2008-04-24

Impact of Jet Grouting on the Lateral Strength of Soil Surrounding Driven Pile Foundations

Matthew E. Adsero
Brigham Young University - Provo

EFFECT OF JET GROUTING ON THE LATERAL RESISTANCE OF SOIL SURROUNDING DRIVEN-PILE FOUNDATIONS

By

Matthew E. Adsero

A thesis submitted to the faculty of

Brigham Young University

in partial fulfillment of the requirements for the degree of

Master of Science

Department of Civil and Environmental Engineering

Brigham Young University

August 2008

BRIGHAM YOUNG UNIVERSITY

GRADUATE COMMITTEE APPROVAL

of a thesis submitted by

Matthew E. Adsero

This thesis has been read by each member of the following graduate committee and by majority vote has been found to be satisfactory.

Date	Kyle M. Rollins, Chair
Date	Travis M. Gerber
Date	Paul W. Richards

BRIGHAM YOUNG UNIVERSITY

As chair of the candidate's graduate committee, I have read the thesis of Matthew Adsero in its final form and have found that (1) its format, citations, and bibliographical style are consistent and acceptable and fulfill university and department style requirements; (2) its illustrative materials including figures, tables, and charts are in place; and (3) the final manuscript is satisfactory to the graduate committee and is ready for submission to the university library.

Date

Kyle M. Rollins
Chair, Graduate Committee

Accepted for the Department

E. James Nelson
Graduate Coordinator

Accepted for the College

Alan R. Parkinson
Dean, Ira A. Fulton College of Engineering and Technology

ABSTRACT

EFFECT OF JET GROUTING ON THE LATERAL RESISTANCE OF SOIL SURROUNDING DRIVEN-PILE FOUNDATIONS

Matthew E. Adsero

Department of Civil and Environmental Engineering

Master of Science

Jet grouting was used to strengthen the soft soil surrounding the piles and the pile cap of two full-scale driven pile foundations. Soilcrete columns, created by jet grouting, were placed underneath the pile cap and surrounding the piles of the first foundation. Two rows of soilcrete columns were placed around the perimeter of one-side of the second. All of the jet grouting took place after construction of the pile caps. Laboratory testing of the soilcrete slurry showed the columns as having a design unconfined compressive strength of 550-650 psi, compared with the native soil strength of only 6-8 psi (850-1150 psf). Lateral loading of the pile foundation was then performed on these foundations. The results of this test were compared with a similar test performed on the same foundations under native soil conditions. The total lateral capacity of the pile foundation treated underneath the pile cap was increased by 500

kips, which equals an increase of 175%. The total lateral capacity of the pile foundation treated adjacent to the pile cap was 150%. Results of testing suggest that each of the jet-grout treated zones displaced as a rigid block. A majority of the increased lateral resistance came from the passive soil resistance acting on the face of the blocks and the adhesive soil resistance acting on the sides and bottom of the block as it displaced through the native soil. The remaining soil resistance, not accounted for by the passive and adhesive soil resistance, can potentially be attributed to increased soil pile interaction, which is predicted from the decrease in pile head rotation during loading following soil treatment.

ACKNOWLEDGMENTS

I wish to thank my Professor Dr. Kyle Rollins for giving me the opportunity to work on such an exciting project, and for all of his technical assistance and support. I also couldn't have done this without the assistance of my fellow students, Mark Herbst (2008) and Nate Lemme (In Press). A special thanks should also be made to the Utah Department of Transportation and Hayward Baker Inc. for their respective volunteer contributions to the project. Also, funding for this project came from the National Cooperative Highway Research Program (NCHRP), without which this research would not have been possible. The support of my wife, Charlotte, and the rest of my family has also been invaluable.

TABLE OF CONTENTS

LIST OF TABLES

LIST OF FIGURES

1 Introduction

Many of the bridge structures in the aging United States transportation infrastructure were designed and built many years before seismicity and associated engineering parameters were taken into consideration for bridge design. In other cases, seismic design forces may have increased significantly with new codes which have been adopted since construction. These bridge structures and the associated foundations are in need of being retrofitted or replaced to meet current seismic code specifications. In the past, additional piles or drilled shafts have been added to the deep foundations to improve lateral resistance, which improves the foundation performance in the event of an earthquake. However, this can be quite difficult to do, particularly when dealing with foundations constructed in soft soils. Furthermore, tying the new foundations to the existing foundations and pile cap can be expensive and time intensive. Recently, strengthening the soft soil surrounding the foundations, in lieu of structural retrofits, has been suggested as a potentially cost-effective alternative to increase the lateral resistance of deep foundations.

Jet grouting, a soil strengthening technique which uses hydraulic and pneumatic energy to erode in situ soil and replace the eroded material with soil-cement columns, has been used in numerous projects to increase the strength of soft soils. Jet grouting has generally been used for excavation support and underpinning buildings adjacent to

excavations. Jet grouting has proven to dramatically increase the stiffness and strength of all soil types, including soft clays.

The application of jet grouting to increase the lateral strength of soils surrounding driven pile foundations has not previously been verified or quantified although it seems particularly well suited to the problem. The lateral resistance of deep foundations is primarily developed within 5 to 10 pile diameters of the ground surface. For typical piles with diameters of 1 to 2 ft, this corresponds to a total depth of 10 to 20 ft. Fortunately, it is possible to treat soils with jet grout to these depths. In addition, jet grouting offers the potential to treat soil underneath a pile cap using holes at the periphery of a pile cap so that the treated soil can extend to the face of the piles. Therefore, jet grouting offers the potential of significantly increasing lateral pile foundation resistance without the need for an expensive structural retrofit In addition, increased strength produced from jet grouting could also increase the passive resistance acting against bridge abutments and pile caps, which would further increase the lateral resistance of a bridge foundation system.

1.1 Project Objectives

The objectives of our research were four-fold.

- Evaluate the increase in lateral pile group resistance due to jet grouting
- Evaluate the increase in lateral passive resistance due to jet grouting
- Produce a well-documented case history of field performance for calibration of computer models so that additional parametric studies can be performed

- Perform a basic cost analysis as to the cost effectiveness of jet grouting to retrofit an existing foundation, in lieu of structural additions

The research for this project was one component of a much larger research project which is funded by the National Cooperative Highway Research Program (NCHRP). The NCHRP has outlined specific tasks that it would like to ultimately accomplish through this investigation. The above list represents four of the specific tasks that were to be accomplished through this research.

This report will focus only on the increased lateral resistance to pile group foundations through jet grouting treatment of the soft soil surrounding the foundation; however, jet grouting was not the only soil improvement technique implemented during this phase of research. Pile foundations were also tested after the soft soil surrounding the foundations was treated with various geometries of compacted fill, mass mixing, flowable fill, and geopiers. Reports of the results associated with these particular soil treatments can be found in the related thesis work of Lemme (In Press), Herbst (2008), and others.

1.2 Scope of Investigation

Four identical full-scale foundations, placed 32 feet apart, were designed, constructed and tested during this phase of research. Each foundation consisted of nine piles, in a 3 x 3 configuration, driven to a depth of approximately 40 ft below grade. Prior to driving, the piles were also instrumented with strain gages at predetermined depths. Inclinometer and shape accelerometer shape array casings, which extended the

length of the driven piles, were also placed in selected middle row piles. A 9.25 ft square reinforced concrete pile cap which extended from the ground surface to 2.5 feet below grade, was constructed on top of the piles. A reinforced concrete corbel was attached to the concrete pile cap to create a load transfer surface during testing of the various foundation systems. A hydraulic actuator was placed between two foundations which were being tested. Steel pipe extensions were attached to each end of the actuator to span the distance between the actuator and foundation. The extensions were then attached to the corbel to enable lateral load transfer from the actuators to the pile caps.

The foundations were first tested under native-virgin soil conditions. One test was performed with soil directly behind the pile cap; the second test was performed with the soil directly behind the pile cap excavated to the depth of the pile cap. The results of these two tests were used to determine the total and passive force acting on the foundation when it is loaded laterally under native soil conditions. Shape arrays, strain gages, and inclinometers were also used to determine the deflections and moments in the piles with respect to depth below grade. After these tests were completed, jet grouting was used to treat the soil surrounding each of the pile caps. Jet grouted columns were inserted below the pile cap and between the piles of one of the pile caps. The soil was treated to a depth of 10 feet below the bottom of the pile cap.

Jet grouted columns were also inserted adjacent to another pile cap. These columns formed a treated soil zone which extended 5 feet from the face of the pile cap to a depth of 12 feet below the top of the pile cap. Subsequently, lateral load tests were performed on the same foundations both with soilcrete columns directly in front of the pile cap, and after excavating the soil-cement in front of the pile cap to eliminate any

passive force contribution. The results of these tests were then compared with the results obtained when the foundation was loaded under native soil conditions to determine the degree of improvement to both lateral pile resistance and passive resistance on the pile cap itself.

2 Jet Grouting Literature Review

Jet grouting has been around for many years, and hundreds of projects around the world have utilized jet grouting to strengthen weak soils. The following chapter will give a more detailed description of the jet grouting process, and its various applications. As has been stated previously, the application of jet grouting to improve the lateral strength of soils has never before been validated or quantified.

2.1 Basic Overview

Jet grouting is a ground improvement method which uses hydraulic and pneumatic energy to erode in situ soil and mix/replace the eroded material with a soil-cement slurry to produce a product known as “soilcrete”. These internal soilcrete structures can be constructed in many different geometries and diameters, and are most ofeeten interconnected to provide underpinning of structures, excavation support, groundwater control, or in situ stabilization for a variety of civil and environmental engineering projects. These construction practices can apply to new construction projects or retrofitting of pre-existing structures. Jet grouting is a very diverse soil improvement technique that can be used for an extremely broad range of soil conditions and applications. Four different styles of jet grouting (double fluid, single fluid, triple

fluid, and superjet) are available for use depending on the erodibility of the in-situ soil and other design considerations for individual projects.

Single fluid jet grouting uses a grout slurry pumped at a high velocity through a nozzle near the end of a rotating drilling rod. The slurry breaks down the soil and replaces/mixes with eroded soil to form the soilcrete structure. Single fluid jet grouting is the best approach for cohesionless soils, and can produce soilcrete columns up to 3.5 feet in diameter. *Double fluid* jet grouting also uses a grout slurry to erode and replace the in situ soil; however the erosion energy of the slurry jet is increased by shrouding the slurry jet with air. The higher erosion energy of this method makes it more effective in cohesive soils than single fluid grouting, and can produce soilcrete columns up to 6 feet in diameter. Triple *fluid* jet grouting utilizes a slightly different approach than single or double fluid jet grouting. A coaxial-air enshrouded water jet is shot at a high velocity from a nozzle to form the erosion medium. A lower-velocity grout slurry is shot from a nozzle located below the erosion jet to form the soilcrete structure. The separation of the erosion and grouting processes in this technique leads to a higher quality soilcrete. This form of jet grouting is most effective for cohesive soils, and can produce columns up to 4 feet in diameter in clays. *Superjet* grouting is basically a modified version of the double fluid system which reduces the dispersion of the erosion media from the monitor (nozzle), increasing the erosive energy of the air-enshrouded grout slurry. Superjet grouting can produce soilcrete columns up to 16 feet in diameter, and is most effective for projects where mass stabilization or surgical treatment is necessary. Figure 2-2 shows the potential strength gains that can be achieved through jet grouting in the various types of soils. For a given cement content and curing time, sands and gravels develop the

highest compressive strengths while organic silts and peats develop the lowest. For clays, the in-situ compressive strength can typically be increased to between 250 and 500 psi using jet grouting. (Burke, 2004).

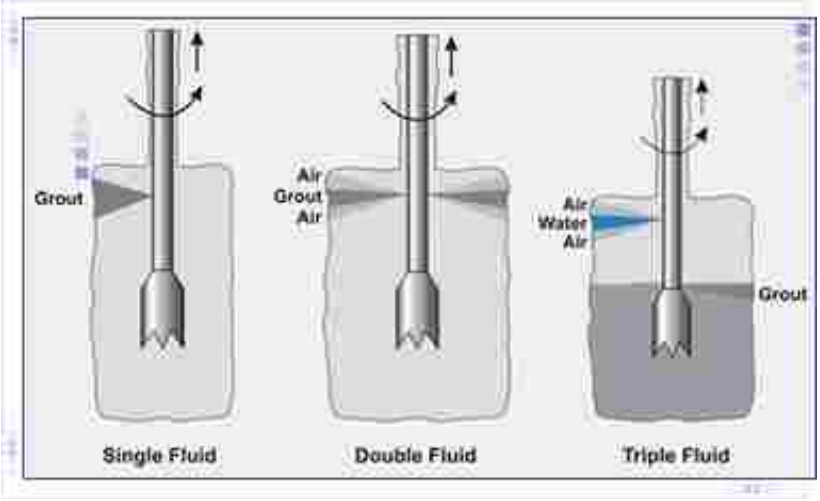

Figure 2-1 Basic overview of jet grouting styles (Hayward-Baker, 2007).

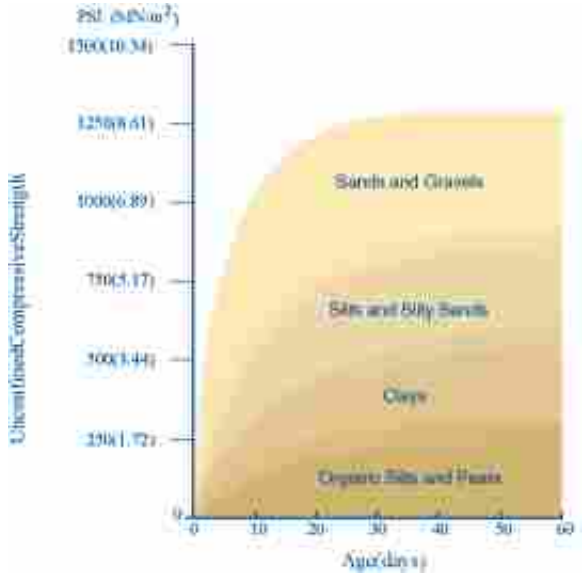

Figure 2-2 Ranges of compressive strength possible from jet grouting for various soil types (Hayward-Baker, 2007).

2.2 Basic Approach

A detailed understanding of the soil profile is necessary in order to determine which type of jet grouting and jet grouting parameters will be utilized to produce the required soilcrete structures. Parameters for each type of jet grouting can include the following: water pressure, water volume, air volume, air pressure, slurry volume, slurry pressure, slurry density, rotation rate, lift rates and specifications, and depth.

Table 2-1 provides typical range of parameters used for the various types of jet grouting. Generally, clays require greater amount of erosive energy and cement content to treat a volume of soil. Therefore, the upper ranges of slurry pressure, volume and density found in

Table 2-1 are used when treating clays. The cement content of the slurry is generally controlled by the slurry density. Typical cement contents for the various soil types treated with jet grouting are found in Table 2-2. If the soil is extremely varied it may be necessary to vary these parameters with depth in order to achieve uniform soilcrete geometry. The determination of these parameters requires a high degree of familiarity with the different jet grouting systems and should generally be done by engineers who specialize in jet grouting.

Typcial jet grouting is a bottom-up procedure, which means that a borehole is drilled to the desired depth; then erosion and mixing/replacing of the soil with the jet grouting fluids begins as the drill shaft gradually moves back up the borehole. This means that the drill rig must be able to set up directly over the area to be treated. An illustration of this process is provided in Figure 2-3.

Table 2-1 Typical design parameters used in jet grouting (Burke, 2004).

		Single Fluid	Double Fluid	Triple Fluid
Water	Pressure (bar)	na	na	300-400
	Volume (l/min)	na	na	80-200
	No. Nozzels	na	na	1-2
	Nozzel Sizes (mm)	na	na	1.5-3.0
Air	Pressure (bar)	na	7-15	7-15
	Volume (m^3/min)	na	8-30	4-15
Grout Slurry	Pressure (bar)	400-700	300-700	7-100
	Volume(l/min)	100-300	100-600	120-200
	Density (S.G.)	1.25-1.6	1.25-1.8	1.5-2.0
	No. Nozzels	1-6	1-2	1-3
	Nozzel Sizes (mm)	1-4	2-7	5-10
Lift	Step Height (cm)	0.5-60	2.5-40	2-5
	Step Time (sec)	4-30	4-30	4-20
Rotation	Speed (rpm)	7-20	2-20	7-15

Table 2-2 Typical cement contents for soilcrete (Burke, 2004).

Soil Type	Cement Content of Soilcrete (kg/m^3)
Sands	150-200
Silts and Silty Sands	200-275
Clays	250-350
Organic Silts and Peats	300-400

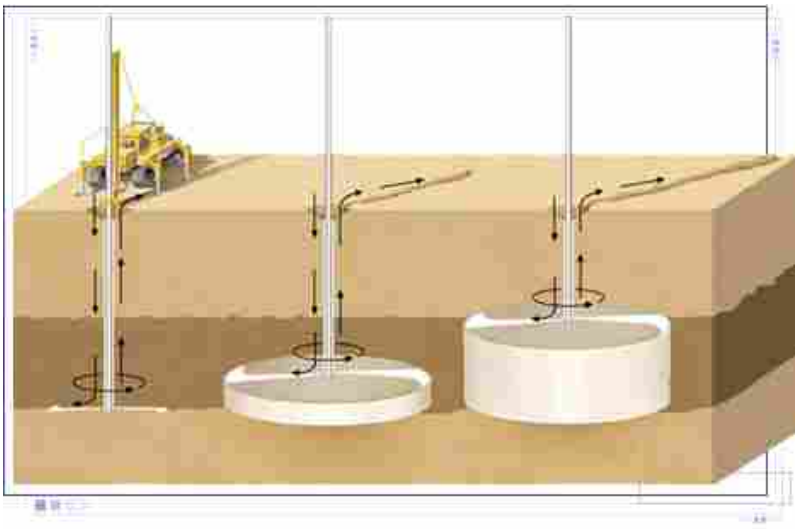

Figure 2-3 Schematic illustration of typical jet grouting procedure (Hayward-Baker, 2007).

2.3 Quality Control

Prior to the decision to use jet grouting, it is typical to perform a laboratory investigation to evaluate the effect of cement content on the unconfined compressive strength. Samples of the soil types at the site are thoroughly mixed with varying percentages of cement, test cylinders are formed and cured, then broken. These tests define the compressive strength vs. cement content relationship under laboratory conditions. This testing aids in selecting an appropriate value for the desired application and refining the cost of the treatment.

In the field, it is also common practice to construct test sections of soilcrete columns on or near site to ensure that the soilcrete columns meet the design-specified parameters. The columns can be excavated to evaluate the diameter of the columns which are actually produced by the selected jet grouting process. Wet grab as well as hardened core samples of the test soilcrete structures are taken and evaluated to ensure that the soilcrete meets the design strength specifications. Generally, wet grab samples are taken from various depths of the installed column. The samples are then placed into test cylinders and mixed to a uniform density. The samples are then allowed to cure, and are tested in a laboratory for compressive strength at various cure times. It is general practice among Hayward Baker engineers to reduce the compressive strengths obtain from the laboratory by a factor of 2.5 to 3 to estimate the in-situ field strength of the soilcrete. If it is determined that these test soilcrete columns meet the ground improvement design specifications, then construction can commence. Additionally, cored samples can be taken from hardened soilcrete columns and tested in compression to determine if the soilcrete meets design strength specifications.

Another important aspect of quality control of soilcrete column construction is the control and disposal of the spoil from the boreholes. The spoil must be allowed to freely flow up the annulus of the borehole throughout the erosion and grouting phases of jet grouting. If the annulus gets clogged (which is a common occurrence in highly plastic soils), this greatly changes the erosion environment in the borehole and can lead to hydrofracturing of the soil and inconsistent soilcrete properties and geometries. Also, there must be a system in place to divert the spoil return to a specified location where it can be stored and disposed of.

2.4 Advantages

Jet grouting can be performed in nearly any soil type and variable treatment diameters are possible. It is also possible to treat specific subsurface layers rather than the entire thickness from the ground surface down as with stone columns or rammed aggregate piers. The strength and permeability of the resulting soilcrete can be controlled, and the method does not produce significant noise or vibration as with pile driving for dynamic compaction or dynamic replacement. With respect to soil treatment around deep foundations, jet grouting offers several important advantages relative to other soil improvement methods. Jet grouting is one of the few methods which can be used to treat the soil underneath an existing pile cap. However, this procedure might require that access holes be cored through the pile cap in some cases where treatment can not be achieved from the periphery of the pile cap. Jet grouting could also be used to produce an "equivalent pier" foundation by enclosing the existing pile foundations within a mass of soilcrete. This would be highly desirable in dealing with scour.

2.5 Disadvantages

One major disadvantage of the method is the need to control the spoil return through the borehole annulus. The quality of the resulting columns is directly related to the ability of the field crew to prevent clogging and maintain flow. Clogging can lead to variations in column diameter and strength. The potential for clogging increases as the soil becomes more cohesive. A second major disadvantage is need to store and dispose of the spoil. If there are questions regarding contamination of the soil, then spoil disposal becomes even more problematic. Fortunately, cement stabilized spoils generally make reasonably good compacted fill material. Lastly, because the method is a highly sophisticated process, it requires specialized labor, equipment and design teams. As a result, mobilization and demobilization costs are high as are treatment costs. Therefore, this method is one of the most expensive treatment methods available. Because of the high mobilization costs, the method becomes more economical as the size of the project increases.

3 Geotechnical Site Characterization

The following chapter will describe the soil conditions of the site used for testing. The site was located north of Salt Lake City at the interchange of Redwood Road and I-215 on a Utah Department of Transportation (UDOT) right-of-way. An aerial view of the site is shown in Figure 3-2. The site was chosen because it was known to have deep soft clay deposits. The top 4 feet of the site consisted of fill materials containing large pieces of asphalt, and was excavated from the entire test site prior to testing. All of the geotechnical field investigations took place before the excavation, and the results from these investigations have been modified to reflect the soil conditions below the excavation.

3.1 Field Investigations

Geotechnical site conditions were evaluated using field and laboratory testing. Field testing included one drilled hole with undisturbed sampling, four cone penetration test (CPT) soundings, and shear wave velocity testing. Laboratory testing included unit weight and moisture content determination, Atterberg limits testing, and undrained shear testing. A plan view drawing showing the locations of the borehole and CPT soundings relative to the finished pile caps is shown in Figure 3-2.

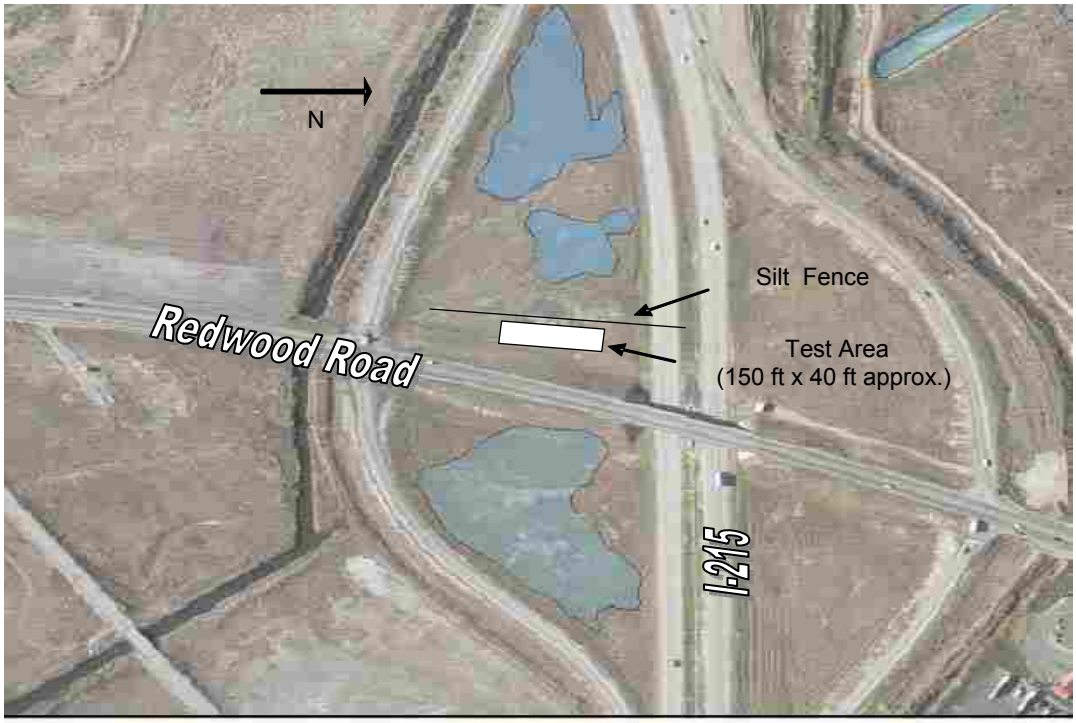

Figure 3-1Arial photo of test site location.

3.2 Soil Profile, Classification and Shear Strength.

A generalized soil boring log at the test site is provided in Figure 3-3 (a). The depth is referenced to the top of the excavation which was 2.5 feet above the base of the pile cap as shown in the figure. The soil profile consists predominantly of cohesive soils; however, some thin sand layers are located throughout the profile. The cohesive soils in the upper 15 feet of the profile typically classify as CL or CH materials with plasticity indices of about 20 as shown in (a). In contrast, the soil layer from a depth of 15 to 25 feet consists of interbedded silt (ML) and sand (SM) layers as will be highlighted by the subsequent plots of CPT cone tip resistance. The liquid limit, plastic limit and natural moisture content are plotted in Figure 3-3 (b) at each depth where Atterberg limits were determined. The water table is at a depth of 2.0 feet, which is equivalent to a depth of 6.0 feet below the pre-excavation ground surface. The natural

water content is less than the liquid limit near the ground surface suggesting that the soil is overconsolidated. However, the water content is greater than the liquid limit for soil specimens from a depth of 5 to 27 feet, suggesting that these materials may be sensitive. Below a depth of 30 feet, the water content is approximately equal to the liquid limit, suggesting that the soils are close to normally consolidated.

The undrained shear strength is plotted as a function of depth in Figure 3-3 (c). Undrained shear strength was measured using a miniature vane shear test (Torvane test) on undisturbed samples immediately after they were obtained in the field. In addition, unconfined compression tests were performed on most of the undisturbed samples. Both the Torvane and unconfined compression tests indicate that the undrained shear strength decreases rapidly from the ground surface to a depth of about 6 feet. However, the undrained shear strengths from the unconfined compression tests are typically about 30% lower than that from the Torvane tests. After a depth of 6 feet the trend reverses, and the shear strength begins to increase with depth. This profile is typical of a soil profile with a surface crust that has been overconsolidated by desiccation. The unconfined compression tests performed on samples taken at the depths of 27 and 48 feet yielded soil strengths substantially lower than that from the Torvane test. These unconfined compression tests appear to have been conducted on soil with sand lenses, and are not likely to be representative of the in-situ soil. The undrained shear strength was also computed from the cone tip resistance using the following correlation equation:

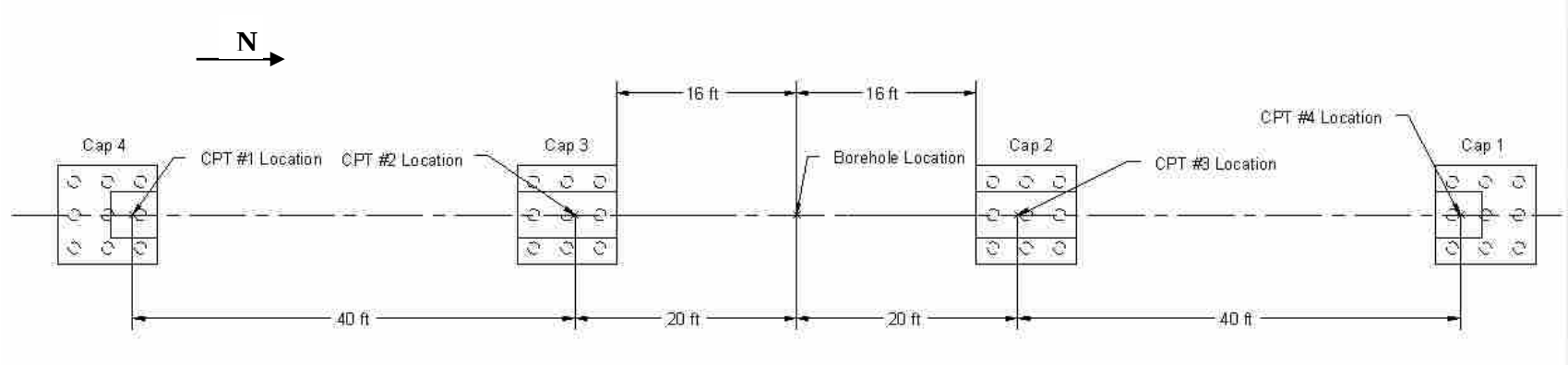

Figure 3-2 Plan view showing location of boring andCPT soundings relative to completed pile caps.

$$s_u = \frac{(q_c - \sigma)}{N_k} \quad \textbf{(3-1)}$$

where q_c is the cone tip resistance, σ is the total vertical stress, and N_k is a variable which typically ranges from 10 to 20 and was taken to be 15 for this study (Riaud and Miran, 1992). The undrained shear strength obtained from the above equation is also plotted vs. depth in (c), and the agreement with the strengths obtained from the Torvane and unconfined compression tests is reasonably good. Nevertheless, there is much greater variability with depth, as the penetrometer displaces through the sand lenses. The shear strength in the sand layers has been excluded because the correlation with cone tip resistance is not applicable in these materials. A summary of laboratory test results is provided in Table 3-1.

Table 3-1 Laboratory test results.

	In-Place		Atterberg Limits				Miniature	
Depth below Excavated Surface (ft)	Saturated Unit Weight (pcf)	Natural Water Content (%)	Liquid Limit (%)	Plastic Limit (%)	Plastic Index (%)	Unconfined Compressive Strength (psf)	Vane Shear Strength (Torvane) (psf)	Unified Soil Classification Symbol
1.25	117.6	34.2	39	18	21	1104	-	CL
2.75	117.4	34.4	38	18	20	626	620	CL
5.75	104.6	56	51	21	30	384	320	CH
8.5	112.4	41.5	38	18	20	684	534	CL
11.5	110.8	44.1	38	19	19	741	500	CL
16.5	126.6	24.2	19	18	1	1081	560	ML
26.75	116.9	35	27	14	13	237	780	CL
33.5	124.6	26.1	27	14	13	1306	780	CL
36.75	117.1	34.8	35	17	18	1381	840	CL
41.75	112.0	42.1	46	17	29	1037	520	CL
48	117.2	34.6	33	16	17	297	660	CL

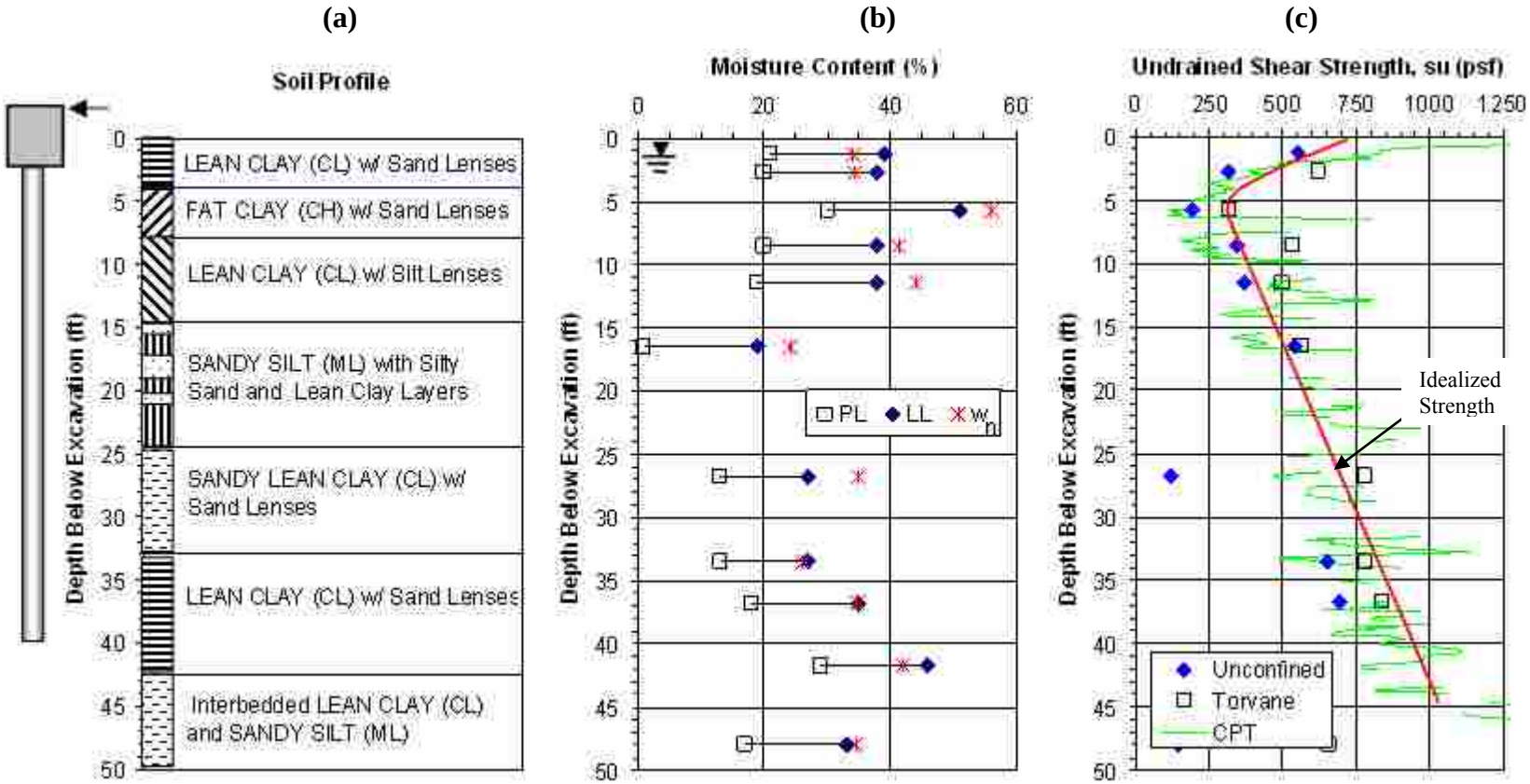

Figure 3-3 Plot of (a) soil profile, (b) Atterberg limits and natural water content vs. depth, and (c) undrained shear strength vs. depth.

3.3 Cone Penetration and Seismic Cone Testing

Four cone penetration tests (CPT) were performed across the test site. Plots of cone tip resistance, friction ratio, and pore pressure for the centermost test are provided as a function of depth in Figure 3-4. In addition, the interpreted soil profile is also shown. From the ground surface to a depth of about 15 feet the soil profile appears to be relatively consistent with a cone tip resistance of about 6 tsf and a friction ratio of about 1%. However, a thin sand layer is clearly evident between 6 and 8 feet. The cone tip resistance, friction ratio, and pore pressure plots clearly show the interbedded silt and sand layering in the soil profile between 15 and 27 feet below the ground surface. Figure 3-5 provides plots of the cone tip resistance, friction ratio and pore pressure as a function of depth for all four of the CPT soundings. The measured parameters and layering are generally very consistent for all four sounding which indicates that the lateral pile load tests can be fairly compared from one foundation to the next.

Penetration of the cone penetrometer through a soft soil causes compression of the soil surrounding the cone. This increases the pore pressures measured by the cone beyond hydrostatic pressure conditions. As the cone penetrometer enters a granular soil, the measured pore pressures typically decrease back to static pressure conditions (USDOT, 1992). This behavior is displayed in Figure 3-4(d). The pore pressures measured through the clay layers are much larger than those measured as the penetrometer enters a sand lens. The porous filter used for measuring the pore pressure was in location 2 on the penetrometer.

Figure 3-6 also provides a plot of the shear wave velocity as a function of depth obtained from the downhole seismic cone testing. The interpreted soil profile and cone tip resistance are also provided in Figure 3-6 for reference. The shear wave velocity in the upper 10 feet of the profile is between 300 and 400 feet/sec. This velocity is relatively low and suggests low shear strength. Between depths of 10 to 20 feet the velocity increases to about 550 feet/sec. This increase in velocity is likely associated with the interbedded sand layers in these depths. Below 20 feet, the velocity drops to a value of around 500 feet/sec and remains relatively constant to a depth of 45 feet, the maximum depth of testing.

For comparison purposes a site with an average shear wave velocity of 600 ft/sec in the upper 100 feet of the profile is classified as a soft clay site (Site E) according to the International Building Code (IBC, 2006). A table of the specifying the site class definitions, taken from the IBC, is displayed in Table 3-2. Knowledge of the average shear wave velocity, standard penetration resistance, and undrained shear strength of the soil to a depth of 100 feet is generally necessary to determine a specific International Building Code (IBC) seismic site classification. However, this is not necessarily the case if the site is classified as Site Class E. Regardless of the average shear wave velocity, any soil profile with more than 10 feet of soil having the following characteristics is classified as a Site Class E, namely:

1. Plasticity index, $PI > 20$
2. Moisture content, $w \geq 40\%$
3. Undrained Shear strength, $S_u < 500$ psf

A close look at Table 3-1 or Figure 3-3 shows that the zone from about 4 to 15 ft has an undrained shear strength less than 500 psf and a moisture content greater than 40% which both meet the criteria for site class E. The PIs in this layer are 30, 20 and 19 which are either above or right at the boundary of 20 specified in the code, which makes evaluation of the third criterion somewhat more problematic. Considering that the 11 ft layer clearly meets two of the criteria and that the average PI of 23 for the layer would meet the third criteria, the site could reasonably considered to be site class E. In any event, knowledge of the site conditions in the last 50 feet of the profile would likely show that the site would at least classify as a site class D.

Table 3-2 Seismic site class definitions from the IBC 2006 code.

Site Class	Soil Profile Name	AVERAGE PROPERTIES IN TOP 100 feet		
		Soil Shear Wave Velocity, v_s, (ft/s)	Standard Penetration Resistance, N	Soil Undrained Shear Strength, s_u, (psf)
A	Hard Rock	$v_s > 5{,}000$	N/A	N/A
B	Rock	$2{,}500 < v_s \leq 5{,}000$	N/A	N/A
C	Very dense soil and soft rock	$1{,}200 < v_s \leq 2{,}500$	N > 50	$s_u \geq 2{,}000$
D	Stiff soil profile	$600 < v_s \leq 1{,}200$	$15 \leq N \leq 50$	$1{,}000 \leq s_u \leq 2{,}000$
E	Soft soil profile	$v_s < 600$	N < 15	$s_u < 1{,}000$
E		Any Profile with more than 10 feet of soil having the following characteristics: 1. Plasticity index PI > 20 2. Moisture content w ≥ 40% 3. Undrained Shear strength Su < 500 psf		
F		Any Profile with more than 10 feet of soil having the following characteristics: 1. Soils vulnerable to potential failure or collapse under seismic loading such as liquefiable soils, quick and highly sensistive clays, collapsible weakly cemented soil 2. Peats and/or highly organic clays (H > 10 feet of peat and/or highly organic clay where H = thickness of soil) 3. Very high plasticity clays (H > 25 feet with plasticity index PI > 25) 4. Very thick soft/medium stiff clays (H > 120 feet)		

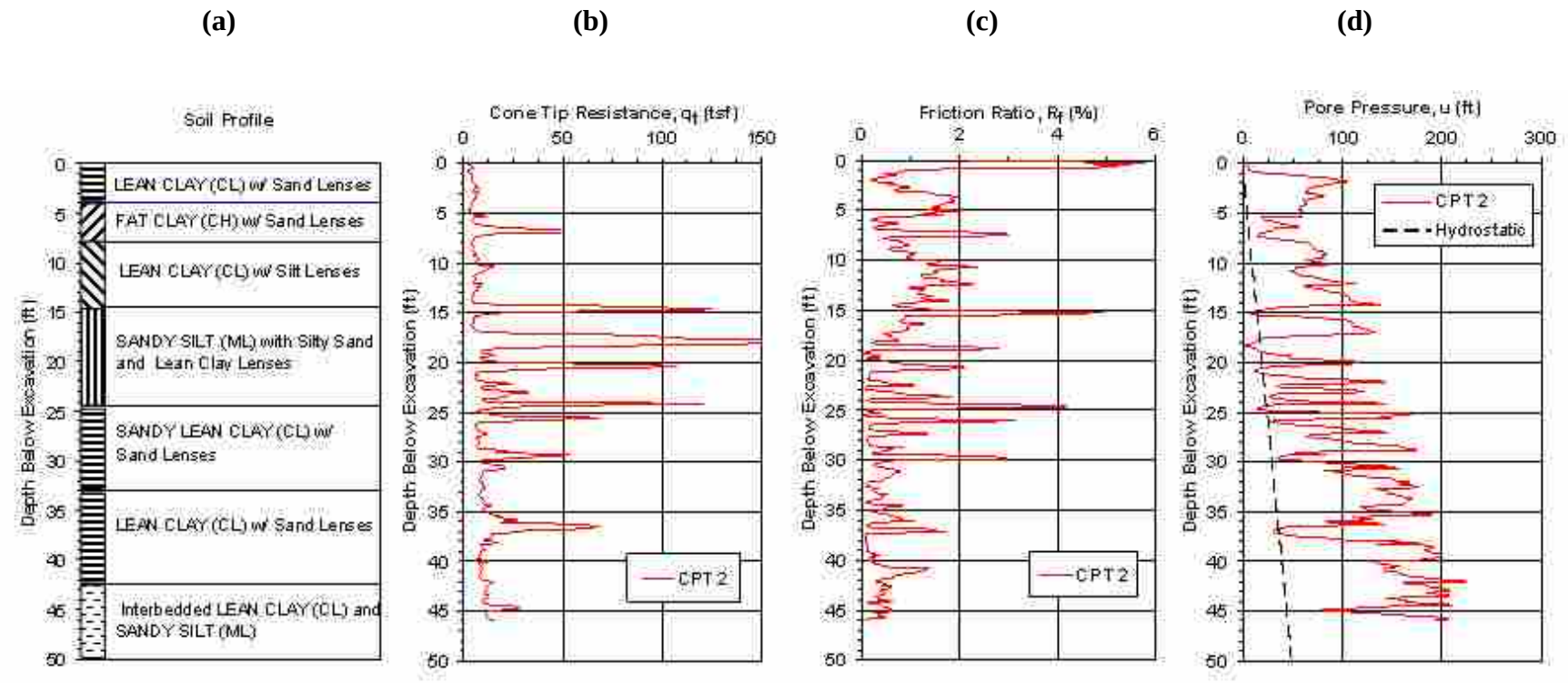

Figure 3-4 Plot of (a) soil profile, (b) cone tip resistance vs. depth, (c) friction ratio vs. depth, and (d) pore pressure vs. depth curves from cone penetration test (CPT) sounding 2 near the center of the site.

(a) **(b)** **(c)** **(d)**

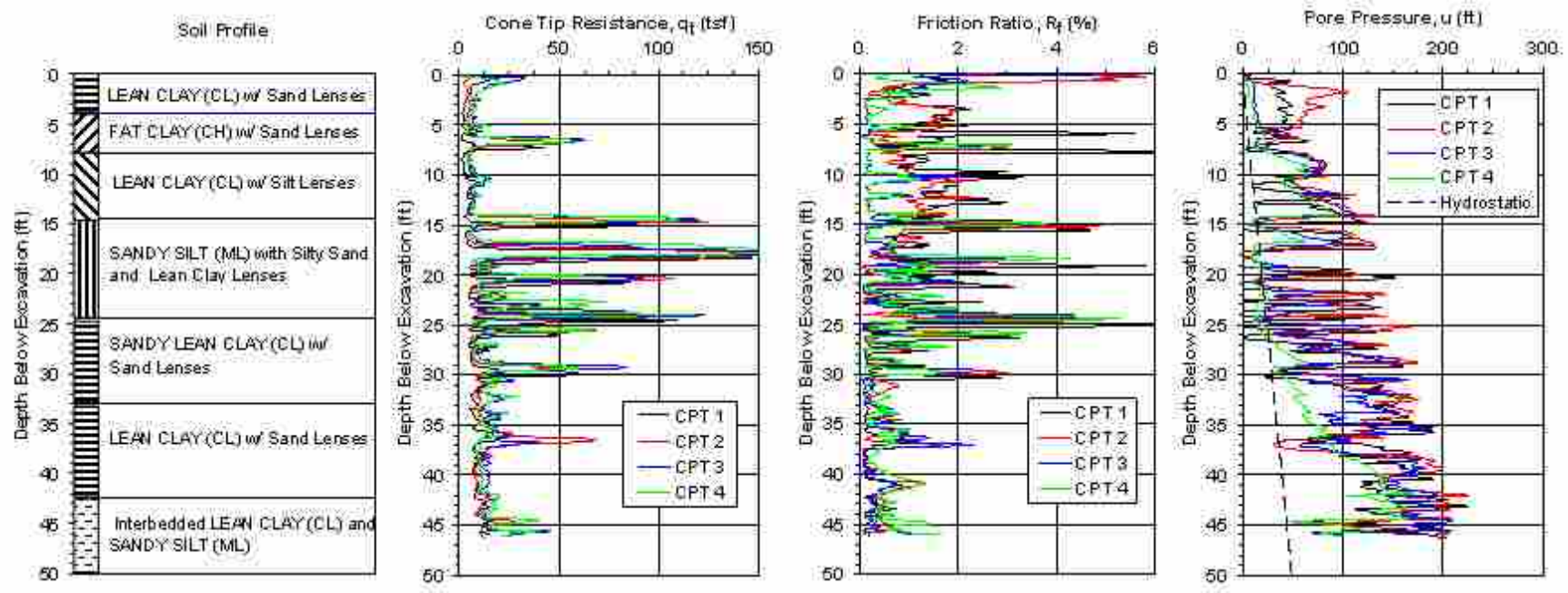

Figure 3-5 Plot (a) soil profile, (b) cone tip resistance vs. depth, (c) friction ratio vs. depth and, (d) pore pressure vs. depth from all four cone penetration test (CPT) soundings.

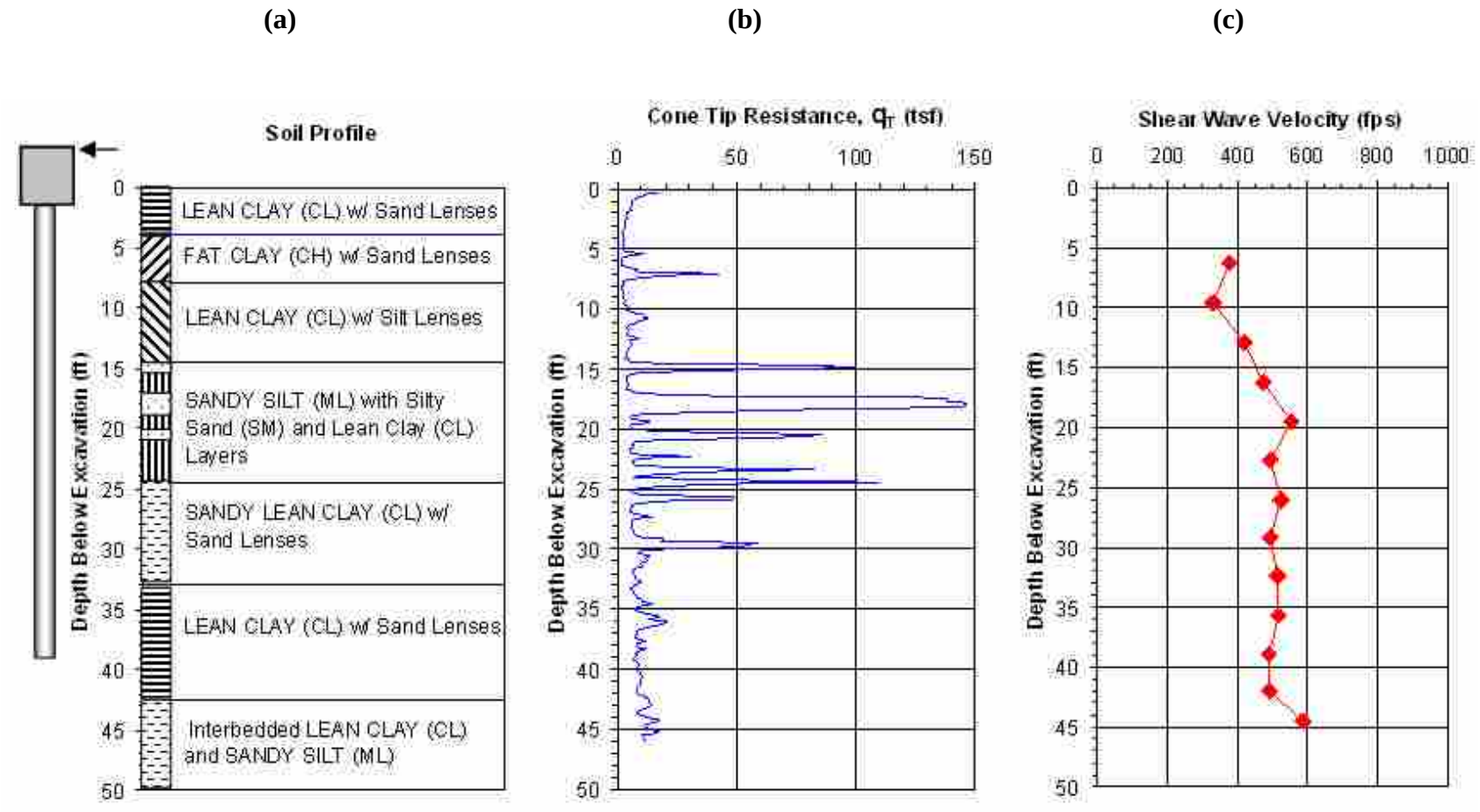

Figure 3-6 Plot of (a) soil profile, (b) cone tip resistance vs. depth, and (c) shear wave velocity vs. depth from seismic cone testing.

4 Test Layout and Procedure

The following section will detail the construction process for the foundations and define the properties of the materials used to create the foundations. This section will also explain the basic layout of the actuators and pile caps, along with the instrumentation configuration for each of the foundations.

4.1 Construction, Layout, and Materials

Once the site had been excavated to the proper elevation of 4 feet below the original grade, the four pile groups were driven. An overall plan view of the four pile group locations is shown in Figure 3-2. As shown in Figure 4-1, each pile group consisted of nine test piles which were driven in a 3 x 3 orientation with a nominal center-to-center spacing of 3 feet in both directions. The test piles were 12.75 inch OD pipe piles with a 0.375 inch wall thickness, and they were driven closed-ended with a hydraulic hammer to a depth of approximately 45 feet below the excavated ground surface on June 13-15, 2007. The test piles had a beveled end which allowed a 1.5 inch thick plate to be welded flush with the edge of the pile at the bottom. The steel pile conformed to ASTM A252 Grade 2 specifications and had a yield strength of 58,700 psi based on the 0.2% offset criteria. The moment of inertia of the pile itself was 279 in^4; however, angle irons were welded on opposite sides of two to three test piles within

each group, as discussed subsequently, which increased the moment of inertia to approximately 342 in^4.

The center piles of each row were instrumented with strain gages prior to installation for pile caps 1 and 3 (see Figure 4-1). However, for caps 2 and 4, the middle pile of the center row was not instrumented with strain gages. The strain gages were placed at pre-determined depths of 2, 6, 11, and 13.5 feet below the tops of the piles. Strain gages were placed along the north and south sides of the piles in the direction of loading. The strain gage depths were determined through computer modeling to be the most critical depths relative to maximum bending moment for the laterally loaded piles. Figure 4-2 is a photo of an installed pile group.

The piles were driven so that they would extend 2 ft into the base of the pile cap. In some cases this was not accomplished so the piles were cut off to this elevation. A steel reinforcing cage was installed at the top of each test pile to connect the test piles to the pile cap. The reinforcing cage consisted of 6 - #8 reinforcing bars which were confined within a #4 bar spiral with a diameter of 8 inches and a pitch of 6 inches. The reinforcing cage extended 2.25 feet above the base of the cap and 8.75 feet below the base. The steel pipe pile was filled with concrete which had an average unconfined compressive strength of 5150 psi based on tests of four specimens. A drawing showing the cross-section for the test piles is provided in Figure 4-3. Once the piles were filled, construction of the pile cap was then commenced.

Figure 4-4 shows plan and profile drawings of pile caps 1 and 2. Pile caps 1 and 2 (the two northern most pile caps) were constructed by excavating 2.5 feet into the virgin clay. The concrete was poured directly against vertical soil faces on the front and

back sides of each pile cap. This construction procedure made it possible to evaluate passive force against the front and back faces of the pile caps. In contrast, plywood forms were used along the east and west sides of all of the caps and were braced laterally against the adjacent soil faces. This construction procedure created a gap between the cap sidewall and the soil so that side friction along the cap would be eliminated.

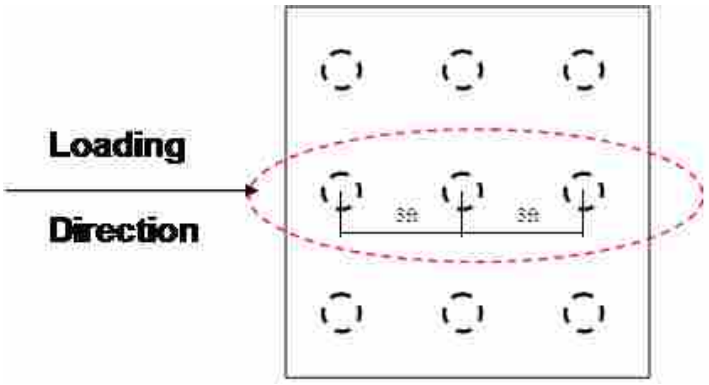

Figure 4-1 Driven 3x3 pile group all 3ft on center in both directions (piles instrumented with strain gages circled in red).

Figure 4-2 Driven pile layout prior to cap construction.

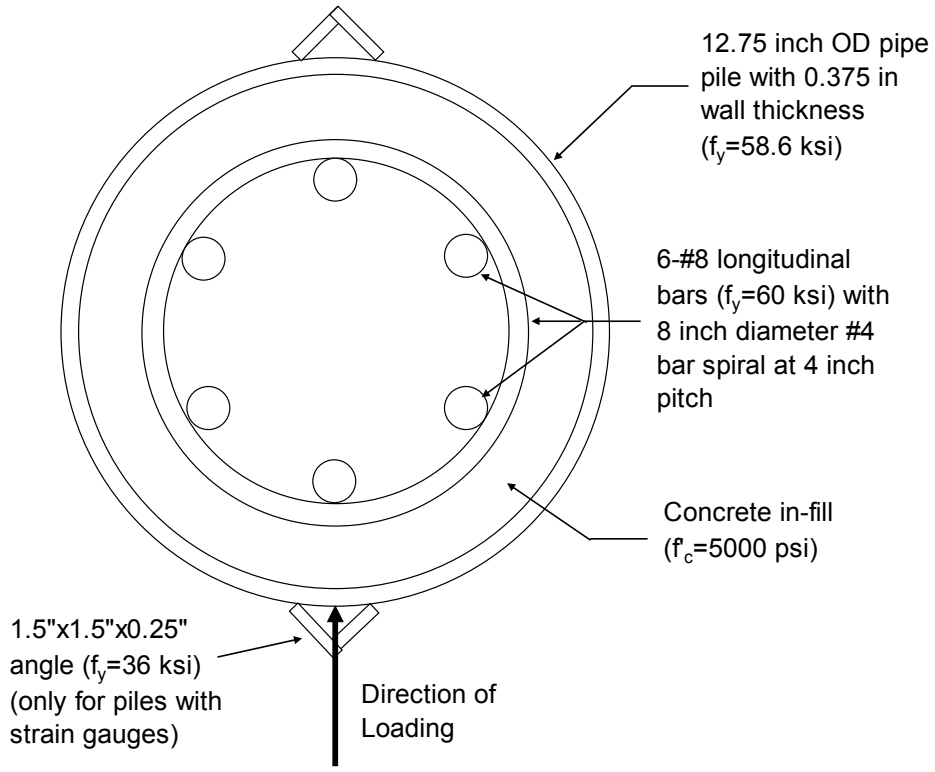

Figure 4-3 Cross-section of piles within the pile groups.

Pile cap 3 was constructed in a similar manner, except that flowable fill was installed prior to pile cap placement to a depth of 7 feet below the top of the finished cap, 9 feet wide, and 13.5 feet in the direction of loading before piles were driven. Flowable fill was also installed on the north side of the cap to the same depth as that installed under the cap and then, after cap installation, up the side at a width of 4.5 feet from the pile cap to the level of the top of the cap. Pile cap 4 was constructed in the same way as cap 3, except that compacted fill was installed prior to pile driving. The compacted fill was installed to a depth of 3 feet below the bottom of the pile cap with a width of 9 feet transverse to the load direction and a length of 14 feet in the direction of loading. Compacted fill was also installed along the north side of the cap level.

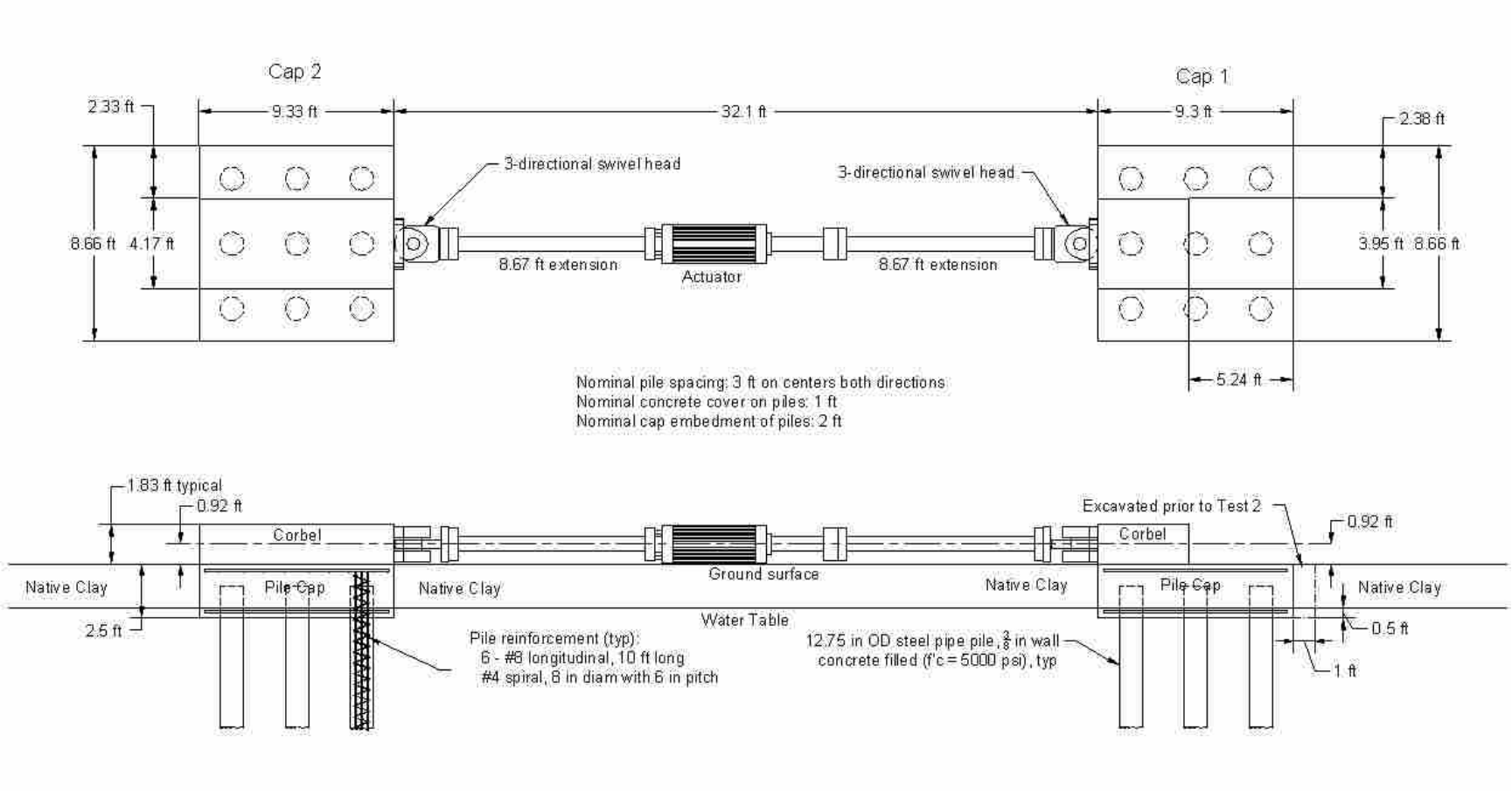

Figure 4-4 Plan and profile drawings of pile caps 1 and 2 during Test 1 when the pile groups were pulled together by the actuator. During Test 2 the soil adjacent to the pile cap was excavated to the base of the cap and the pile caps were pushed apart by the actuator.

Steel reinforcing mats were placed in the top and bottom of each cap with a three inch concrete cover. The top reinforcing mat in the pile caps was designed with #7 bars at 10 inch spacing in both directions, with a decrease in spacing to 6 inches in the transverse direction under the short corbel on caps 1 and 4. The bottom mats were designed with #9 bars at 6.5 inch spacing longitudinally and #7 bars at 10 inch spacing transverse to the load direction. Plan view drawings of the top and bottom reinforcing mats for piles caps 1, 2, 3, and 4 are provided in Figure 4-5 and Figure 4-6.

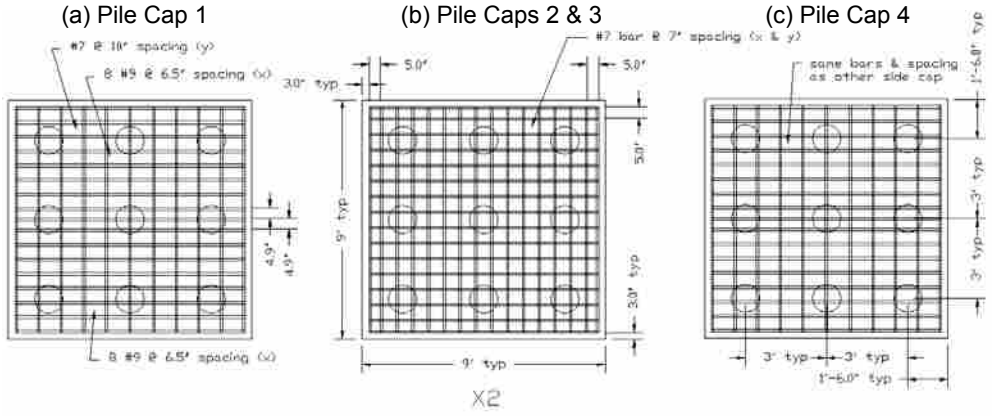

Figure 4-5 Layout of bottom reinforcing mat for the test pile groups.

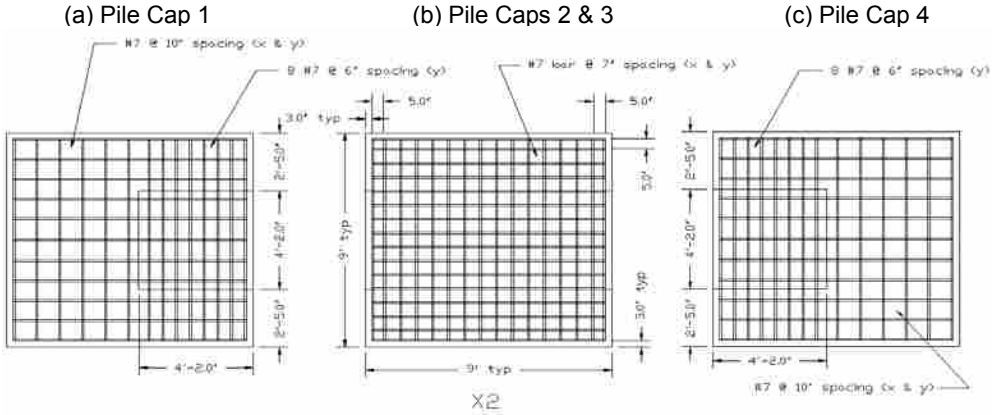

Figure 4-6 Layout of top reinforcing mat for the test pile groups.

A corbel was constructed on each cap to allow the actuator to apply load above the ground surface without affecting the soil around the pile cap. The corbel extended the full length of the pile cap for caps 2 and 3 to allow the actuators to be attached to both sides of the caps. In contrast, the corbel only extended about half of the pile cap length in cap 1 and 4 as only one side was needed for the actuator attachment. This is shown in Figure 4-4 which illustrates the corbel configuration on top of caps 1 and 2. The corbel was designed using the design method found in section 11.9 of the ACI code. The corbel was reinforced with #5 bar hoops and #9 bars as the main reinforcement as shown in Figure 4-7 and Figure 4-8. Also included in Figure 4-9 is a cross sectional view of the corbel steel looking at the interface where the actuator connects to the corbel. Design calculations and more detailed steel reinforcement drawings are provided in the Appendix A.

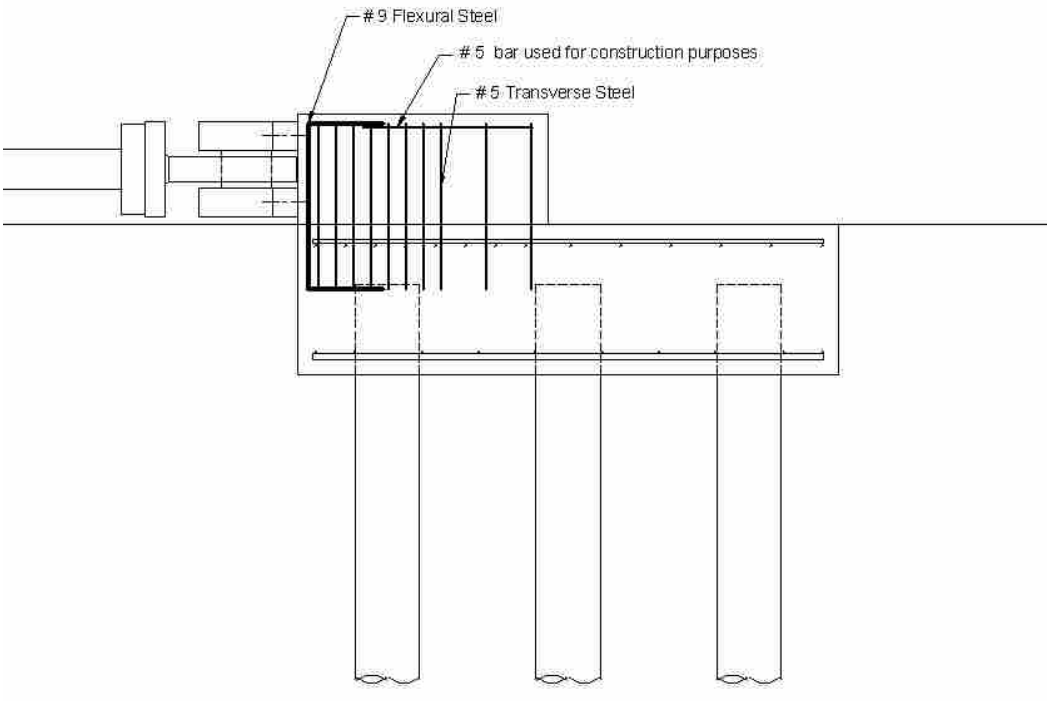

Figure 4-7 Corbel steel layout for caps 1 and 4.

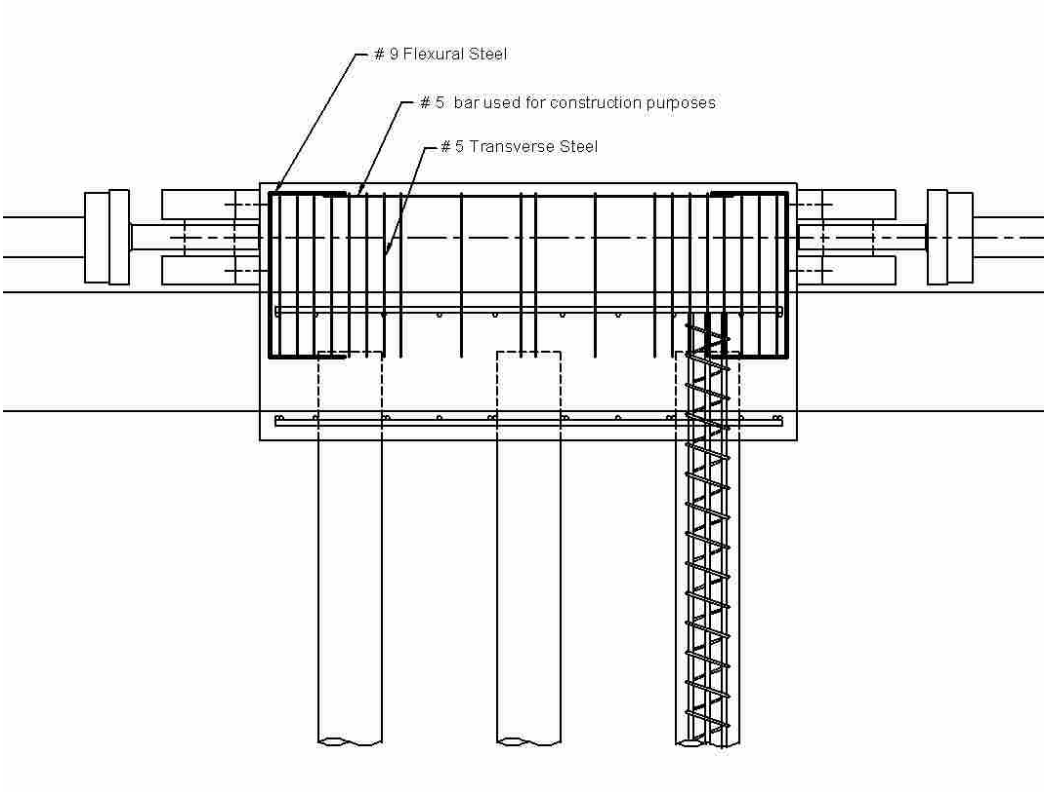

Figure 4-8 Corbel steel layout for caps 2 and 3.

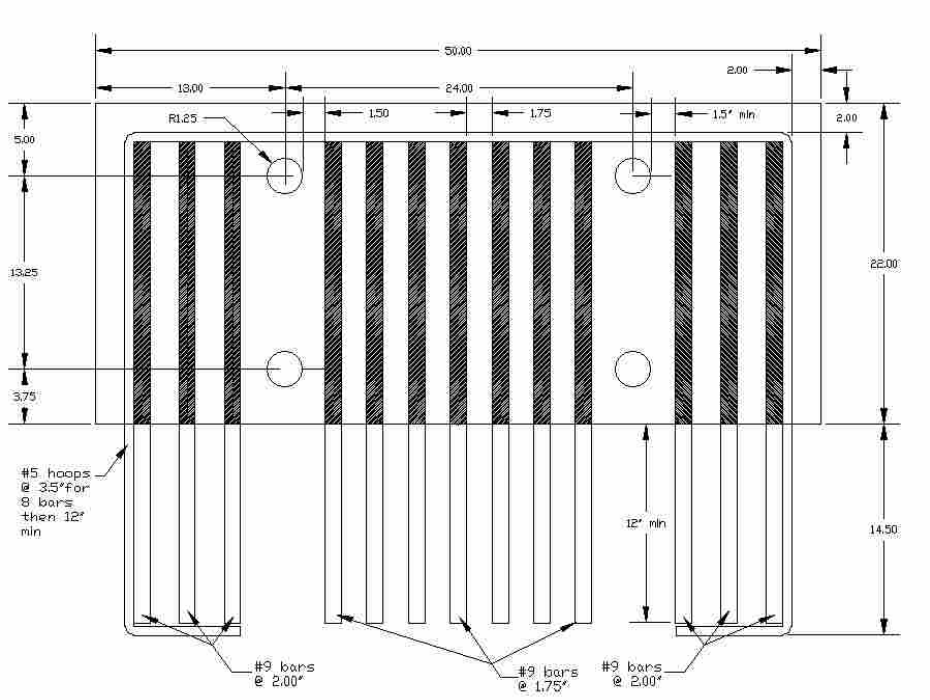

Figure 4-9 View of corbel steel looking at the actuator connection interface.

4.2 Actuator Layout

The lateral pile group load tests were performed by reacting one pile group against another. The lateral load was applied with an MTS actuator with the load centered at a height of 0.92 (11 inches) above the top of the pile cap. Each of the actuators had a capacity of about 600 kips in compression and 450 kips in tension. The pile groups were spaced approximately 32 feet apart edge to edge. This spacing was considered to be large enough to ensure that the volumes soil affected by the displacement of each foundation would not significantly interfere with each other. The actuators were fitted with two 8.67-ft extension pieces each made of 8.5 inch outside diameter steel pipe (f_y= 69 ksi) with a wall thickness of 0.75 inches in order to span the distance between the two foundations. Steel plates (f_y= 36 ksi), 18 in x18 in square and 5 in thick of were welded to the ends of the extensions to connect the extensions to the actuators and the pilecaps. The extension pieces were then bolted to the actuator and swivel heads.

The actuators were attached to each corbel using steel tie-rods which extended through PVC sleeves in the corbel and were bolted to the back face of the corbel. The tie-rods were post-tensioned to minimize displacement of the steel during the load tests. A three-dimensional swivel head was located at each end of the actuator/extension assembly to provide a zero moment or "pinned" connection. Each swivel could accommodate ± 5º of pile head rotation about a horizontal line (pitch) and ± 15º of pile head rotation about a vertical line (yaw). A photo of the actuators and extensions positioned between the two pile caps in the field is provided in Figure 4-9.

Figure 4-10 Photo of actuator setup between caps 1 & 2.

4.3 Instrumentation

Six types of instrumentation were used during the tests, namely: strain gages, inclinometers, shape accelerometer arrays, string potentiometers, actuator pressure transducer for load measurements, and surface grids to evaluate heave/settlement or crack patterns. As noted previously, the middle piles were instrumented with waterproof electrical resistance type strain gages (Texas Measurements Group model WFLA-6-120-*LT) at depths of 2, 6, 11, and 13.5 feet below the top of the pile. Angle irons (as shown in Figure 4-4) were welded on opposite sides of the instrumented piles to a depth of 20 ft to protect the strain gauges during pile driving. Figure 4-11 provides a detailed drawing

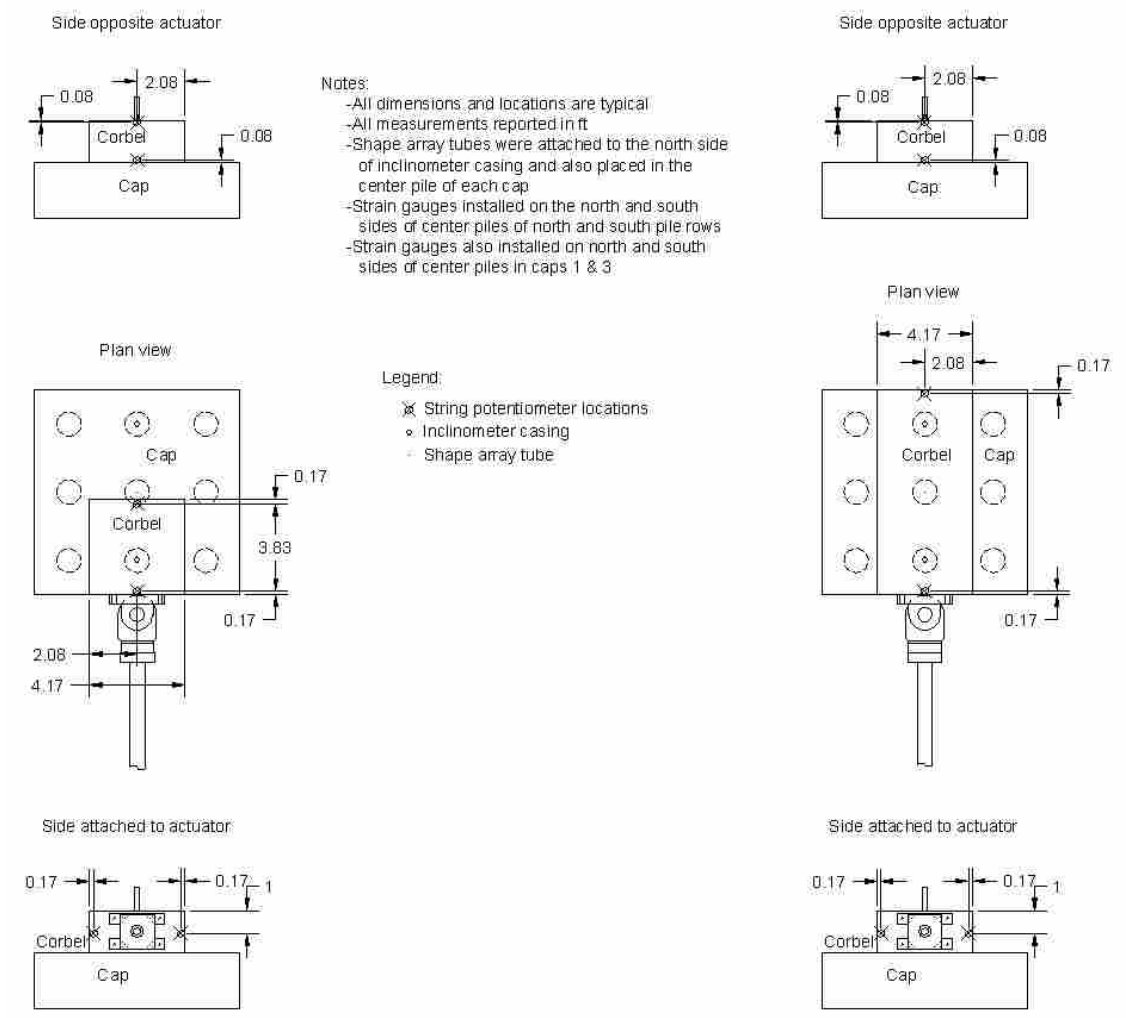

Figure 4-11 Typical instrumentation layout.

of the instrumentation on a typical pile cap. The figure displays the instrumentation for each of the 2 pile cap designs. The left-side of the figure provides the location of the instrumentation for the one-side corbel design, and the left-side of the figure displays the instrumentation for the two-sided corbel design. The strain gauge depths were selected to provide the maximum negative and positive moments along the pile. For a "fixed-head" or "restrained-head" pile the maximum negative moment is expected to occur at the pile-pile cap interface. Preliminary LPILE analyses suggested that the maximum positive moment would likely occur between 11 and 13 feet below the top of

the piles. The depths of the strain gages varied due to the different driving depths of each pile. However, the individual driving depth of each pile was carefully recorded so the actual depths of the strain gages could be obtained. Also, some of the strain gages were damaged in the installation process and, therefore, some instrumented piles do not have data for all strain gage depths.

In addition to the strain gages, the middle pile in the north and south rows of piles in each pile group were instrumented with inclinometer tubes. These tubes were placed in the center of the piles before they were filled with concrete and ran the entire depth of the pile. After the concrete was poured and cured, the inclinometer tubes served as a means of obtaining the pile and pile cap deflections during testing. Inclinometer measurements were typically performed before testing and then again once the final displacement increment had been reached. Using a standard inclinometer and corresponding acquisition box ("data mate"), the slope in the pile was recorded at 2 ft depth intervals. This procedure made it possible to develop displacement vs. depth curves at the maximum deflection level and to determine the deflected shape of the pile at the start of each test. Inclinometer readings typically provide displacement measurements with an accuracy of 0.05 inches in 100 ft.

Next to the inclinometer tubes, a 1-inch outside diameter PVC pipe was also placed before the concrete pour. These tubes were fitted with a new measuring technology called a shape accelerometer array manufactured by Measurand, Inc. The center piles were additioanlly equipped with the shape arrays. Each shape array consists of a 25-ft long flexible waterproof cable with triaxial micro-electrical-mechanical (mems) type accelerometers embedded at 1 ft intervals. By double

integrating the accelerations at each level throughout time, the shape arrays provided real-time displacement vs. depth profiles relative to the initial deflected shape at 1-ft intervals throughout the entire testing period. The shape arrays were designed to provide displacements with accuracy similar to that from an inclinometer. To provide accurate measurements from the shape arrays, a tight fit between the 1-inch PVC pipe and the shape array must be maintained. To accomplish this, nylon straps of various thicknesses was inserted along with the shape array minimizing any gaps between the shape array and the PVC pipe.

Lateral pile cap displacement was measured using two string potentiometers (string pots) attached to the pile cap at the elevation of the loading point (0.92 ft above the top of the cap) on the east and west sides of the actuator attachment point. Lateral pile cap displacement was also measured on the back side of each corbel with two string potentiometers attached 0.167 ft (2 inches) and 1.75 ft (21 inches) above the top of the pile cap directly in line with the load direction. Finally, vertical pile cap displacement was measured at two points along the length of each pile cap to evaluate pile head rotation. Each potentiometer was attached to an independent reference beam supported at a distance of about 6 ft from the side of the pile cap.

Applied load was measured by pressure transducers on the actuator which were calibrated in the laboratory prior to testing in the field. Load data were recorded using the actuator control computer and software, with a data sampling rate of 20 scans per second. Surface grids were painted on the surface area behind the cap being tested. Grid generally 12 feet wide by 10 feet long and segmented at 2-ft intervals. The grids were

typically surveyed before the test and at the maximum deflection during the test. Thegrid was also used to map the shear planes that developed during lateral loading.

4.4 Test Procedure

This section describes the general lateral load test procedure used for this series of tests. If there are variations to an individual test, they will be noted in their individual section. Lateral pile group load testing was conducted from July 16 to August 29, 2007. The piles had been in the ground for about one month prior to the first test. Load was applied to the pile caps using the actuator which was powered by a portable pump with a 60 gallon/minute capacity. The pump unit was powered by a portable diesel generator. At times, the actuators loaded the pile caps for an extended period of time; which caused the circulating hydraulic fluid in the pumps to rapidly rise in temperature. The hydraulic pumps were programmed to disengage when the temperature of the fluid reached about 132° F. In order to keep the temperature of the hydraulic fluid from reaching this critical temperature, water was circulated through the hydraulic pumps to cool the hydraulic fluid. The lateral load tests were carried out with a displacement control approach with actuator displacement increments of approximately 0.125, 0.25, 0.50, 0.75, 1.0, and 1.5 inches. Due to small seating movements and distortion in the actuator displacement, the displacement increments of the actuators did not exactly match the displacements of the pile caps. However, these increments were used as approximate indicators of the displacement of the pile caps. During this process the actuator extended or contracted at a rate of about 1.5 inches/minute. In addition, at each increment 10 cycles with a peak displacement amplitude of about ±0.05 inches were

applied with a frequency of approximately 1 Hz to evaluate dynamic cyclic response of the pile cap. After this small displacement cycling at each increment, the actuator was pulled back to the initial starting point prior to loading to the next higher displacement increment. Due to differences in resistance between the adjacent pile groups, the pile caps were not pulled back to their exact starting positions along with the actuators. Typically, the testing procedure was paused at the end of the 1.5 inch (final) test increment cyclic portion and held for 20 to 30 minutes while inclinometer measurements were made before ramping the actuator load back down to zero displacement. Schematic layouts of each of tests performed will be shown with the test results in the following chapters.

5 Jet Grouting Procedure

Jet grouting was used to strengthen the soft clay surrounding two of the full-scale pile caps. All of the jet grouting took place following construction of the pile caps to evaluate the potential improvement in lateral resistance that could be produced by retrofitting an existing pile supported cap foundation. Jet grouted soilcrete columns were created under the pile cap and between the piles of the first foundation (pile cap 2). On the second foundation (pile cap 1), soilcrete columns were used to create a soilcrete wall along the perimeter of one side of the pile cap. All of the jet grouting design and installation work was performed by engineers and a construction crew from Hayward-Baker Inc. The following sections will detail the jet grouting installation process, the jet grouting layout at each foundation, and the quality assurance procedures used to evaluate the strength of the resulting soilcrete columns.

5.1 Basic Setup and Testing

Jet grouting requires that a drill rig be allowed to set up directly above the installation area. To accommodate this need, the previously constructed foundations were buried with soil back to the original ground level to allow the drill rig to set up directly over the foundation. Figure 5-1 below shows the drill rig in position over a buried foundation. The buried foundations were adjacent to one another, and the

excavated area between the buried foundations was used as a spoil collection area during jet grouting. The spoil collection area was filled and re-excavated a number of times during jet grouting.

A double fluid jet grout approach was employed to improve the soil around both foundations. The jet grout drill head was initially advanced to the base of the treatment zone, 10-ft below the pile cap, using water jets and a drilling bit located at the bottom of the drill rod (see photo in). Afterwards the drill head was rotated at a constant rate, while being pulled upward at a specified rate and cement slurry was injected at a specified pressure and flow rate from the inner orifice as shown in. At the same time, compressed air was also injected from the outer orifice (Figure 5-3) to form a protective shroud around the slurry jet. Throughout the jet grouting process, the flow rates, pressures, pull rate and drill rod rotation rate were controlled by a computerized system which also monitored and recorded these parameters. As the slurry was injected and mixed with the surrounding soil, the air pressure would aid in moving the excess soilcrete spoil upward to the ground surface where it would typically erupt from the ground. The spoils were then washed into the storage area between the two pile caps using high pressure water hoses as shown in Figure 5-4. Several times during the jet grouting process, a clog developed and the return flow of spoils was interrupted. In these cases, the drill operator simply interrupted the grouting, reamed out the hole, and resumed the grouting process at a slightly lower elevation than the clog in an effort to maintain a continuous jet grout column. This process somewhat slowed the installation of the soilcrete columns, but did not pose any significant problem.

Figure 5-1 Photo of drill rig in position above buried foundation.

The grout slurry mix had a specific gravity of 1.52, which is equivalent to a 1:1 water to cement ratio by weight. The specific gravity was continually monitored using an optical sensor at the mixing tank. Extra water was added if the specific gravity was too high and extra cement was supplied if the specific gravity was too low. The cement was initially mixed with water in a venture-type mixer and then kept in suspension with the paddles in the mixing tank. The mixing tank was supplied with bulk cement through a pipe attached to a large hopper and with water through a portable water tank (Figure 5-5). The cement slurry was then pumped to the jet grout drilling rig using a large pump unit which could produce a maximum pressure of 9000 psi. The pump and mixer were powered by a portable generator

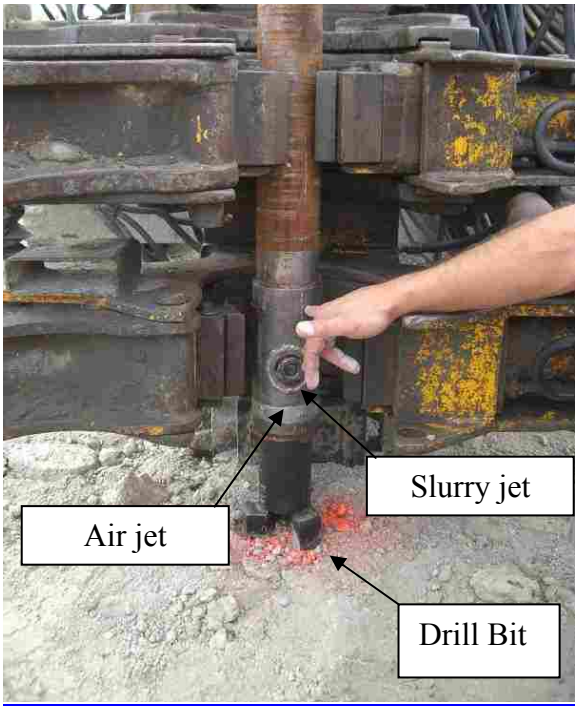

Figure 5-2 Jet grout drill head showing drill bit along with the inner jet orifice for the cement slurry and the outer jet orifice for compressed air shroud.

Figure 5-3 Jet grout drill rods with central pipe for cement slurry and annular space for compressed air.

Figure 5-4 Photo of jet grout drill rig in position above buried foundation with spoil being ejected and washing down into the storage area.

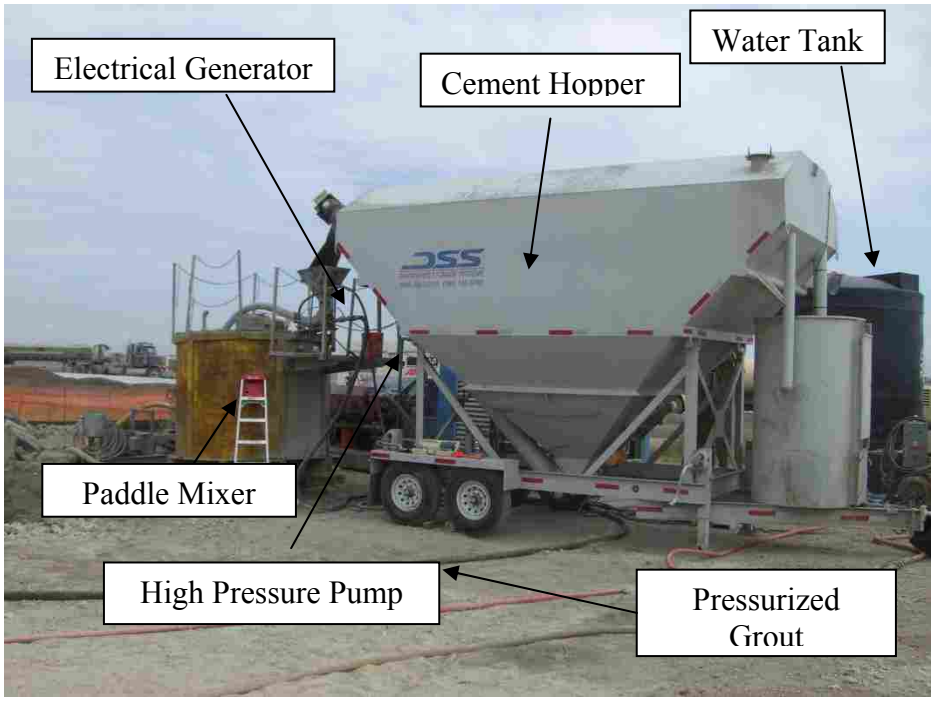

Figure 5-5 Layout of pressurized grout production system, consisting of a portable water tank, cement hopper, paddle mixer, electrical generator, high pressure pump, and pressurized grout line.

5.2 Jet Grouting Beneath Pile Cap

Plan and profile views of the jet grout columns around pile cap 2 are shown in Figure 5-6 and Figure 5-7. A total of eight 5-ft diameter soilcrete columns were installed beneath and around the pile cap. Four of the columns were installed at the periphery of the pile cap while an additional four were installed through the cap itself as shown in Figure 5-6. During construction of the pile cap and corbel, four 6-inch diameter PVC pipes were placed in the pile cap between the rebar. The pipes were sealed before the pile cap concrete was poured, which left four 6-inch diameter holes through the pile cap. The four PVC pipes were extended to the ground surface to provide the jet grout drill rod with an unobstructed path through the fill material and the pile cap. Four of the eight soilcrete columns (2,3,6, and 7) were installed through these pipes. The target diameter of the jet grout columns was 5 feet. The jet grout columns were spaced at approximately 3 ft center-to-center in the north-south direction and 5 ft center-to-center in the east-west direction. This likely produced a 2 ft overlap between columns in the north-south direction and a no overlap between columns in the east-west direction. As can be seen in Figure 5-6 nearly the entire volume of soil beneath the pile cap, including an approximate 3.0 ft extension from both the north and south ends of the pile cap, was treated to a depth of 10 feet below the bottom of the pile cap. Each of the columns was constructed with identical installation parameters. These parameters are summarized in Table 5-1. Based on the column diameter, flow rates, pull rates and rotation rates, the cement content for the jet grout columns would be expected to be about 26 lbs/ft^3. It can be seen that the pull rate (20 cm/min) is greater than the rotation speed (7 rpm).

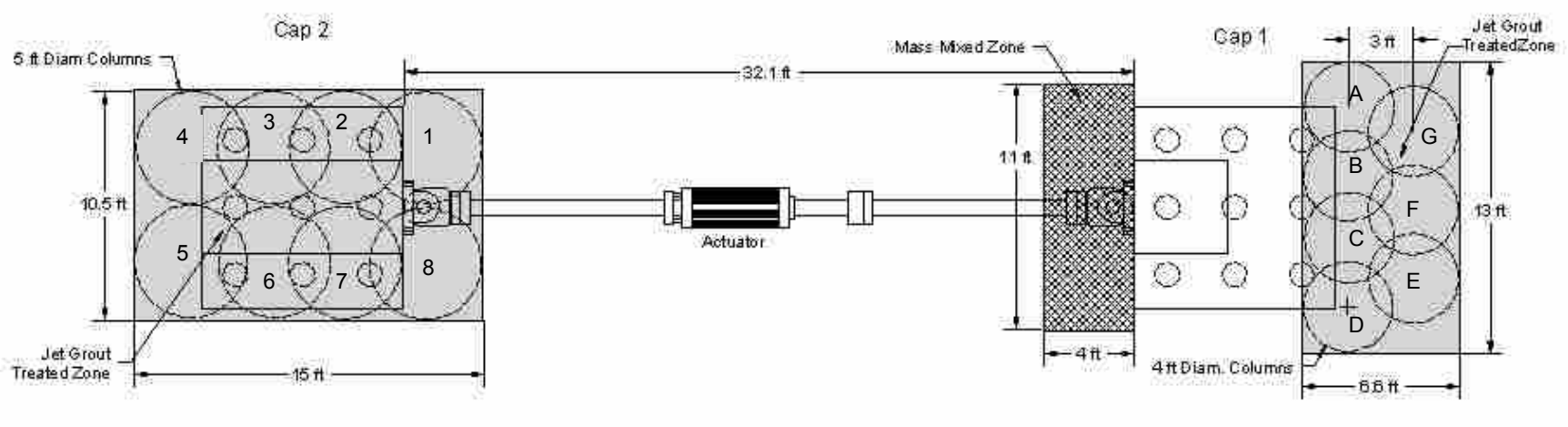

Figure 5-6 Detailed plan view of pile cap 1 (right) and pile cap 2 (left) after mass mixing and jet grouting soil improvement.

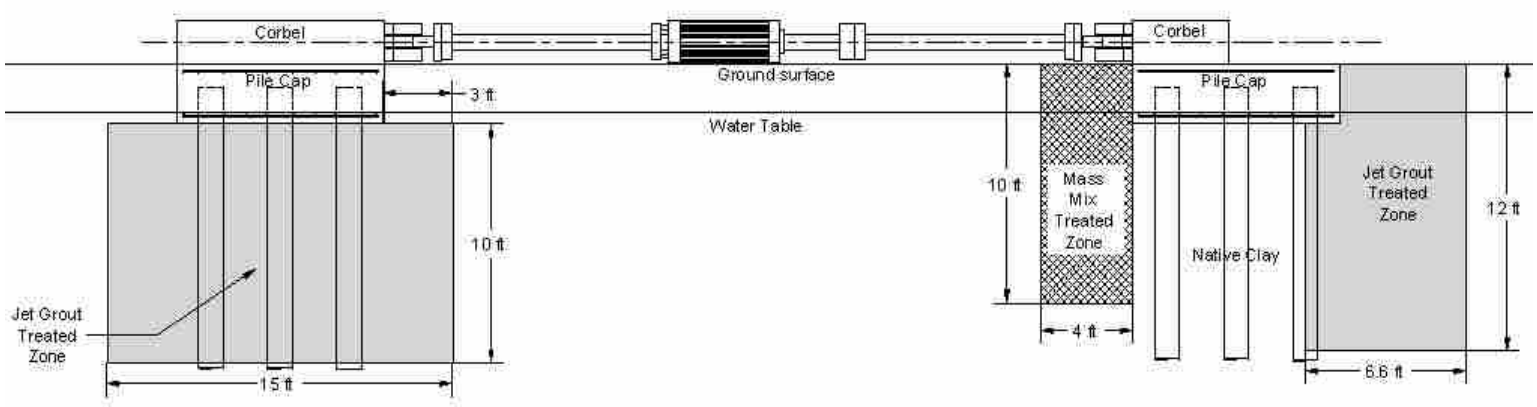

Figure 5-7 Detailed profile view of pile cap 1 (right) and pile cap 2 (left) after mass mixing and jet grouting soil improvement.

Table 5-1 Jet Grouting installation parameters for columns created beneath pile cap 2.

Column Length	10 ft
Estimated Column Diameter	5 ft
Grout pressure	6000 psi
Grout flow rate	90 gpm
Rotation speed	7 rpm
Pull rate	20 cm/min

Thus, one rotation of the high pressure nozzles occurred in an approximate 1.2 in (3cm) lift. Detailed daily construction records providing the construction times, gallons of grout pumped, grout pressure, grout flow-rate, column geometry, rotation speed, and pull rate for each of the columns are provided in Appendix B. Wet grab samples were taken from completed columns 1, 2, 3, 6, and 7. The samples were taken from locations near the top, middle, and bottom of the columns. These samples were tested at various curing times will be described subsequently.

5.3 Jet Grouting Adjacent to Pile Cap

The jet grouting procedure for the second foundation was much less complicated than the first. A total of seven soilcrete columns were installed in two rows to create a wall along one edge of the foundation. Plan and profile views of the jet grout columns adjacent to pile cap 1 are shown in Figure 5-6 and Figure 5-7. These figures also display that the soil adjacent to the other side of pile cap 1 was treated with mass mixing. The target diameter of each of the columns was 4 feet and they were spaced 3 feet on center in a triangular pattern. This created an overlap between columns of approximately 1 ft. Each jet grout column extended from the top of the pile cap to a depth of 12 feet below the top of the pile cap. The centers of the first row of jet grout columns were positioned

so that the jet could cut underneath the pile cap and produce a soilcrete wall which would intersect the front row of piles. The length of soilcrete columns created extending laterally underneath the pile cap would have been about 1.5 feet for 4 ft diameter columns.

Each of the columns was constructed using identical construction parameters, which are summarized in Table 5-2. Based on the column diameter, flow rates, pull rates and rotation rates, the cement content for each jet grout column would be expected to be about 24 lbs/ft^3. One rotation of the high pressure nozzles occurred in an approximate 1.6 in (4cm) lift. Detailed daily construction records for each of the installed columns can be found in Appendix B.

Wet grab samples were taken at various depths of columns 10 and 14. Also, one cored sample each was taken from the top of the columns E and F and tested 38 days following installation. The cored samples measured 4 inches in diameter with an approximate length to diameter ratio of 2.0. Just as with the previous samples, each of the samples taken from the columns was tested in compression at various curing times.

Table 5-2 Jet grouting installation parameters for columns installed adjacent to pile cap 1.

Column Length	12 ft
Estimated Column Diameter	4 ft
Grout pressure	6000 psi
Grout flow rate	90 gpm
Rotation speed	8 rpm
Pull rate	25 cm/min

5.4 Soilcrete Strength

The unconfined compressive strength of the soilcrete produced by the jet grouting process was evaluated using web grab samples as well as cored sample. Wet grab

samples were taken from random soilcrete columns during each of the three days of installation. To obtain samples, a plugged 3-4 inch diameter PVC pipe was inserted into the wet soilcrete column. The plug was attached to a smaller diameter pipe which was inserted through the sampling pipe and extruded about 2 feet out of the top of the sampling pipe. Once the pipe was inserted to the desired depth, the plug was pulled up 2 to 3 feet from the end of the sampling pipe and secured. The sampling pipe was then pumped up and down to fill the un-plugged end of the pipe with soilcrete. The sampling pipe was then pulled from the hole and the soilcrete sample was extracted. The sample was then placed in a bucket and stirred until it reached an even consistency. The sample was then placed in a capped, 3-inch diameter plastic mold with a height to diameter ratio of about 2.0. The samples were placed in the molds in three lifts, with 25 rods per lift with a 0.25 inch diameter rod to consolidate the samples. Photos taken during the various phases of wet-grab sampling are found in Figure 5-8. In addition, two 4-inch diameter core samples were obtained from the upper 2 ft of the jet grouted columns 13 and 14 near pile cap 1 about one month after jet grouting. The samples were capped with either sulfur capping mortar or plaster, and were compression tested at various curing times to evaluate the strength gain with time. The vertical strain rate during compression testing was 0.05 in/min.

A plot showing the laboratory soilcrete strengths from each of the respective columns as a function of curing time is provided in Figure 5-9. From the plot it can be seen that there is a "shotgun" scatter to the data, which is typical for soilcrete columns installed using jet grouting. To improve our understanding of the average unconfined

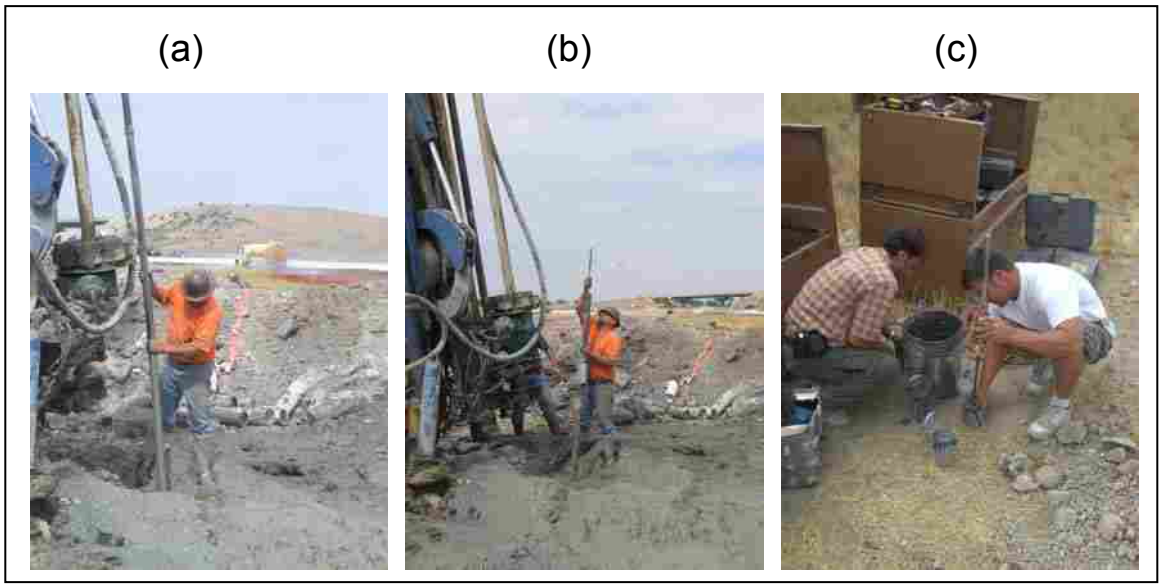

Figure 5-8 Photos taken during (a) insertion of sampling pipe to desired depth, (b) extrusion of small pipe connected to the sampling pipe plug , and (c) rodding of wet grab samples in plastic molds.

compressive strength, a standard statistical analysis was performed on the samples. Each of the samples tested within three days of each other were grouped into four separate categories. A mean strength and standard deviation were calculated for each of these sample groups. Curves representing the mean ± one standard deviation are also plotted in the figure. Prior to treatment, the mean compressive strength of the untreated clay was only 6 to 8 psi. Two weeks after jet grouting, the mean compressive strength had increased to about 440 psi and after four weeks the strength had increased to about 650 psi. From the mean plot it can be seen that the strength curves begins to flatten out after about 25 days of curing.

The strengths of the two cored samples taken from columns 13 and 14 installed adjacent to the pile cap are also shown in the graph; however, these values were not used in the statistical analysis because they represent tests on soil mixed in the field.

The average strength from the two cored samples was about 460 psi, which is about 30% lower than the strength obtained from the wet grab samples. The lower strength is likely attributable to the poorer mixing produced by the jet grouting process relative to the hand mixing employed with the wet grab samples. However, these strengths are assumed to be the most accurate measurement of in-situ strength, due to the fact that they represent soilcrete cured and mixed under actual field conditions. Additionally, the cored samples were taken from the top of the soilcrete columns. Generally it is assumed that the strength of soilcrete will increase with depth, due to the higher specific gravity of cement which causes greater cement contents and water-cement ratios at depth. The greater water-cement ratios would higher soilcrete strength. Therefore, the cored sample strengths taken from the top of the columns represent the low-end of the in-situ compressive soilcrete strengths.

It is common practice among the engineers at Hayward Baker to divide the sample strengths found in the laboratory by a factor of 2 to 2.5 to estimate the design strength of the soilcrete columns in the field. This is done, because it is assumed that the in situ soilcrete is not as uniformly mixed as the laboratory samples. Also, planes of weakness, caused by inconsistencies of soilcrete geometry due to clogging of the borehole annulus in highly plastic soils, could also contribute to a lower in-situ soilcrete strength. Figure 5-9 also provides the range of mean design strength curves for the soilcrete columns installed beneath the pile cap. The range of design strengths was calculated according to the Hayward Baker standard of practice. The values for the design strength of the soilcrete are quite conservative, and the actual field strengths may be higher than the design curves suggest as indicated by the core samples. The lateral

load tests on the foundations with jet grouted soil around the pile cap were performed 17-34 days after installation of the soilcrete columns. This correlates to a compressive strength range from 550-675 psi based on the wet grab samples and design compressive strength range of about 200 to 275 psi.

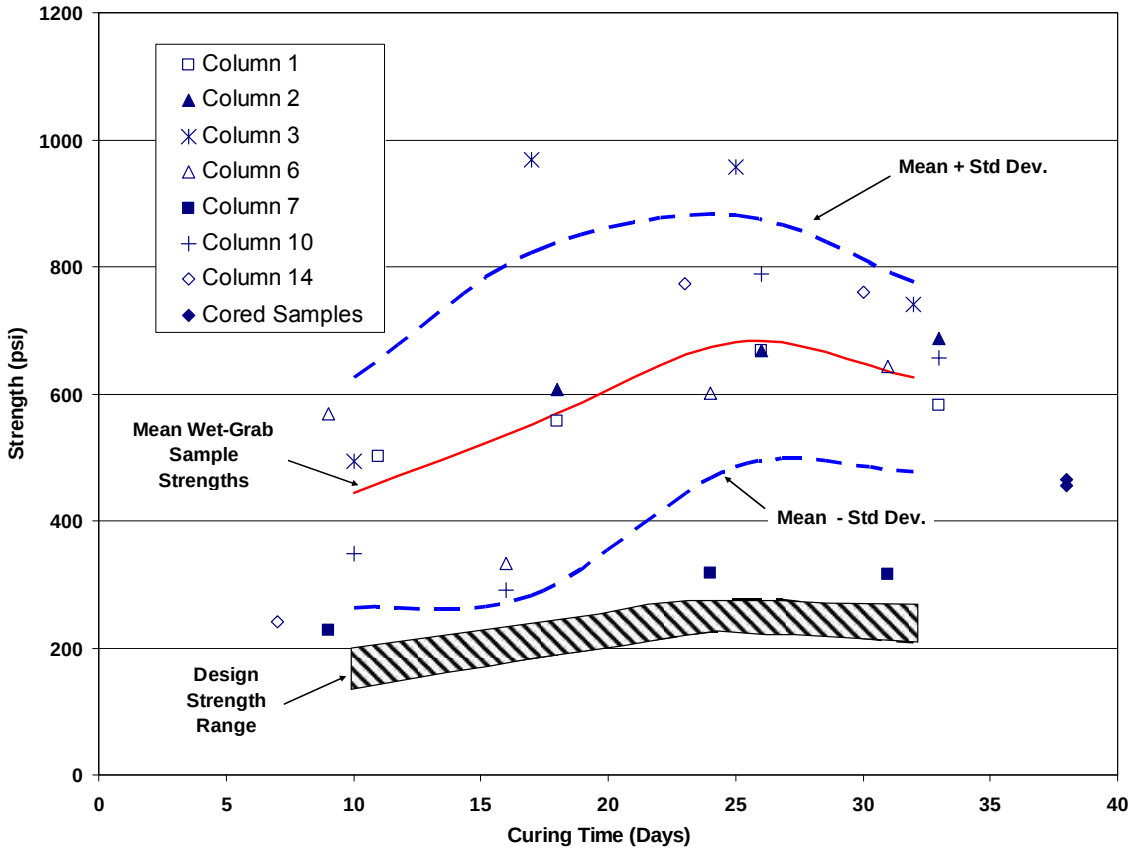

Figure 5-9 Compressive strengths of installed soilcrete columns.

6 Test Results Introduction

The first two sections of this chapter will present the results of the two tests performed in untreated native clay. The following sections will present the results from the subsequent tests performed in soil treated with jet-grouted soilcrete columns. The basic approach to each of the tests was to first laterally load the pile groups in either the virgin native clay or "virgin" treated clay. Next, the soil adjacent to the pile cap was excavated away from the cap and the pile cap was once again laterally loaded. This was done to determine the approximate passive soil resistance which acted on the face of the pile cap during virgin loading. Test 1 was the test performed on the virgin clay, and tests 3 and 4 were the "virgin" tests performed following jet grouting treatment. Test 2 was the test performed in the native clay following excavation, while tests 5 and 6 were the tests performed following excavation of the treated soil.

Table 6-1 displays the excavation and loading details of each of the tests presented in the following chapters. Also, schematic plan views of the tests are included in each chapter. Refer to Figure 3-2 for the layout of the pile caps relative to one another. Also, detailed plan and profile views of pile caps 1 and 2 following jet grouting soil treatments can be found in Figure 5-6 and Figure 5-7, respectively.

Table 6-1 Testing details for each lateral load test.

Test No.	Pile Caps	Loading Conditions	Excavations
1	1 and 2	Virgin loading of native soil	None
2	1 and 2	Virgin loading of native soil	North face of pile cap 1
3	1 and 2	First loading of treated soil	None
4	1, 2, and 3	Second loading of treated soil	None
5	2 and 3	Third loading of treated soil	South face of pile cap 2
6	1 and 2	Fourth loading of treated soil	South face of pile cap 2 & North face of pile cap 1

A number of other data were also collected during the tests. The following list introduces the results which will be displayed for each of the tests, as well as the instruments which were used to obtain the data from which the results were based.

1. Continuous plot of actuator load vs. pile cap displacement
    - Instruments: pressure transducers and string potentiometers
2. Plot of peak actuator load vs. pile cap displacement per test increment
    - Instruments: pressure transducers and string potentiometers
3. Plot of pile head rotation vs. actuator load
    - Instruments: pressure transducers and string potentiometers
4. Plot of displacement vs. depth below bottom of pile cap for instrumented piles
    - Instruments: shape arrays and inclinometers
5. Plot of moment vs. depth below bottom of pile cap for instrumented piles
    - Instruments: shape arrays and inclinometers
6. Plot of maximum bending moment vs. applied load for instrumented piles
    - Instruments: shape arrays, strain gages, and pressure transducers

6.1 Baseline Selection and Test Numbering

Each of the pile caps were displaced multiple times and in opposite directions. Thus, each of the displacements and strains measured with the above instrumentation are all measured relative to the original position of the piles and pile caps prior to testing. Therefore, any residual displacement created from previous tests will result in a non-zero value for the initial displacement of the foundation. Also, deflections were all measured as positive in the direction of loading during a particular test. A good example of this can be seen in the plots of actuator load vs. pile cap displacement for the two native clay tests in chapter 7 and chapter 8. For the first test, pile caps 1 and 2 were pulled together during testing. Following the test and disengagement of the actuators, pile caps 1 and 2 were displaced towards each other approximately 0.3 inches from their original positions. This value is the starting displacement of each of the pile caps in test 2, and can be seen in Figure 8-4. The starting displacement is plotted as a negative value because the residual displacements left over from test 1 were a result of pulling the pile caps together; and were in the opposite direction of loading during test 2. Two different foundation positions were chosen as the baseline for foundation displacement during testing.

The first baseline was chosen as the position of the pile cap prior to the beginning of any testing (i.e. before test 1). This baseline was used to measure displacements for test 1 and test 2. The second baseline was chosen as the position of the foundation prior to test 3. This was the position of the foundation directly following jet grouting, before any testing of the improved soil had begun. The reference frames and instrumentation were necessarily removed from the foundations prior to jet

grouting, making it nearly impossible to continue using the original baseline. Therefore, this new baseline was selected. The new baseline was used for test 3 through test 6.

Additionally, the numbered tests in the following sections only relate to those tests which were performed to evaluate the strength improvement of the soil from installation of soilcrete columns; the tests numbers do not represent the actual number of tests performed. For example, pile cap 2 was used as a reaction foundation for two separate tests between test 3 and test 4. The two tests between test 3 and test 4 were performed to evaluate the improvement of the soil through excavation and replacement of the native soil with flowable fill and the spoils from jet grouting, respectively. As mentioned previously, the results of these intermediate tests will not be explained in this thesis. However, the foundations reported on in this work did undergo appreciable displacements during these intermediate tests, even though the foundations were merely used as reactions blocks. Knowledge of these intermediate loadings and displacements is necessary when analyzing the results obtained from the tests outlined in the sections below.

6.2 Bending Moment Curve Construction

When evaluating the lateral resistance of deep foundations, it is important to know the maximum bending moment and the depth in the pile where it occurs. The bending moment, M, was calculated from the shape array and inclinometer deflection data using the equation

$$M = EI\frac{\partial^2 y}{\partial x^2} \quad \textbf{(6-1)}$$

where E is the modulus of elasticity, I is the moment of inertia, and $\partial^2 y / \partial x^2$ is the curvature along the length of the pile. This equation is approximated using the equation

$$M = \frac{EI(f_{-1} - 2f_0 + f_1)}{h^2} \quad \textbf{(6-2)}$$

where f_{-1} is the horizontal displacement one level above the point of consideration , f_0 is the displacement at the point of interest, f_1 is the displacement one level below the point of interest, and h is the distance between displacement equally spaced measurement depths. The moment computed using Equation 6-2 is very sensitive to minor variations or errors in the measured displacement vs. depth curves. To reduce the influence of minor variances in the measured displacement data on the computed moment, a multi-order polynomial equation was developed based on the measured data to smooth the displacement vs. depth curves. Fourth through sixth order polynomial curves were used to develop the smoothed curves depending on the curvature of the measured curve. The polynomial curve which gave the most realistic results was chosen to define the smoothed curve. The displacements used in Equation 6-2 were then based on smoothed values computed with the polynomial equation. While the difference in the displacement values at any depth were generally very small, this procedure produced moment vs. depth curves with more realistic shapes.

As indicated previously, the vertical spacing between the shape array nodes was 12 inches, which corresponds to the interval h. A composite EI of 14.15 x 10^9 lbs-in^2 for the concrete filled pile was used based on the EI of the steel pile and the uncracked EI of the concrete used to fill the pile. To calculate the EI of the steel pile, a modulus of elasticity of 29 x 10^6 psi and a moment of inertia of 344 in^4 was used. Similarly for the EI of the concrete, a modulus of elasticity of 4.1 x 10^6 psi based on the 5100 psi unconfined compressive strength and a moment of inertia of 1018 in^4 was used. Potentially, the concrete in the piles could crack, which would make it more appropriate to use the cracked EI for the concrete section. However, due to the amount of reinforcement in the piles, the uncracked EI was assumed to sufficiently represent the actual behavior of the concrete during deflection. Additionally, using equation (5-2) a positive displacement will produce a maximum bending moment directly under the cap which will be negative.

To compliment the bending moments obtained from the shape arrays, strain gages were also used to derive bending moments. As mentioned before, strain gages were placed at depths of 2, 6, 11, and 13.5 feet below the top of the pile and the top of the piles were driven with approximately 2 feet of stickup. Since piles cannot be driven precisely to a given elevation, these depths vary by no more 8-12 inches. The bending moments from the stain gages where obtained from the equation.

$$M = \frac{EI\varepsilon_{Combined}}{y} \qquad \textbf{(6-3)}$$

where EI is the composite modulus of elasticity and moment of inertia for the pile which are the same values used in the shape array bending moments equation, $\varepsilon_{Combined}$ is the difference in strain obtained from the strain gages located opposite each other at the depth of interest, and y is the diameter of the pile or 12.75 inches.

The notation chosen to describe the sign convention of the moments was that a positive displacement of the cap would result in a negative moment at the pile-pile cap interface, and a positive moment at depth. The datum of these plots was changed to be measured as the depth below the bottom of the pile cap. This was done because once the piles enter the pile cap the EI changes and becomes difficult to estimate without a large degree of uncertainty. The negative bending moments measured at the interface of the piles and pile cap will have some degree of error due to the changing EI. This error is minimized to some degree by the fact that the displacements used to derive the bending moments included those that were obtained from within the pile cap. These bending moments were then truncated to the bottom of the pile cap where the EI could be estimated.

Using equations (6-2) and (6-3) with the procedures described above, bending moment vs. depth plots were obtained. The curves were obtained from the shape arrays and inclinometer readings, while point moments were computed at the locations of the strain gages. The maximum total load associated with each target displacement is also listed in the legend for each figure.

Occasionally, the polynomial-based bending moment calculations produced unrealistic curves after the point of maximum bending moment and at the pile-pile cap interface. The bending moment calculations are based on curvature, and a knowledge of

the curvature of the pile above and below the point of interest is needed to calculate a realistic value for bending moment in the pile. The shape arrays generally only extended about 18 to 20 feet below the bottom of the pile cap. The maximum positive bending moment in the piles generally occurs between 10 to 15 feet below the bottom of the pile cap for the maximum loads applied during testing. Therefore, the bending moment curves are not always well defined below the point of maximum positive bending moment. The top 4 to 5 feet of the shape array exited the pile and measured the deflections of the pile cap. Deflection inside the pile cap didn't generally follow the parabolic deflection of the pile. At times, this caused a significant change in the slope of the depth vs. deflection curve at the pile-pile cap interface, which affected the bending moment calculations for the upper few feet of the pile before it entered the pile cap. The slope of the upper few feet of the bending moment curve would increase dramatically, or at times the slope would change signs. If the bending moment curves exhibited a drastic change or even a reversal in slope near the pile-pile cap interface, those curves were truncated back to the point where curvature started changing drastically. The results for both the extrapolated and calculated maximum negative bending moment at the pile-pile cap interface should not be considered as accurate as the rest of the bending moment curve (unless validated by strain gage data). The bending moment curves in the following sections are generally truncated at two locations; the pile-pile cap interface and the point at which the bending moment curve comes back below the point of maximum bending moment.

7 Test 1 Virgin Clay Test

The first test was performed on the virgin clay between pile cap 1 and pile cap 2, the northern most pile caps. This particular test pulled pile caps 1 and 2 together, as can be seen in the schematic layout in Figure 7-1. The objective of this test was to find the lateral resistance of the virgin soil conditions for comparison to later soil improvements.

All instrumentation of string potentiometers, shape arrays, inclinometers, actuator pressure transducer, and strain gages were in place and initial measurements taken prior to the test. The location of all the instrumentation for pile caps 1 and 2 is found in Chapter 4 Test Layout and Procedure. Strain gages on pile cap 1 were located on the three middle piles, but only on the south and north piles of pile cap 2. The test followed the standard testing procedure with one exception. Once the maximum displacement was reached (1.5 inches), the actuator proceeded to perform the cyclic loadings, and then ramped back down to zero displacement and was not held at the maximum displacement increment for inclinometer readings. In order to obtain the inclinometer readings for the 1.5 inch test increment, an additional reload ramp was necessary from which the inclinometer measurements were taken. Finally, since this was the first test, the values measured were all zero set to the initial values of this test just prior to commencement.

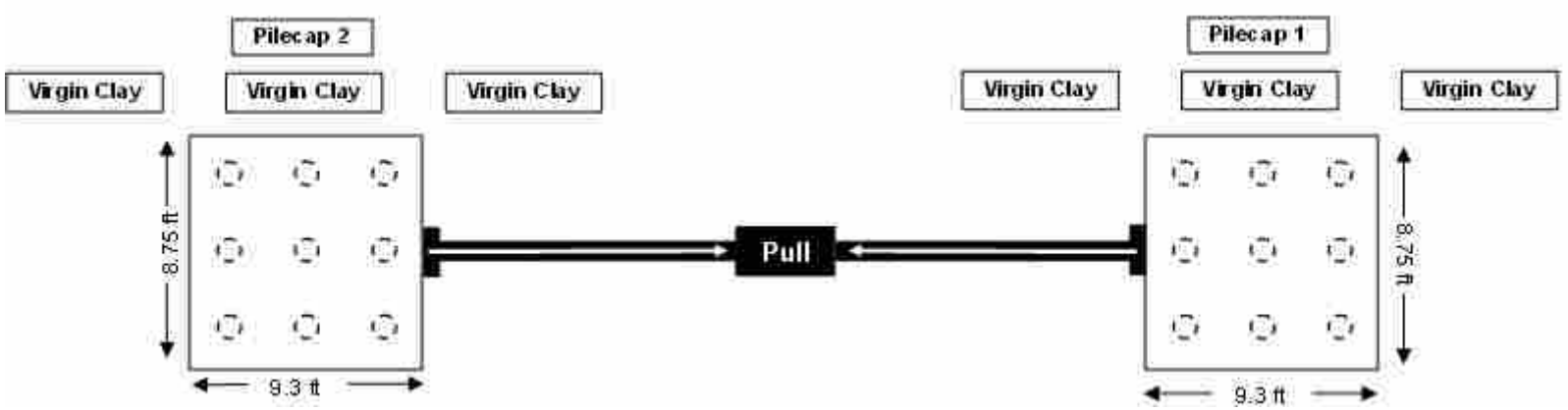

Figure 7-1 Schematic plan view of test 1.

7.1 Load vs. Pile Cap Displacement

Plots of the continuous pile cap load vs. displacement curves for pile cap 1 and pile cap 2 for test 1 are presented in Figure 7-2 and Figure 7-3. These curves were obtained from the actuator pressure transducer and the string potentiometers attached to their corresponding pile cap. These plots illustrate the load path taken during loading, unloading and reloading for each cycle. At the end of each loading cycle it was necessary to apply a tensile force to bring the actuator deflection back to zero. This does not appear to be a result of yielding in the pile based on measured bending moments. The behavior could result from a flow of weak soil into the gap behind the pile during loading or lateral resistance due to side shear on the pile as it moves in the opposite direction. During re-loading, the load is typically less than that obtained during virgin loading and considerably more linear. The peak load during reloading is typically about 90% of the peak load during the initial loading. After the deflection exceeds the maximum previous deflection for a given cycle, the load increases and the load-deflection curve transitions into what appears to be the virgin loading curve.

The virgin pile head load vs. displacement curves for each pile group have been developed in Figure 7-4 by plotting the peak values and eliminating the unload and reload segments. Although the actuator was set to push the pile caps to target displacement increments of 0.125, 0.25, 0.5, 0.75, 1.0, 1.5 inches, small seating movement and rotations in actuator connections during loading led to somewhat smaller displacements than anticipated. For example, the actual peak displacement increments for pile cap 1 were 0.08, 0.18, 0.38, 0.59, 0.85, and 1.51 inches respectively. Peak displacement increments for pile cap 2 were 0.08, 0.19, 0.39, 0.61, 0.87, and 1.48

inches respectively as measured by the corresponding string potentiometers. Because selection of increments was somewhat arbitrary, these small discrepancies are insignificant

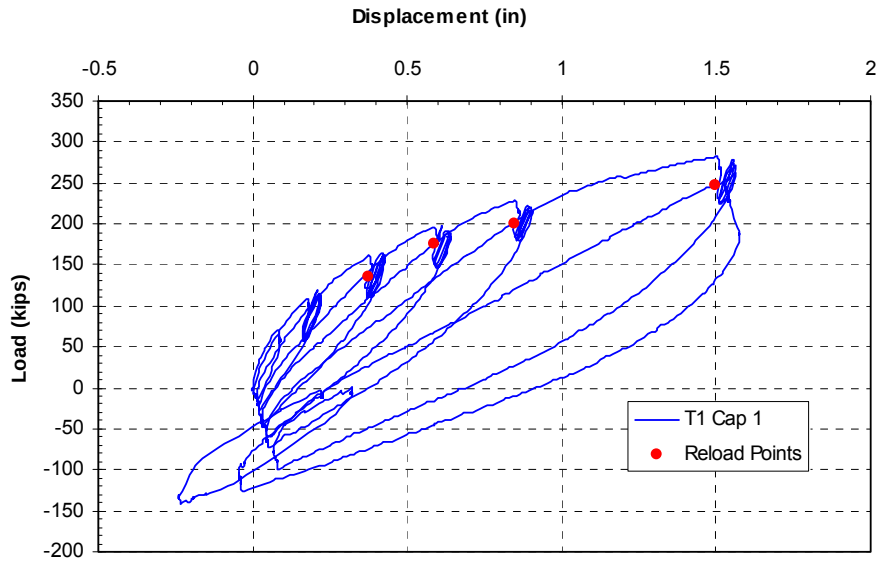

Figure 7-2 Plot of continuous pile cap displacement vs. applied load for pile cap 1 during test 1.

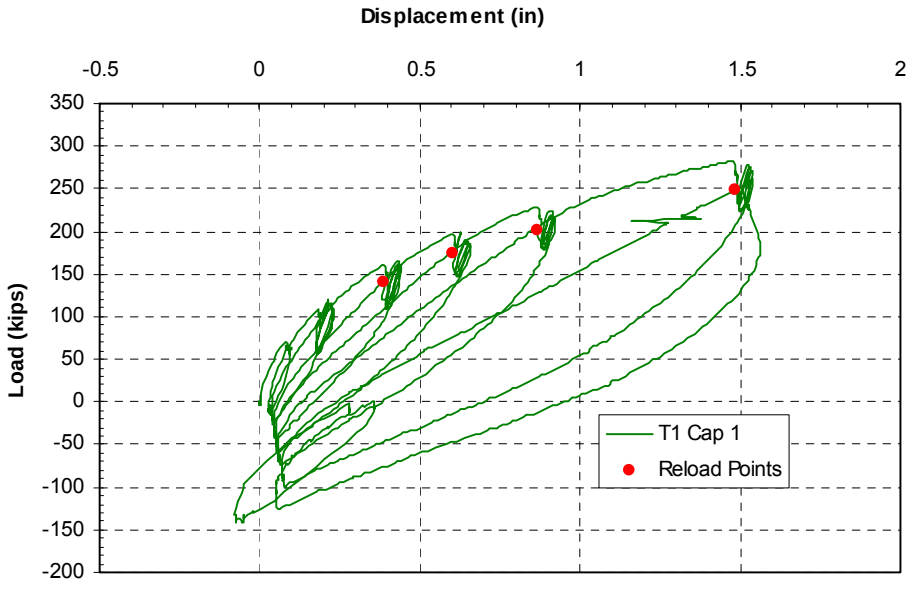

Figure 7-3 Plot of continuous pile cap displacement vs. applied load for pile cap 2 during test 1.

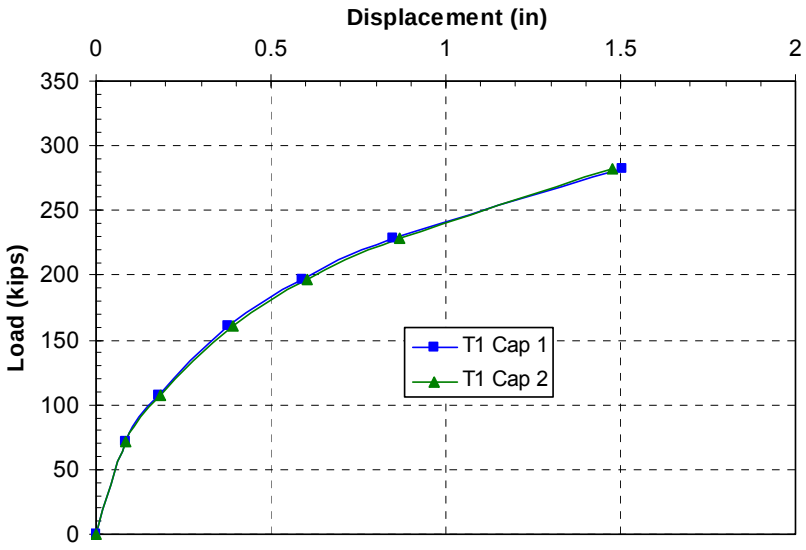

Figure 7-4 Plot of pile cap displacement vs. peak applied load for each increment of test 2.

The curves in Figure 7-4 exhibit the conventional hyperbolic shape that would be expected for a pile in soft clay. However, because the peak displacement was limited to 1.5 inches to prevent excessive moments in the pile, the slope of the load vs. displacement curve never reached a nearly horizontal asymptote. Nevertheless, the last part of the curve is relatively linear suggesting that the lateral resistance is primarily due to the flexural resistance of the piles. The maximum applied load during the last pull was 282.2 kips and resulted in a displacement of 1.50 inches for pile cap 1 and 1.48 inches for pile cap 2. For comparison purposes this load of 282 kips at 1.5 inch displacement will be used for the virgin soil. Despite the fact that the two pile groups were 32 ft apart and had minor variations in construction details, the two load-displacement curves shown in Figure 7-4 are nearly identical. These results suggest that the soil properties across the site are sufficiently uniform that valid comparisons can be made between the pile caps with various soil improvement techniques relative to the untreated conditions.

7.2 Pile Head Rotation vs. Load

Pile head rotation vs. applied load curves based on the shape array and string potentiometer measurements for pile cap 1 during test 1 are provided in Figure 7-5. Rotation was measured from the string potentiometers located directly above the corbel of pile cap 1. The distance between the string potentiometers was approximately 45.25 inches. Refer to Figure 4-11 for a review on the position of the string pots on pile cap 1. Rotation was also measured from the shape arrays. measured from the shape arrays. The difference in node deflections near the bottom of the pile cap and the top of the corbel were used to measure rotation from shape array 115 and shape array 134; the distance between these nodes was 48 inches. The rotations measured from the string potentiometers and either shape array differ by a maximum 0.03 degrees throughout the test. This level of agreement suggests that the rotations measured by each of the instruments are relatively accurate.

Pile head rotation vs. load curves based on the string potentiometer and shape array measurements for pile cap 2 during test 1 are provided in Figure 7-6. Rotation was measured from the string potentiometers located directly above the corbel of pile cap 2. The distance between the string potentiometers was approximately 108.9 inches. Refer to Figure 4-11 for a review on the position of the string pots on pile cap 2. The difference in node deflections near the bottom of the pile cap and the top of the pile cap were used to measure rotation from the shape array 134 and 115; the distance between these nodes was 24 inches. The rotations measured from the string potentiometers and shape arrays differ by a maximum 0.7 degrees until the final peak load. During the final loading the rotation measured from the string potentiometers increased more rapidly.

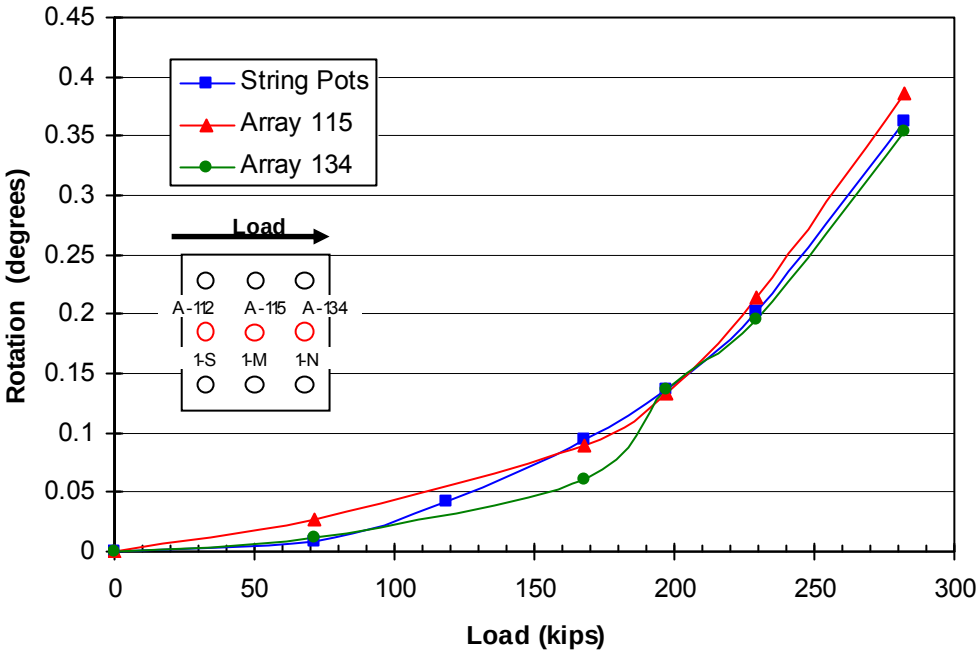

Figure 7-5 Peak pile cap load vs. pile head rotation for pile cap 1 during test 1 obtained from string potentiometer and shape array measurements.

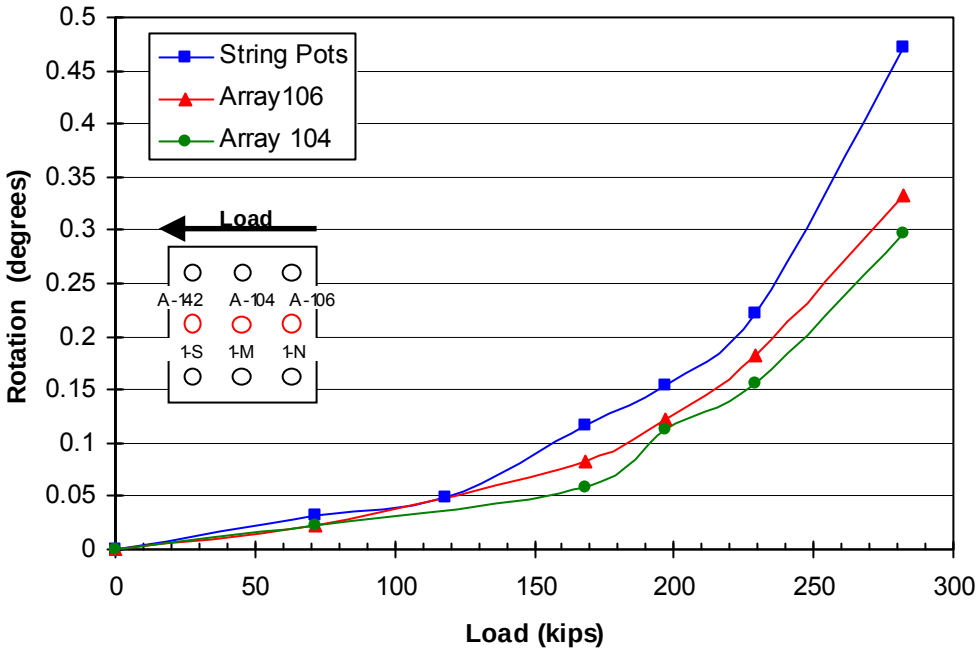

Figure 7-6 Peak pile cap load vs. pile head rotation for pile cap 2 during test 1 obtained from string potentiometer and shape array measurements.

The difference in measurement during the final loading was 0.14 degrees for shape array 104 and 0.17 degree for shape array 104. The reason for these discrepancies could have been the fact that the string potentiometers were measuring rotation over a much longer distance. It is assumed therefore, that the string potentiometers are more accurate.

7.3 Pile Deflection vs. Depth

The shape arrays and inclinometers were used to record pile deflection vs. depth profiles in the piles during the tests. The shape arrays recorded continuously during loading and could therefore be used to provide displacement profiles at any point in the test. In contrast, 15 to 20 minutes were required to make inclinometer measurements on the four instrumented piles at a given displacement increment. Therefore, inclinometer measurements were only made immediately prior to testing and after the final maximum displacement increment to prevent disruption of the testing procedure. To provide an indication of the accuracy of the downhole measurements, displacements from the string potentiometers at the elevation of the applied load are compared to those obtained from the shape arrays at the maximum load for each loading increment. In addition, displacement profiles from the inclinometers were compared to those from the shape arrays during the extended hold portion of the final loading test increment.

Defelction vs. depth curves obtained from the accelerometer shape arrays in the piles within pile cap 1 and 2 are provided in Figure 7-7 and Figure 7-8, respectively. The location of the shape arrays relative to the piles in the group and the loading direction are shown by the legends in each figure. The average displacements measured

by the string potentiometers at the elevation of the load application for each load increment are also shown in these figures for comparison purposes. Due to a defective shape array, the data collected from the south (A-142) shape array on pile cap 1 were erroneous. As a result, only the center shape array (A-104) and the north shape array (A-106) are used to compare to the string potentiometer and inclinometer data shown subsequently. Similarly, the south shape array (A-112) on pile cap 2 also produced erroneous data which will not be presented. Nevertheless, the center shape array (A-115) and the north shape array (A-134) provide useful comparisons which are shown in Figure 7-8. Additionally, due to operator error no shape array data were recorded for the target 0.25 inch displacement increment, therefore this data is missing from the plots in Figure 7-7 and Figure 7-8.

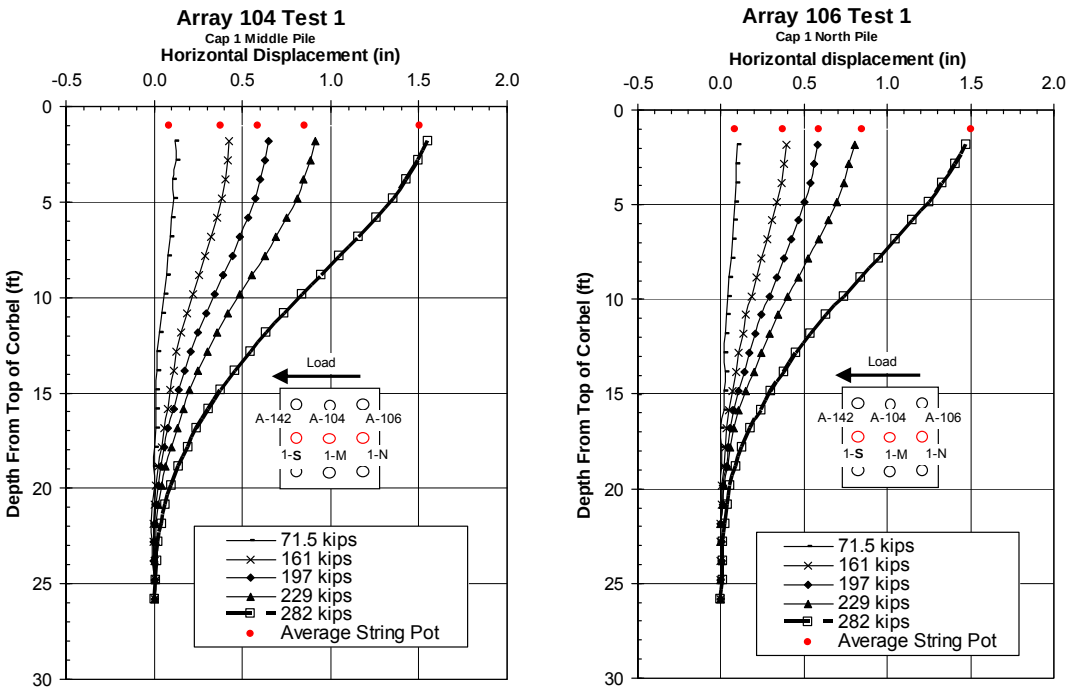

Figure 7-7 Deflection vs. depth curves for pile cap 1 for each increment of test 1, with pile head displacements from the string potentiometers also shown.

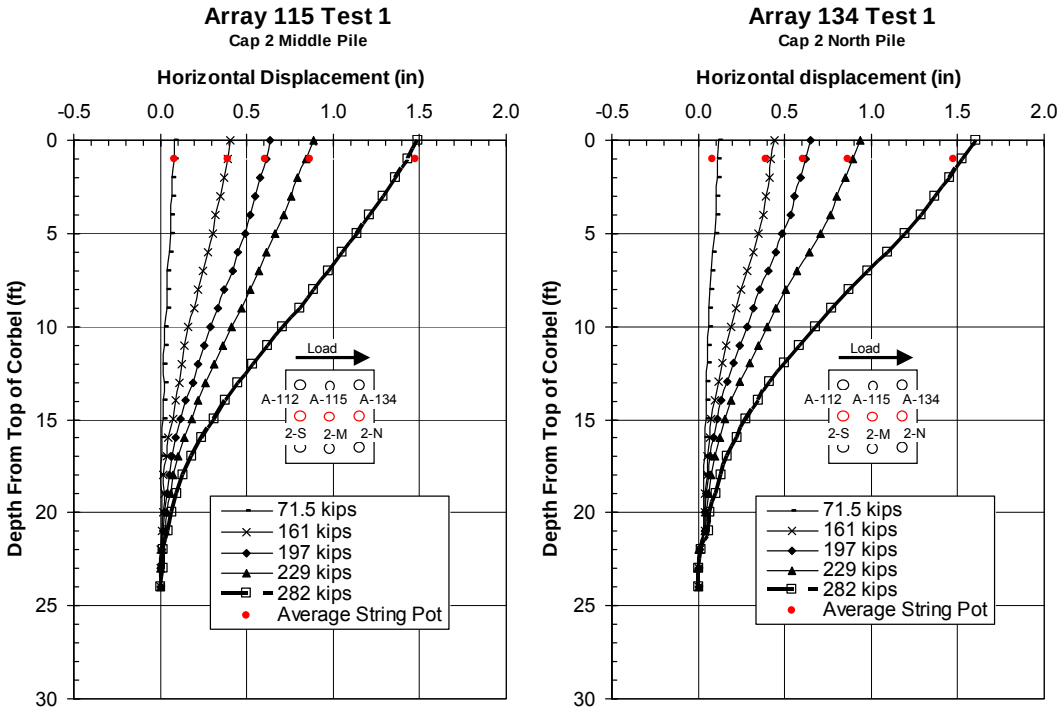

Figure 7-8 Deflection vs. depth curves for pile cap 2 for each increment of test 1, with pile head displacements from the string potentiometers also shown.

To make an accurate comparison between the shape arrays and the string potentiometers in Figure 7-7**,** the shape array data for pile cap 1 had to be extrapolated to the same depth as the string potentiometers since the shape arrays terminated at the base of the corbel. To do this, a linear trendline was created using the measured displacements at depths of 1.83 and 2.83 feet below the top of the corbel and extrapolating 0.92 ft upward to the elevation of the load point At these depths it can be assumed that the shape array would behave linearly as that portion of the shape array was enclosed in the concrete pile cap. Using this approach, the pile head displacement obtained from shape array 106 varied less than 0.05 inches from that measured by the string potentiometer, while the difference in pile head displacement from shape array 104 and the string potentiometer varied from 0.1 inches at 282 kips to 0.01 inches at

71.5 kips. Thus, shape array 106 tends to give more accurate results than shape array 104 when compared to the string potentiometers on pile cap 1.The displacements from the shape arrays on pile cap 2 showed even greater agreement with those from the string potentiometers as seen in Figure 7-8. For example, in the worst case, pile head displacements from shape array 115 in the center pile were less than 0.04 inch different than those from the string potentiometers. Shape array 134 in the north pile also provided close agreement with slightly higher displacements than the string potentiometers and a difference of only 0.04 inch or less.

Figure 7-9 provides comparisons between the displacement vs. depth curves obtained from the shape arrays and the two inclinometer pipes in pile cap 1 at the maximum pile head displacement of 1.5 inches. When looking at the inclinometer and shape array comparison for pile cap 1, the slopes of the center shape array 104 and the inclinometers are nearly identical from the top of the corbel until about 17 feet below the top of corbel; however, the displacements at the same depths during that same interval vary from 0.17 to 0.14 inches. On the other hand, displacements from shape array 106 and the north inclinometer vary by less than 0.05 inch with the greatest discrepancy at a depth of 15 feet below the base of the pile cap. The full reason for the differences in displacements between the center shape array 104 and the inclinometers is to a degree unknown. One reason for the discrepancies could be due to the fact that the shape arrays were only 24 feet long whereas the inclinometers ran the entire length of the piles. If there was any displacement in the pile deeper than the shape arrays could measure, the shape arrays could not account for that since they were set up to reference displacement from the deepest node.

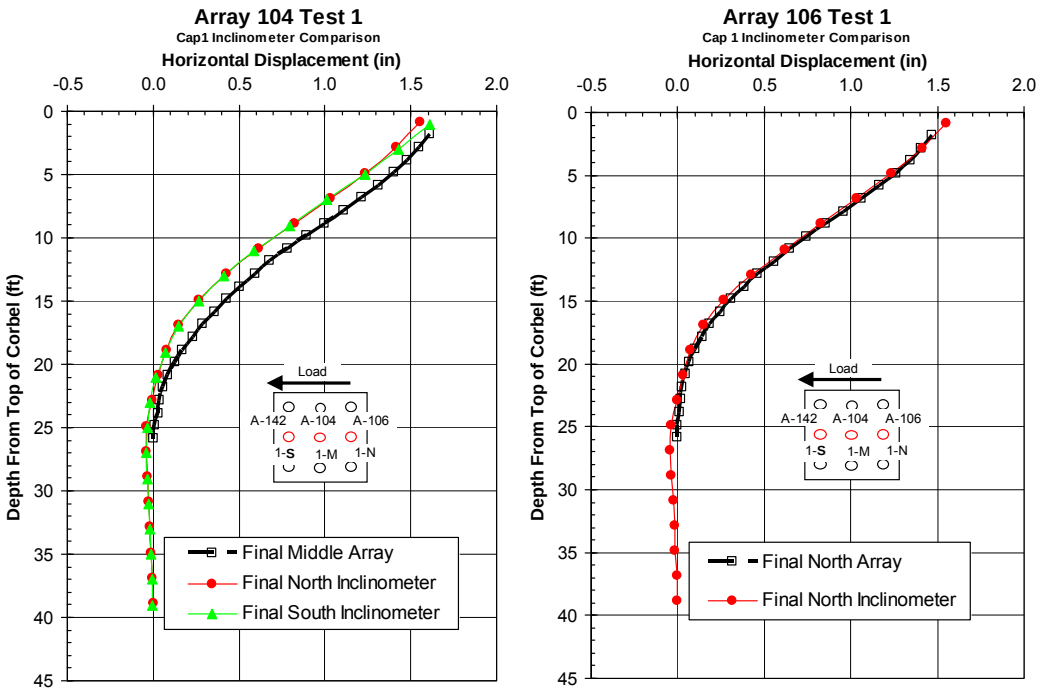

Figure 7-9 Comparison of depth vs. deflection curves for the piles in pile cap 1 from the north and south inclinometers, an shape array 104 and shape array 106.

As seen in Figure 7-9, the inclinometers often indicate a negative displacement at depths below the shape arrays, which could account for some of the discrepancies between the shape arrays and the inclinometers.

Another reason for discrepancies between the shape arrays and the inclinometer could be due to the difficulty of getting a tight fit between the shape array and the pipe. If the fit is not tight, the shape array could move within the PVC pipe housing the shape array and yield displacements which were different, usually less, than those in the pile. One other consideration for the discrepancies could be the fact that shape array 104 and the inclinometers are measuring different piles in the pile cap. This could account for some small discrepancies, but not to the full degree that is shown by shape array 104 in this test. Figure 7-10 show the inclinometer and shape array comparisons for pile cap 2.

Shape array 115 shows a slope variance with the inclinometers, which could be due to the fact that it is the middle pile being compared to the north and south piles. Shape array 134 in the north pile shows almost a perfect match with the north inclinometer, only varying by 0.04 inches at its greatest discrepancy.

Overall, the two inclinometer profiles for each pile cap are remarkably similar in each case. The displacement profiles from the shape arrays are also quite consistent with the profiles from the inclinometers. An overview of the results provide increased confidence in the accuracy of the profiles. An overview of the results shows that the piles start to experience bending at about 23 feet below the top of the corbel. The most significant bending tends to occur between 21 and 16 feet below the top of corbel, which is an indication of the location of the maximum bending moments.

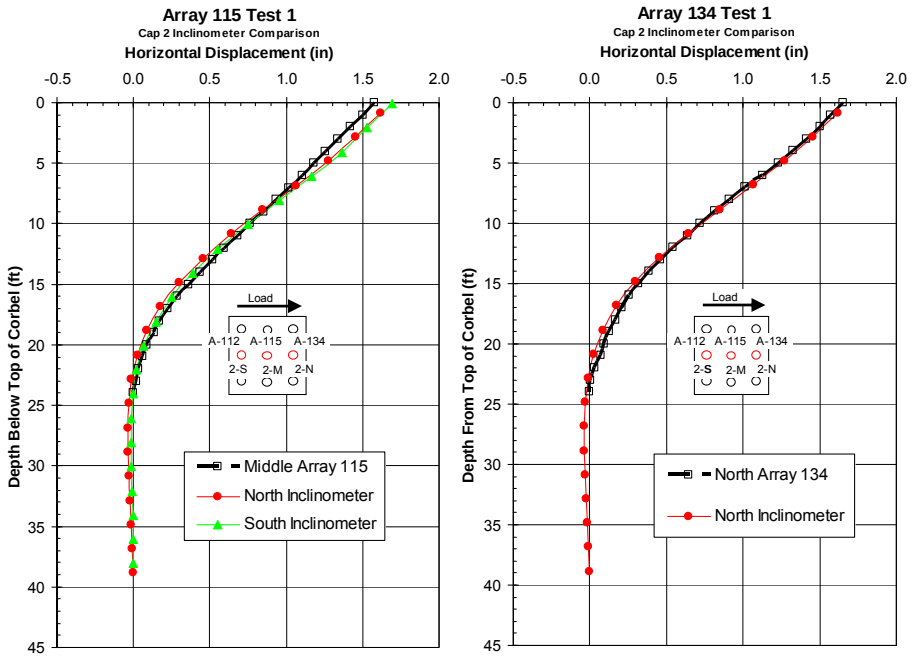

Figure 7-10 Comparison of depth vs. deflection curves for the piles in pile cap 2 from the north and south inclinometers, and shape array 115 and shape array 134.

7.4 Pile Bending Moment vs. Depth

Using equations (6-2) and (6-3) with the procedures described above, moment vs. depth plots were obtained. The curves were obtained from the shape arrays and inclinometer readings while the individual points represent moments computed at the locations of the strain gages. The maximum total load associated with each target displacement is also listed in the legend for each figure.

Figure 7-11 shows the moment vs. depth curves for the middle center pile of pile cap 1. Shape array 104 and the strain gages measured the maximum positive bending moment between the depths of 9 to 11 feet below the bottom of the pile cap. The maximum positive moment created by the 282 kip load was between 69 and 72 kip-ft. The strain gages for the middle pile tend to compliment the shape array by only varying as little at 1 kip-ft, and at most, 7 kip-ft for the positive moments. The negative moments measured by the strain gages in Figure 7-11 tend to be higher than the trend derived by the shape array. However, if the shape array were to continue on its trend into the pile cap there would still only be a 10 kip-ft difference or less for all the loads except the 282 kip load. At the 282 kip load the moment from the strain gage at the bottom of the pile cap measured -79 kip-ft, while the trend of the shape array would be around -59 kip-ft, thus leaving a wide range as to what the actual magnitude of the negative moment might be.

Bending moments for the north pile were also derived and shown in Figure 7-12. The only strain gages on this pile that remained operational for the test were at about the bottom of the pile cap and 4 feet below. The shape array shows the maximum bending moment occurring between 11 to 13 feet. At the 282 kip load the greatest moment the

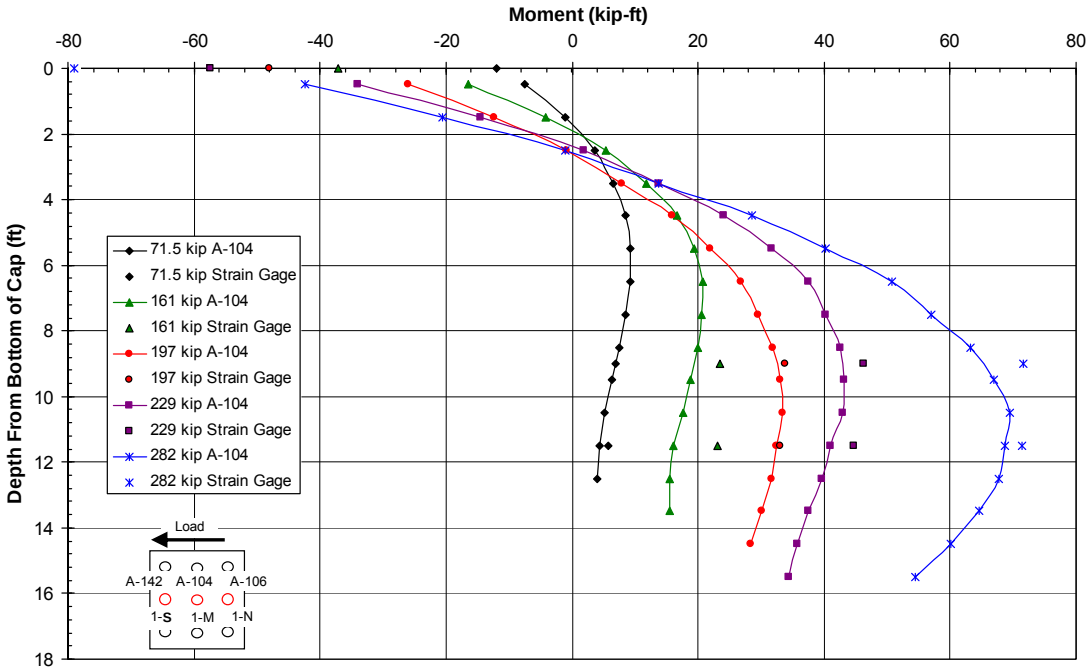

Figure 7-11 Moment vs. depth curve for the middle center pile of pile cap 1 (1-M) based on incremental deflection vs. depth curves measured from shape array 104 during test 1, with point moments measured from strain gages at various depths also shown.

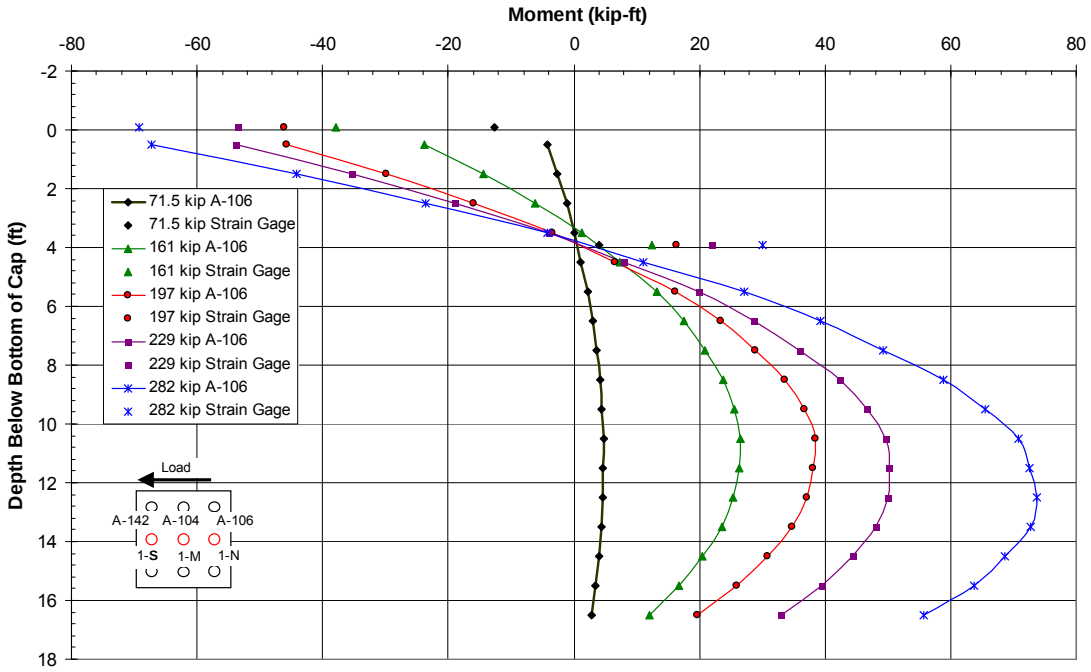

Figure 7-12 Moment vs. depth curve for the north center pile of pile cap 1 (1-N) based on incremental deflection vs. depth curves measured from shape array 106 during test 1, with point moments measured from strain gages at various depths also shown.

pile experienced was 73 kip-ft, which is almost identical to the values measured in the middle pile at the same load. The maximum negative moments derived from shape array 106 tend to be higher than the strain gages if their trend continued to the bottom of the pile cap. At the 465 kip load the moment from the strain gage at the bottom of the pile cap measured -69 kip-ft, while the trend of the shape array would be around -80 kip-ft.

The only significant discrepancy with the data from the north pile is the bending moments at 4 feet below the pile cap. The array data tends to converge to zero moment at that depth, but the strain gages still show a significant amount of positive moment. In comparing the bending moments of the middle and north piles of pile cap 1, both have similar maximum positive moments, but the north piles' moments seem to be about 1.5 feet deeper. The maximum negative moments for the strain gages at the bottom of the pile cap varied up to 10 kip-ft at the maximum load. The arrays vary from -59 kip-ft from the middle pile to -80 kip-ft from the north pile at maximum load. The discrepancies between the arrays are mostly due to the different displacements recorded, but due to similar slopes, the bending moments still demonstrate similar trends.

With the arrays being a fairly new technology, it was interesting to see how the moments derived from them compare to the moments derived from the inclinometer data using the same numerical method. The deflections from Figure 7-9 were used to produce Figure 7-13. When looking at the maximum positive moment the inclinometers show a significant agreement with only 2 kip-ft difference where as the arrays differ by about 10 kip-ft. The maximum negative moments are the opposite. The arrays only vary by 2 kip-ft, while the inclinometers vary by 16 kip-ft.

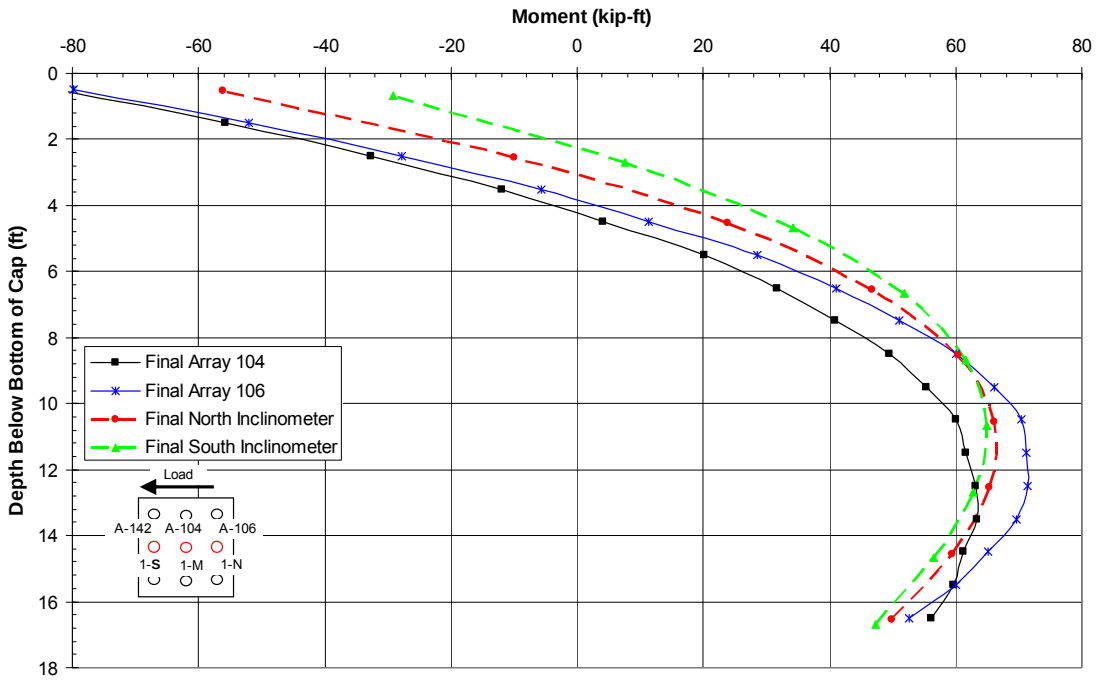

Figure 7-13 Moment vs. depth comparison for the piles in pile cap 2 based on deflections measured from the north and south inclinometers, shape array 104 and shape array 106 during test 1.

The instruments together only varied by 10 kip-ft at 16 feet below the pile cap, but increasingly deviate further apart as the depth decreases and approaches the pile cap. This leads to some evidence that the method used to derive the bending moments is more accurate at greater depths. Just as bending moments vs. depth plots were obtained for pile cap 1, the same analysis was done for pile cap 2. The results are found in Figure 7-14 through Figure 7-16. As mentioned previously, there were no data for the south pile. The middle pile of pile cap 2 had no strain gages so there is no comparison in Figure 7-14. Maximum positive bending moments in the middle pile appear to occur between 13 and 14 feet below the bottom of the pile cap, with the greatest moment being 71 kip-ft. The maximum negative moments directly under the pile cap range from -1 to -33 kip-ft.

The location of maximum positive moments for the north pile of pile cap 2 in Figure 7-15 occur a little higher than the middle pile ranging between 10.5 and 11.5 feet below the bottom of the pile cap. The greatest moment in the north pile at the 465 kip load was 69 kip-ft which is comparable to the middle pile. The maximum negative moments for the north pile are a little greater than the middle pile ranging from -5 to -40 kip-ft, nevertheless, they are still considerably lower then what was measured on pile cap 1. When looking at the maximum positive moment the inclinometers and the north array show a great congruency with about a 4 kip-ft difference where as the middle array shows about the same magnitude of bending moment, just differs in the depth of the moment by almost 3 feet. This gives evidence that the discrepancies in measured displacements, although small, have a great impact on the derived bending moments using the numerical method.

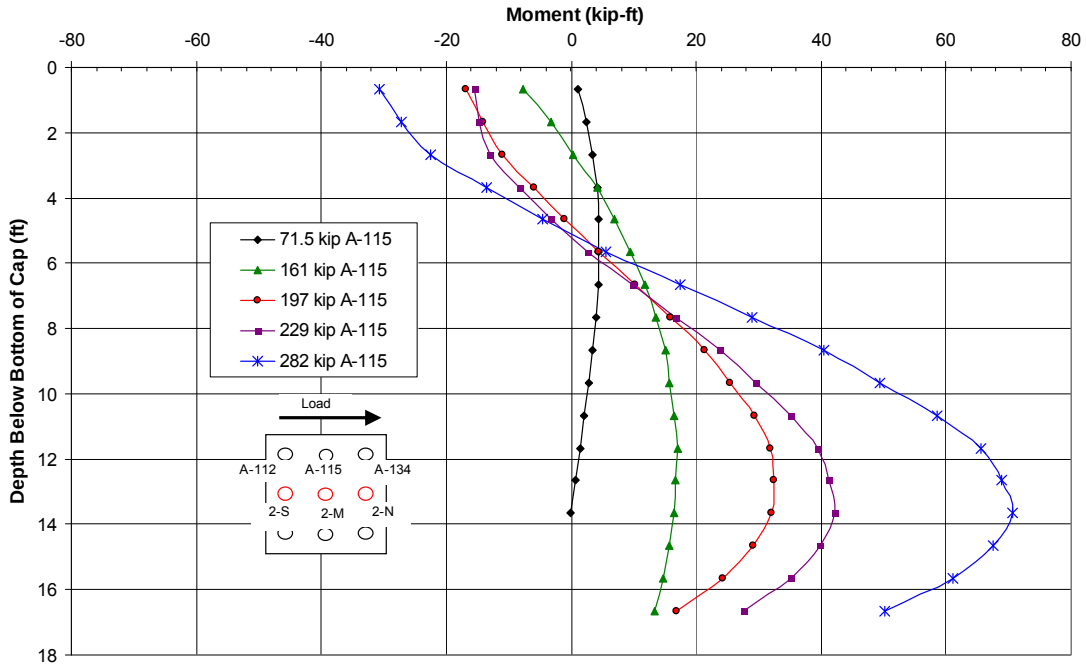

Figure 7-14 Moment vs. depth curve for the middle center pile of pile cap 1 (1-M) based on incremental deflection vs. depth curves measured from shape array 104 during test 1.

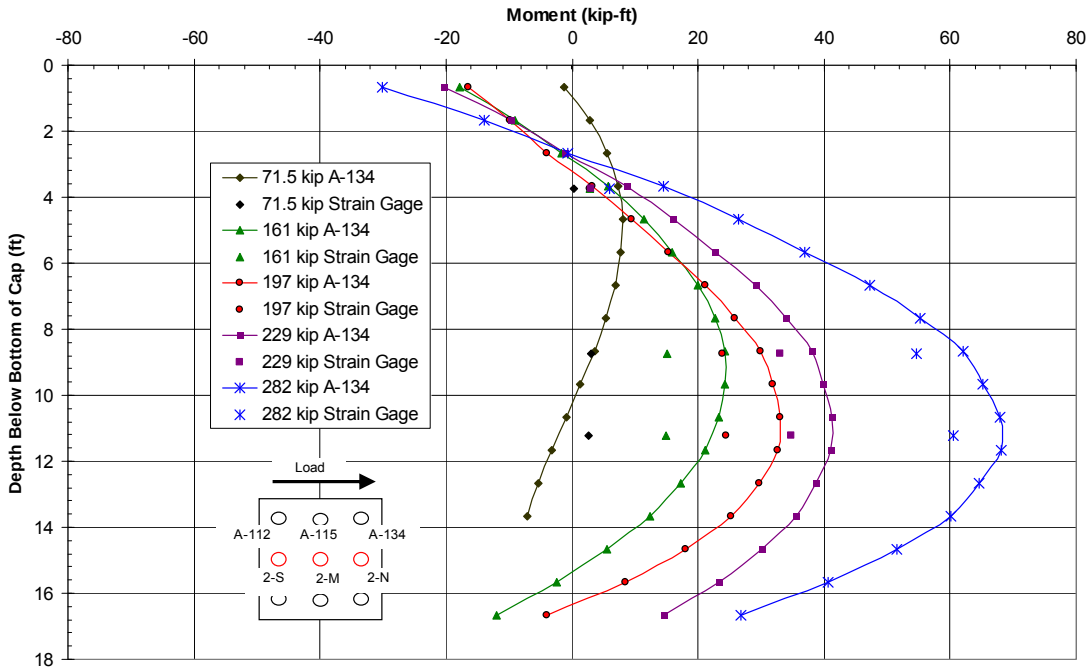

Figure 7-15 Moment vs. depth curve for the north center pile of pile cap 2 (2-N) based on incremental deflection vs. depth curves measured from shape array 134 during test 1 with point moments measured from strain gages at various depths also shown.

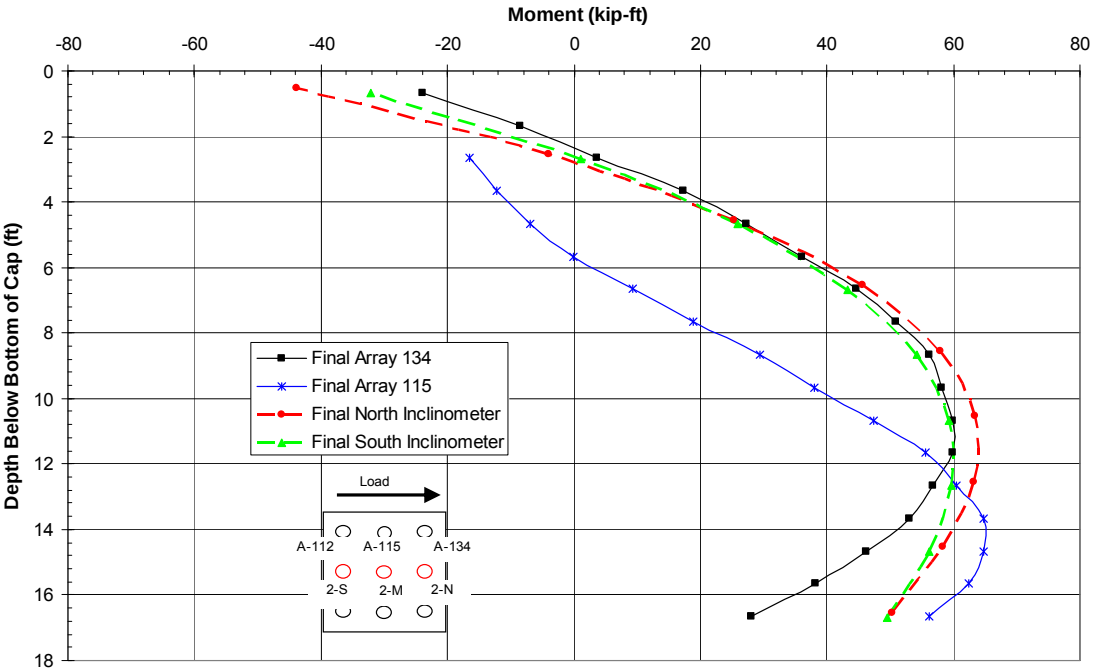

Figure 7-16 Moment vs. depth comparison for the piles in pile cap 2 based on deflections measured from the north and south inclinometers, shape array 104 and shape array 134 during test 1.

The maximum negative moments in Figure 7-16 continue to show a degree of similarity with the north array and the inclinometer. Their results span a range of about 20 kip-ft, but are still 10 to 12 kip-ft lower than what was measured on pile cap 1. Not much can be discerned from the trend of the middle array's negative bending moments as it had to be truncated due to inconsistencies of the numerical method at depths just below the pile cap.

In final review of test 1, the behavior of both pile caps in the weak virgin clay was consistent. Both pile caps displaced close to 1.5 inches at a load of 282 kips. The depth vs. displacement comparisons were consistent with the arrays closely matching the string potentiometers and inclinometers with the exception of the middle array of pile cap 1. The results of the bending moments also demonstrate fairly consistent comparisons with the exception of the middle array in pile cap 2. Since the measured behavior on both pile caps was relatively the same the following can be stated in regards to the bending moments: The negative bending moment is always greatest at the base of the pile cap, while the depth to the maximum moment increases from 9 ft to 12 ft below the pile cap as the pile head deflection increases from 0.5 in to 1.5 inches. Both the maximum negative and positive moments increase as the pile cap displacement increases. The front piles, closest to the load, experienced a maximum bending moment at the depths of 10.5 to 11.5 feet below the bottom of the pile cap, the middle piles 9.5 to 12.5 feet, and the back piles 11 to 13 feet. The difference between the array and strain gage measurements of the maximum positive moments was less than 10 kip-ft. Due to the wide range of values measured, the magnitude of the maximum negative moments will be left at the reader's discretion to discern reasonable results.

8 Test 2 – Virgin Clay - Excavated

In addition to the lateral pull into the virgin soil, a similar test was performed where the passive resistance was removed from the soil directly behind the pile cap. The purpose of this test was to find out how much of the soils strength in test 1, the virgin soil test, was due to the passive strength of the soil behind the pile cap. To accomplish this, a 1 ft wide excavation of the virgin soil along the north face of pile cap 1 to the depth of the pile cap was made as shown in Figure 8-1. The datum for the displacement of test 2 was the initial measurements taken prior to test 1. Since this test took place after the pile caps had been pulled together in the first test of the virgin clay, there was still some residual displacement once the load was released in the direction of the original displacement. Thus, test 2, started with a negative initial displacement of about 0.3 inches. All instrumentation was in place and identical to that of test 1. The test followed the standard testing procedure with one exception; due to the residual gap and initial offset resulting from test 1, the 0.125 inch test increment for test 2 was omitted.

8.1 Load vs. Pile Cap Displacement

The lateral load vs. displacement plots show the entire testing procedures incremental cycles or load paths. Figure 8-2 and Figure 8-3 were obtained from the

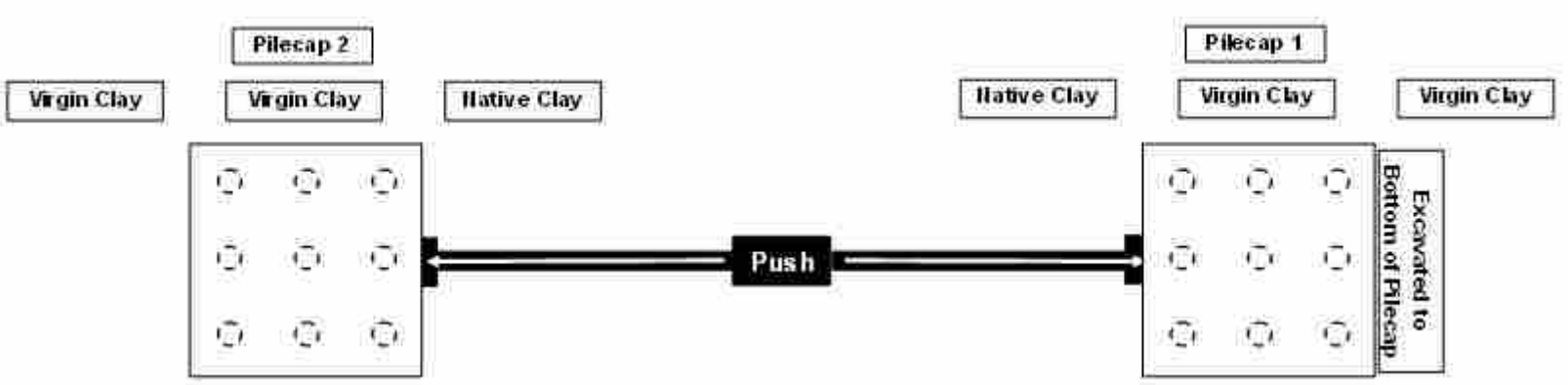

Figure 8-1 Schematic planview of test 2.

actuator pressure transducer and the string potentiometers attached to their corresponding pile caps. The actuator pushed the pile caps to target the prescribed increments of 0.25, 0.5, 0.75, 1.0, 1.5 inches, being referenced to pile cap 1 rather than pile cap 2 which was stronger. The actual displacements for pile cap 1 with the residual offset of -0.27 inches were -0.01, 0.26, 0.48, 0.75, and 1.28, inches respectively. Pile cap 2 displacements with the residual offset of -0.32 inches were -0.12, 0.06, 0.19, 0.34, and 0.63 inches respectively as measured by the corresponding string potentiometers. These displacements are consistent with expectations, as pile cap 1 had no passive resistance directly behind it. A Plot of pile cap displacement vs. peak applied load for each test increment is displayed in Figure 8-4.

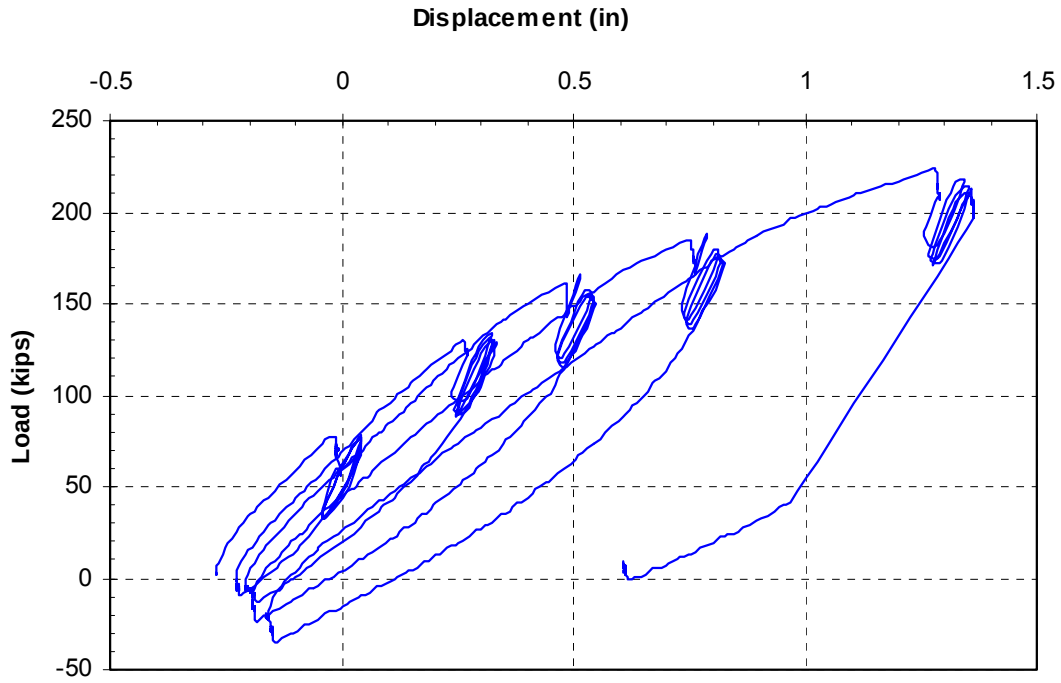

Figure 8-2 Plot of continuous pile cap displacement vs. applied load for pile cap 1 during test 2.

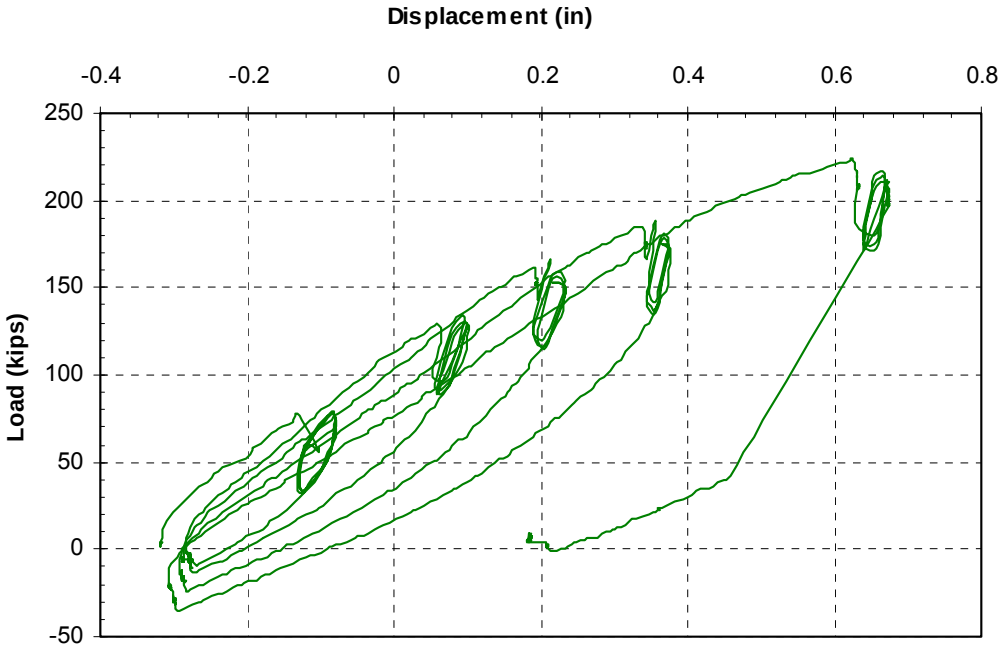

Figure 8-3 Plot of continuous pile cap displacement vs. applied load for pile cap 2 during test 2.

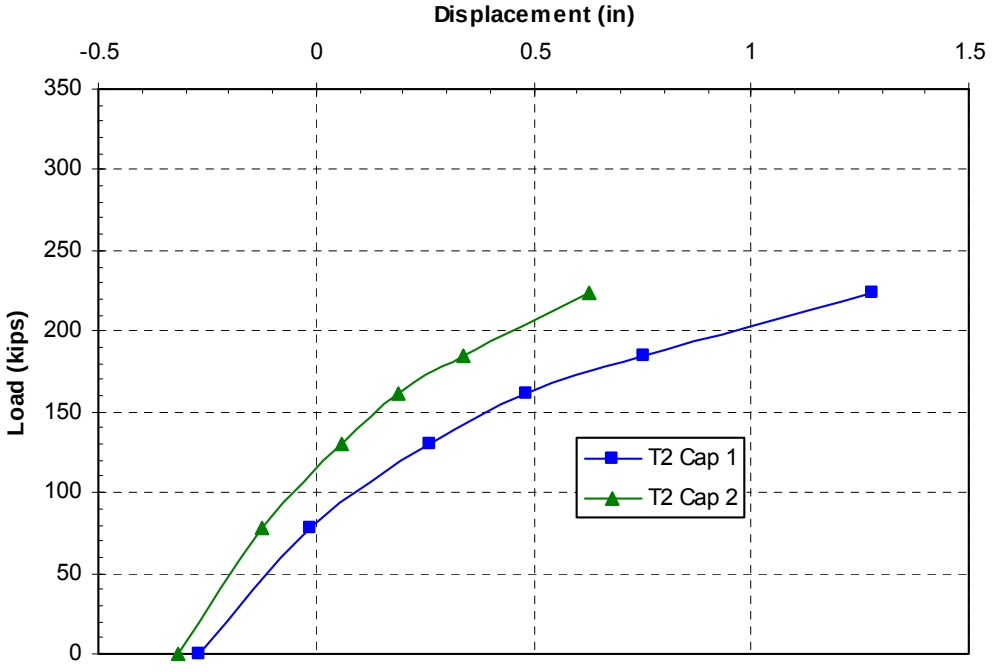

Figure 8-4 Plot of pile cap displacement vs. peak applied load for each increment of test 2.

8.2 Pile Head Rotation vs. Load

Pile head load vs. rotation curves obtained from string potentiometer and shape array measurements for the pile caps 1 and 2 during test 2 are provided in Figure 8-5 and Figure 8-6, respectively. Because of the initial negative offset, the pile caps had a slight negative rotation at the start of the test. As load increased, the rotation shifted to a positive value. Rotation of pile cap 1, where passive force was absent, exceeds that of pile cap 2 at higher load levels as would be expected. The total rotation measured on pile cap 1 was about 0.3 degrees. This value is significantly greater than the rotations observed on both caps during test 1, which measured about 0.17 degrees at the same load. This occurrence also was expected as pile cap 1 during test 2 had the passive force directly behind the cap removed.

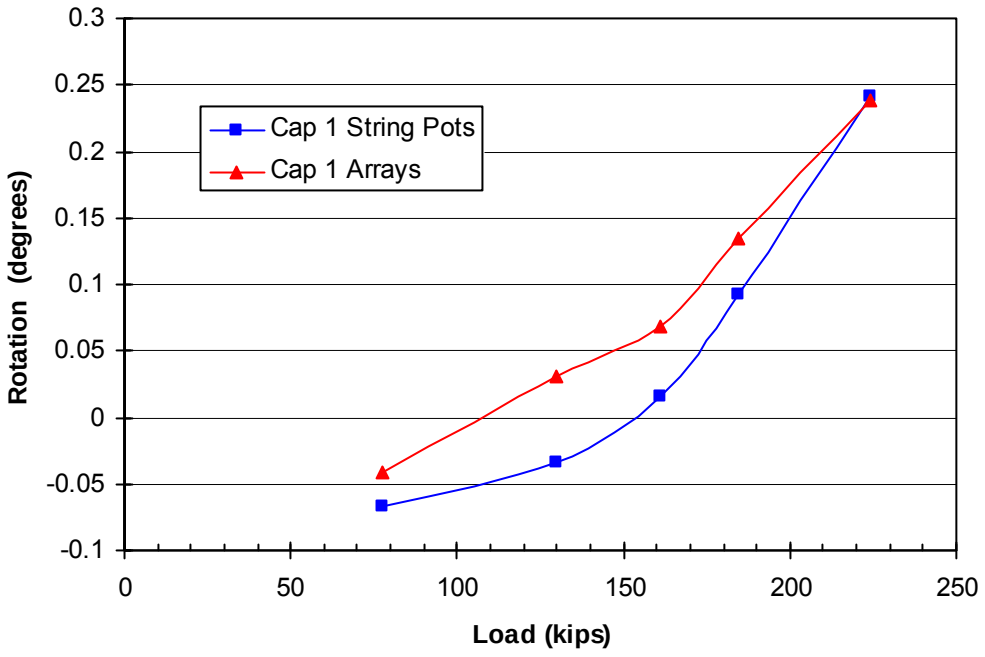

Figure 8-5 Peak pile cap load vs. pile head rotation for cap 1 during test 2 obtained from string potentiometer and shape array measurements.

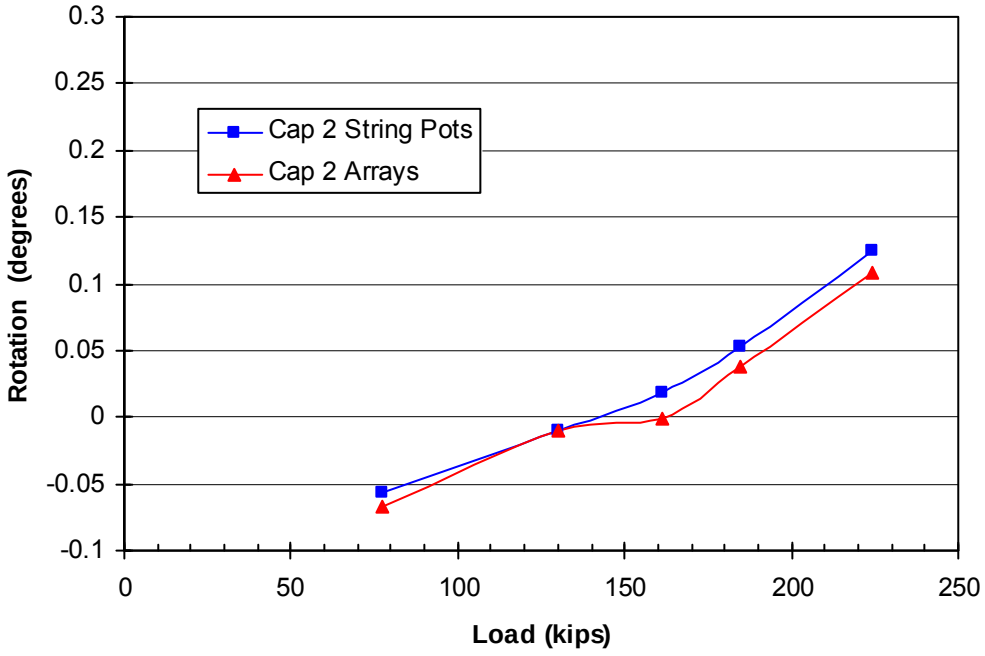

Figure 8-6 Peak pile cap load vs. pile head rotation for pile cap 2 during test 2 obtained from string potentiometer and shape array measurements.

8.3 Pile Deflection vs. Depth

Since pile cap 1 had the passive force on the pile cap removed, the remaining sections in this chapter will focus on the results from pile cap 1. It is sufficient to note that the load-displacement curves for pile cap 2 were plotting consistent with that seen in test 1 and therefore, had it displaced the same increments similar results would be apparent. Figure 8-7 shows the pile deflection vs. depth profiles of the arrays and inclinometer readings on pile cap 1 at the maximum displacement during test 2. There is good agreement in the north pile even though there is a slight discrepancy starting at about 6 feet below the top of the corbel. The instrumentation in the center pile experienced a little more variance with the greatest discrepancy being about 0.1 inches.

This discrepancy is also noted in the string potentiometer comparison with the

inclinometers found in Figure 8-8. In spite of the minor discrepancies, the general trend and slope of the depth vs. displacement profiles are consistent and provide an accurate representation of the deflections the piles experienced.

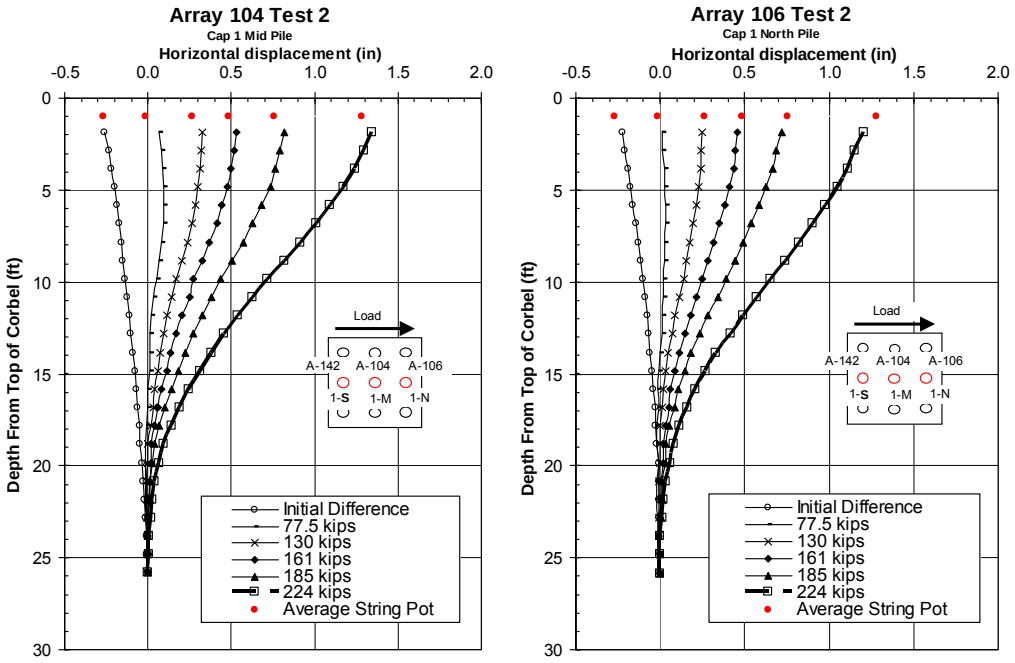

Figure 8-7 Deflection vs. depth curves for pile cap 1 for each increment of test 2, with pile head displacements from the string potentiometers also shown.

8.4 Pile Bending Moment vs. Depth

Bending moments were estimated from the depth vs. displacement profiles from the center and north piles on pile cap 1 using the methods described in section 6.2. Figure 8-9 and Figure 8-10 provide bending moment vs. depth curves for the piles in pile cap 1 at the five target displacement levels during test 2. The curves were obtained from the shape arrays while the individual points represent moments computed from the strain gages. The datum of the figures has been moved from the top of the corbel to the bottom of the pile cap.

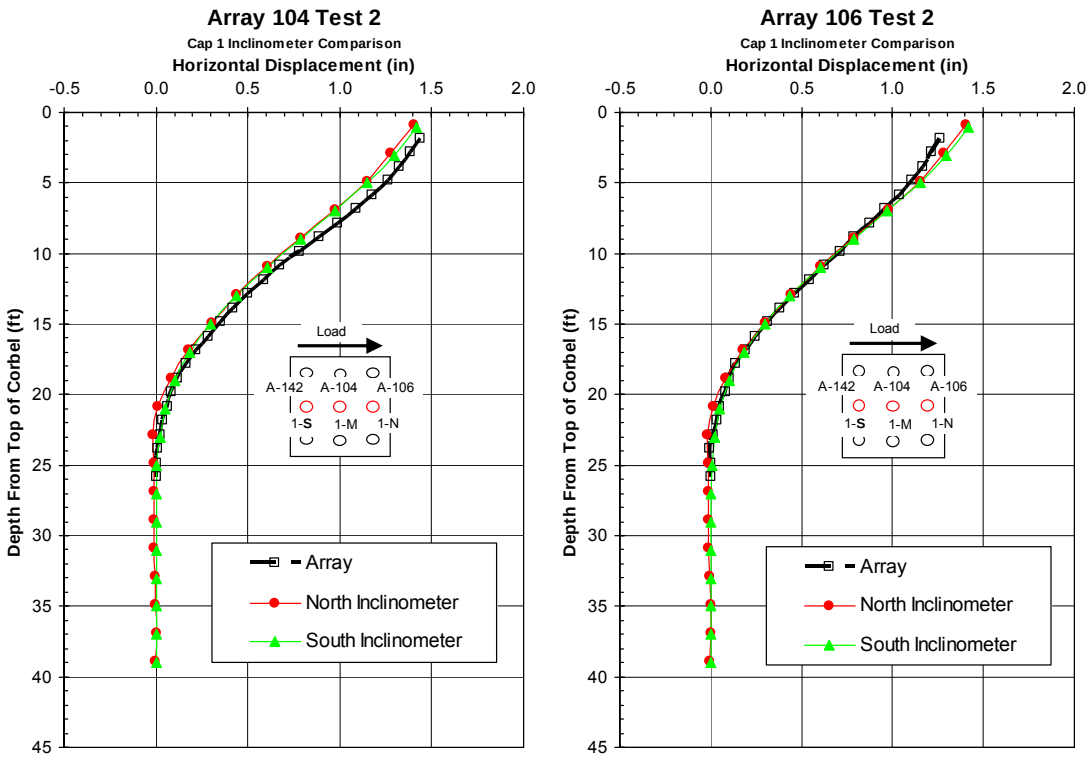

Figure 8-8 Comparison of depth vs. deflection curves for the piles in pile cap 1 from the north and south inclinometers, and shape array 104 and shape array 106.

The maximum positive bending moments from the center pile array in Figure 8-9 tend to occur from about 11.5 feet to 13.5 feet below the bottom of the pile cap. The positive moments measured from the strain gages are within 7 kip-ft or less of the moments from the array, with the only exception of the 185 kip load or 1 inch test increment. The positive moments from the north pile in Figure 8-10 seem to be a little more consistent as the depths of the maximum moments occur at about 13.5 feet below the bottom of the pile cap. The moments from the strain gages are within 7 kip-ft or less of array moments at all test increments. Also, with the exception of the 77.5 kip load or 0.25 inch test increment, the positive moments from the arrays are within 2 kip-ft or less when comparing the two piles at the corresponding load.

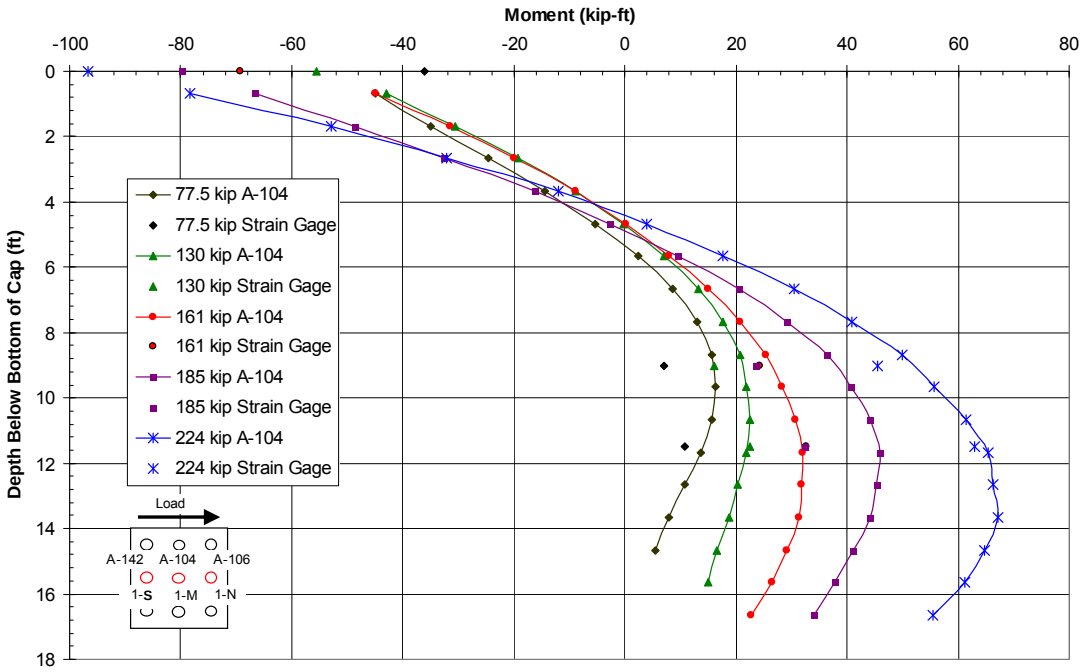

Figure 8-9 Moment vs. depth curve for the middle center pile of pile cap 1 (1-M) based on incremental deflection vs. depth curves measured from shape array 104 during test 2, with point moments measured from strain gages at various depths also shown.

The trends for the negative moments from the array in the center pile are in close agreement with the moments from the strain gages. If the array trends were to continue to the base of the pile cap only the 0.25 inch (77.5 kips) and 0.75 inch (161 kips) test increments would vary by more than 5 kip-ft. On the other hand, the array trends for the negative moments from the north pile are more inconsistent when compared to the strain gages. Most test increments are off by 8 kip-ft if the array trends were to continue to the bottom of the pile cap. The 1.5 inch or 224 kip load is the only one that appears to be in agreement. In addition the magnitude of the maximum negative moment at each test increment is about 13 kip-ft higher on the center pile than on north pile.

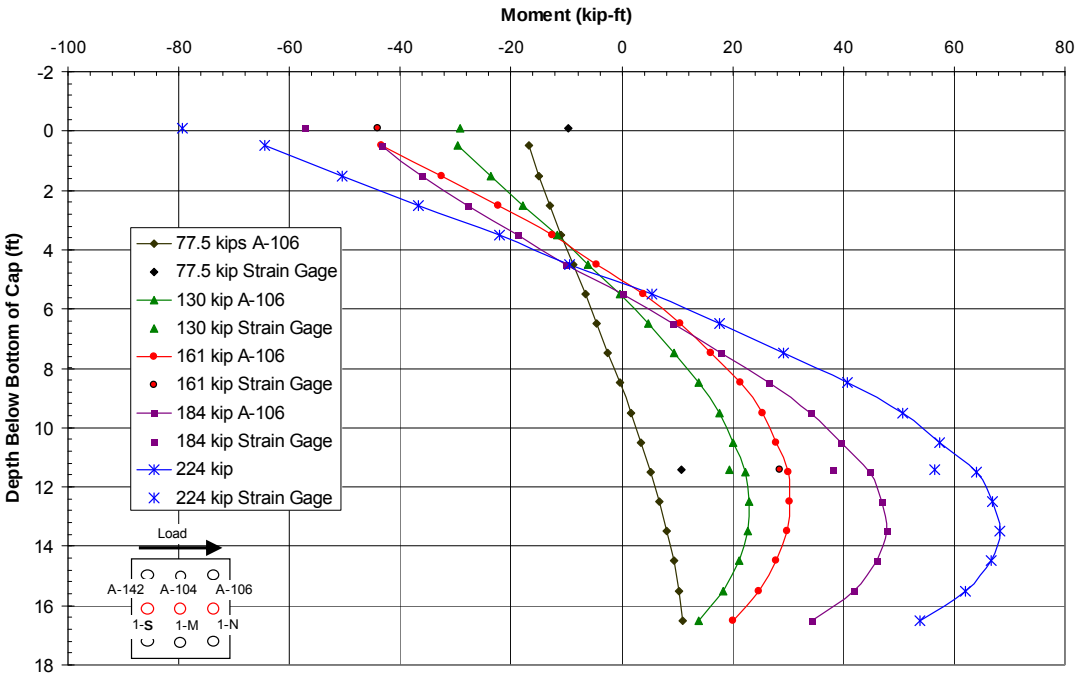

Figure 8-10 Moment vs. depth curve for the north center pile of pile cap 1 (1-N) based on incremental deflection vs. depth curves measured from shape array 106 during test 2, with point moments measured from strain gages at various depths also shown.

A comparison of the moments derived from the arrays and inclinometers at the maximum displacement is shown in Figure 8-11. There is great agreement with the inclinometers; however the arrays vary in their trends to a degree. The inclinometers and the center array place the maximum positive bending moment at about 11.5 feet, but the north array places it lower at 12.5 feet. When looking at the magnitude of the maximum positive moment the inclinometer measure about 58 kip-ft, the north array 66.5 kip-ft, and the center array 69 kip-ft. The north array and the inclinometers are in fair agreement at the maximum negative moment measuring around -60 kip-ft, while the center array measures a higher value at about -95 kip-ft. The discrepancy in the center array's negative moments is due to the fact that it recorded greater displacements at depths closer to the pile cap than the inclinometers as shown in Figure 8-8.

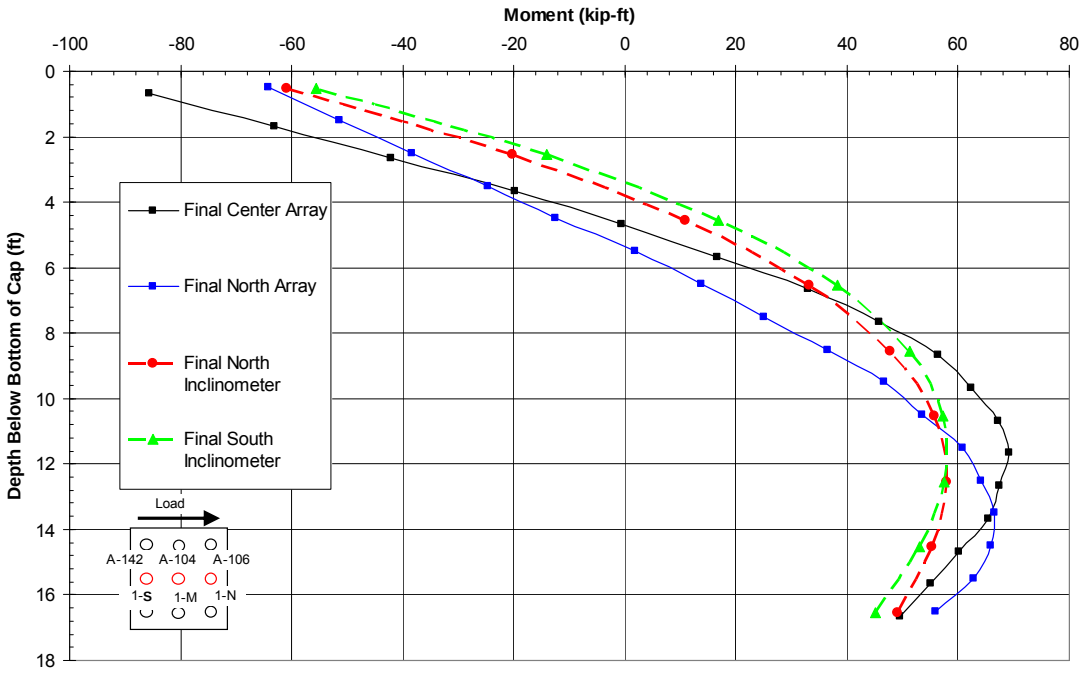

Figure 8-11 Moment vs. depth comparison for the piles in pile cap 1 based on deflections measured from the north and south inclinometers, shape array 104 and shape array 106 during test 2.

Overall when comparing these results to that of test 1 the location of the maximum positive moment on center pile was about 1 ft lower without the passive force behind the pile cap, but the magnitude stayed relatively the same. On the north pile the location of the maximum positive moment stayed within 1 ft or closer, but decreased about 5 kip-ft on average without the passive force. The maximum negative moments on the center pile remained at the bottom of the pile cap, but increased 15 kip-ft on average from test 1. It is believed though, that the negative moments from the center pile array were already low compared to the corresponding strain gages on that test. Therefore, the 15 kip-ft average increase should in reality be much lower if not an overall decrease in moment. The maximum negative moments on the north pile also remained at the bottom of the pile cap, but decreased about 13 kip-ft on average without the passive force.

In summary, without the passive force behind the pile cap, the magnitudes of the positive bending moments decreased slightly, while the negative moments decreased on average 13 kip-ft. The location of the positive moments appeared to have dropped about 1 ft, while the location of the maximum negative moments remained at the bottom of the pile cap.

9 Test 3 – Jet Grout Test I

Both foundations loaded during this test had been loaded twice previously. The two foundations were pulled together during test 1, and they were pushed apart during test 2. However, this test was the first test on the foundations following jet grouting. As explained in the previous section, the position of pile cap 1 and pile cap 2 (including the positions of the instrumented piles at depth) at the beginning of this test were chosen to define the baseline for displacement of the foundations during this and subsequent tests. A schematic of the test can be found in Figure 9-1. As shown in the figure, the pile caps were pushed apart during this test. The figure also shows that the soil adjacent to the south end of the pile cap was treated with mass mixing. The results from the tests involving mass mixing, as well as the particular process used in the mass mixing soil treatment can be found in the MS thesis by Herbst (2008).

Initial measurements from the string potentiometers, shape arrays, inclinometers, actuator pressure transducer, strain gages, were in place and initial measurements were taken prior to the test. The locations of all the instrumentation for pile caps 1 and 2 are found in Chapter 4 Test Layout and Procedure. Strain gages on pile cap 1 were located on the three center piles, but only on the south and north piles of pile cap 2. Shape arrays were placed in the south and middle center piles of pile cap 1, and in the south and north center piles of pile cap 2. Because the treatment zone for cap

1 was smaller than for cap 2, it was expected that It was expected that cap 1 might displacement much more than cap 2. Therefore, while Test 3 followed the standard procedure, the displacements were to be based on the movement of cap 1. Due to the fact that the treated soil was much stronger than the native soil, it was expected that much higher lateral forces would be necessary to displace the pile caps during this test.

As was described in Chapter 4, nearly the entire volume of soil below pile cap 2 was treated to a depth of ten feet below the pile cap. Additionally, approximately 2.5 feet of soil extending from the north and south ends of the pile cap were treated to the same depth. The soil adjacent to the north end of pile cap 1 was treated to a depth of 12 feet below the ground surface. The volume of treated soil adjacent to pile cap 1 was assumed to have extended approximately 5 feet from the north face of the pile cap. Figure 9-2 displays a profile view of the treated soil volumes for pile caps 1 and 2.

This test was performed about 20 days after installation of the soilcrete columns below pile cap 2. From the strength curves in Figure 5-9, the design strength of the soilcrete columns installed beneath pile cap 2 at the time of testing was between 200 and 250 psi, with a mean laboratory strength of about 600 psi. The soilcrete columns installed on the north edge of pile cap 1 had only been curing for approximately 17 days at the time of this test. The design strength of the soilcrete columns adjacent to pile cap 1 was between 175 and 225 psi, with a mean laboratory strength of approximately 550 psi. These strengths are only slightly lower than the strengths of the columns installed beneath pile cap. The actual strengths of the soilcrete are likely between the laboratory strengths and the design strengths calculated according the Hayward Baker standard of practice.

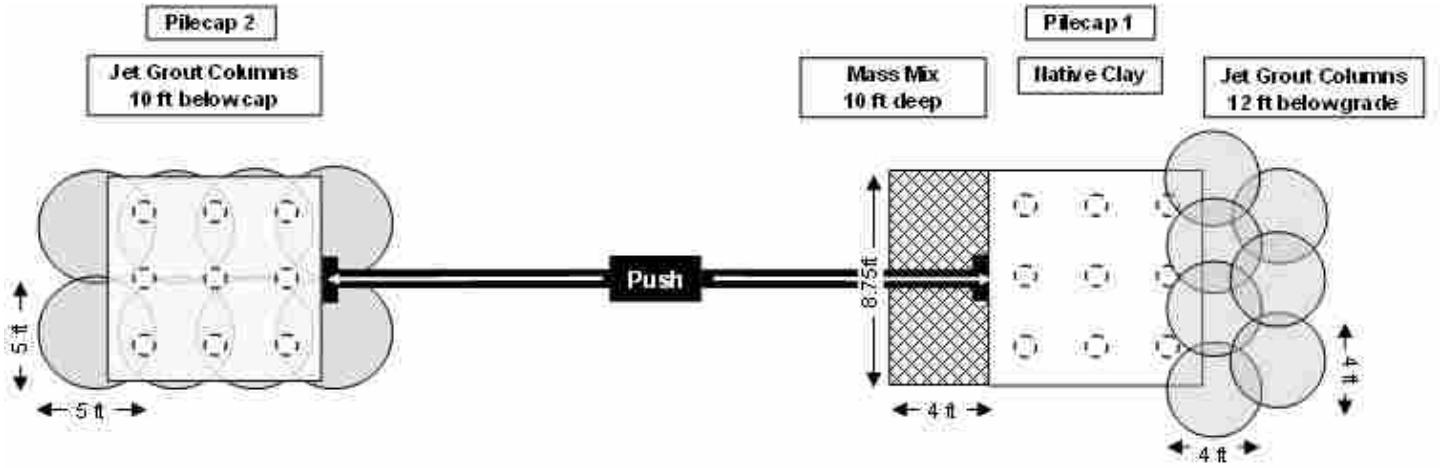

Figure 9-1 Schematic plan view of test 3.

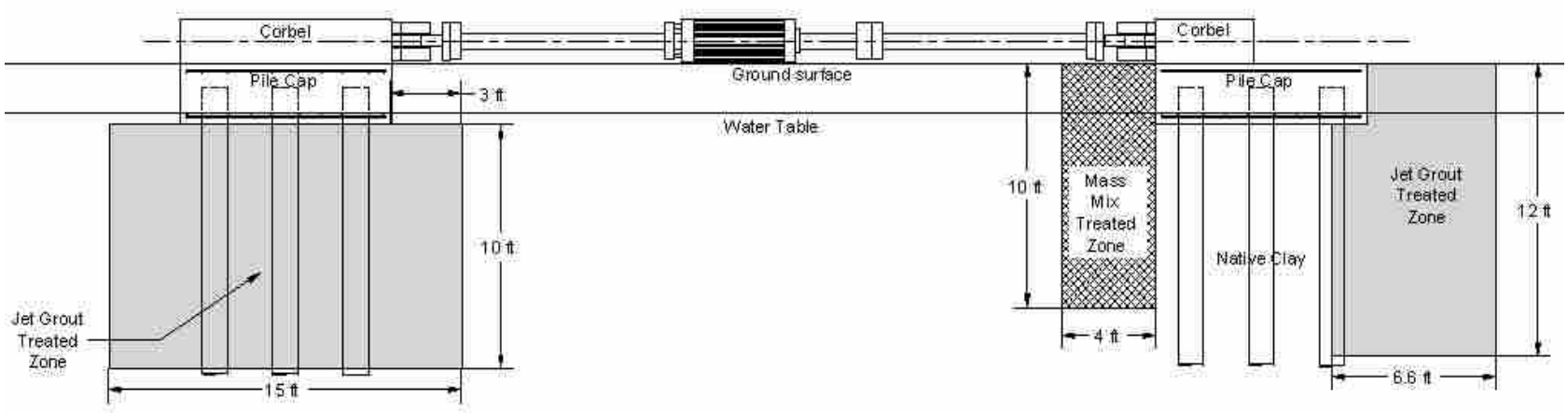

Figure 9-2 Detailed profile view of the treated soil on pile cap 1 (left) and pile cap 2 (right).

9.1 Load vs. Pile Cap Displacement

Continuous plots of load vs. displacement for pile cap 1 and pile cap 2 during this test can be found in Figure 9-3 and Figure 9-4, respectively. Since this test was chosen as the baseline for all subsequent tests, the initial deflection of each of the pile caps was zero. These plots provide the load path taken during loading, unloading and reloading for each cycle. As can be seen in the plots, there were relatively few test increments in this test.

At the end of second loading cycle it was necessary to apply a tensile force to bring the actuator deflection back to zero, which would bring the approximate pile cap deflection back to zero as well.. This does not appear to be a result of yielding in the pile based on measured bending moments. The behavior could result from lateral resistance due to side shear on the pile as it moves in the opposite direction. During re-loading, the load is typically less than that obtained during the first loading. The load deflection curve for pile cap 1 showed a decrease in resistance of about 20% during reloading; while pile cap 2 exhibited a 40% decrease in resistance during reloading. During the third test increment, the steel pipe extensions on the actuator yielded in compression at a load of approximately 500 kips because of inadequate lateral bracing. As the extensions yielded, increasing eccentric load was exerted on the extensions by the actuators. This resulted in excessive lateral deformations in the extensions, and the test was necessarily halted at this point. A picture of the bent actuators can be found in Figure 9-6. After this test, the extensions were straightened and laterally braced, which allowed testing to continue.

A plot of peak actuator load vs. displacement for each test increment is presented in Figure 9-5. The target deflections for each of the test increments were 0.675, 0.25 and 0.35 inches respectively. The actual peak displacements for pile cap 1 were 0.06, 0.23 and 0.30 inches. The actual peak displacements for pile cap 2 were 0.02, 0.16 and 0.34 inches. This plot shows that pile cap 2 is experiencing higher lateral resisting forces than pile cap 1 for nearly the entire test. The last peak point for pile cap 2 shows very little increase in resistance after undergoing a considerable amount of displacement. The curve seems to reach a horizontal asymptote at a displacement of 0.23 inches and a load of 480 kips. The load-deflection curve for pile cap 1 also seems to have flattened out at a displacement of 0.29 inches and 490 kips. This behavior would suggest

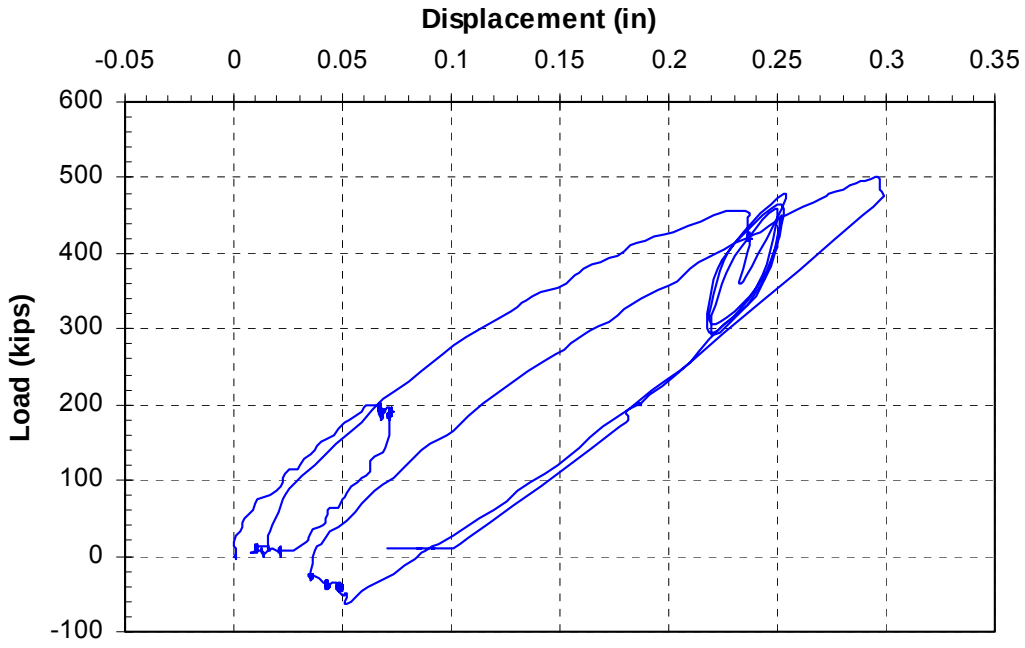

Figure 9-3 Plot of continuous pile cap displacement vs. applied load for pile cap 1 during test 3.

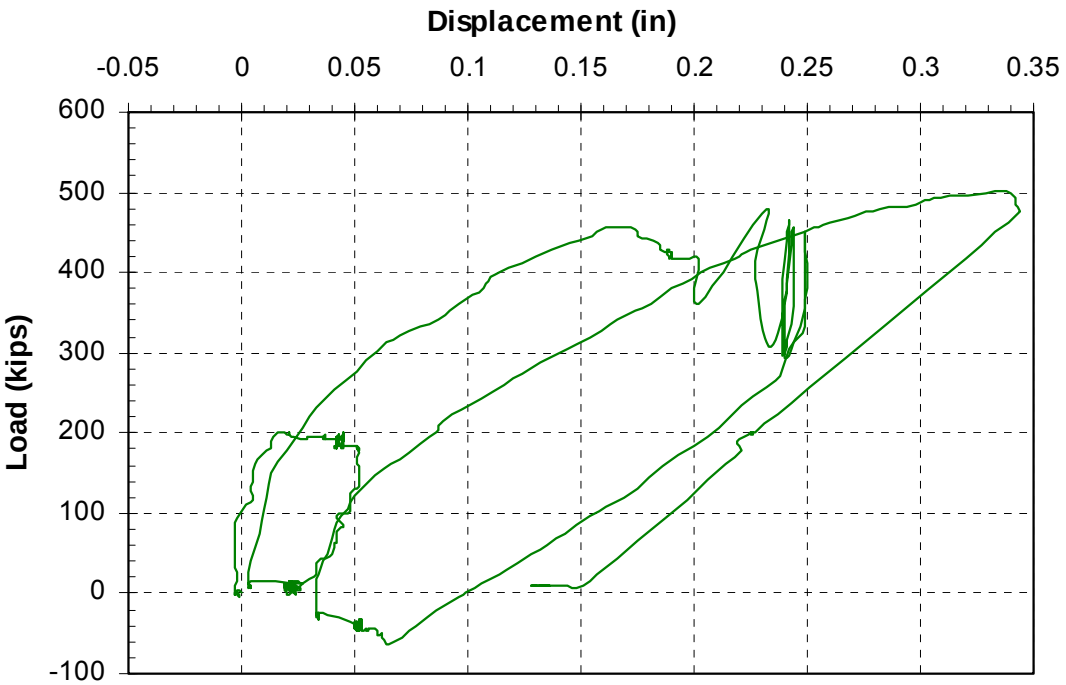

Figure 9-4 Plot of continuous pile cap deflection vs. applied load for pile cap 2 during test 3.

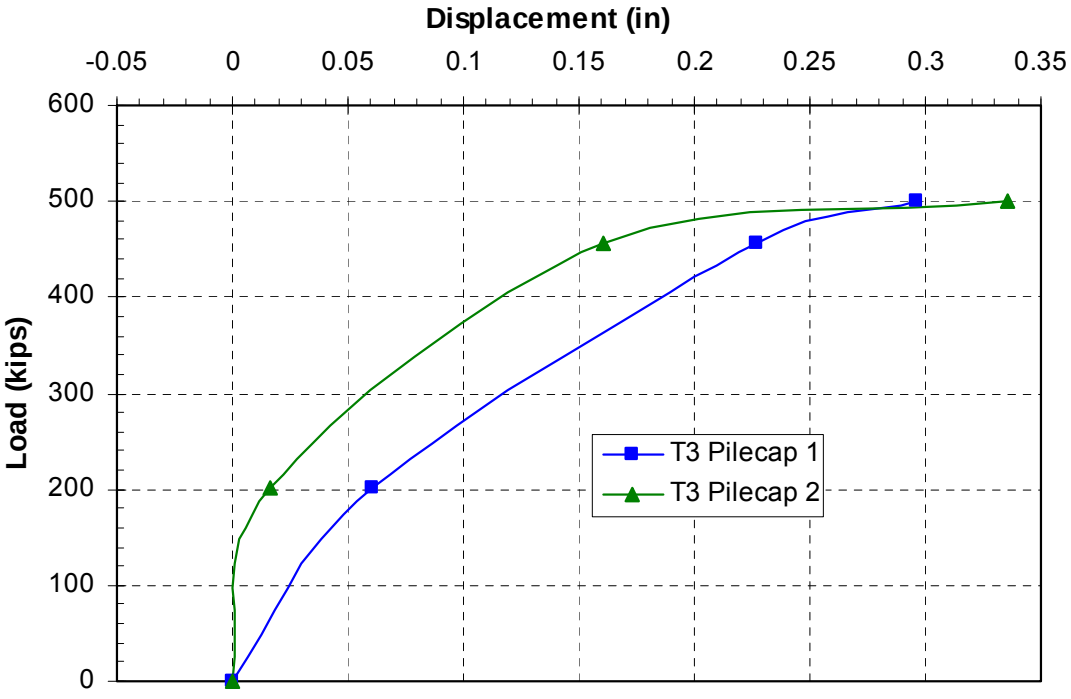

Figure 9-5 Plot of pile cap displacement vs. peak applied load for each increment of test 3.

shear failure of the soil masses in front of the loaded foundations. The violent deformation of the extensions caused rapid pile cap loading and movement. Also, the bending of the extensions changed the orientation of the applied load from the actuators. These factors may have caused either an underestimation of load applied to the pile caps or an overestimation of the pile cap displacement for the final load cycle. This brings the validity of the final point on the load deflection curves into question. The results from test 4 (Figure 10-5), which was a duplicate of test 3 using both actuators, prove that the load deflection curves for pile cap 2 and pile cap 1 are shown to prematurely flatten out during this test.

Figure 9-6 Picture of bent actuator extension.

9.2 Pile Deflection vs. Depth

Unfortunately, the inclinometer casing placed in the northernmost center pile of pile cap 1 (1-N) was broken at the base and filled with hardened jet grout spoil during the jet grouting process. The shape array casing in pile 1-N was also filled with jet grout spoils. This rendered both the inclinometer and shape array casing unusable. In

addition, the inclinometer casing in the southernmost center pile of pile cap 2 (2-S) was broken at the base and filled with jet grout spoils to a depth of approximately 24 feet below the top of the corbel. Thus, for the remaining tests the deflection vs. depth and moment vs. depth curves for this inclinometer will only measure to a depth of 24 feet below the top of the corbel, instead of the original 38 feet. Only four shape arrays were available for measurement during this test. Shape array 104 was placed in the north center pile of pile cap 2 (2-N) and shape array 115 was placed in the south center pile of pile cap 2 (2-S). Shape array 134 was placed in the south center pile of pile cap 1 (1-S), while shape array 112 was placed in the middle center pile of pile cap 1 (1-M). Shape array 112 was placed in pile 1-M because pile 1-N was filled with hardened jet grout spoils

Figure 9-7 shows the incremental deflection vs. depth curves measured from shape array 104 and shape array 115 during test 3. The average displacements measured by the string potentiometers at the elevation of the load application for each load increment are also shown in these figures for comparison purposes. As shown in Figure 9-7, the pile deflections measured at the load point elevation from each of the shape arrays is nearly twice as large as the pile cap displacement measured from the string potentiometers. The reason for this discrepancy is unknown, and does not affect the overall project objectives. It is assumed that the deflections measured from the string potentiometers are more accurate, because they are more consitent with the deflections measured by the actuator. These deflections will be used for subsequent analysis are consistent with the deflections measured from the string potentiometers.

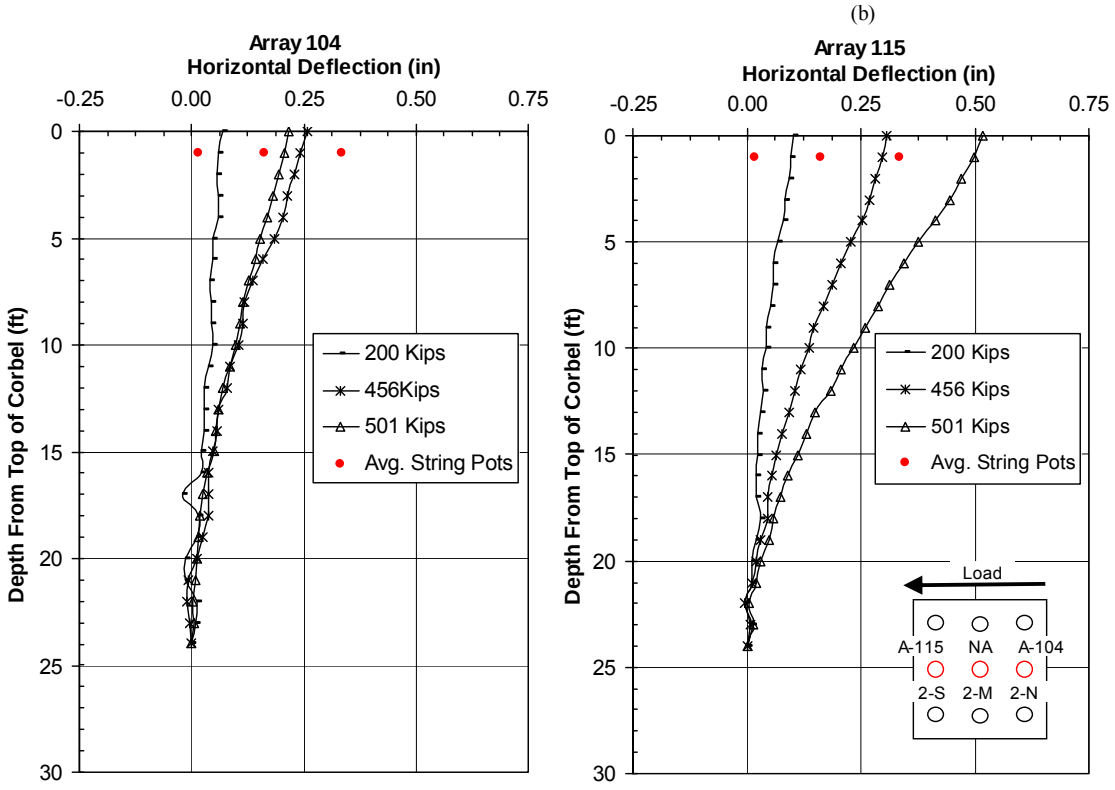

Figure 9-7 Deflection vs. depth curves for (a) the north center pile of pile cap 2 (2-N) from shape array 104 and (b) the south center pile of pile cap 2 (2-S) from shape array 115 for each increment of test 3.

The pile deflection vs. depth curves measured from shape array 134 and shape array 112 are shown in Figure 9-8. The deflections at the load point measured from the shape arrays The deflections from shape array 112 were extrapolated to the elevation of the string potentiometers for comparison. The greatest difference in measured deflection was in the initial increment; shape array 134 measured a deflection 0.035 inches greater than that measured by the string potentiometers. This small difference is within the accuracy tolerance for the shape arrays and string potentiometers. The displacements measured from shape array 134 and shape array 112 can be considered accurate for this test.

Unfortunately, the failure of the actuator extensions did not allow time for inclinometer readings to be taken for any of the piles. Thus, no shape array and inclinometer comparisons were able to be shown for this test. Bending moment vs. depth curves will also not be shown for this test. The pile deflections were relatively small, and the resulting bending moments would not be of consequence for our analysis. Additionally, the rotation vs. load curves will not be displayed in section. This test was duplicated in test 4, with the exception of using both actuators to displace pile cap 2. All of the missing data not shown for test 3 will be shown for test 4.

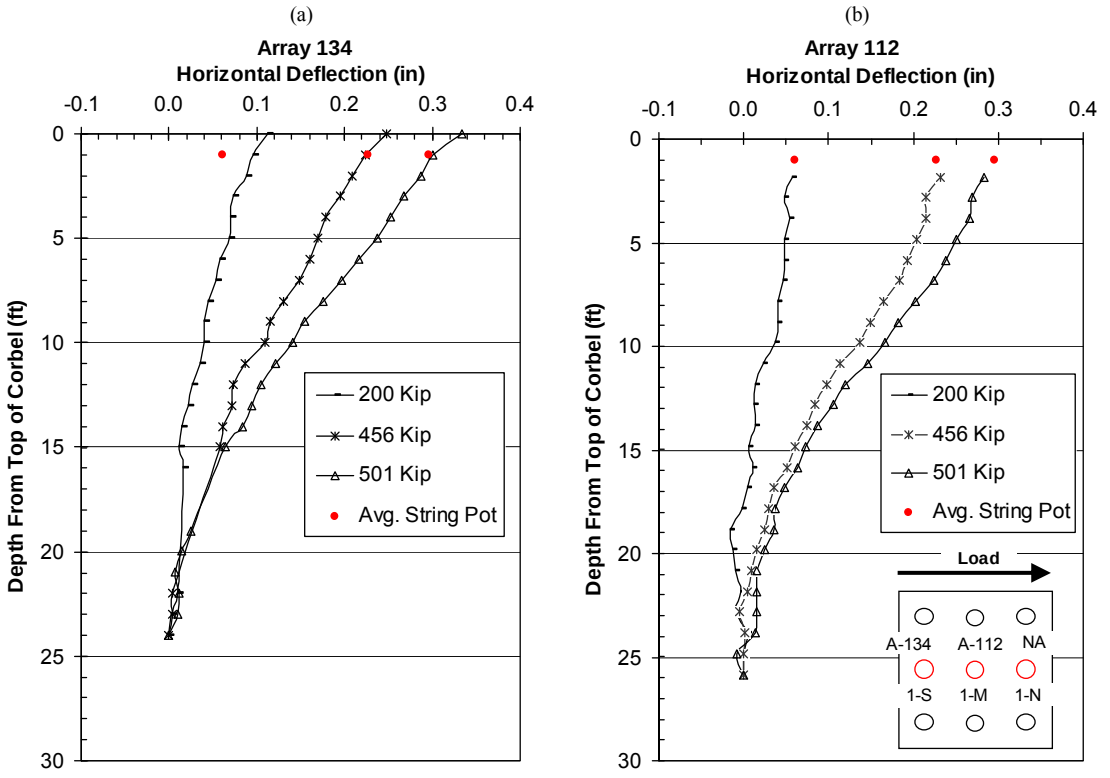

Figure 9-8 Deflection vs. depth curves for (a) the south center pile of pile cap 1 (1-S) from shape array 104 and (b) the middle center pile of pile cap 1 (1-M) from shape array 115 for each increment of test 3.

10 Test 4 (11) – Jet Grout Test II

The results of test 3 proved that, in order to displace pile cap 2 an adequate amount, both actuators would need to be used to displace the pile cap. Therefore, the first actuator was placed between pile caps 2 and 3, and the second was placed between pile caps 1 and 2 so they could act in concert. During this test, the actuators simultaneously pushed pile caps 1 and 2 apart, while pulling pile caps 2 and 3 together. Figure 10-1 shows a schematic layout for this test. A profile view of the treated soil is also found in Figure 9-2. The jet grout columns placed below pile cap 2 had been curing for 30 days. The design strength was approximately 500 psi, with a mean laboratory strength of 625-650 psi. The soilcrete placed adjacent to pile cap 1 had been curing for 27 days, and had achieved similar strength.

Between test 3 and test 4, two intermediate tests were performed. The first test pulled pile cap 1 and pile cap 2 together. The second test pushed pile cap 2 and pile cap 3 apart. Thus, before test 4 began, pile cap 2 had been displaced 2 times in the north direction and 1 time in the south direction since installation of the soilcrete columns. Pile cap 1 had been displaced once in the north direction and once in the south direction. Pile cap 2 was loaded 0.6 inches to the north, while pile cap 1 was loaded 1.85 inches to the south. During test 4, cap 2 was displaced to the north and cap 1 to the south. For a review on where the pile caps are located relative to one another please refer back to

Figure 3-2. All instrumentation such as string potentiometers, shape arrays, inclinometers, actuator pressure transducer, and strain gages were in place and initial measurements taken prior to the test. The instrumentation used during this test was not changed from test 3, except that the shape arrays in pile cap 1 were pulled from the piles in pile cap 1 for use in pile cap 3 for the two intermediate tests. The shape arrays were reinserted into the piles of pile cap 1 before test 4 began. A discussion of how this affected the results is found in section 10.3. Test 4 followed standard testing procedures, except the testing increments were load-controlled, instead of displacement-controlled as in previous tests. It was necessary to use load-controlled tests because of the large lateral loads needed to displace the pile caps. The actual loads exerted by the actuator during a displacement- controlled test could not be predicted, which could have resulted in the actuators loading the extensions to the point of buckling again during this test.

10.1 Load vs. Pile Cap Displacement

Continuous load-displacement plots for pile cap 1 and pile cap 2 during this test can be found in Figure 10-3 and Figure 10-4, respectively. These plots provide the load path taken during loading, unloading and reloading for each cycle. The test increments in test 4 were not displacement-controlled like the previous tests. The specified loading increments for this test were 200, 400, 600, and 800 kips of combined actuator load from both of the actuators. These increments were the total force that was exerted on pile cap 2 from both of the actuators. The load exerted on pile cap 1 was from just one actuator. The loading increments on pile cap 1 were 100, 200, 300, and 450 kips, respectively.

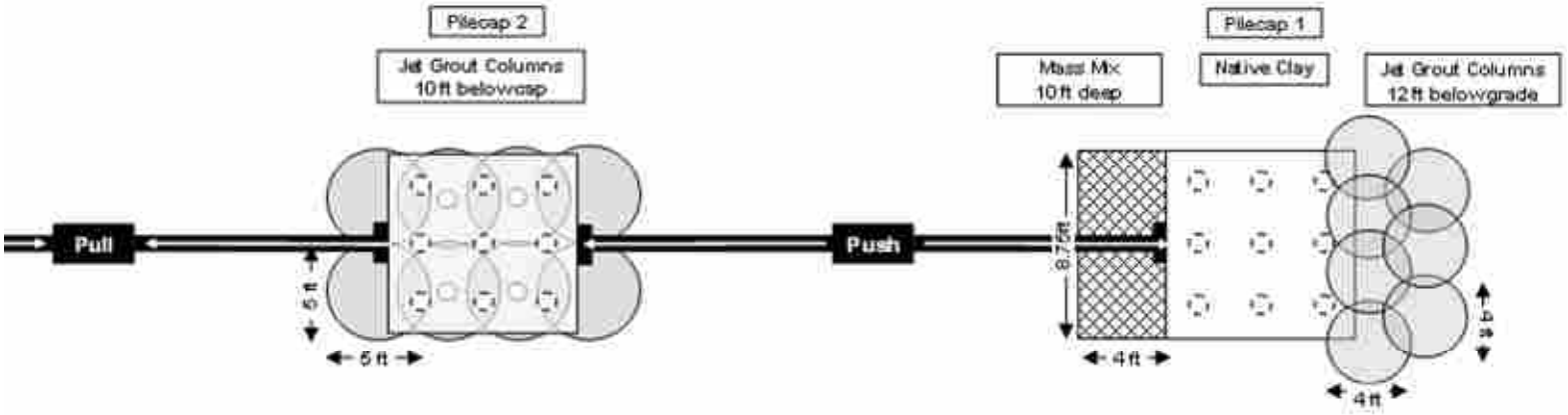

Figure 10-1 Schematic plan view of test 4.

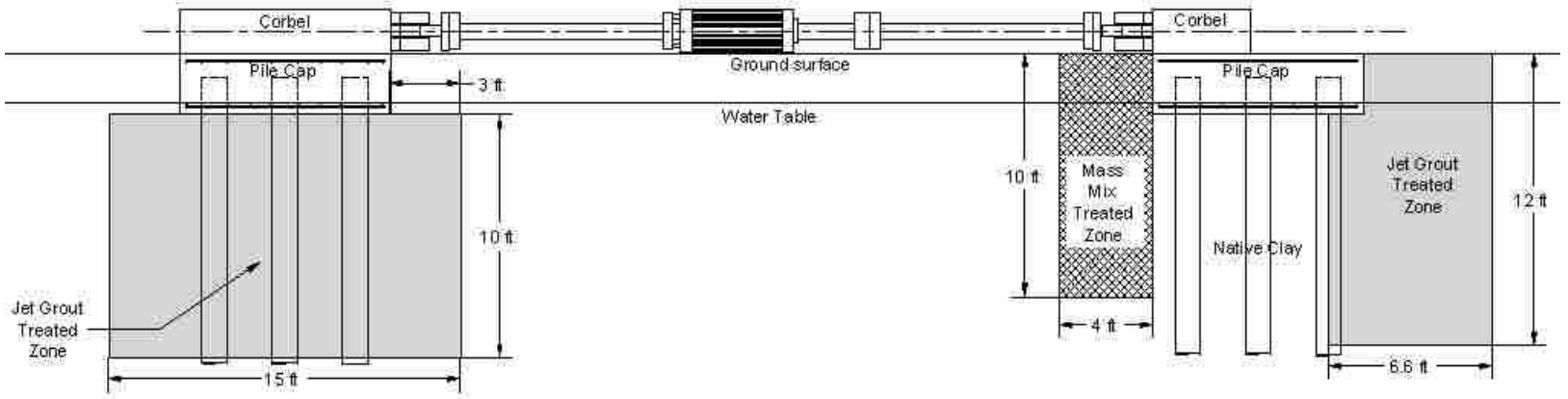

Figure 10-2 Detailed profile view of the treated soil on pile cap 2 (left) and pile cap 1 (right).

The initial displacement of pile cap 1 was a negative 0.67 inch due to previous testing. Pile cap 2 had an initial displacement of negative 0.48 inches. At the end of the final loading cycle, it was necessary to apply a tensile force to bring each of the actuator displacements back to zero. This behavior was not exhibited for the first three test increments. It appears that the tensile force needed to bring pile cap 2 back to its original position was due to yielding in the piles caused by a lateral pile cap displacement of nearly 4 inches during the 800 kip load increment. The yielding of the piles is also indicated by the horizontal asymptote of the load deflection curve for pile cap 2 which starts at a displacement of 1.6 inches and a load of 800 kips, as shown in Figure 10-4. The asymptote continues to a displacement of 3.95 inches with no increase in lateral resistance. The reload curve appears to follow the same trends as the reload curves for the previous tests. However the reload curves exhibit only 40-50% of the resistance during the first loading. This response is most likely due to the effect of having loaded the pile caps multiple times previously in the direction of loading.

Figure 10-5 is a plot of peak pile cap load vs. displacement for each test increment. From this plot it can be seen that the initial portion of the load deflection curve for pile cap 1 creates an “s” shape. This “s” shape is consistent with having an initial gap between the pile cap and the treated soil. The lateral soil resistance is initially low, but the resistance dramatically increases as the gap is closed. The gap appears to have closed at a deflection of about negative 0.36 inches. From this point on, the load-deflection curve follows a reasonable trend. In fact, the curve for pile cap 1 seems to match the pile cap 2 curve reasonably well for small deflections. The pile cap 1 curve never reached a horizontal asymptote; thus, the soil surrounding the foundation did not

appear to reach a failure state. However, the curve for pile cap 2 reached a horizontal asymptote at a displacement of 1.6 inches and a load of about 800 kips, indicating failure of the soil.

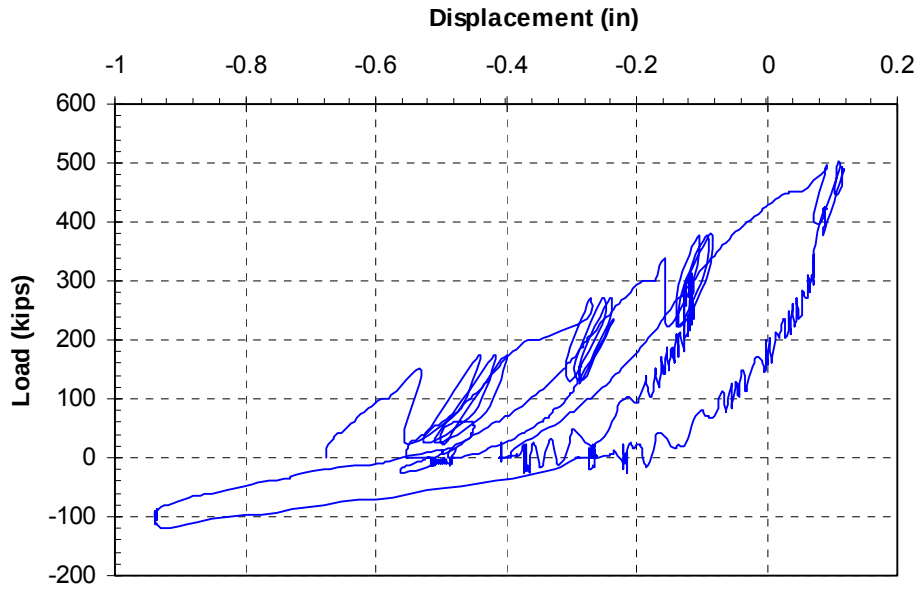

Figure 10-3 Plot of continuous pile cap displacement vs. applied load for pile cap 1 during test 4.

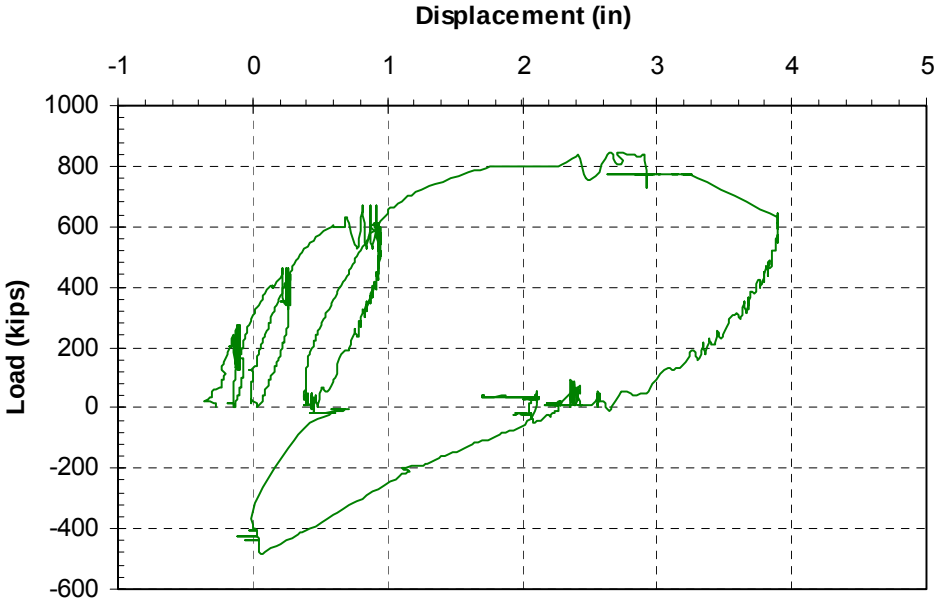

Figure 10-4 Plot of continuous pile cap displacement vs. applied load for pile cap 1 during test 3.

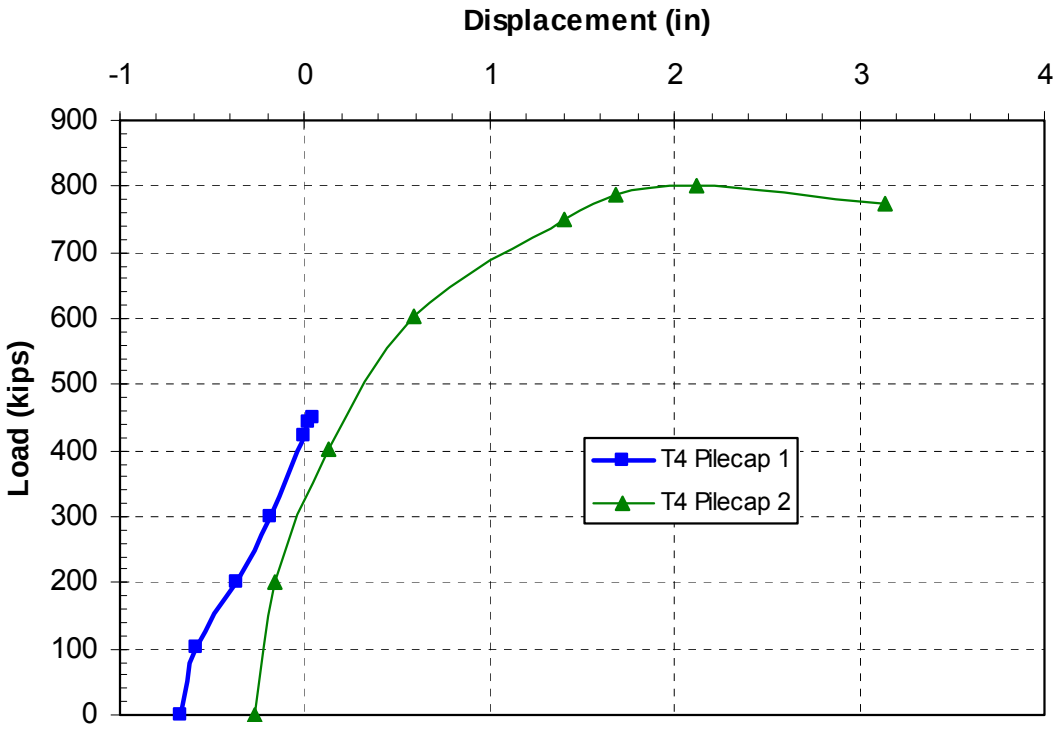

Figure 10-5 Plot of pile cap displacement vs. peak applied load for each increment of test 4.

10.2 Pile Head Rotation vs. Load

Pile head rotation vs. load curves based on the shape array deflections for pile cap 1 during test 4 are provided in Figure 10-6. There was no appreciable rotation measured from the string potentiometers during this test; thus the values are not shown in this figure. It is assumed that the string potentiometers malfunctioned during this test, because both of the shape arrays in pile cap 1 measured appreciable rotations during test 4. The difference in node deflections near the bottom of the pile cap and top of the corbel was used to measure rotation from shape array 134; the distance between these nodes was 48 inches. The difference in node deflections near the bottom and top of the pile cap was used to measure rotation from shape array 112; the distance between these nodes was 24 inches. Initially, pile cap 1 was rotated in the direction opposite to that

induced through loading. This is indicated by an initial negative rotation value. The rotations measured from two shape arrays show similar trends but the measured values are somewhat different throughout the test. These discrepancies could be caused by the smaller distance between the nodes measuring rotation in shape array 112.

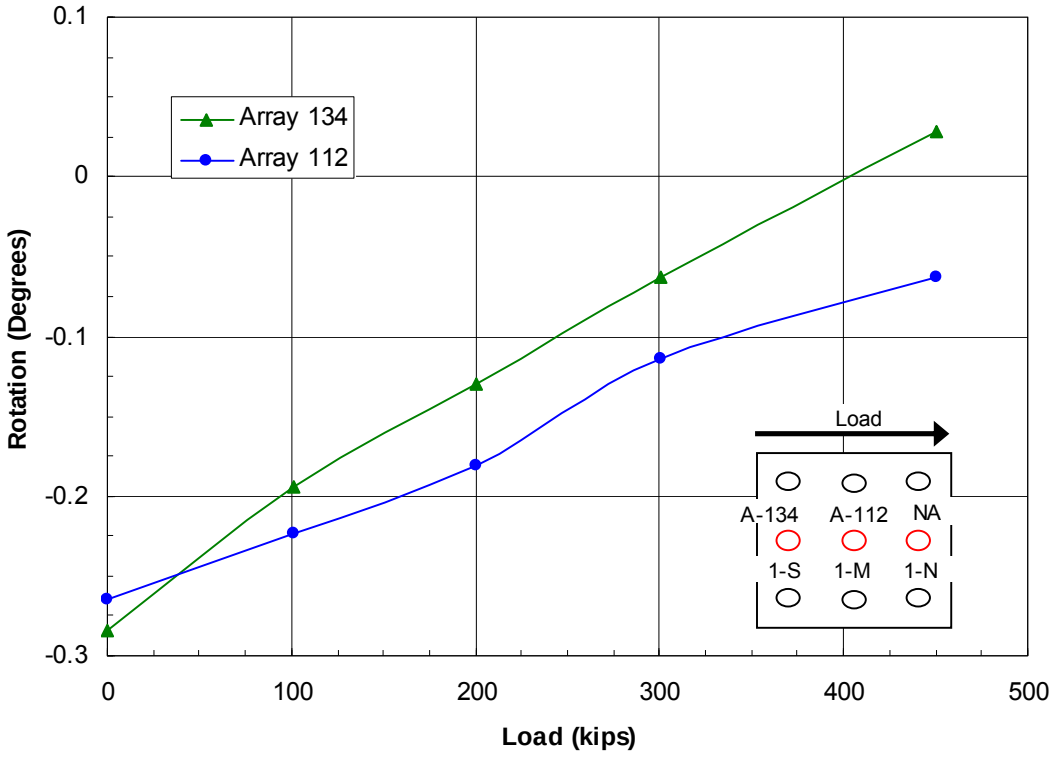

Figure 10-6 Peak pile cap load vs. pile head rotation for pile cap 1 during test 4 obtained from string potentiometer and shape array measurements.

Pile head rotation vs. load curves based on the shape array deflections for pile cap 2 during test 4 are provided in Figure 10-7. Rotation was measured from the string potentiometers located directly above the corbel of pile cap 2. The distance between the string potentiometers was 108.9 inches. Refer to Figure 4-11 for a review on the position of the string pots on pile cap 1. Rotation was also measured from the shape

arrays. The difference in node deflections near the bottom of the pile cap and top of the corbel were used to measure rotation from shape array 104 and shape array 115, the distance between these nodes was 48 inches. Initially, pile cap 2 was rotated in the direction opposite to that induced through loading. The rotations measured by the string potentiometers and shape array 104 differ by a maximum of 0.2 degrees throughout the test. Rotations measured by shape array 115 are consistently between 0.1 and 0.15 degrees lower than those measured by the string potentiometers. The reason for this discrepancy may simply be the difference in the initial measured rotation.

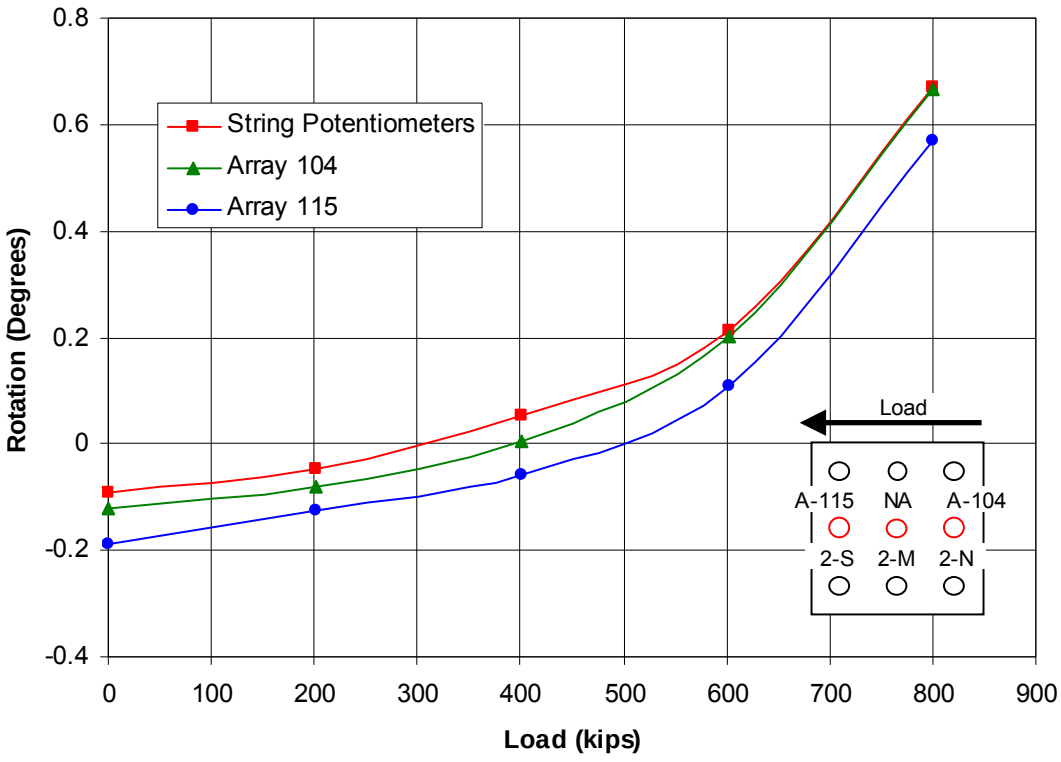

Figure 10-7 Peak pile cap load vs. pile head rotation for pile cap 2 during test 4 obtained from string potentiometer and shape array measurements.

10.3 Pile Deflection vs. Depth

As stated in the introduction to test 4, there were only four shape arrays available for measurement in this test. Shape array 134 was placed into the southernmost pile of pile cap 1, while shape array 112 was inserted into the middle center pile of pile cap 1. The shape array placement for pile cap 2 did not change between test 3 and test 4.

Figure 10-8(a) displays the deflection vs. depth curves for the north center pile of pile cap 2 (2-N) measured from shape array 104 at each load increment during test 4. The deflections measured by shape array 104 at the elevation of loading are comparable to those measured by the string potentiometers; however, the initial deflection reading of the shape arrays at the loading point (-0.5 inches) is nearly twice as large as the initial string potentiometer reading (-0.27 inches). This discrepancy is somewhat unexplainable, since the rest of the deflections measured from the shape arrays are comparable with the string potentiometer readings. The second greatest discrepancy in measurement was 0.06 inches during the 800 kip loading increment. This equates to a difference of about 3%. Figure 10-8(b) shows a comparison of the deflection vs. depth curve for pile 2-N measured from shape array 104 and from the inclinometer.

The initial readings from the north inclinometer and shape array differ. The shape array shows a deflection at the point of loading of -0.5 inches, while the inclinometer measured a deflection of -0.33 inches. The inclinometer deflection is consistent with the measurement from the string potentiometers. This seems to suggest that the initial shape array readings for this test were not accurate. There were no appreciable differences in measured deflections for any depth during the final loading.

Just as with the string potentiometers for this test, the shape array data is more consistent with the inclinometer measurements at greater deflections. The final loading in Figure 10-8(b) was also taken during the 800 kip loading increment, but the loading was held for an extended period to allow time for inclinometer readings to be performed. The extended loading of pile cap 2 caused the lateral soil resistance on the foundation to gradually decrease. Since this final test increment was load controlled, the actuator continued to displace pile cap 2 in order to keep a constant load of 800 kips. Hence, there is a difference of about 2 inches of deflection in the top of the north center pile of pile cap 2 (2-N) in the 800 kip loading increment in Figure 10-8(a) and the final load increment in Figure 10-8(b).

Figure 10-9(a) provides plots of the deflection vs. depth curves for the south center pile of pile (2-S) measured from shape array 115 for each load increment during test 4. The deflections of the shape arrays at the loading elevation are reasonably close to the displacements measured from the string potentiometers. The measurements from shape array 115 do not agree quite as well with the string potentiometers as the measurements from shape array 104. The greatest difference in displacement measured by the string potentiometers and shape array 115 was 0.21 inches during the 800 kip loading. This equates to a difference of about 10%.

Figure 10-9(b) shows a comparison pile 2-S deflection vs. depth curves measured from shape array 115 and the south inclinometer for pile cap 2. The comparison shows that the initial readings for the shape array and inclinometer are similar; however, the final reading of the inclinometer measured consistently greater deflections (about 0.25 inches) than that of the shape array. This could be due to an

error in recording the new height of the broken inclinometer casing, since the curvature of the inclinometer curve is nearly identical with that measured from shape array 115. Just as was the case for

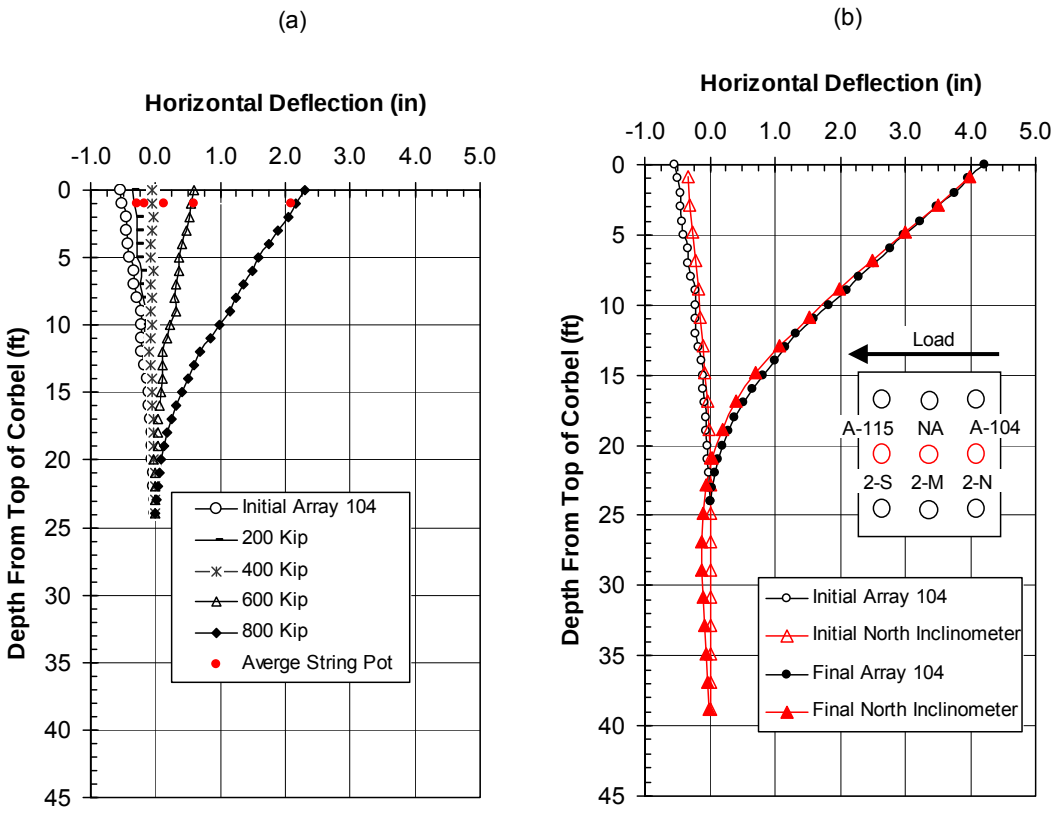

Figure 10-8(a) Deflection vs. depth curves for the north center pile of pile cap 2 (2-N) from shape array 104 for each increment of test 4, with pile head displacements from the string potentiometers also shown. (b) Comparison of depth vs. deflection curves for the north center pile of pile cap 2 (2-N) from shape array 104 and the north inclinometer of pile cap 2 during test 4.

Figure 10-8, the final loading deflections in Figure 10-9(b) are much larger than the deflections for the 800 kip increment in Figure 10-9(a). Unfortunately, we only had the use of 4 shape arrays for testing, which forced us to remove the shape arrays from the piles in pile cap 1 (shape array 134 and shape array 112), and place them in pile cap 3 for the two intermediate tests performed between test 3 and test 4. The shape arrays were reinserted into the pile cap 1 piles prior to the beginning of test 4. However, the

shape arrays could not be reliably reinserted in the exact position as they were in before extraction. Consequently, the deflections of the reinserted shape arrays in piles of pile cap 1 could not be measured from there original position before test 3.

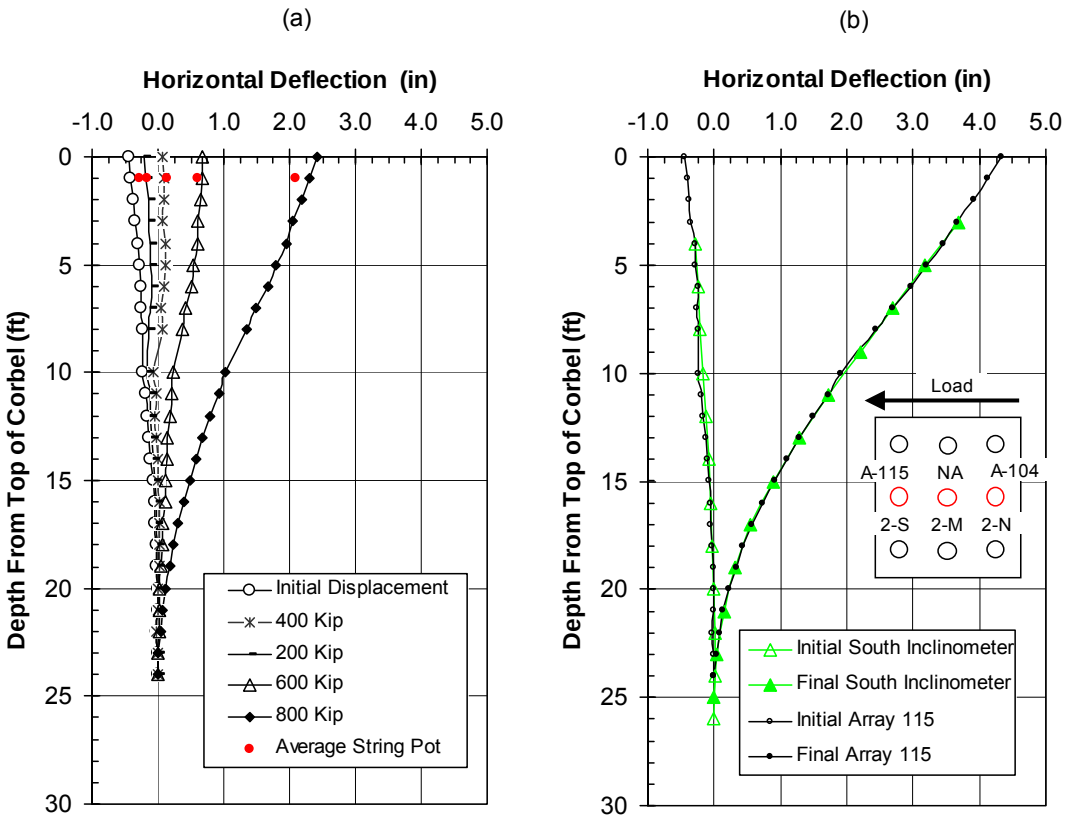

Figure 10-9(a) Deflection vs. depth curves for the south center pile of pile cap 2 (2-S) from shape array 115 for each increment of test 4, with pile head displacements from the string potentiometers also shown. (b) Comparison of depth vs. deflection curves for the south center pile of pile cap 2 (2-S) from shape array 115 and the south inclinometer of pile cap 2 during test 4.

Fortunately, the inclinometer casing in the southernmost center pile of pile cap 1 was still in good condition. The displacements measured from the inclinometers could be measured from the baseline position before test 3. Throughout the tests, the pile deflections measured from the inclinometers and shape arrays were fairly agreeable. Therefore, the initial inclinometer position for this test was also used as the initial position of both of the reinserted shape arrays. The deflections measured by shape array

134 and shape array 112 for all of the test increments during test 4 were taken relative to this initial inclinometer/shape array position.

The deflections of the south center pile of pile cap 1 (1-S) measured from shape array 134 for each increment of test 4 are found in Figure 10-10(a). The deflection measured by shape array 134 for the 200 kip increment as the loading elevation was twice as large as the string potentiometer measurement. However, shape array 134 gave accurate readings for the larger deflections. During the rest of the test increments, the greatest difference between the string potentiometers and shape array 134 was only 0.02 inches. This small discrepancy is within the measurement accuracy of the string potentiometers and shape arrays. Figure 10-10(b) shows a comparison of the south center pile of pile cap 2 (2-S) deflection vs. depth measured from shape array 134 and the south inclinometer. Note that, due to the removal and reinsertion of shape array 134, there is no initial shape array 134 reading to compare with the inclinometer. The final inclinometer and shape array 134 deflections are very comparable to a depth of 9 feet below the bottom of the pile cap. The shape array seems to measure slightly less deflection (between 0.01 and 0.04 inches) than the inclinometer from 10-20 feet below the pile cap. These discrepancies are also within the accuracy of the inclinometers and shape arrays.

The deflections of the middle center pile of pile cap 1 (1-M) measured from shape array 112 for each increment of test 4 are found in Figure 10-11(a). The small deflections measured by shape array 112 for the 200 kip increment are once again too large, while the larger deflections were much more accurate. Figure 10-11(b) shows a comparison of the pile 2-S deflection vs. depth measured from shape array 112 and the

south inclinometer. It can be seen that the final deflection measured from shape array 112 at the point of loading is consistent with that measured from the south inclinometer; however, the shape of the curves vs. depth are very dissimilar.

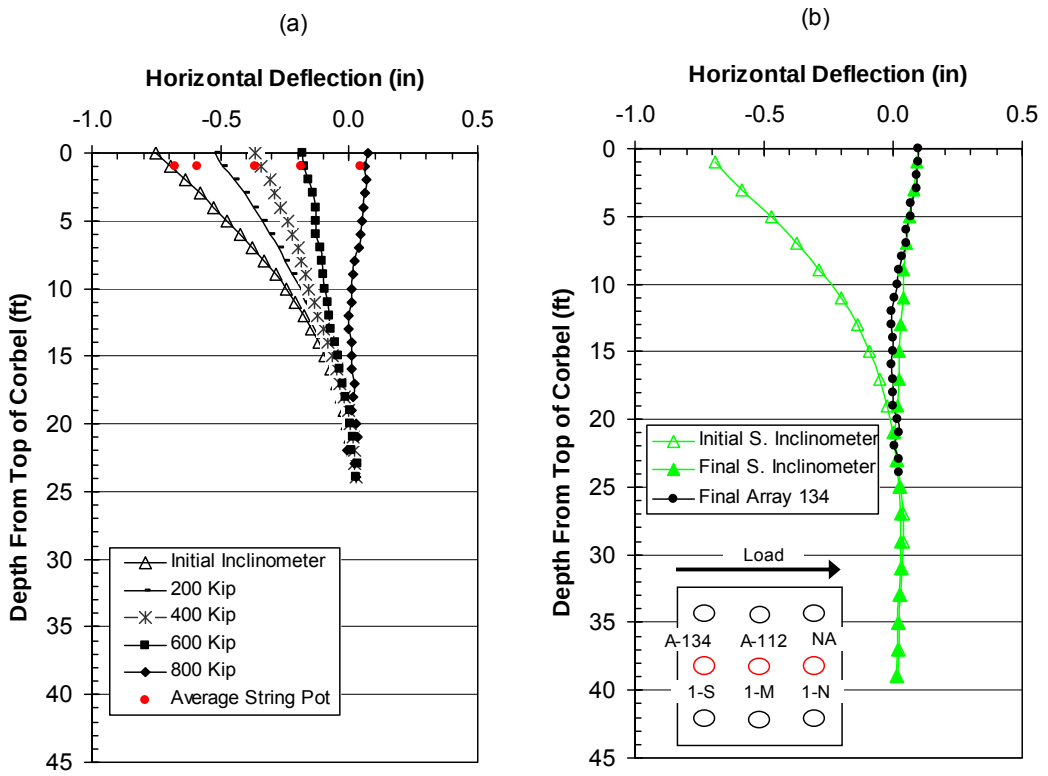

Figure 10-10 (a) Deflection vs. depth curve for the south center pile of pile cap 1 (1-S) from shape array 134 for each increment of test 4, with pile head displacements from the string potentiometers also shown (b) Comparison of depth vs. deflection curves for the south center pile of pile cap 1 (1-S) from shape array 134 and the south inclinometer in pile cap 1 during test 4.

This is most likely due to the initial inclinometer readings being taken from pile 1-S, while the shape array readings were taken for the middle center pile of pile cap 1 (1-M). However, the consistency of the deflections measured at the load point (approximately 1 ft below the top of the corbel) helps to validate the accuracy of the readings from shape array 112 during test 4.

10.4 Pile Bending Moment vs. Depth

Figure 10-12 displays the bending moments vs. depth curves for the north center pile of pile cap 2 (2-N) during test 4. The bending moment curves were generated from the deflection profiles displayed in Figure 10-8(a). A fourth order polynomial curve was used to calculate the bending moment curves for the initial, 200 kip and 400 kip load increment. A fifth order polynomial curve was used to calculate the 600 kip and 800 kip increments. Inclinometer and shape array 104 readings were taken after the final 800 kip loading increment was held for an extended period of time.

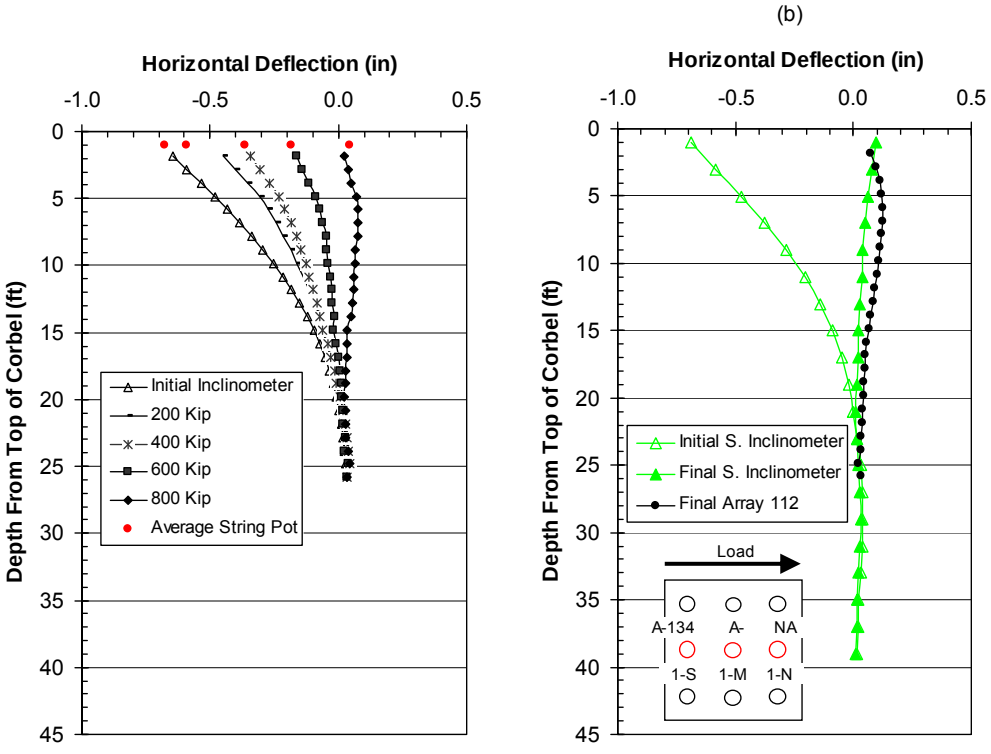

Figure 10-11(a) Deflection vs. depth curve for the middle center pile of pile cap 1 (1-M) from shape array 112 for each increment of test 4, with pile head displacements from the string potentiometers also shown (b) Comparison of depth vs. deflection curves for the middle center pile of pile cap 1 (1-M) from shape array 112 and the south inclinometer in pile cap 1 during test 4.

Figure 10-13 displays the bending moment vs. depth curves calculated during this extended loading from the deflections in Figure 10-8(b). Fifth order polynomial curves were used for all of the bending moment curves except the initial curve for shape array 104.

The initial bending moments were calculated from the initial pile deflections measured relative to the pile position before the beginning of test 3. The initial bending moments calculated from the shape array deflections give a maximum initial bending moment of -16 kip-ft at a depth of 10 feet; the bending moments from the inclinometer deflections yield a maximum initial moment of -12 kip-ft at a depth of 12.5 feet. These results are very comparable, and define the range of reasonable initial bending moments. Having a "negative" maximum initial bending moment at depth, means that the initial curvature of the pile was opposite to that produced by loading the piles during the test due to residual stresses developed during previous loading. The maximum positive bending moment in pile 2-N from the initial 800 kip load was 100 kip-ft, and occurred at a depth range of 12.5-13.5 feet. The maximum positive bending moment from the shape array 104 deflections measured during the extended 800 kip loading was 158 kip-ft acting at a depth of 12.5-13.5 feet. The maximum inclinometer-based bending moment was 141 kip-ft at a depth of 12 feet. These maximum moments are quite similar and suggest that the maximum bending moment range for the extended loading was between 140-160 kip-ft, acting at a depth of 12-14 ft. These bending moments for the extended 800 kip load in Figure 10-13 are much larger than the 800 kip load bending moments in Figure 10-12 due to the larger pile deflections during the extended 800 kip loading.

Additionally, the curves in Figure 10-12 indicate that the depth to the maximum positive bending moment increased with increasing applied load during this test. For the 200 kip loading, the pile cap was displaced very little and there was no definite curvature to the bending moment vs. depth profile. The depth to the maximum positive bending moment for the 400 kip loading was about 7ft, while the depth to the maximum moment for the 600 kip loading was about 10 feet below the pile cap. The 800 kip load, which displaced the pile cap about 2 inches, caused the depth to the maximum positive bending moment to shift to about 13 feet below the bottom of the pile cap.

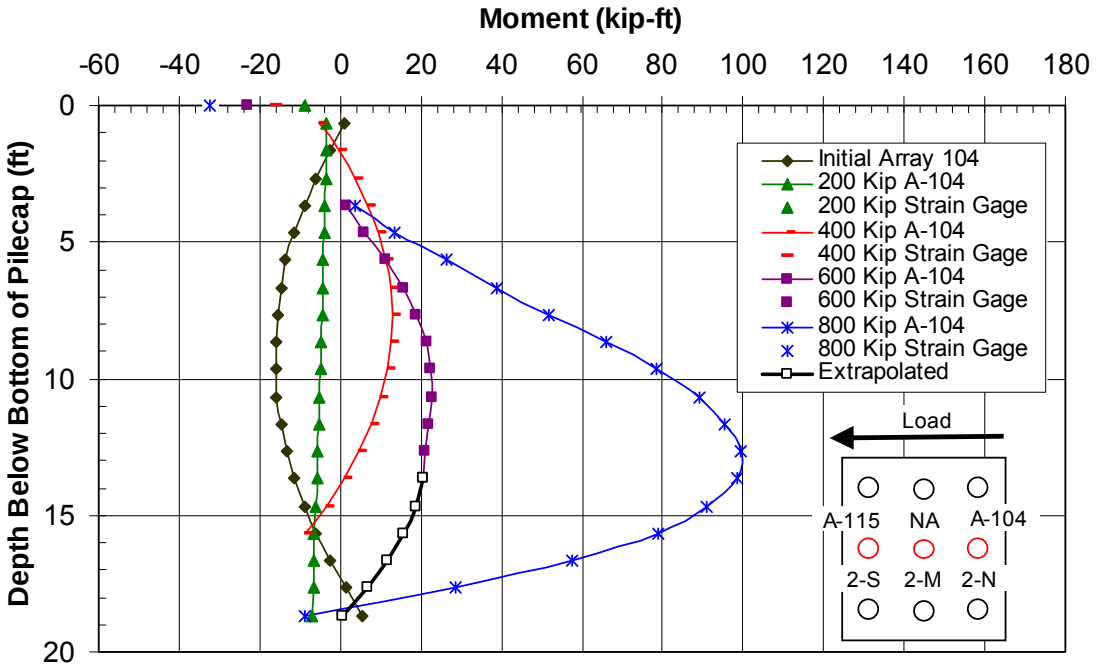

Figure 10-12 Moment vs. depth curve for the north center pile of pile cap 2 (2-N) based on incremental deflection vs. depth curves measured from shape array 104 during test 4, with point moments measured from strain gages at the bottom of the pile cap also shown.

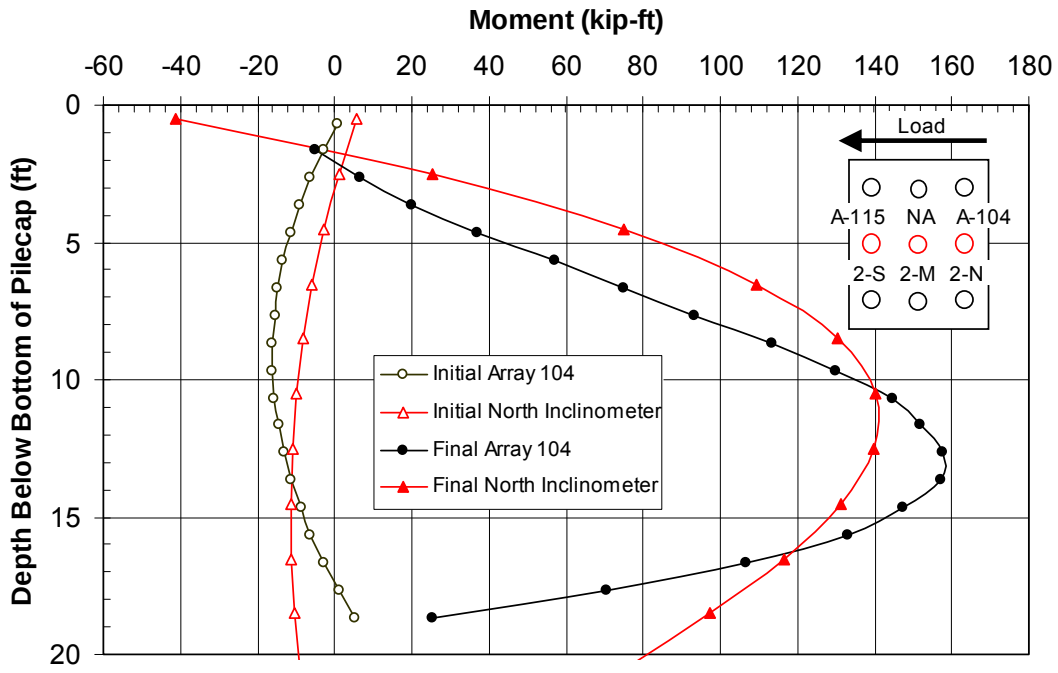

Figure 10-13 Moment vs. depth comparison for the north center pile of pile cap 2 (2-N) based on deflections measured from the north inclinometer and shape array 104 for test 4.

Nearly all of the wires coming from the strain gages in pile cap 2 were damaged during burial or during the jet grouting process. The only remaining working strain gage was at the pile-pile cap interface in the north center pile of pile cap 2 (2-N). The maximum negative moments calculated from the strain gages (Figure 10-12) seem to be in line with the truncated bending moment curves generated from the shape array deflections.

Figure 10-14 displays the bending moment vs. depth curve for the south center pile of pile cap 2 (2-S) for each load increment of test 4. These curves were calculated from the deflection profiles found in Figure 10-9(a). A fourth order polynomial curve was used to calculate the bending moment curves for all of the increments. Figure 10-15 displays the bending moment vs. depth curves calculated from the inclinometer and shape array 115 deflection profiles found in Figure 10-9(b). Fourth order polynomial

curves were used to create each of the four bending moment curves in this figure as well.The initial bending moments calculated from shape array 115 deflections give a maximum positive initial bending moment of 5 kip-ft at a depth between 7-8 feet. The inclinometer deflections yield a maximum initial moment of negative 10 kip-ft at a depth between 10-12 feet. The initial results from the inclinometer are much more comparable to the initial readings shown for the north center pile in Figure 10-13. The initial moments from the inclinometer are recommended for use in future analysis. The maximum bending moment in pile 2-S from the initial 800 kip load was 100 kip-ft, and acted at a depth range of 12.5-13.5 feet. This bending moment is approximately 20 kip-ft lower than the maximum moment in the north center pile of pile cap 2 (2-N) for the same loading increment.

The maximum bending moment from the shape array 115 deflections measured during the extended 800 kip loading was 142 kip-ft acting at a depth of 13-16 feet. The maximum inclinometer-based bending moment was 153 kip-ft at a depth of 16-18 feet. Based on the results from all of the previous tests and pile 2-N from this test, it appears that a depth of 16-18 feet below the bottom of the pile cap for the maximum positive bending moment may be excessive. Therefore, the maximum bending moment range for the final loading was likely to be between 140-150 kip-ft, occurring at a depth of 12 to 15 feet below the bottom of the pile cap.

Once again, the depth to the maximum positive bending moment increased with increasing applied load during this test. For the 200, 400, and 600 kip loadings, pile cap 2 was displaced less than 1 inch. The depth to the maximum positive bending moment for these testing increments stayed constant at about 7 feet below the pile cap. However,

the 800 kip load, which displaced the pile cap about 2 inches, caused the depth to the maximum positive bending moment to shift to about 13 feet below the bottom of the pile cap. At this stage of the testing, there were no working strain gages in the south center pile of pile cap 2 (2-S) which could be used to calculate bending moments.

Figure 10-16 displays the bending moment vs. depth curves for the south center pile of pile cap 1 (1-S) for the load increments of test 4 based on the curves in Figure 10-10(a). A fourth order polynomial curve was used to calculate the bending moment curves for the initial, 400 kip and 800 kip increments. A fifth order polynomial was used for the 600 kip increment, and a sixth order polynomial for the 200 kip increment. Figure 10-17 shows the bending moments calculated from the inclinometer and shape array 134 deflection vs. depth curves found in Figure 10-10(b).

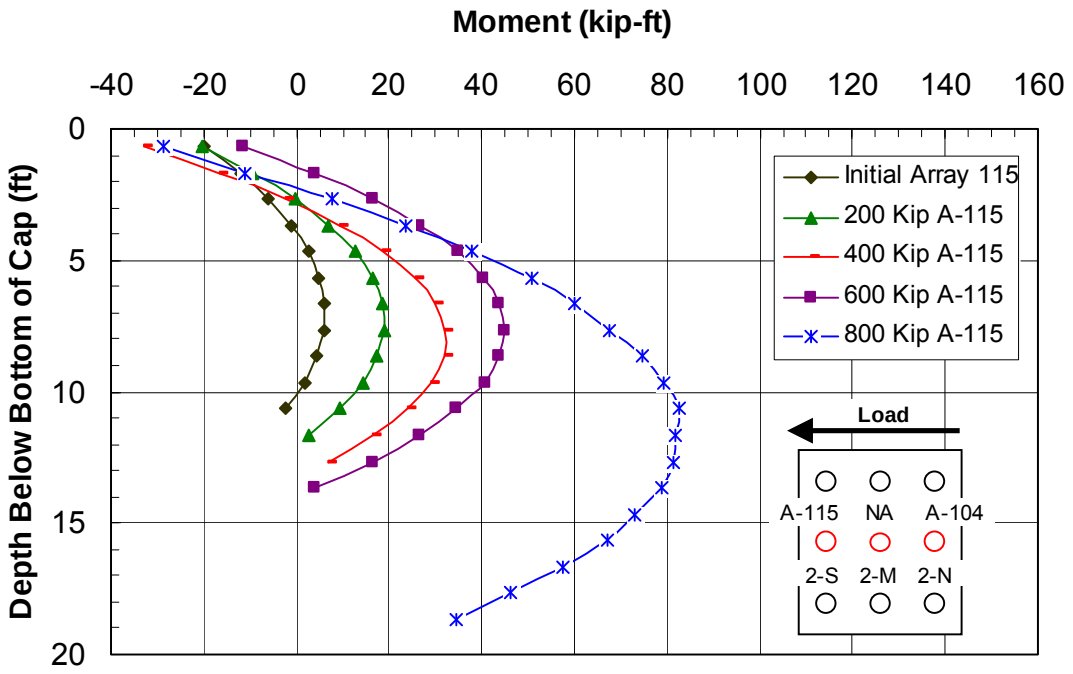

Figure 10-14 Moment vs. depth curve for the south center pile of pile cap 2 (2-S) based on incremental deflection vs. depth curves measured from shape array 115 during test 4.

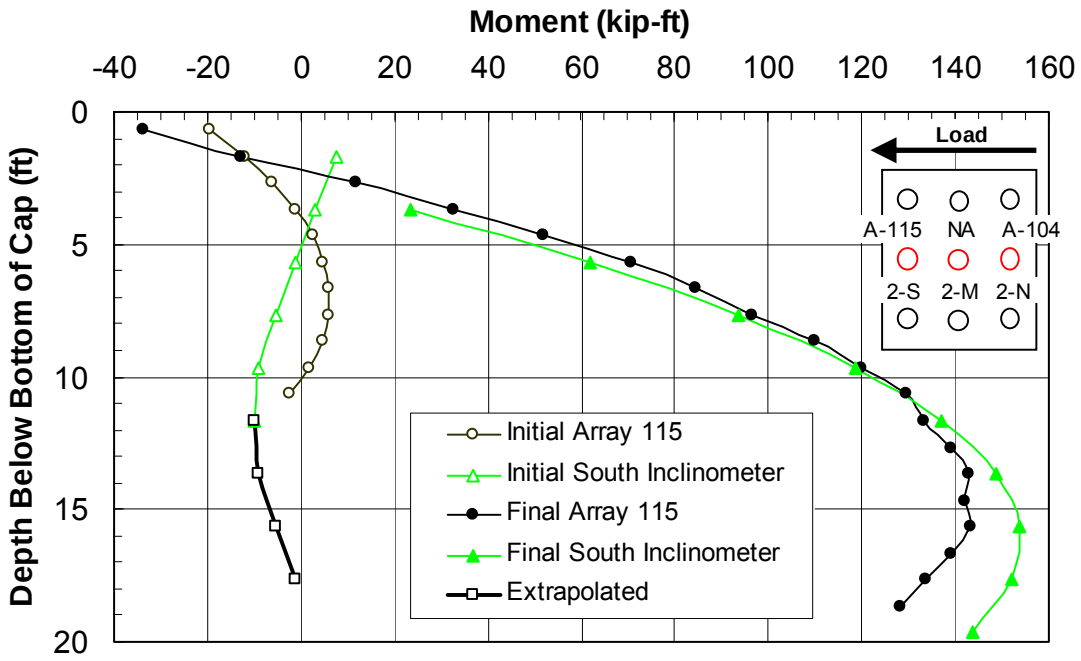

Figure 10-15 Moment vs. depth comparison for the south center pile of pile cap 2 (2-S) based on deflections measured from the south inclinometer and shape array 115 during test 4.

Fifth order polynomial curves were used to create each of the bending moment curves in this figure except the initial curve from shape array 134. The initial pile deflection vs. depth curves were only able to be calculated from the south inclinometer of pile cap 1 (see discussion in section 10.3). The maximum initial bending moment from the initial south inclinometer deflection vs. depth curve was negative 24 kip-ft at a depth between 6 to 9 feet. Having a "negative" maximum initial bending moment at depth, means that the initial deflected shape of the pile was opposite to that produced by loading the piles during the test. The maximum bending moment in the south center pile of pile cap 1 (1-S) from the 800 kip load was about 10.5 kip-ft, and acted at a depth range of 12-13 feet.

The maximum bending moment from the shape array 134 deflections measured during the extended 800 kip loading was 13.5 kip-ft acting at a depth of 13-14 feet. The maximum inclinometer-based bending moment was 4 kip-ft at a depth of 13-15 feet. In summary, the test results suggest that a maximum bending moment range for the final loading was between 5-15 kip-ft and occurred within a depth range of 12 to 15 ft. Once again, the depth to the maximum positive bending moment increased with increasing applied load during this test. It should be noted that the bending moment vs. depth curve for the 200 kip test increment does not follow the trends of the other bending moment vs. depth curves generated for this test. However, the location and value for the maximum positive bending moment are comparable to the other tests. This may be caused by errors in small deflections from the shape array.

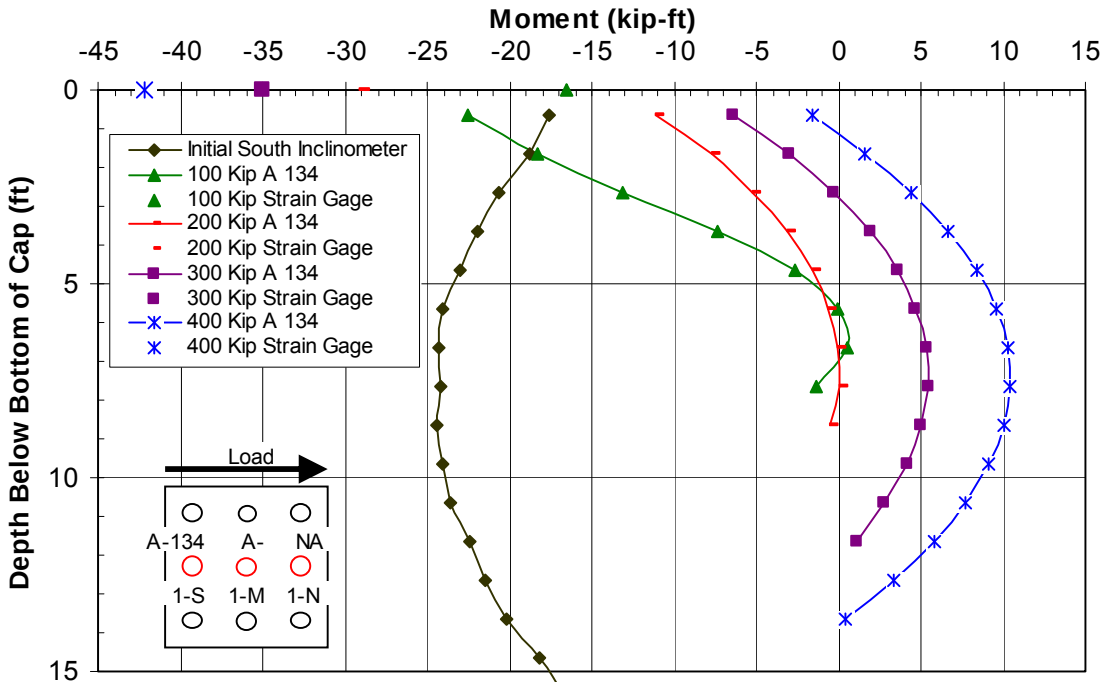

Figure 10-16 Moment vs. depth curve for the south center pile of pile cap 1 (1-S) based on incremental deflection vs. depth curves measured from shape array 134 during test 4, with point moments measured from strain gages at the bottom of the pile cap also shown.

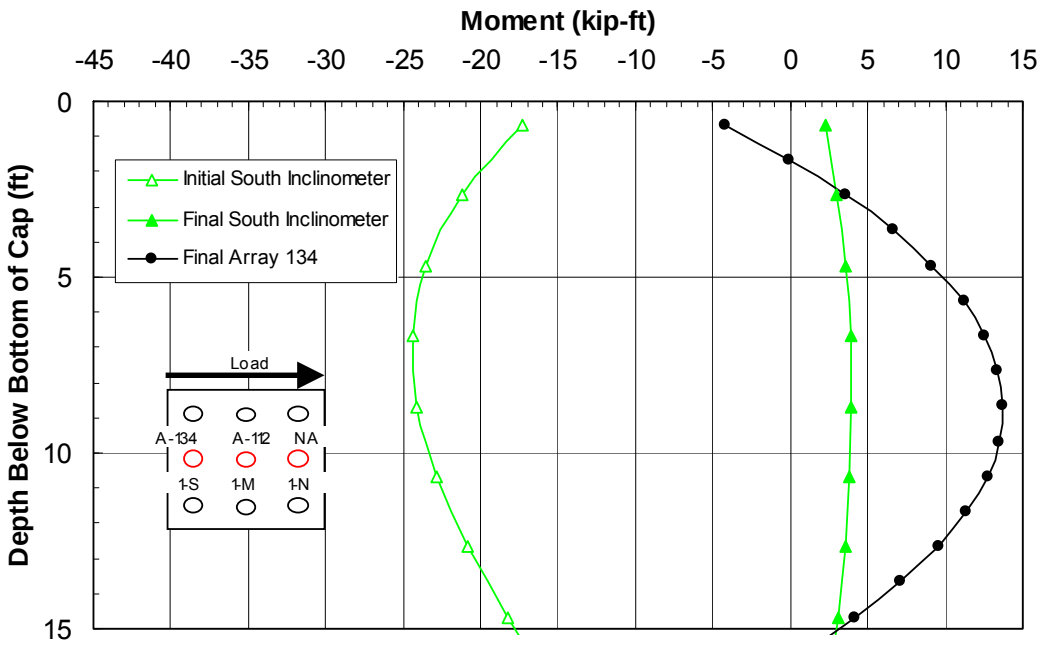

Figure 10-17 Moment vs. depth comparison for the south center pile of pile cap 1 (1-S) based on deflections measured from the south inclinometer and shape array 134 during test 4.

The strain gages generally measure negative bending moments at the pile-pile cap interface which are much greater than those which would be expected by extrapolating the bending moment curves calculated from the shape array and inclinometer measured deflections. The strain gages could have been damaged during installation or during the jet grouting process. Thus, it is very difficult to determine if the bending moments measured from the strain gages are more accurate than the moments calculated from the shape array and inclinometer deflections.

Figure 10-18 displays the bending moment vs. depth curves for the middle center pile of pile cap 1 (1-M) for the load increments of test 4 based on the curves in Figure 10-11(a). A fourth order polynomial curve was used to calculate the bending moment curves for the initial and 200 kip increments. A fifth order polynomial was used for the 400 kip, 600 kip, and 800 kip increments. Figure 10-19 shows the bending

moment vs. depth curves calculated from the inclinometer and shape array 112 deflection vs. depth comparison curves found in Figure 10-11(b). Fifth order polynomial curves were used to create each of the bending moment vs. depth curves in this figure except for the initial curve for shape array 112.

The initial pile depth vs. deflection curves were only able to be calculated from the south inclinometer of pile cap 1 (see discussion in 10.3). Having the deflections zeroed to a different pile (pile 1-N), potentially brings all of the calculated bending moment curves into question. However, the location and magnitude of the maximum positive bending moments are consistent with those measured in pile 1-S. The maximum initial bending moment from the initial south inclinometer deflections was a -24 kip-ft at a depth between 6-9 feet. The maximum positive bending moment pile 1-M from

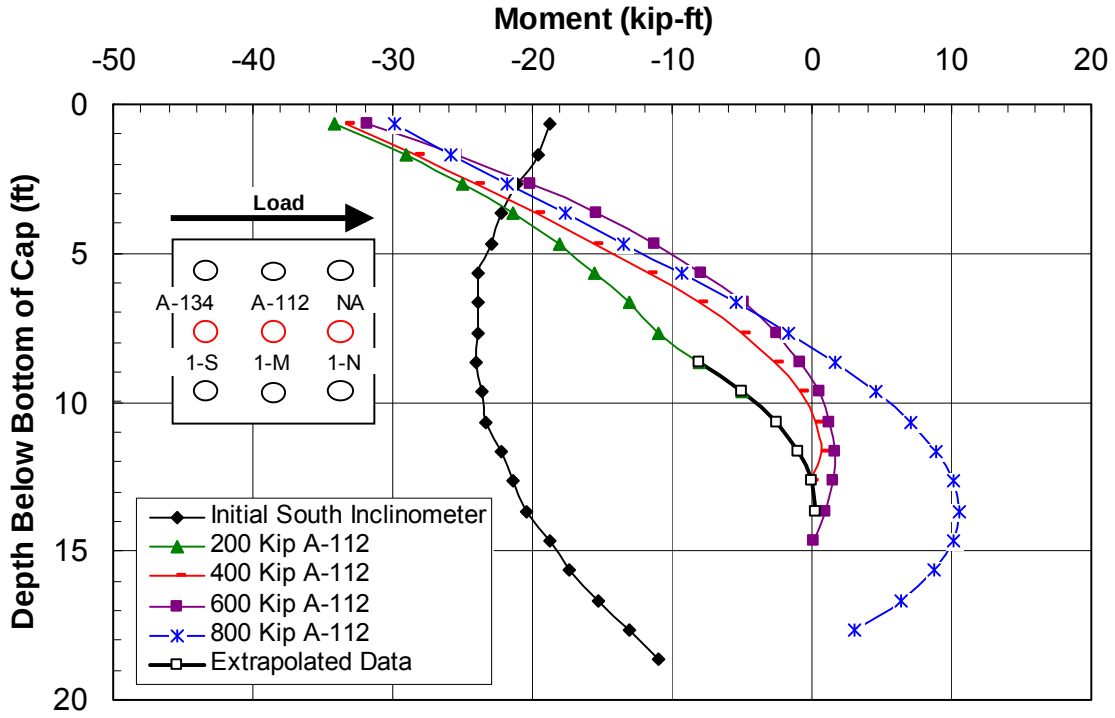

Figure 10-18 Bending moment vs. depth curve for the middle center pile of pile cap 1 (1-M) based on incremental deflection vs. depth curves measured from shape array 112.

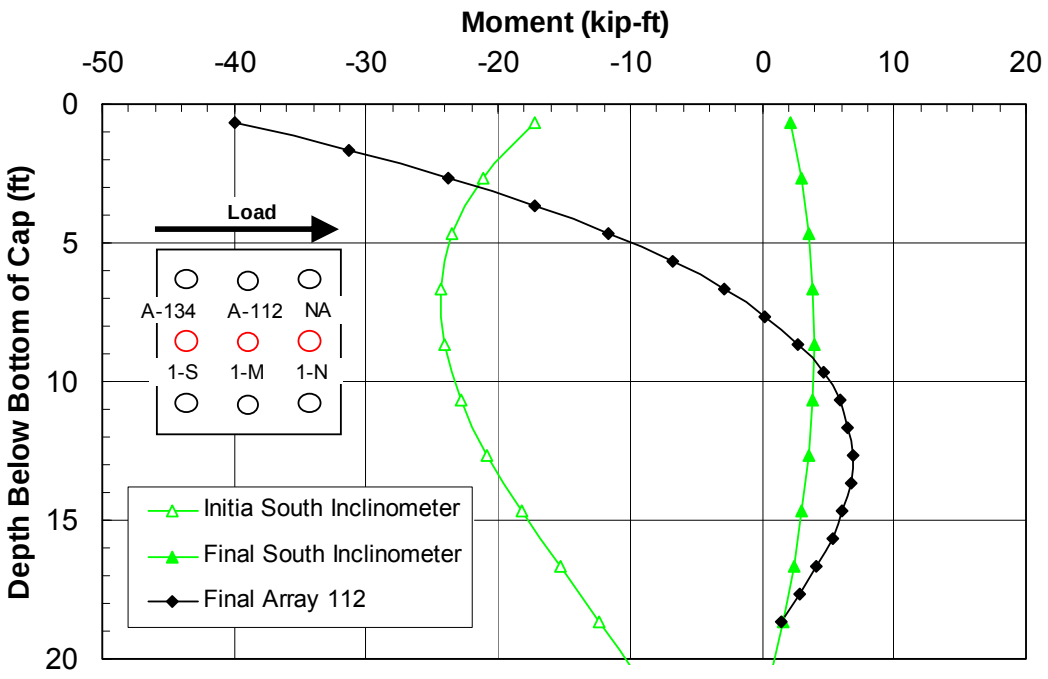

Figure 10-19 Moment vs. depth comparison for the middlecenter pile of pile cap 1 (1-M) based on deflections measured from the north inclinometer and shape array 112 for test 4.

the initial 800 kip load was about 10.5 kip-ft, located at a depth range of 13-15 feet. The maximum bending moment from the shape array 112 deflections measured during the extended 800 kip loading was 8 kip-ft acting at a depth of 13-14 feet.

The maximum inclinometer-based bending moment for the extended load was 4 kip-ft at a depth of 12-14 feet. In summary, the test results suggest that the maximum bending moment range for the extended loading was between 5-15 kip-ft and occurred with a depth range of 12-15 ft. The depth to the maximum positive bending moment increased only slightly with increasing applied load during this test. The bending moments measured from the strain gages attached to pile cap 1-M did not appear to give reasonable results; and have not been included in the following figures.

11 Test 5 – Jet Grout - Excavated Test I

In test 5, pile cap 2 and pile cap 3 were pulled together. Prior to testing, the volume of soil extending approximately 1 ft from the southern face of pile cap 2 to the depth of the pile cap was excavated. The excavation extended the entire width of the pile cap. A schematic drawing of the test is shown in Figure 11-1. A detailed profile of the treat soil around pile cap 2 is also shown in Figure 11-2. Only the results associated with the deflection of pile cap 2 will be given in the following section. Just one intermediate test was performed between test 4 and test 5. This test involved pushing pile cap 2 to the north about 0.5 inches (from -0.65 to -.15 inches) and pile cap 3 to the south, and was performed on the same day as test 5. Thus, prior to the beginning of test 5, pile cap 2 had been displaced three times in the north direction and twice in the south direction since the beginning of test 3. The jet grout columns placed below pile cap 2 had cured for 32 days. The design strength was approximately 250 psi, with a mean laboratory strength of 625-650 psi (Figure 5-9). The instrumentation for pile cap 2 used during this test was not changed from test 4. Test 5 followed standard testing procedures, except that this test was the second of two tests performed between pile caps 2 and 3 on the same day. Initial measurements were not taken between the two tests. Thus, initial pile cap displacement, pile deflection and actuator load measurements are based on the conditions before the beginning of intermediate test.

11.1 Load vs. Deflection

Continuous plots of applied actuator load vs. deflection of pile cap 2 for this test are shown in Figure 11-3. This plot provides the load path taken during loading, unloading and reloading for each cycle. At the end of each of the loading cycles, it was necessary to apply a tensile force to bring each of the actuators' deflections back to the initial actuator position. It appears that the tensile force needed to bring pile cap 2 back to its original position was due to yielding in the piles caused by a lateral pile head displacement of nearly 4 inches during test 4. The reload curve appears to follow the same trends as the reload curves for the virgin tests. The peak load during reloading is about 90% of the peak load during the initial loading.

Figure 11-4 is a plot of peak pile cap load vs. displacement for each test increment. The initial displacement of pile cap 2 during the test was 0.68 inches. This offset indicates that the pile cap was already displaced 0.68 inches in the direction of loading before the test began. The target deflections for the 6 test increments in this test were 0.125, 0.25, 0.5, 0.75, 1.0, and 1.25 inches from the initial displacement. The actual pile cap displacements were 0.1, 0.24, 0.44, 0.72, 1.05, and 1.31 inches. It can be seen that there was also an initial load of 44 kips exerted on the pile cap before the test began. This was the result of zeroing the actuator deflection following the intermediate test, which pushed pile caps 2 and 3 apart. The force needed to bring the actuator back to the position it was in before the intermediate test was 44 kips. The slope of the load-deflection curve in Figure 11-4 for pile cap 2 remained relatively constant throughout the test. This suggests that the soil in front of the foundation did not reach a failure state.

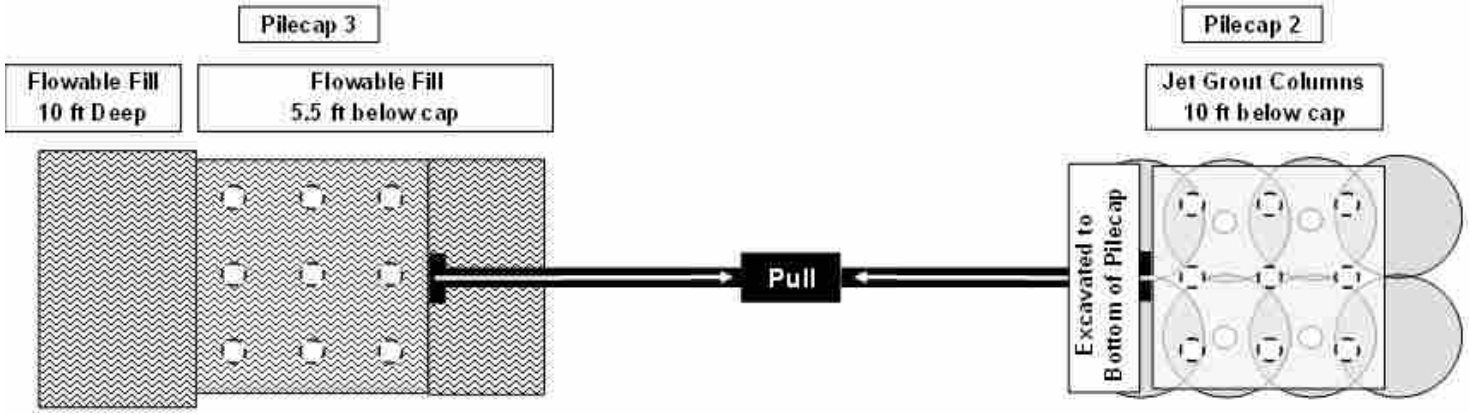

Figure 11-1 Schematic plan view of test 5.

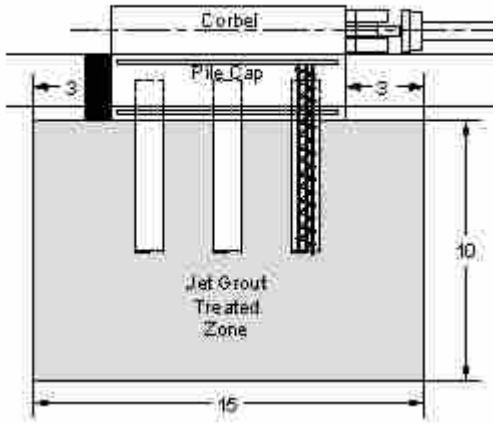

Figure 11-2 Detailed profile view of the treated soil on pile cap 2 during test 5 with the excavated area is shaded in black.

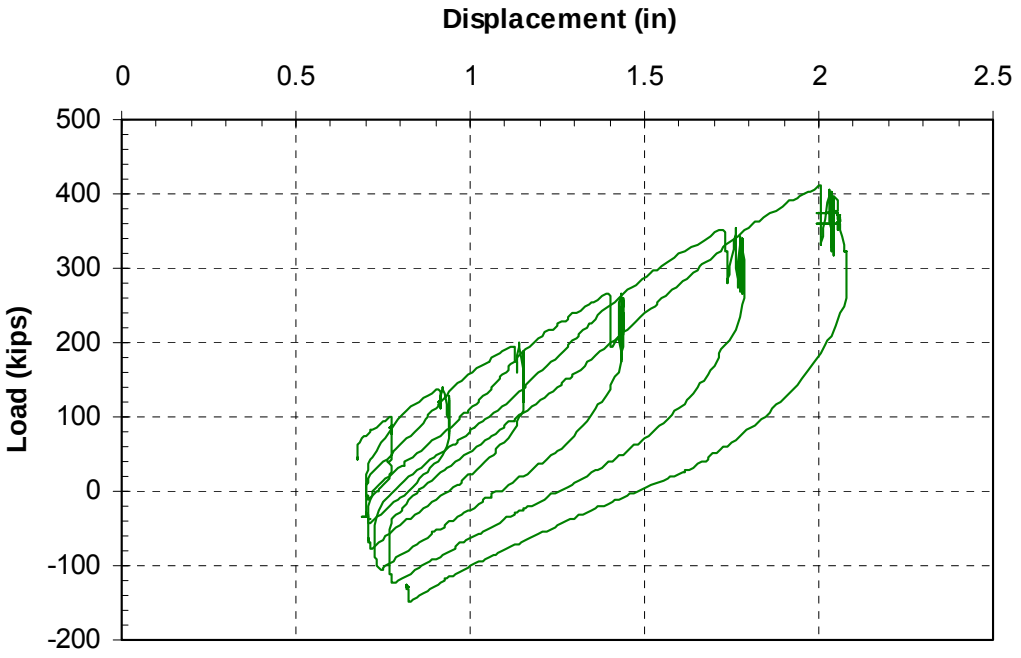

Figure 11-3 Plot of continuous pile cap displacement vs. applied load for pile cap 2 during test 5.

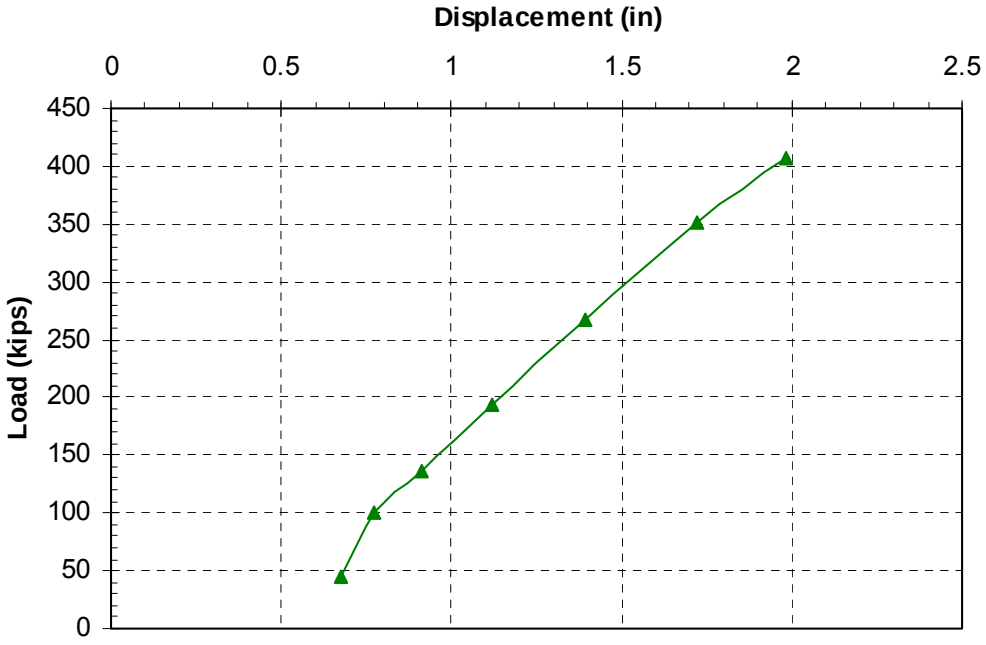

Figure 11-4 Plot of pile cap 2 displacement vs. peak applied load for each increment of test 2.

11.2 Pile Head Rotation vs. Load

Pile head rotation vs. load curves based on the shape array and string potentiometer measurements for pile cap 2 during test 5 are provided in Figure 11-5. Rotation was measured from the string potentiometers located directly above the corbel of pile cap 2. Refer to Figure 4-11 for a review on the position of the string pots on pile cap 1. The location of the string potentiometers and shape arrays had not changed from test 4. The pile cap was initially rotated in the same direction as that induced by loading, as indicated by the initial positive rotation. The rotations from the string potentiometers and the shape arrays follow the same general trend as the rotations measured during test 4. The rotations measured from the string potentiometers and shape array 104 differ by only 0.02-0.04 degrees throughout the test.

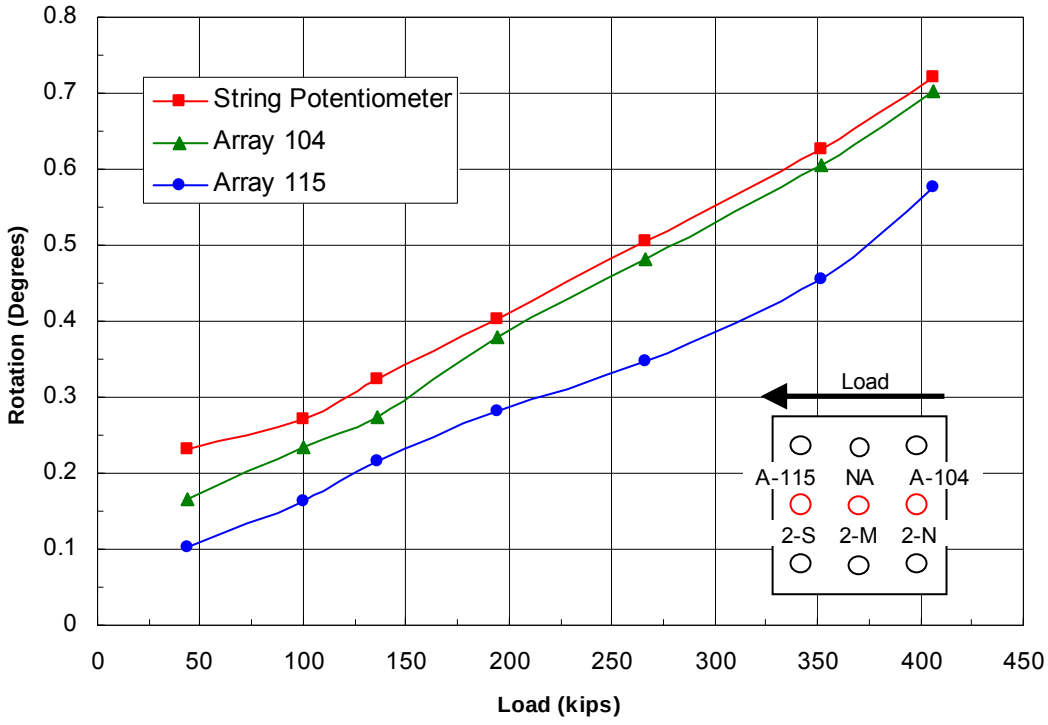

Figure 11-5 Peak pile cap load vs. pile head rotation for pile cap 2 during test 5 obtained from string potentiometer and shape array measurements.

Shape array 115 measures rotations which are consistently between 0.10 and 0.15 degrees lower than those measured by the string potentiometers. The difference in rotation measurements may come because the string potentiometers are measuring rotation over a much longer distance than the shape arrays. Just as with the previous tests, the major difference in measured rotations between the various instruments comes in the initial rotation measurement. The rotations induced during the test are basically the same for the string potentiometers and shape arrays.

11.3 Pile Deflection vs. Depth

The shape array placement for pile cap 2 did not change from test 4. Figure 11-6(a) displays the incremental deflection profiles of the north center pile of pile cap 2 (2-N) measured from shape array 104 during test 5. The initial deflection reading of the shape arrays at the loading point was 0.49 inches, while the initial string potentiometer reading was 0.66 inches. This is a difference of about 30%, which is quite large. However, the deflections measured from the shape arrays from the larger testing increments are comparable with the string potentiometer readings. For the final four testing increments, the greatest difference in measurements from the string potentiometers and shape arrays was 0.08 inches. This equates to a difference of 4%. Figure 11-6(b) shows a comparison of pile 2-N deflection vs. depth curve measured from shape array 104 and from the north inclinometer. The initial readings from the north inclinometer and shape array differ. The shape array measured an initial deflection at the point of loading of 0.49 inches, while the inclinometer measured a deflection of 0.72 inches. The inclinometer deflection is consistent with the

measurement from the string potentiometers. This same behavior was exhibited in test 4. Measurements from shape array 104 seem to not be consistent with the initial measurements from both the inclinometers and string potentiometers. However, at larger pile cap displacements the measurements from the shape array are comparable with those from the other instruments. Also, the curvature of the shape array and inclinometer deflection vs. depth curves is very similar until a depth of 5 feet below the top of the corbel. This depth is the approximate depth of the pile-pile cap interface. This could be the reason for the sudden shift in the shape array data.

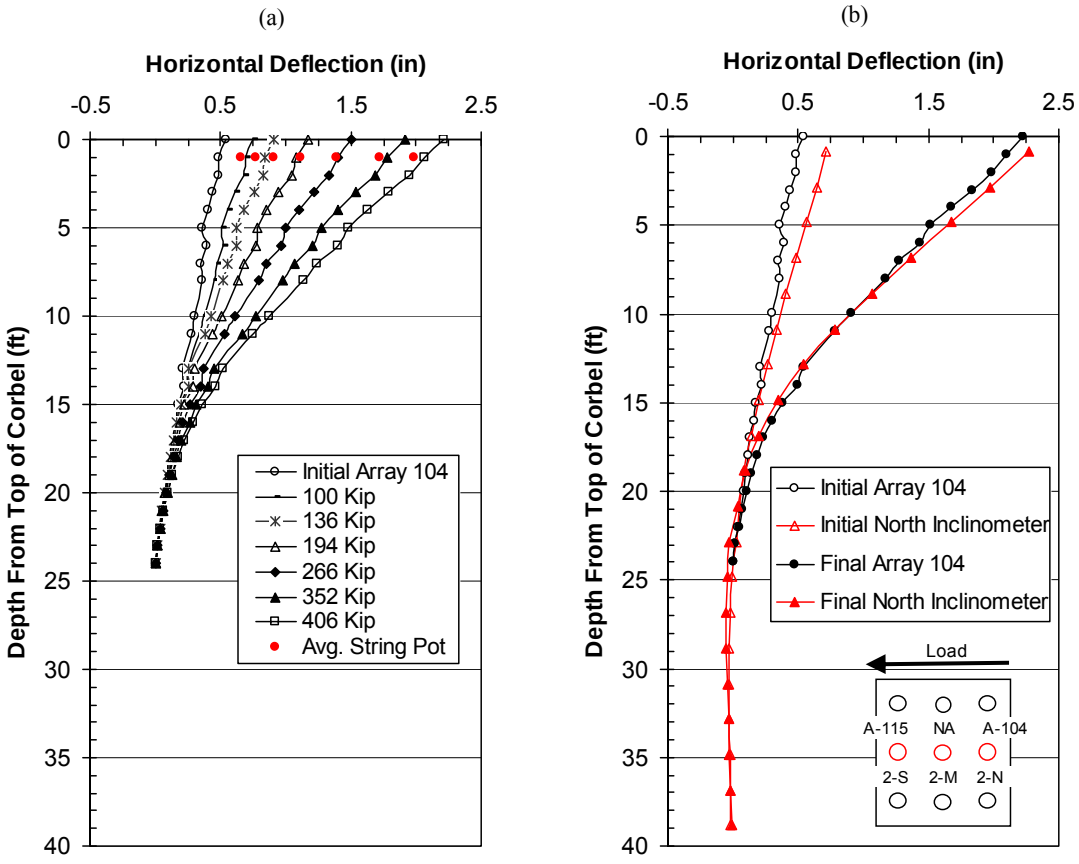

Figure 11-6(a) Deflection vs. depth curve for the north center pile of pile cap 2 (2-N) from shape array 104 for each increment of test 5, with pile head displacements from the string potentiometers also shown (b) Comparison of depth vs. deflection curves for pile 2-N from shape array 104 and the north inclinometer in pile cap 2 during test 5.

Figure 11-7(a) displays the incremental deflections of the south center pile of pile cap 2 (2-S) measured from shape array 115 during test 5. The deflections from shape array 115 shown in Figure 11-7 have been reduced by 15% from the original deflections measured from the shape arrays. During the process of data reduction, the deflections measured by shape array 115 were found to consistently measure deflections at the load point which were 15% larger than those measured by the string potentiometers. This exact trend proved to be true for the last five tests, which were all performed on the same day.

Also, as can be seen in Figure 11-7(b), reducing the deflections by 15% does not too adversely affect the agreement of the shape array curve with the curve generated from the south inclinometer. Incomplete connection of the shape array to the computer ports could be the reason for the deflections measured by shape array 115 being 15% larger than actual for the final five tests. The greatest difference in measurement between the corrected shape array 115 and the string potentiometers was 0.14 inches, which occurred during the first loading increment of test 5.

This difference is quite large; however, for the final 5 testing increments the greatest difference was only 0.03 inches, which equals a difference between 2-3%. In Figure 11-7(b), the inclinometer curve matches the curve from the shape array from a depth of 10 to 24 feet below the pile cap. Above 10 feet, the curves separate. This could be due to concrete in the piles crushing, which could cause a gap between the inclinometer and shape array casings in pile 2-S during the test. Inclinometers have been proven to work well for downhole pile applications. Therefore, the profile from the inclinometers is assumed to be most accurate.

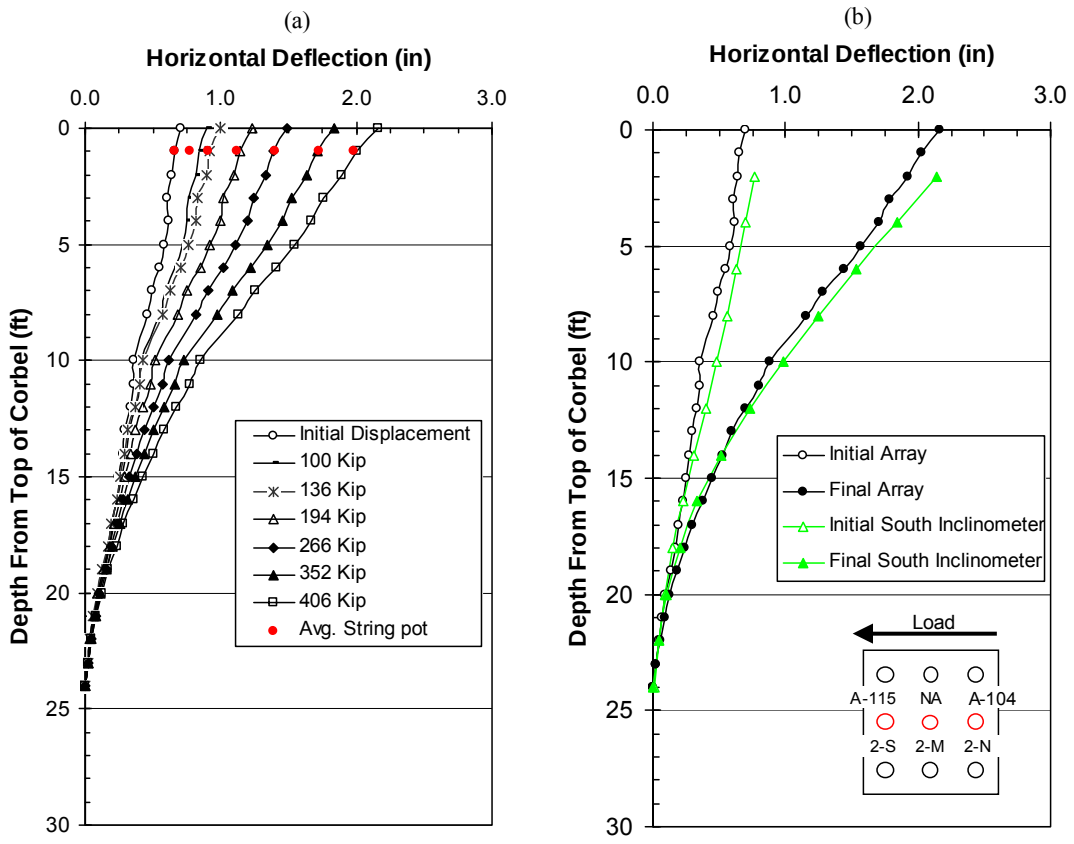

Figure 11-7(a) Deflection vs. depth curve for the south center pile of pile cap 2 (2-S) from shape array 115 for each increment of test 5, with pile head displacements from the string potentiometers also shown (b) Comparison of depth vs. deflection curves for pile 2-N from shape array 115 and the north inclinometer in pile cap 2 during test 5 (The deflections measured by shape array 115 are all reduced by 15%).

11.4 Pile Bending Moment vs. Depth

Figure 11-8 displays the bending moments for the north center pile of pile cap 2 (2-N) during test 5. The bending moment curves were generated from the pile deflection profiles displayed in Figure 11-6(a). Fifth order polynomial curves were fit to the displacement vs. depth curves measured from shape array 104 for each of the increments of test 5. Inclinometer and shape array 104 readings were taken after the final loading increment was held for an extended period of time. Figure 11-9 displays the bending moments calculated from the comparison pile deflection profiles provided

in Figure 11-6(b). Fourth order polynomial curves were fit to the deflection profiles generated from the north inclinometer for both the initial measurement and final loading.

The initial bending moments calculated from the shape array 104 deflections give a maximum initial bending moment of positive 10 kip-ft at a depth of 13-14 feet below the bottom of the pile cap; the bending moments from the inclinometer deflections yield a maximum initial moment of positive 18 kip-ft at a depth of 15 feet below the bottom of the pile cap. These results are very comparable, and define a good range of initial bending moments in the pile. The maximum positive bending moment in pile 2-N from the initial 406 kip loading increment was 83 kip-ft, and acted at a depth range of 12.5-13.5 feet below the pile cap. The maximum positive bending moment from the shape array 104 deflections measured during the extended loading was 82 kip-ft acting at a depth of 19 feet below the pile cap. The maximum inclinometer-based bending moment for the extended loading was 72 kip-ft at a depth of 12 feet below the pile cap. The recommended range for maximum positive bending moments is 70-80 kip-ft, acting 12-15 feet below the pile cap. Nearly all of the wires coming from the strain gages in pile cap 2 were damaged during burial, or were damaged during the jet grouting process. The only remaining working strain gage was at the pile-pile cap interface in the north center pile of pile cap 2 (2-N). The maximum negative moments calculated from the strain gages in Figure 11-8 seem to be producing negative moments which are too low to fit the bending moment curves generated in the same figure. This could be due to damage to the strain gages during pile driving, or damage to the strain gage connection some time during testing or the jet grouting process.

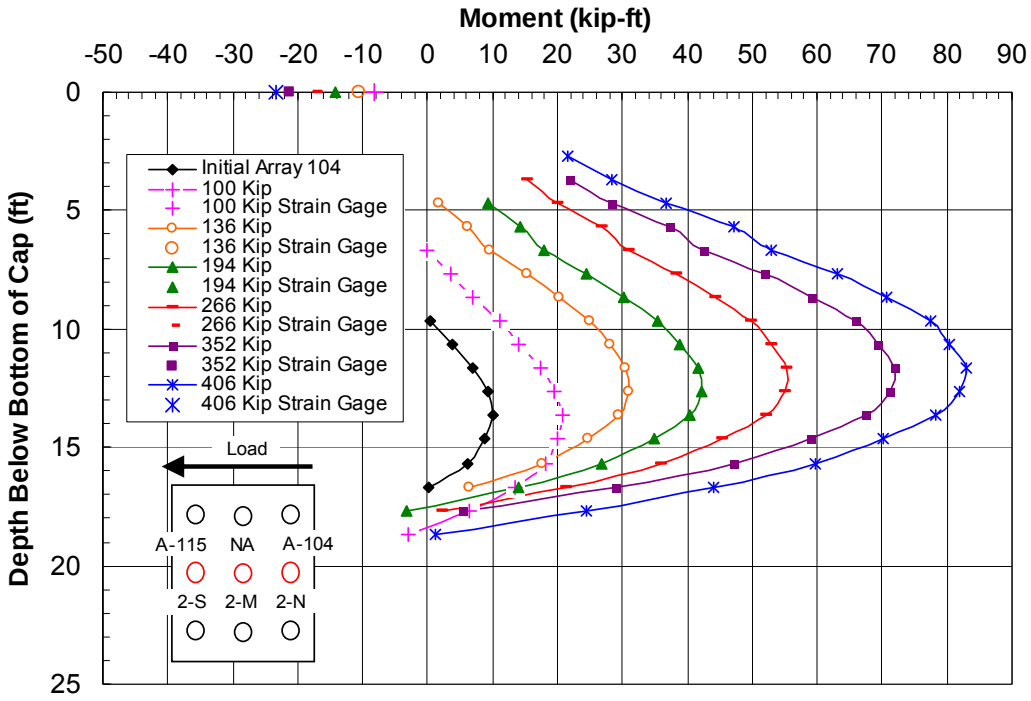

Figure 11-8 Test 5 moment vs. depth curve for the north center pile of pile cap 2 (2-N) based on incremental deflection vs. depth curves measured from shape array 104 during test 5.

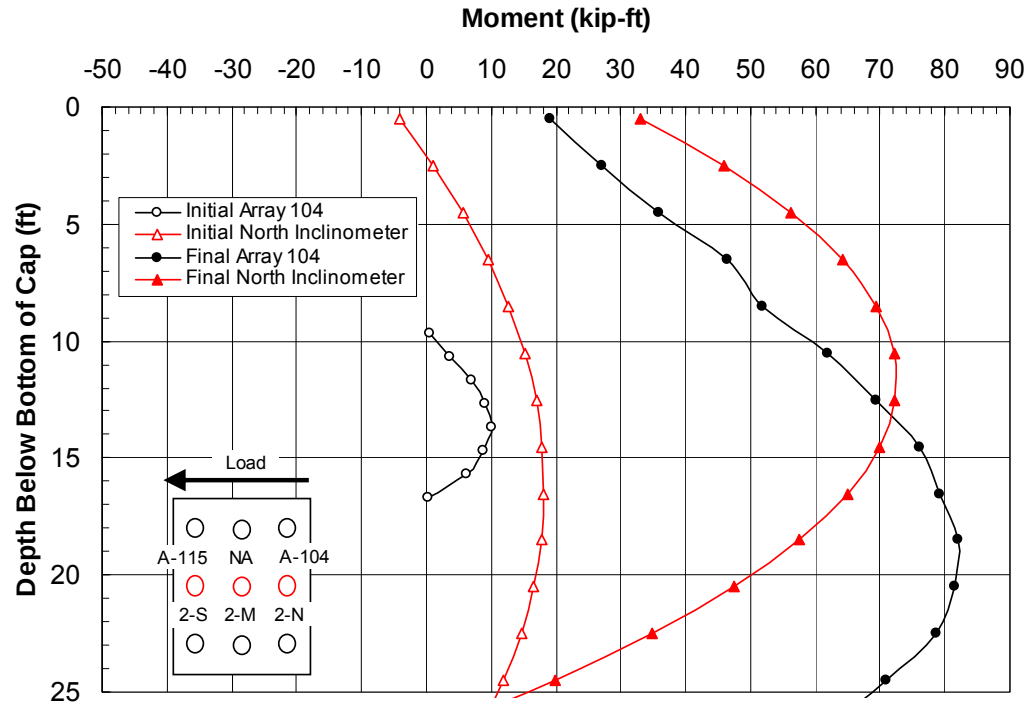

Figure 11-9 Moment vs. depth comparison for the north center pile of pile cap 2 (2-N) based on deflections measured from the north inclinometer and shape array 104 for test 5.

Figure 11-10 displays the bending moments for the middle center pile of pile cap 2 (2-M) during test 5. The bending moment curves were generated from the deflection profiles in Figure 11-7(a). Inclinometer and shape array 104 readings were taken after the final loading increment was held for an extended period of time. Figure 11-11 displays the bending moments calculated for the north inclinometer and shape array 104 from the deflection profiles Figure 11-7(b). Fourth order polynomial curves were fit to the displacement vs. depth curves used to generate all of the bending moment curves in both of the following figures.

The initial bending moments calculated from the shape array 115 deflections give a maximum initial bending moment of positive 10 kip-ft at a depth of about 9 feet below the bottom of the pile cap; the bending moments from the inclinometer deflections yield a maximum initial moment of negative 9 kip-ft at a depth of 7 feet below the bottom of the pile cap. The results from the shape array 115 more closely match the initial bending moment results for pile 2-N for this test, and are assumed to be more accurate. A recommended range of initial bending moments is between 10-15 kip-ft acting at a depth of about 10 feet below pile cap 2. The maximum positive bending moment in pile 2-M from the initial 406 kip loading increment was 67 kip-ft, and acted about 10 feet below the pile cap. The maximum positive bending moment from the shape array 104 deflections measured during the extended 406-kip loading was also 67 kip-ft acting at a depth of 10 feet below the pile cap. The maximum inclinometer-based bending moment for the extended loading was 79 kip-ft at a depth of 12-13 feet below the pile cap. The recommended range for maximum positive bending moments is 65-80 kip-ft, acting between 10-13 feet below the pile cap.

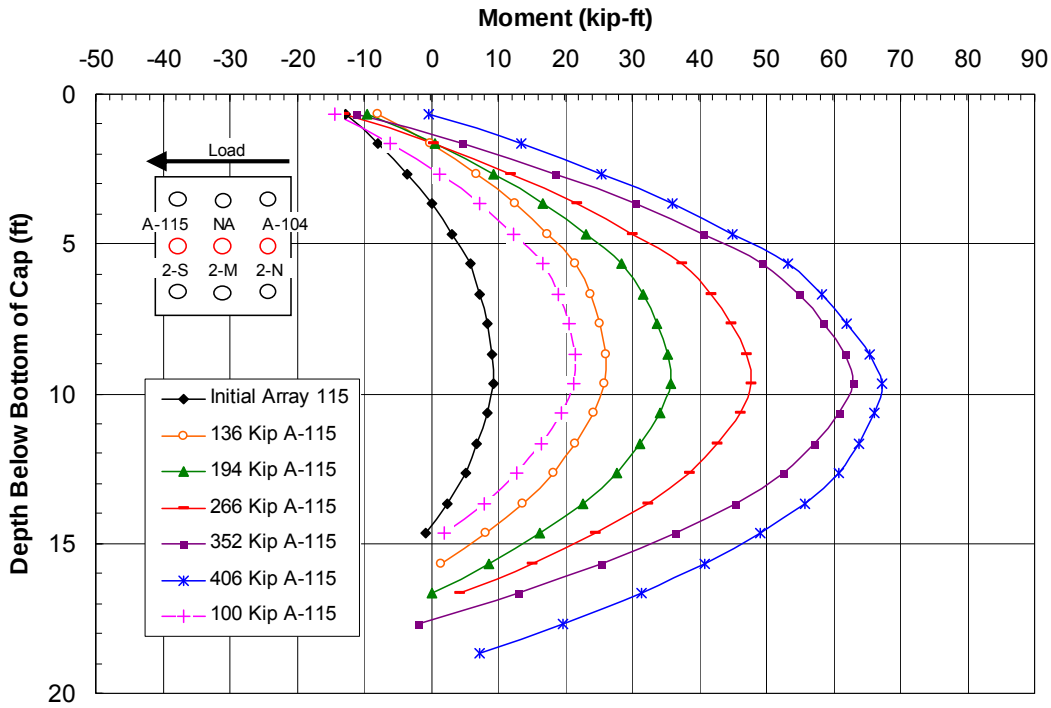

Figure 11-10 Moment vs. depth curve for the south center pile of pile cap 2 (2-S) based on incremental deflection vs. depth curves measured from shape array 115 during test 5.

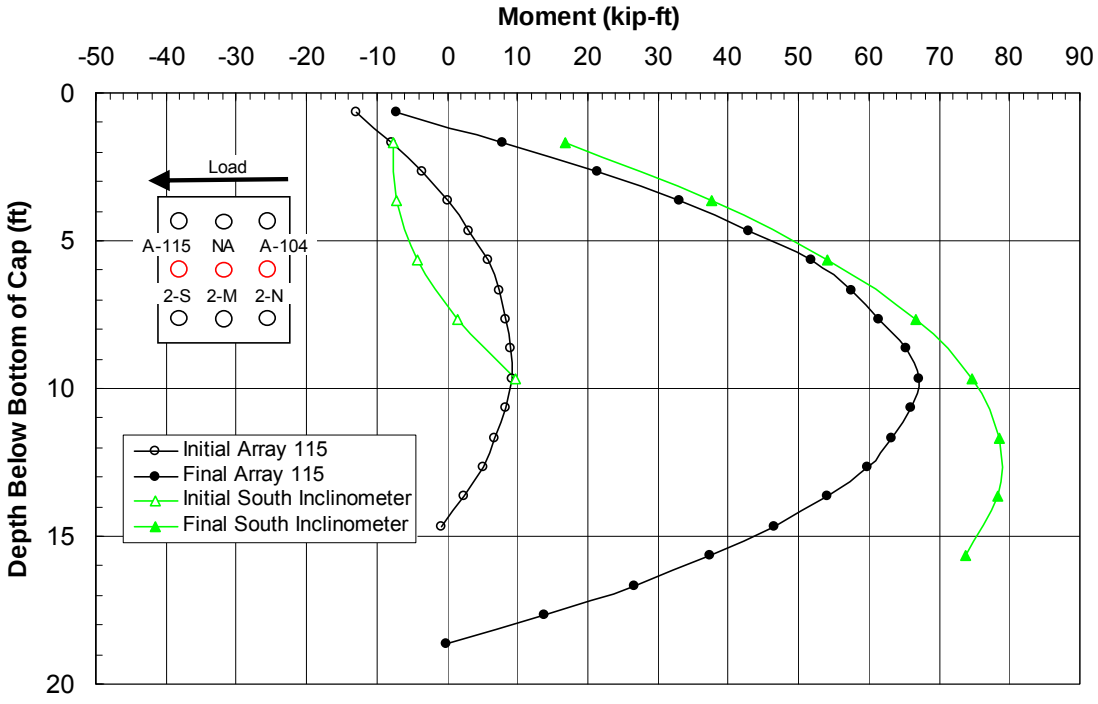

Figure 11-11 Moment vs. depth comparison for the south center pile of pile cap 2 (2-S) based on deflections measured from the north inclinometer and shape array 115 for test 5.

12 Test 6 – Jet Grout – Excavated Test II

During test 6, pile cap 2 was pushed to the south and pile cap 1 was pushed to the north. Thus, since installation of the jet grout columns, pile cap 1 had been displaced twice to the north and once to the south; and pile cap 2 had been displaced 3 times to the north and 3 times to the south. A volume of soil, similar to that excavated from the south side of pile cap 2, was also excavated from the north side of pile cap 1. A schematic of test 6 is shown in Figure 12-1. A detailed profile view of the treated soil around pile caps 1 and 2 is displayed in Figure 12-2. There were no intermediate tests performed between test 5 and test 6. Test 6 was the first of three tests which were performed on pile caps 1 and 2 on the same day. Test 6 was also performed on the same day as test 5. Therefore, test 6 was the third of five tests performed on pile cap 2 in the same day.

Just as in test 4, the shape arrays placed in the piles of pile cap 1 were extracted and reinserted before test 6 began. The initial position of the south inclinometer in pile cap 1 was once again used as the initial position for each of the shape arrays. Test 6 followed standard testing procedures, except that inclinometer readings were not taken during the final loading. The maximum possible actuator load (~600 kips) was applied to the pile caps during the final two loading increments, and inclinometer readings were not taken during this loading because it was deemed unsafe to hold the maximum load

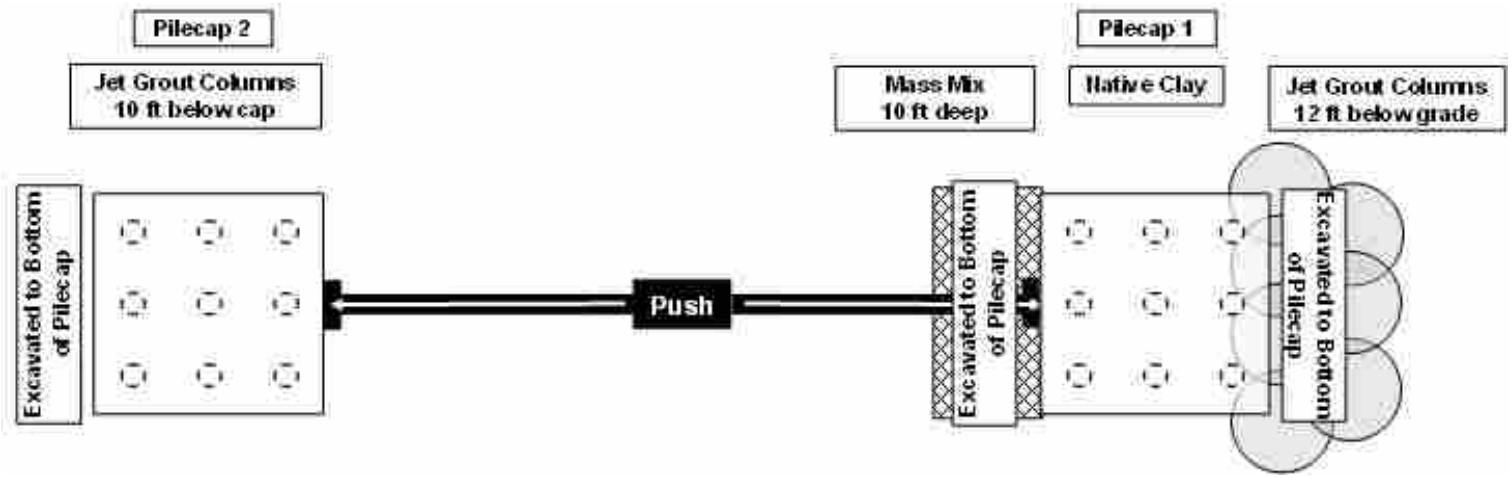

Figure 12-1 Schematic plan view of test 6.

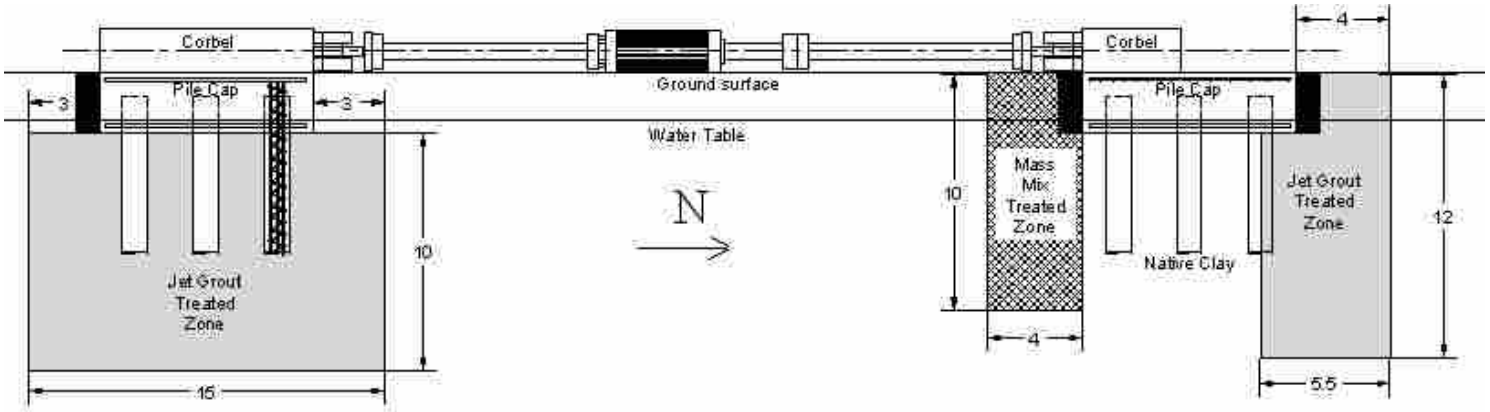

Figure 12-2 Detailed profile view of the treated soil on pile cap 2 (left) and pile cap 1 (right) during test 6; with the black areas adjacent to the pile caps representing the excavated areas.

for an extended period of time. Also, the initial measurements for pile caps 1 and 2 were taken at different times. The initial pile cap 2 displacement and pile deflection used for test 5 was also used for this test. The initial measurements for pile cap 1 were taken before the beginning of this test. The design strength of the soilcrete columns placed below pile cap 2 and adjacent to pile cap 1 was approximately 250 psi, with a mean laboratory strength of 625-650 psi (Figure 5-9).

12.1 Load vs. Displacement

Continuous plots of applied actuator load vs. deflection of pile caps 1 and 2 for this test can be found in Figure 12-3 and Figure 12-4. This plot provides the load path taken during loading, unloading and reloading for each increment of test 6. At the end of each of the loading increments it was necessary to apply a tensile force to bring the actuator deflection back to the initial actuator position. In pile cap 1 this does not appear to be a result of yielding in the pile, because of the measured bending moments from this and previous tests. The behavior could result from a flow of weak soil into the gap behind the pile during loading; however the flow of soil would have been inhibited by the volume of mass mix treated soil on the south side of the pile cap. Lateral resistance due to side shear on the piles as they move in the opposite direction is the most likely reason for the need to apply a tensile force to bring the actuator deflection back to its initial position. The tensile force needed to bring pile cap 2 back to its original position was due to yielding in the piles caused by a lateral pile cap displacement of nearly 4 inches during test 4. For each of the curves, it can be seen that each of the pile caps displace a great deal during the final two loading cycles. This indicates that the soil is at

or near failure around both of the foundation. It can be seen that the pile cap displaced nearly 0.1 inches with no increase in load during the final loading increment. The final displacement value of the last loading increment is used in subsequent analysis.

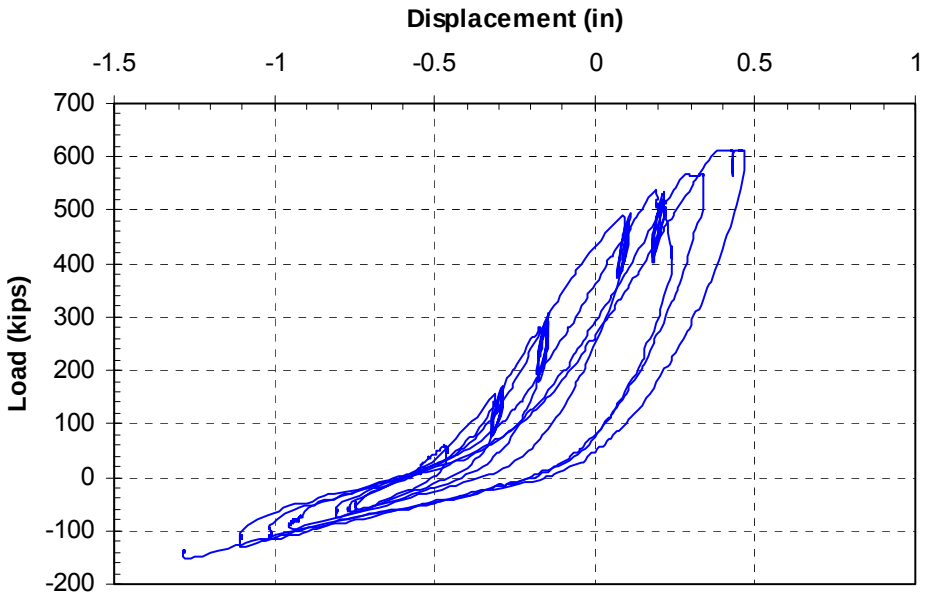

Figure 12-3 Plot of continuous pile cap displacement vs. applied load for pile cap 1 during test 6.

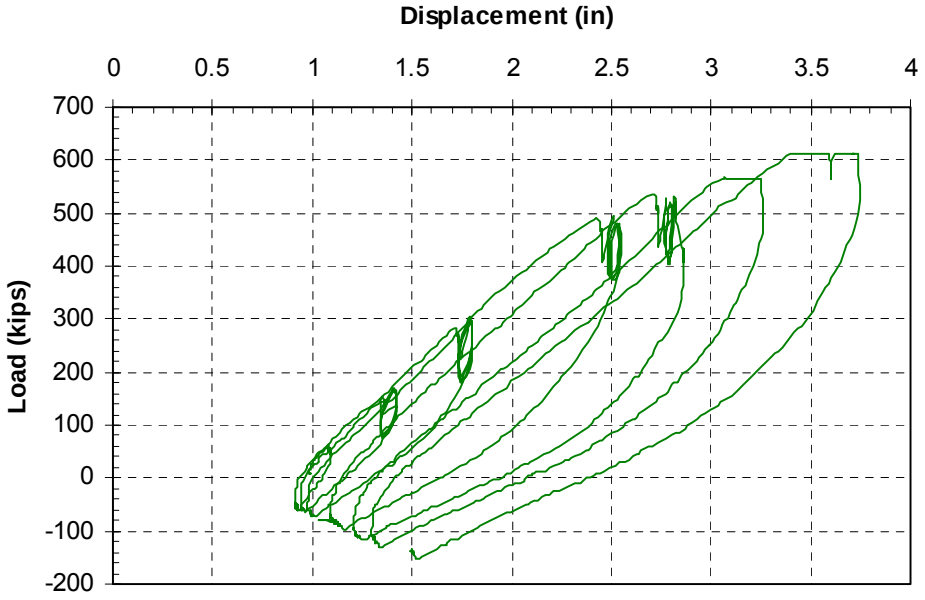

Figure 12-4 Plot of continuous pile cap displacement vs. applied load for pile cap 2 during test 6.

Plots of pile cap deflection vs. peak actuator load for pile caps 1 and 2 for this test can be found in Figure 12-5. The initial displacement of pile cap 2 was a positive 0.99 inches. Pile cap 1 was initially displaced a negative 0.55 inches, indicating it was initially displaced in the direction opposite of loading. The first 5 testing increments for this test were displacement controlled, while the final two testing increments were load controlled. The target displacements for the first 5 test increments in this test were 0.125, 0.25, 0.5, 0.6, 0.75 inches of pile cap 1 displacement. The actual pile cap 1 displacements were 0.08, 0.23, 0.38, 0.63 and 0.74 inches from the initial pile cap 1 location. The final two loadings were load controlled, in an attempt to fail the soilcrete columns adjacent to pile cap 1. The load applied by the actuator for these tests were 567 and 612 kips respectively. It appears that the load-displacement curves for each of the pile caps are displaying initial signs of failure; however, it appears that additional loading was necessary to document complete failure of the soil surrounding the foundations.

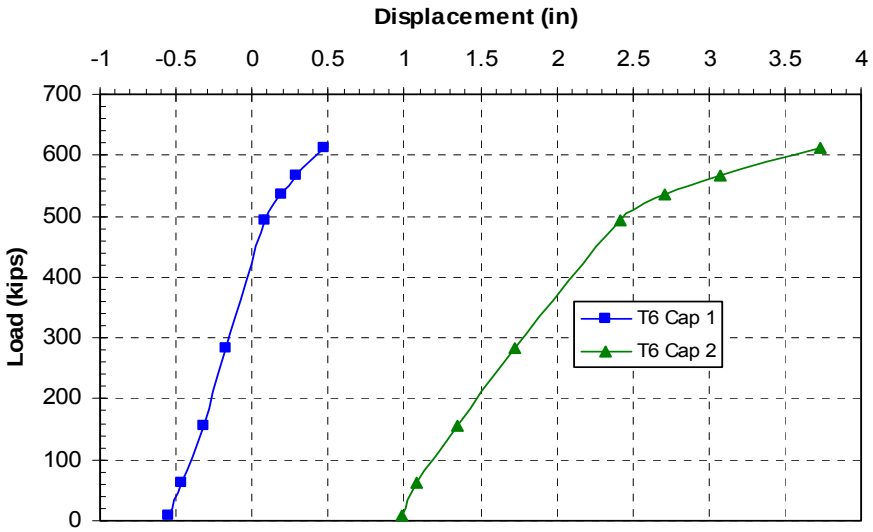

Figure 12-5 Plot of pile cap displacement vs. peak applied load for each increment of test 6.

12.2 Pile Head Rotation vs. Load

Pile head rotation vs. load curves based on the shape array deflections for pile caps 1 and 2 during test 6 are provided in Figure 12-6 and Figure 12-7. Refer to Figure 4-11 for a review on the position of the string pots on the pile caps. The location of the string potentiometers and shape arrays had not changed from the previous tests.

There was no appreciable rotation measured from the string potentiometers on pile cap 1 during this test. Thus, the values are not shown in Figure 12-6. It is assumed that the string potentiometers malfunctioned during this test, because both of the shape arrays in pile cap 1 measured appreciable rotations during test 6. Initially, pile cap 1 was rotated in the direction opposite to that induced through loading. This is indicated by an initial negative rotation value. The rotations measured from the two shape arrays are somewhat different throughout the test; however, the greatest difference in measured rotation is only 0.05 degrees. The discrepancies could have been caused by the smaller distance between the measured nodes of shape array 112.

The string potentiometers and the arrays measured appreciable rotations for pile cap 2. The initial positive rotation value indicates that the pile cap was initially loaded in the direction induced through loading during this test. The rotations measured from the string potentiometers and each of the shape arrays follow the same general trend. However, shape array 104 is shifted down about 0.05 degrees and shape array 115 is shifted down about 0.2 degrees. This initial difference in measured rotation can be seen to be fairly constant throughout the test. Thus, instruments measured similar rotations throughout the test; the only difference in measured rotation came from the difference in initial measurements.

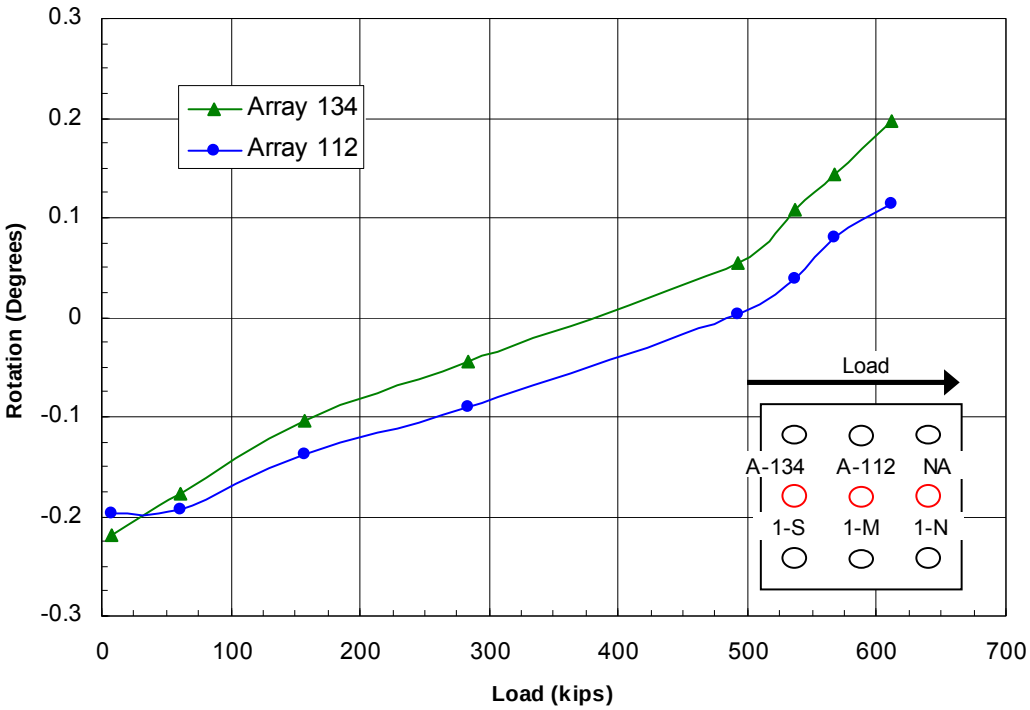

Figure 12-6 Peak pile cap load vs. pile head rotation for pile cap 1 during test 6 obtained from string potentiometer and shape array measurements.

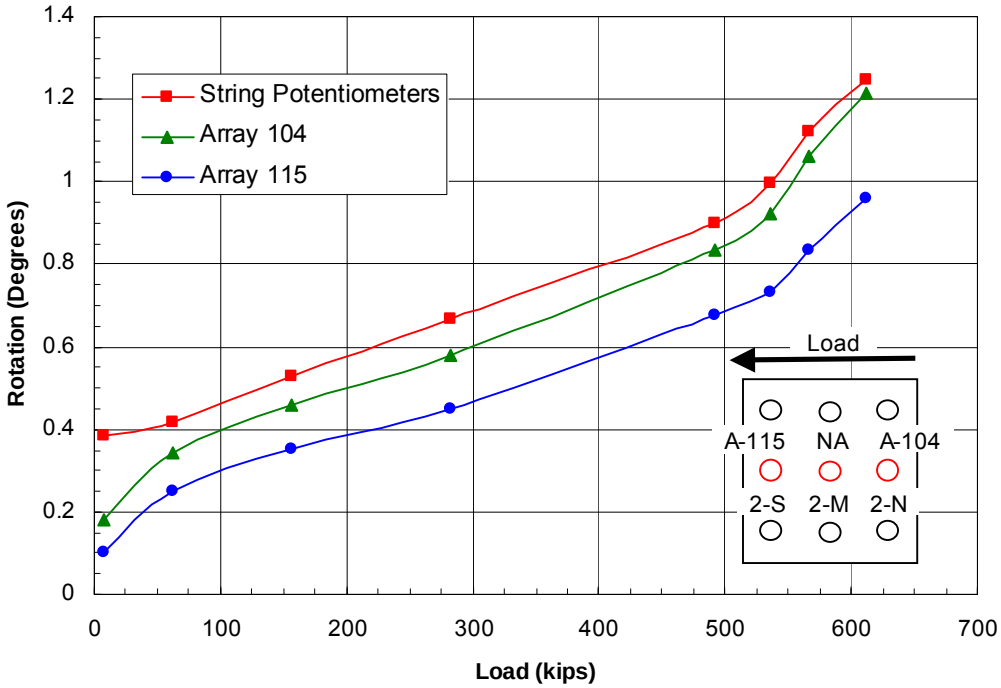

Figure 12-7 Peak pile cap load vs. pile head rotation for pile cap 2 during test 6 obtained from string potentiometer and shape array measurements.

12.3 Pile Deflection vs. Depth

The shape array placement for pile caps 1 and 2 did not change from test 5. However, the shape arrays in pile cap 1 were removed and reinserted prior to the beginning of this test. Figure 12-8(a) displays the incremental deflections of the north center pile of pile cap 2 (2-N) measured from shape array 104 during test 6. The deflections measured by shape array 104 at the elevation of loading are comparable to those measured by the string potentiometers. The initial deflection measurements are the same as those from the previous test, with a 30% difference in measured deflection between the string potentiometers and shape array 104. The deflections measured from the shape arrays from the larger testing increments are much comparable with the string potentiometer readings. The greatest difference in measurement during the 4 subsequent displacement controlled test increments was 0.36 inches, or 12.5%.

For the final two load-controlled testing increments, the greatest difference in measurements from the string potentiometers and shape arrays was 0.28 inches, or 8%. Once again, it is assumed that the string potentiometers are more accurate than the shape arrays. Figure 12-8(b) shows a comparison of the deflection profiles calculated from array 104 and the north inclinometer. The initial readings from the north inclinometer and shape array 104 are the same as those from the previous test, with the initial measurements from the inclinometer matching that string potentiometers initial measurements more closely than shape array 104. However, during the extended final loading increment, the deflection profile from the shape arrays matches the deflection profile from the inclinometers very closely. Once again, the curves separate slightly at the pile-pile cap interface.

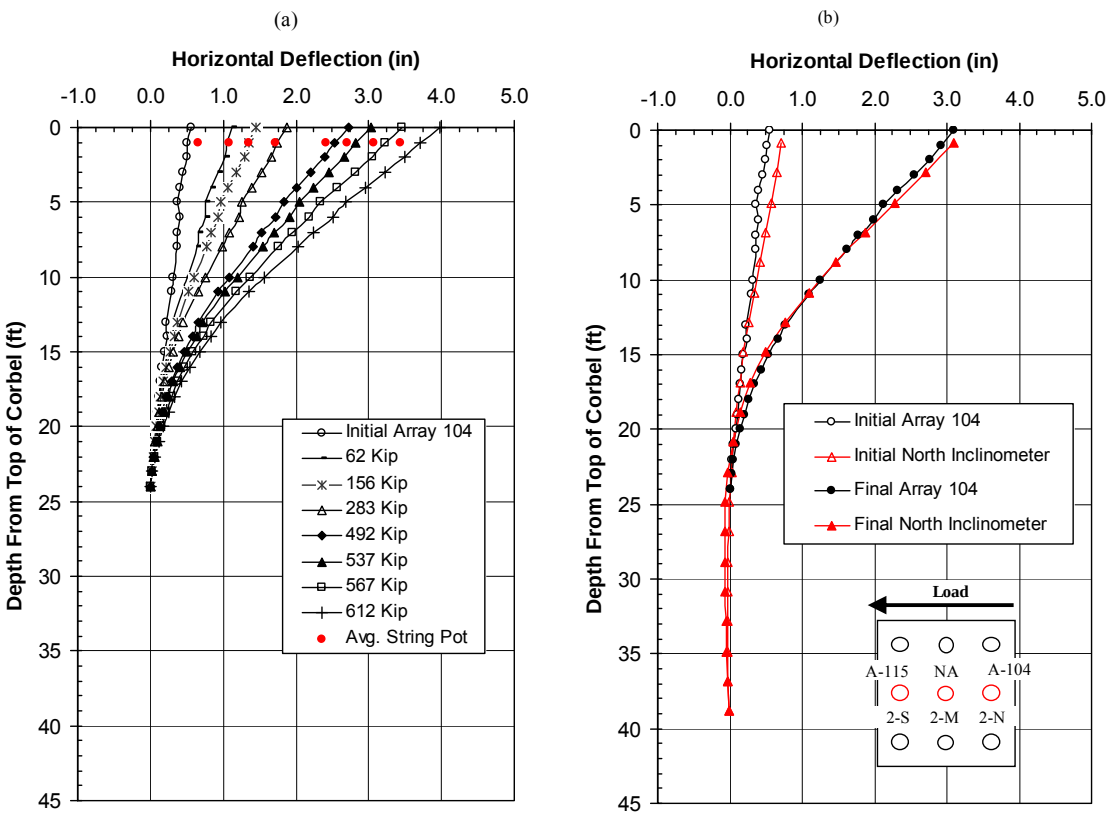

Figure 12-8 (a) Deflection vs. depth curves for the north center pile of pile cap 2 (2-N) from shape array 104 for each increment of test 6, with pile head displacements from the string potentiometers also shown. (b) Comparison of depth vs. deflection curves for the north center pile of pile cap 2 (2-N) from shape array 104 and the north inclinometer of pile cap 2 during test 6.

Figure 12-9(a) displays the incremental deflections of the south center pile of pile cap 1 (1-S) measured from shape array 115 during test 5. As explained in the section 11.3, the deflections measured by array 115 have been reduced by 15% from the original deflections measured from the shape arrays. The greatest difference in measurement between the corrected shape array 115 and the string potentiometers was only 0.05 inches from the first test increment. In Figure 12-9(b), the inclinometer curve matches the curve from the shape array from a depth of 10 to 24 feet below the pile cap. Above 10 feet, the curves separate. This trend was exhibited in the previous test, and could be the result of gaps created between the inclinometer and shape array casing.

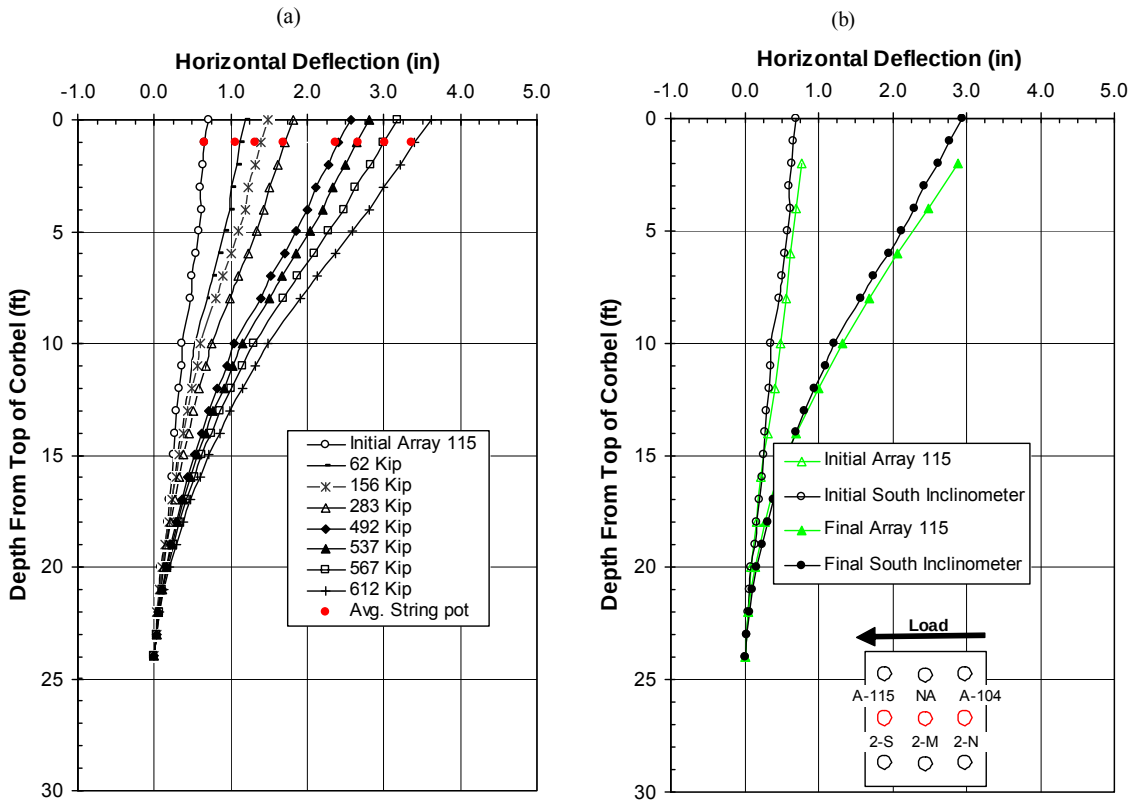

Figure 12-9(a) Deflection vs. depth curves for the south center pile of pile cap 2 (2-S) from shape array 115 for each increment of test 6, deflections at the point of loading measured from the string potentiometers are also shown (b) comparison of depth vs. deflection curves for the north center pile of pile cap 2 (2-N) from shape array 104 and the north inclinometer of pile cap 2 during test 6.

Figure 12-10(a) displays the incremental deflections of the south center pile of pile cap 1 (1-S) measured from shape array 134 during test 6. The measured deflections of shape array 115 are comparable with the string potentiometers for the initial reading and the final two readings. Greater discrepancies were encountered for the first four test increments. The results from the previous tests show that the string potentiometers are most inaccurate (when compared to the string potentiometers) at deflection less than 0.5 inches. The deflections measured during this test are all much less than 0.5 inches, except the initial and the 2 final test increment measurements. This would explain why the initial and final 2 test increment measurements are in much better agreement with

the string potentiometers than those from the first four test increments. Figure 12-10(b) displays the deflected pile profiles measured from shape array 134 and the south inclinometer of pile cap 1 during test 6. There was no initial shape array reading due to the fact the shape arrays had been extracted and reinserted into pile 1-S before test 6 began. The measured deflections from shape array 115 and the inclinometer show good agreement in the top 5 feet of the profile. However, the results are quite different for profile depths between 5 and 20 feet. This may be the result of zeroing the deflections of the shape array to the initial inclinometer measurements.

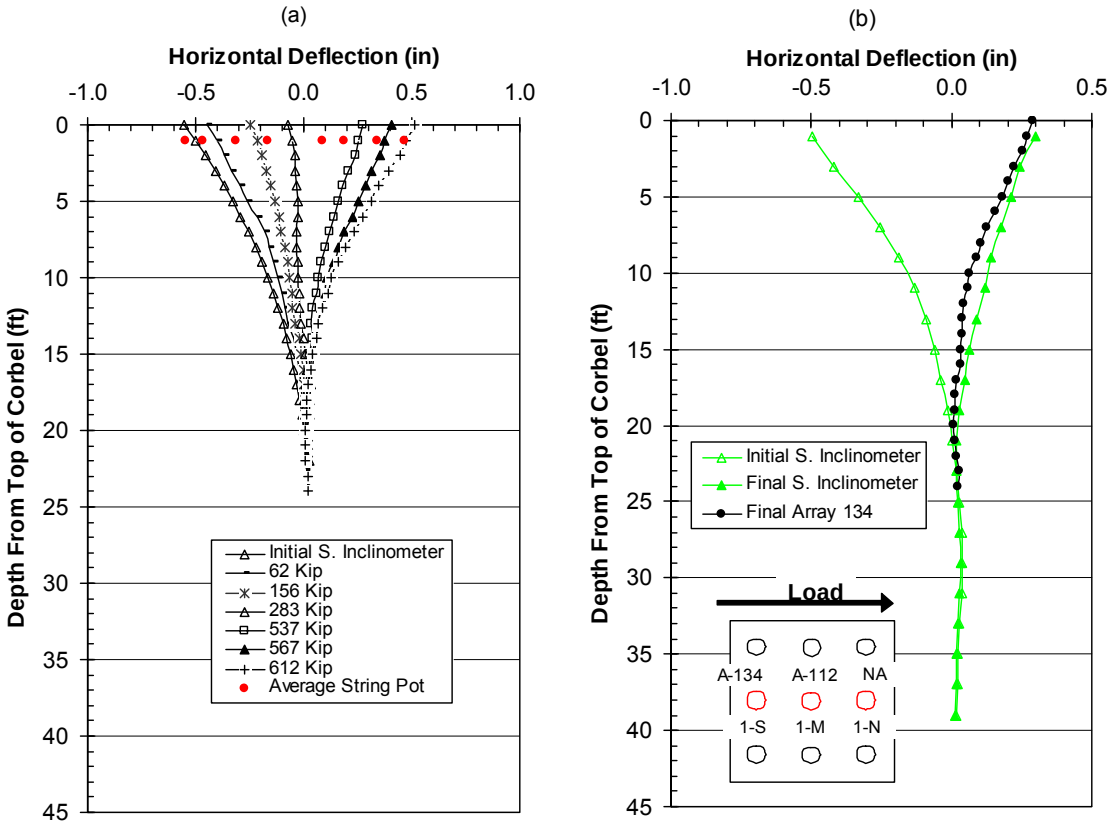

Figure 12-10(a) Deflection vs. depth curves for the south center pile of pile cap 1 (1-S) from shape array 134 for each increment of test 6, deflections at the point of loading measured from the string potentiometers are also shown (b) Comparison of depth vs. deflection curves for the south center pile of pile cap 2 (2-S) from shape array 134 and the southinclinometer of pile cap 1 during test 6.

Figure 12-11(a) displays the incremental deflections of the middle center pile of pile cap 1 (1-M) measured from shape array 134 during test 6. The measured deflections of shape array 115 are comparable with the string potentiometers for the initial reading and the final two readings. The measurements were compared by extrapolating the deflections of the shape arrays to the elevation of the string potentiometers. The greatest difference in measurement from string potentiometers and extrapolated shape array was 0.1 inches during the final displacement-controlled test increment. Once again, the initial and final two load-controlled test increments provided the best agreement between the measurements from the two types of instrumentation. A comparison of the deflected pile profiles from shape array 112 and the inclinometer is found in Figure 12-11(b). The deflected profiles from the inclinometer and shape array 112 are very similar. This is somewhat surprising, because the inclinometer is located in pile 1-S, while the shape array is located in pile 1-M. This level of agreement, however, helps to validate the accuracy of the deflections measured from both types of instrumentation.

12.4 Pile Bending Moment vs. Depth

Figure 12-12 displays the bending moments for the north center pile of pile cap 2 (2-N) during test 6. The bending moment curves were generated from the pile deflection profiles displayed in Figure 12-8(a). Figure 12-13 displays the bending moments calculated from the pile deflection comparison profiles provided in Figure 12-8(b). Fifth order polynomial curves were fit to the deflection profiles to generate the bending moment curves in both of the figures.

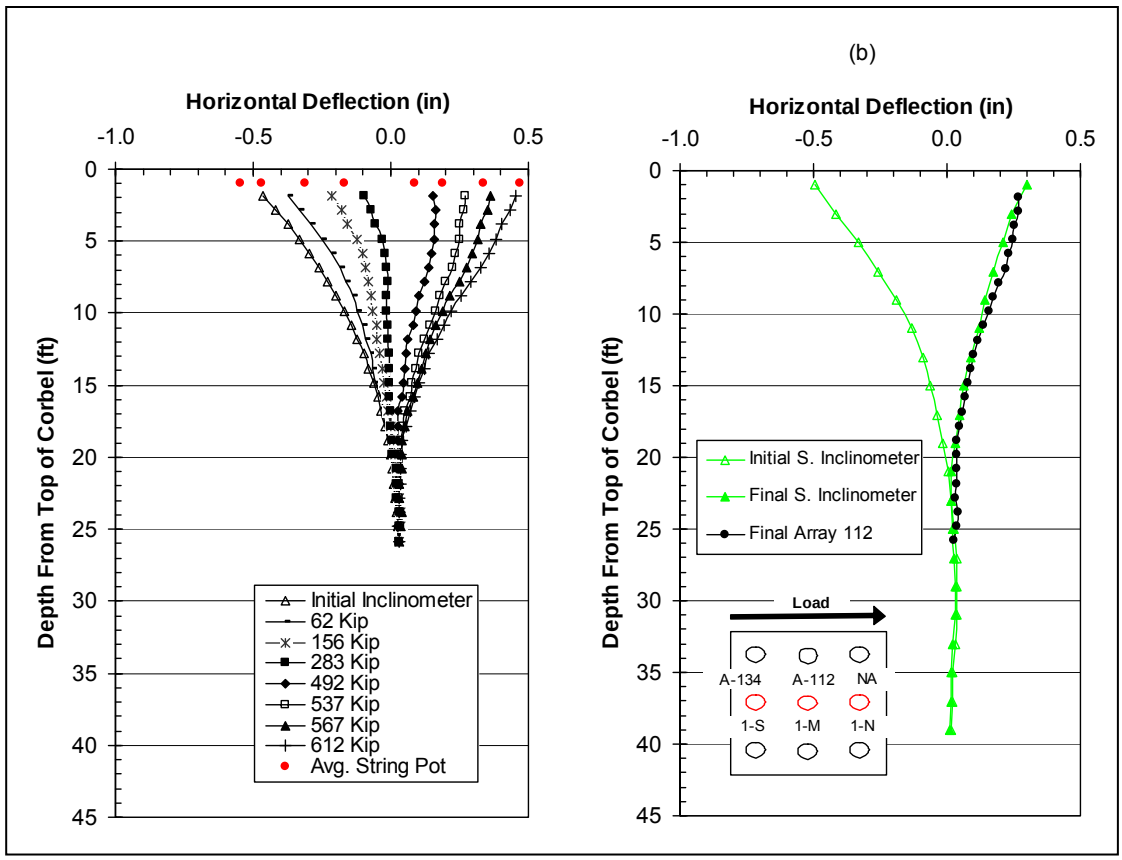

Figure 12-11 (a) Deflection vs. depth curves for the middle center pile of pile cap 1 (1-M) from shape array 112 for each increment of test 6, deflections at the point of loading measured from the string potentiometers are also shown (b) Comparison of depth vs. deflection curves for the middle center pile of pile cap 2 (1-M) from shape array 112 and the south inclinometer of pile cap 1 during test 6.

The initial bending moments calculated from the shape array 104 deflections give a maximum initial bending moment of positive 10 kip-ft at a depth of 14-16 ft below the bottom of the pile cap; the bending moments from the inclinometer deflections yield a maximum initial moment of positive 18 kip-ft at a depth of 15 feet below the bottom of the pile cap. These results are very comparable, and define a good range of initial bending moments in the pile. The maximum positive bending moment in pile 2-N from the initial 612 kip loading increment was 134 kip-ft, and acted at a depth range of 11-13 ft below the pile cap. The bending moments in the pile during the

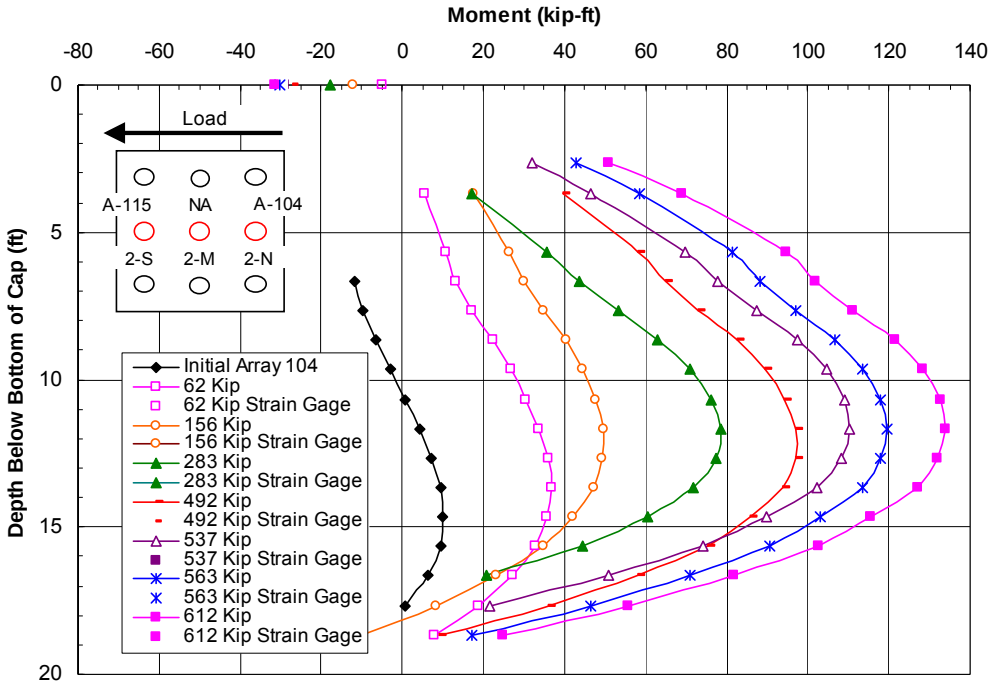

Figure 12-12 Moment vs. depth curve for the north center pile of pile cap 2 (2-N) based on incremental deflection vs. depth curves measured from shape array 104 during test 6, with point moments measured from strain gages at the bottom of the pile cap also shown.

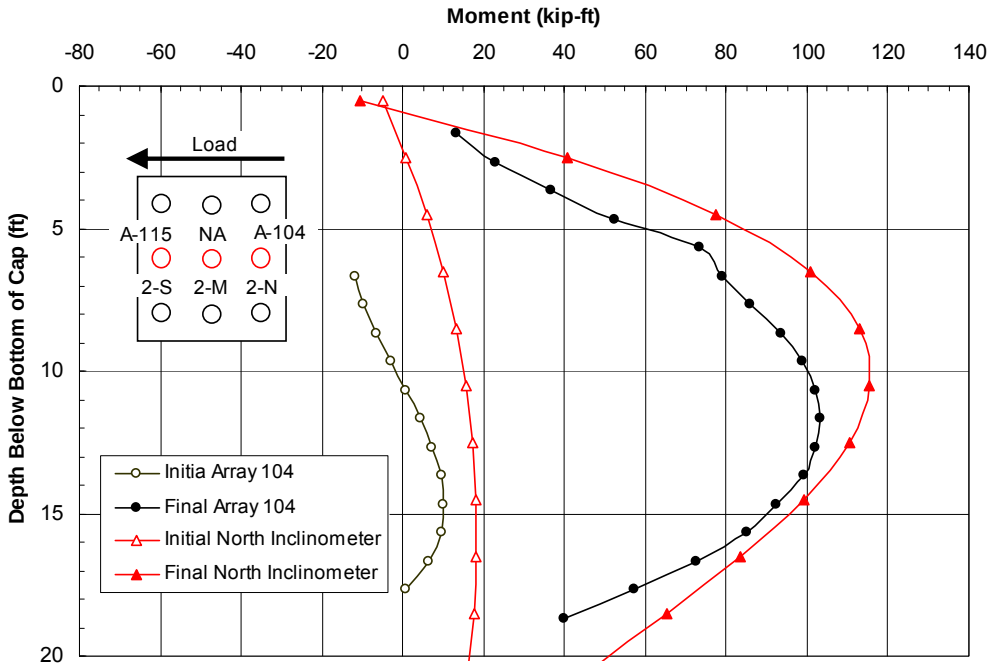

Figure 12-13 Moment vs. depth comparison for the north center pile of pile cap 2 (2-N) based on deflections measured from the north inclinometer and shape array 104 for test 6.

extended 537 kip loading were 103 kip-ft occurring at a depth of 12 feet below the pile cap from the shape array 104 readings and 115 kip-ft at 10 feet below the pile cap from the inclinometer. A range of 105-115 kip-ft occurring at a depth between 10-13 feet below the pile cap is a recommended maximum bending moment range for this test.

Figure 12-14 displays the bending moments for the south center pile of pile cap 2 (2-S) during test 6. The bending moment curves were generated from the pile deflection profiles displayed in Figure 12-9(a). Figure 12-15 displays the bending moments calculated from the pile deflection comparison profiles provided in Figure 12-9(b). Fourth order polynomial curves were fit to the deflection profiles to generate the bending moment curves in both of the figures.

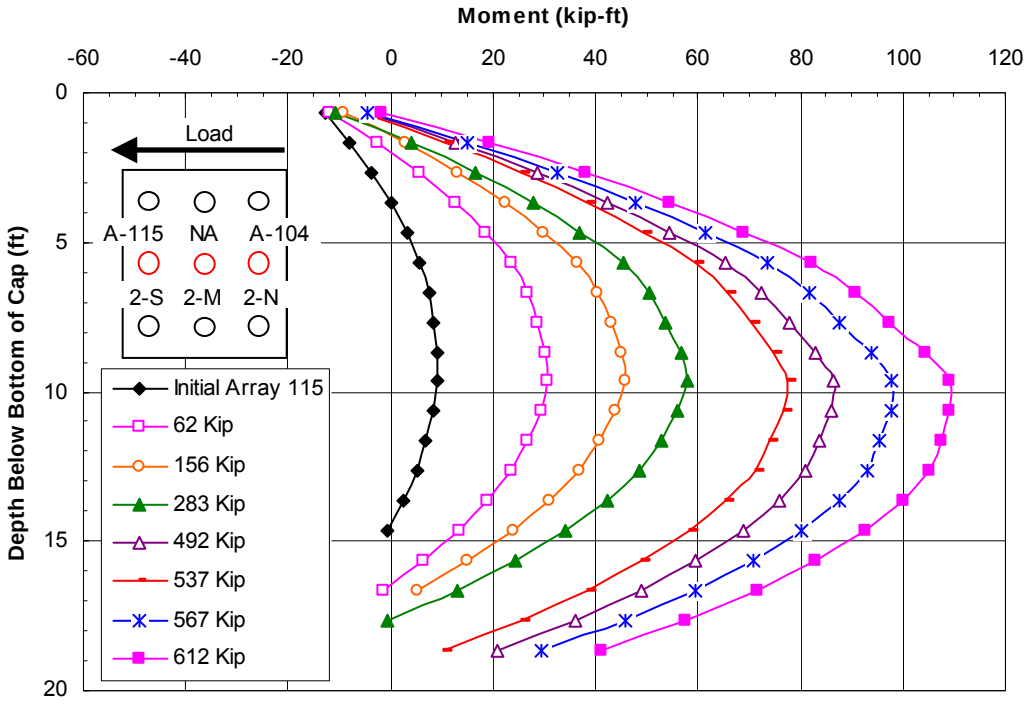

Figure 12-14 Moment vs. depth curve for the south center pile of pile cap 2 (2-S) based on incremental deflection vs. depth curves measured from shape array 115 during test 6.

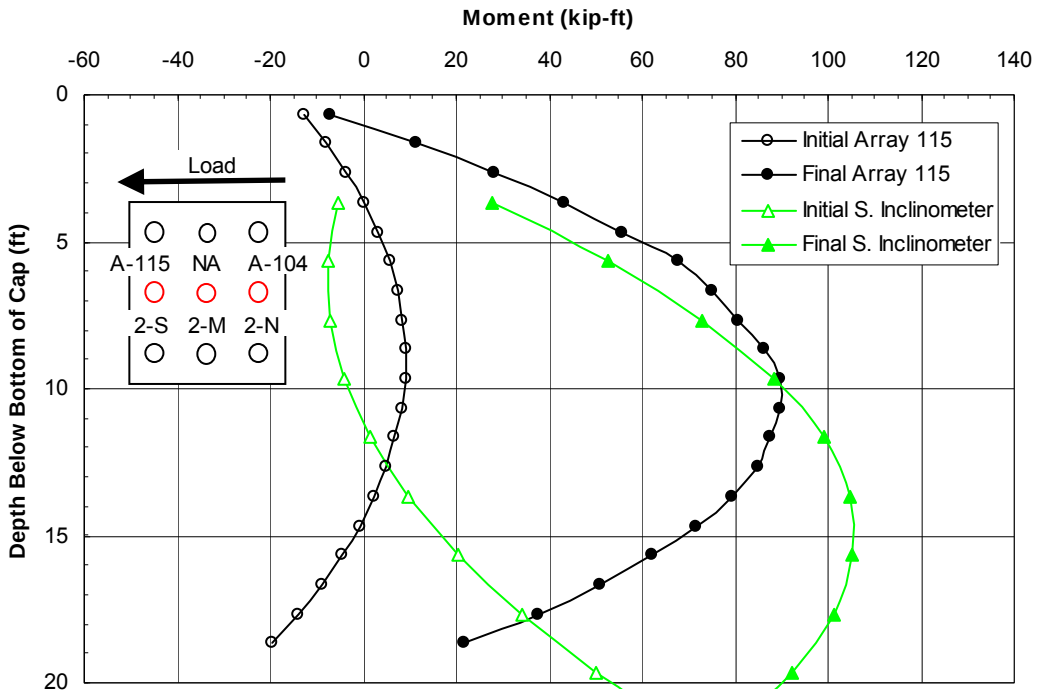

Figure 12-15 Moment vs. depth comparison for the south center pile of pile cap 2 (2-S) based on deflections measured from the north inclinometer and shape array 115 for test 6.

The initial maximum bending moment calculated from the shape arrays was 9 kip-ft occurring 10 feet below the pile cap. The initial bending moment from the inclinometer deflections was -7 kip-ft occurring about 8 feet below the pile cap. These data suggest that the initial bending moment was close to zero. The results define a realistic range of initial bending moments from -10 to 10 kip-ft acting about 10 feet below the pile cap. The maximum bending moment calculated from array 115 for the initial 612 kip loading was 109 kip-ft at a depth of 10-11 feet below the pile cap. During the extended 537 kip loading, the deflections measured from shape array 115 resulted in a bending moment of 90 kip-ft at 10-11 feet below the pile cap, the inclinometer deflections resulted in a 105 kip-ft bending moment occurring at 14-15 feet below the pile cap. A bending moment range between 90-105 kip feet acting 10-15 below the

pilecap defines the range of acceptable bending moments for the subsequent parametric studies.

Figure 12-16 displays the bending moments for the south center pile of pile cap 1 (1-S) during test 6. The bending moment curves were generated from the pile deflection profiles displayed in Figure 12-10(a). Figure 12-17 displays the bending moments calculated from the pile deflection comparison profiles provided in Figure 12-10(b). Fourth order polynomial curves were fit to the deflection profiles to generate the bending moment curves in both of the figures. Sixth order polynomial curves were fit to the initial deflection profiles from the inclinometer and the 537 kip loading increment, with a 5^{th} order polynomial was used for the 492 kip loading curve. The rest of the bending moment curves were generated from 4^{th} order curves fit to the deflection profiles.

The maximum initial bending moment was calculated to be -20 kip-ft at 5 feet below the pile cap. This negative initial bending moment at depth comes from the piles being initially strained in the direction opposite to that induced through loading. The initial maximum bending moment from the 612 kip loading measured from shape array 134 was 34 kip-ft at a depth of 7-8 feet below the pile cap. The bending moment during the extended 537 kip load (Figure 12-17) from the shape array 134 deflections was 30 kip-ft at a depth of 5-6 ft below the pile cap, and 10 kip-ft at 11 feet below the pile cap for the inlinometer-based bending moments. The depths to maximum positive bending moment calculated from the shape array 134 deflections are much lower than expected, and the depths from the inclinometer-based bending moment curves are more consistent with previous results. Therefore, the recommended bending moment range for pile 1-S

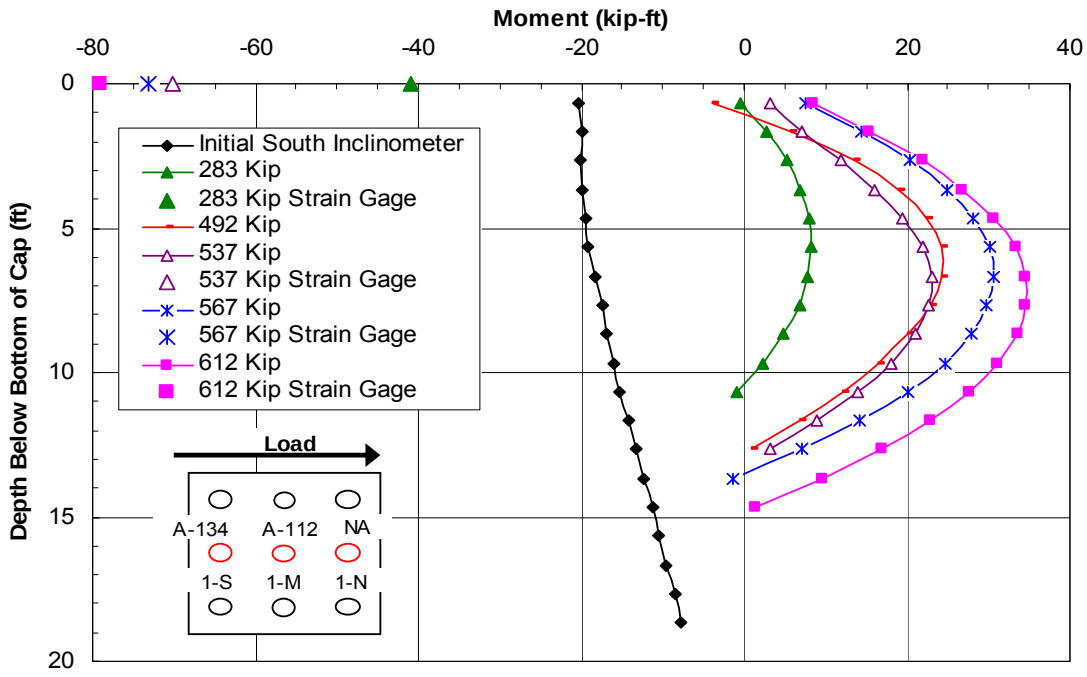

Figure 12-16 Moment vs. depth curve for the south center pile of pile cap 1 (1-S) based on incremental deflection vs. depth curves measured from shape array 134 during test 6, with point moments measured from strain gages at the bottom of the pile cap also shown.

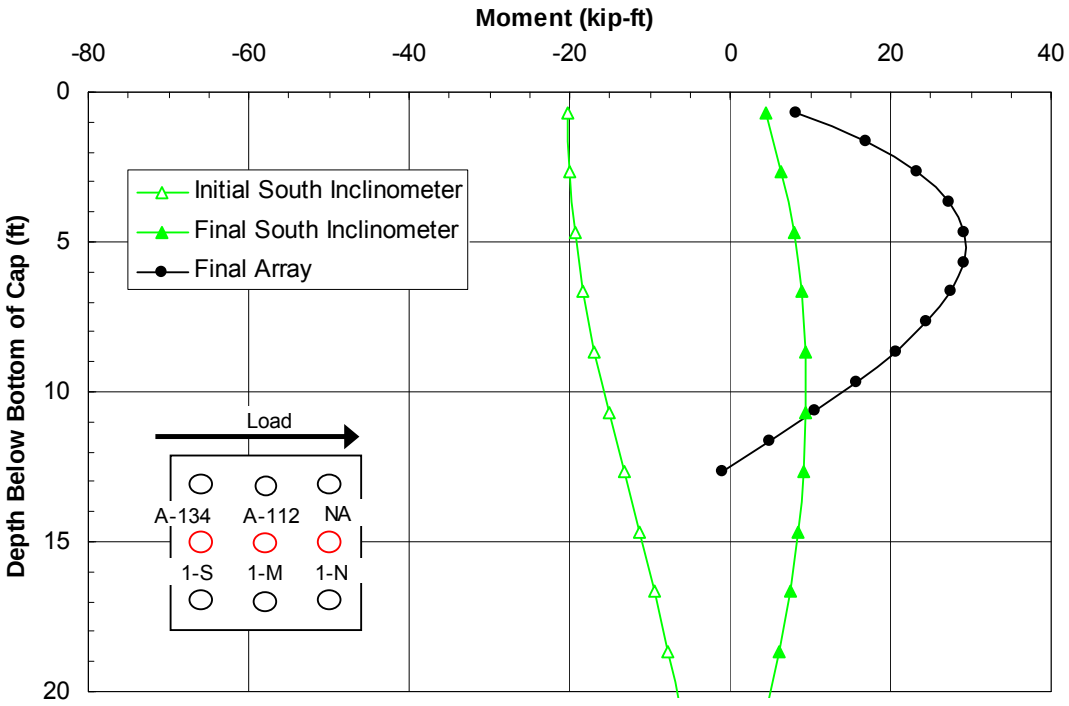

Figure 12-17 Moment vs. depth comparison for the south center pile of pile cap 1 (1-S) based on deflections measured from the north inclinometer and shape array 134 for test 6.

for test 6 is 10-30 kip-ft occurring at a depth of 10-12 feet below the pile cap. The bending moments calculated from the strain gages results are quite high for the measured pile deflections, and do not match the general trends from extrapolating the curves generated from shape array 134. Once again, it is difficult to determine which bending moments are most accurate, but, when compared to the results from previous tests with similar pile deflections, the moments calculated from the strain gages seem too high.Figure 12-18 displays the bending moments for the middle center pile of pile cap 1 (1-M) during test 6. The bending moment curves were generated from the pile deflection profiles displayed in Figure 12-11(a). Figure 12-19 displays the bending moments calculated from the pile deflection comparison profiles provided in Figure 12-11 (b). Fourth order polynomial curves were fit to the deflection profiles to generate the bending moment curves in both of the figures. Sixth order polynomial curves were fit to the initial deflection profiles from the inclinometer and the 537 kip loading increment, with a 5^{th} order polynomial was used for the 492 kip loading curve. The rest of the bending moment curves were generated from 4^{th} order curves fit to the deflection profiles.The initial bending moment in pile 1-M was not able to be calculated; the initial inclinometer deflections from pile 1-S were used to estimate the initial moment values for pile 1-M, and were reported previously. The maximum positive bending moment for the initial 612 kip load was 27 kip-ft at a depth of about 10 feet below the pile cap. The maximum bending moment for the extended 537 kip loading from the shape array 112 deflections was 17 kip-ft at 12-13 feet below the pile cap, and 10 kip-ft at 11 feet below the pile cap from the inclinometer deflections. There were no working strain gages on pile 1-M during this test.

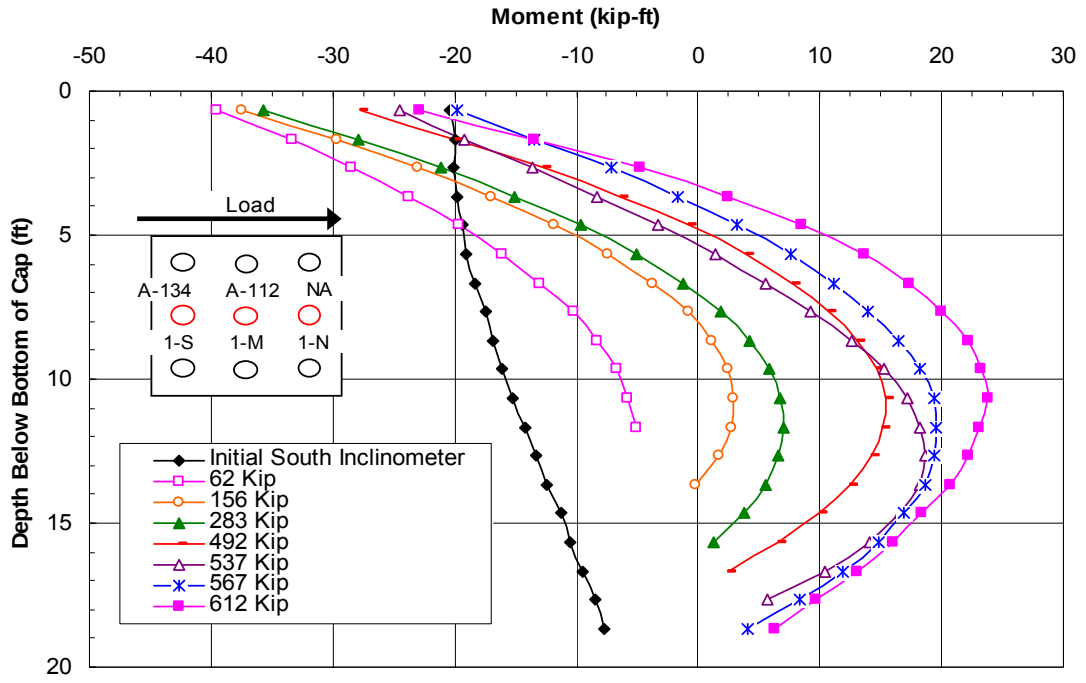

Figure 12-18Moment vs. depth curve for the middle center pile of pile cap 1 (1-M) based on incremental deflection vs. depth curves measured from shape array 112 during test 6.

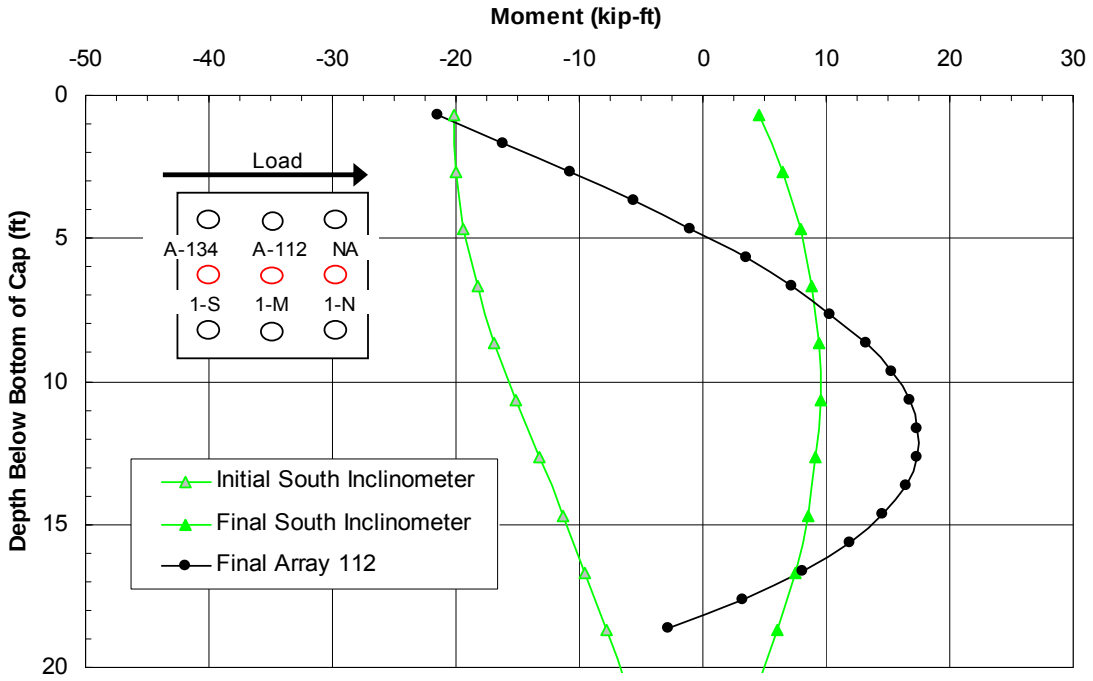

Figure 12-19Moment vs. depth comparison for the middle center pile of pile cap 1 (1-M) based on deflections measured from the north inclinometer and shape array 112 for test 6.

13 Test Comparisons

This chapter will compare the results from the tests reported in the previous chapters. Tests 1 and 2 are compared to determine the amount of passive soil resistance which acted directly on the pile cap during virgin soil loading. The test results from tests 3 through 6 will then be compared to determine the increase in lateral resistance caused by treating the soil with jet grouting. With results from these tests, various failure mechanisms for the soilcrete mass will be explored and the ultimate lateral resistance from the jet grout treated zone will be determined. Finally, a basic cost analysis will be presented to examine the relative cost of jet grouting compared to a structural retrofit with additional piles and an expanded pile cap.

13.1 Virgin Tests Comparisons

Figure 13-1 provides a comparison between the load-displacement curves for pile caps 1 and 2 during tests 1 and 2. The load-displacement curves for test 2 have been shifted to the right 0.15 inches to account for reloading effects. With this minor adjustment, the load-displacement curve for pile cap 2 then matches the curves for pile caps 1 and 2 during test 1 at larger displacements, as would be expected. The development of passive force on the pile cap was then determined by computing the difference in the lateral load as a function of displacement for the tests on pile cap 1.

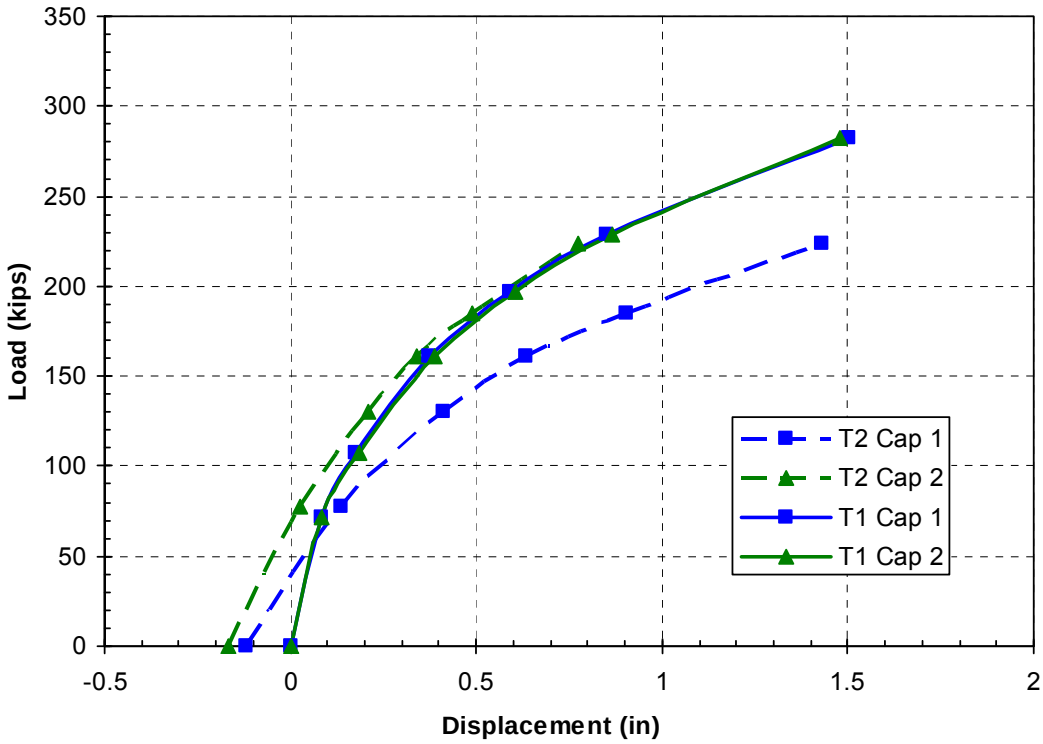

Figure 13-1 Comparison of peak pile cap load vs. pile head displacement curves for pile caps 1 and 2 during tests 1 and 2.

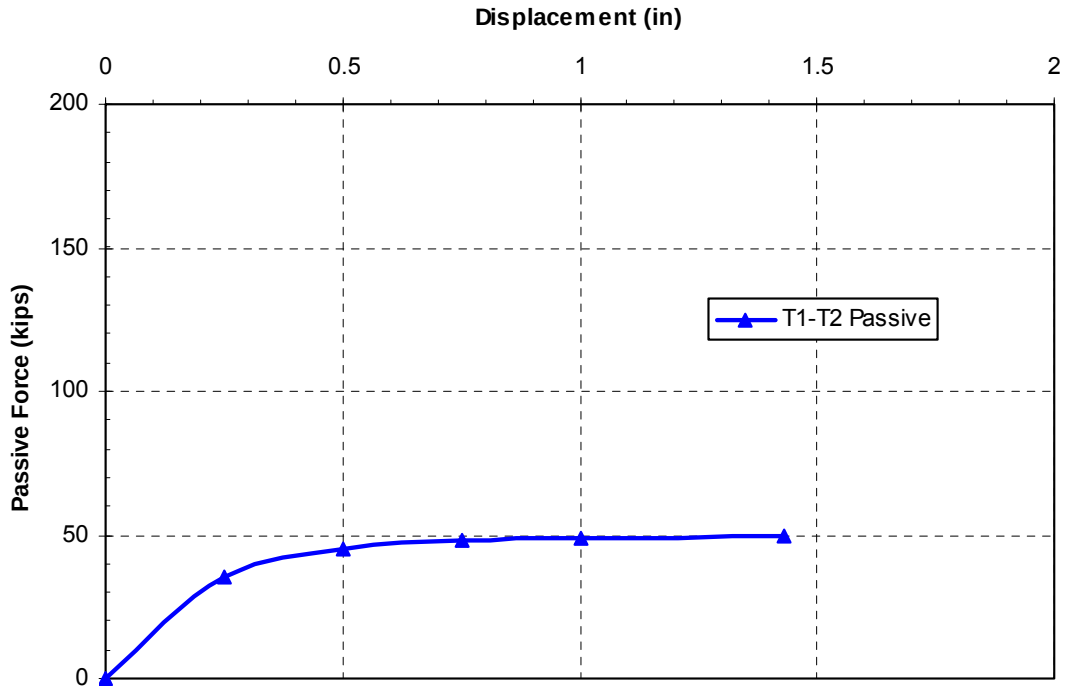

Figure 13-2 Development of passive force for virgin clay around pile cap 1.

with and without soil against the pile cap. These calculations were performed at displacements of 0.25, 0.5, 0.75, 1.0, and 1.5 inches. The resulting passive force-displacement curve is displayed in Figure 13-2. The curve indicates that the ultimate passive force was approximately 50 kips, and was fully developed at a displacement of about 0.75 inches (2.5% of cap height). In this case, the passive soil resistance behind the pile cap represents about 18% of the total lateral resistance of the pile group foundation.

13.2 Jet Grout Test Comparisons for Pile Cap 1

13.2.1 Load vs. Displacement Comparison

Figure 13-3 displays the peak load-displacement curves from tests 1, test 3 and test 6. Test 3 was the test performed just after the soil was treated with jet grouting. Test 6 was the test performed after excavating the treated soil from the face of the pile cap. The results from the virgin tests are also shown for comparison. In this figure it can be seen that the loads developed during test 6 are greater than loads from test 3 for similar deflections. Because test 6 involved reloading after soil had been excavated adjacent to the cap, the loads would have been expected to be lower than for test 3. For example, reloading in tests 1 and 2 typically decreased the peak load by about 10%, and excavation of the soil in front of the pile cap reduced the fully developed peak load by 50 kips.

One explanation for the loads from test 6 being greater than test 3 is the flow of the soil into the gap between the treated soil and pile cap, which was generated from previous tests on pile cap 1. This would cause greater loads to be developed while the

initial gap was being closed, due to the additional resistance on the pile cap from the soil which flowed into the gap. Additionally, passive resistance theory states that fully developed passive soil resistance is incrementally developed as the pile group is displaced through the soil. If soil flowed into the initial gap, the pile cap and piles would begin displacing through the soil before "zero" displacement is reached. Thus, greater passive resistance would be expected for similar pile group displacements if soil flowed into the initial gap. A second explanation deals with the development of the adhesive resistance between the piles and the soil. As with passive soil resistance, the adhesive resistance of the soil on the piles is developed incrementally as the piles are displaced through the soil. Adhesive resistance is generally fully developed at much smaller displacements. Therefore, a greater amount of adhesive resistance would have been developed at similar displacements for test 6 when compared with test 3.

To account for these "gap" effects, the load-displacement from test 6 was shifted to the right. Figure 13-3 shows the results from test 6 shifted a positive 0.25 inches, which was the smallest shift necessary to have the results from test 6 plot below test 3. This shift causes the loads on the curve from test 6 to only be about 10% difference is less than the peak load from test 3 at the maximum previous displacement, which was the expected behavior for the pile cap during reloading. For all of the previous tests, the soil resistance decreased considerably after the soil on the face of the pile cap was excavated. However, the 10% difference in load-deflection curves for test 3 and test 6 is what would be expected if the soilcrete block adjacent to the pile cap displaced as a rigid block. The soilcrete block is in contact with the piles beneath the pile cap, and thus would have displaced similarly before and after excavation. The 10% decrease in

strength is caused by reloading effects, and is the same percentage decrease found during the virgin tests. Additionally, the results of the lateral load tests on soil improved with mass mixing suggested that the mass mix zone on the south side of pile cap 1 displaced as a rigid block as the pile cap was displaced (Herbst, 2008). In order to determine whether or not the soilcrete mass could have displaced as a rigid block, further analysis must be performed to determine if the soilcrete mass had the shear and bending moment capacity to transfer the loads from the pile group along the entire length of the block.

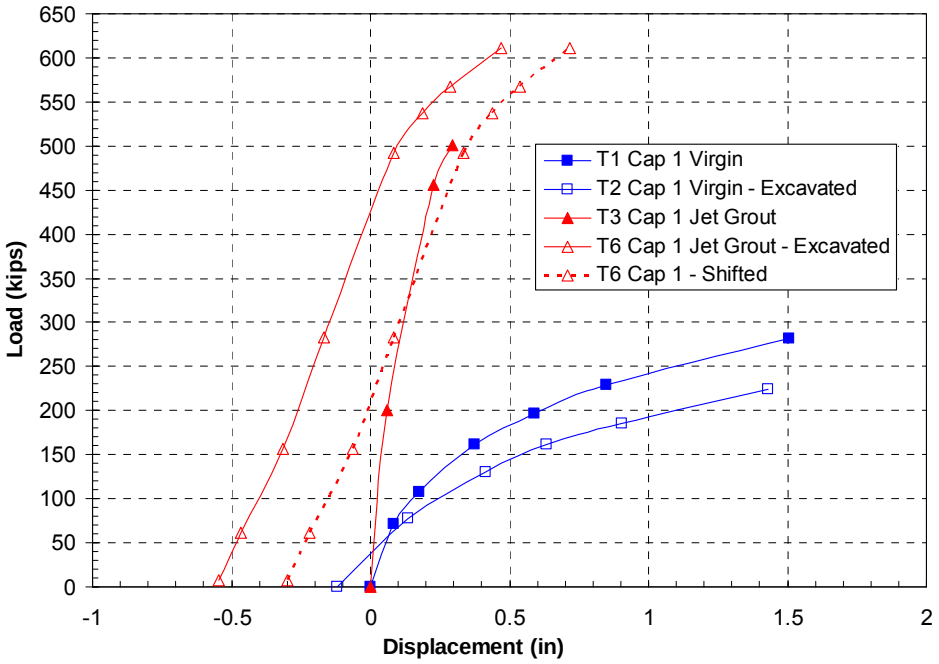

Figure 13-3 Load-displacement curves for tests performed on pile cap 1 following jet grouting. The results from the virgin test are also shown for comparison.

Treating the soil adjacent to pile cap 1 with jet grouting increased the lateral resistance of the pile cap dramatically. The results from test 3 and test 6 were combined to create a composite load-displacement curve for the pile cap following jet grouting.

The combined curve is found in Figure 13-4. The combined curve had a maximum load of 612 kips at a pile cap displacement of 0.72 inches, which is 398 kips greater than the 214 kip maximum load from the virgin curve for the same displacement.

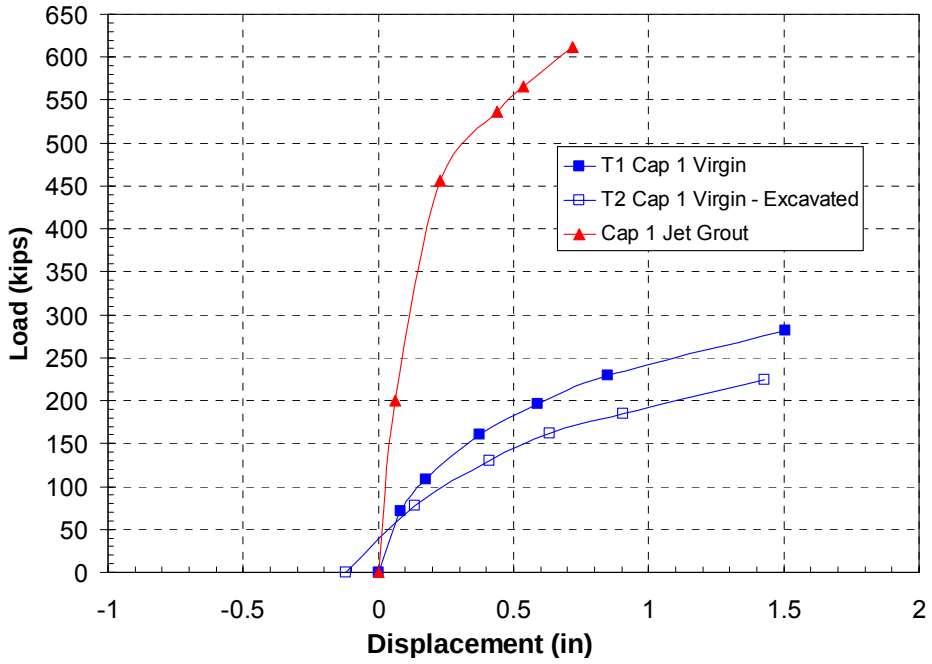

Figure 13-4 Combined load-displacement curves for all tests performed on pile cap 1 following jet grouting. The results from the virgin test are also shown for comparison.

This equals about a 185% increase in lateral resistance at the maximum measured deflection. The increased lateral resistance curve from jet grouting is calculated by subtracting the composite curve in Figure 13-4 from the virgin curve, and is found in Figure 13-5. From this figure it can be seen that the increased resistance curve has begun to flatten out at a displacement of about 0.26 inches, but it has not yet reached a maximum, which would signify that the increased resistance has been fully developed. Additionally, the initial stiffness of the load-displacement curve following jet grouting is substantially higher that the initial stiffness from the virgin curve.

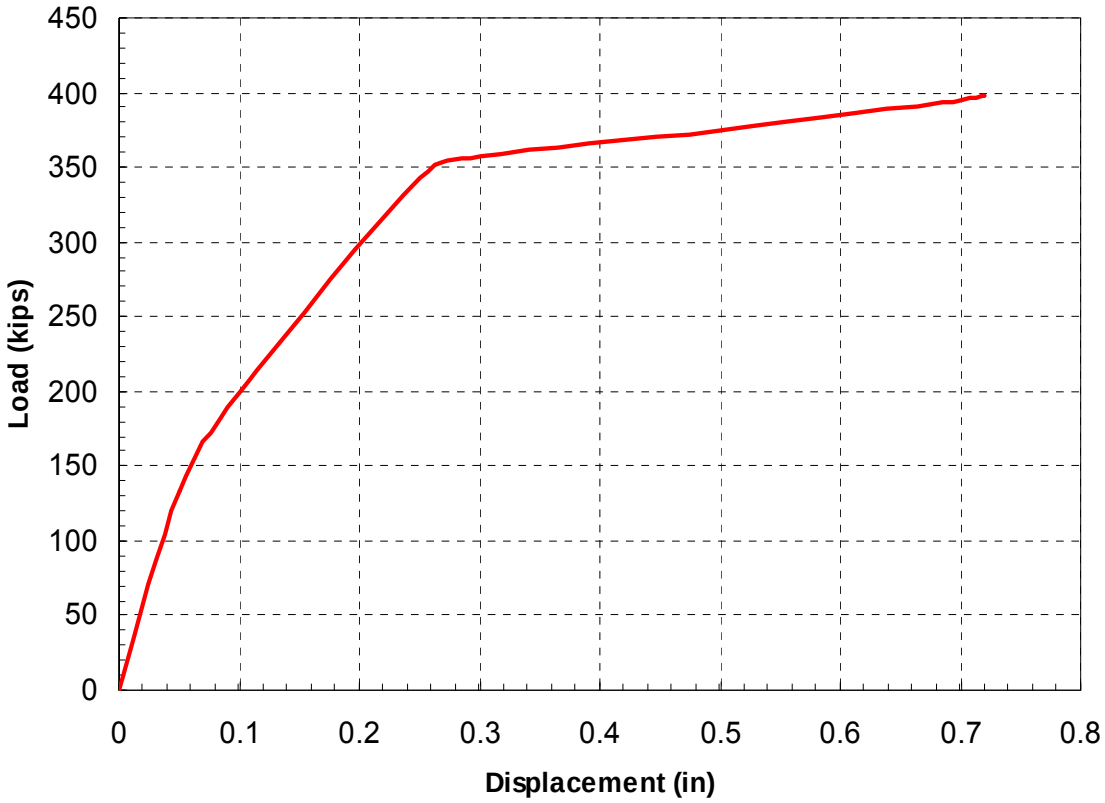

Figure 13-5 Total measured increase in lateral resistance due to jet grouting adjacent to pile cap 1.

13.2.2 Failure Mechanisms

Although the 185% increase in lateral resistance appears to result from the movement of the soilcrete mass, it is not immediately apparent how this resistance was generated and what failure mechanisms were involved. To answer this question a few scenarios need to be considered. One scenario is that the soilcrete zone could have sheared, and thus only a portion of the mass contributed to strength gain, as shown in Figure 13-6. The exact location of the maximum shear force acting on the soilcrete will be predicted in a later analysis. Another scenario is that the entire soilcrete mass acted as a rigid block of soil. Figure 13-7 displays how the soilcrete block would displace as a rigid block.

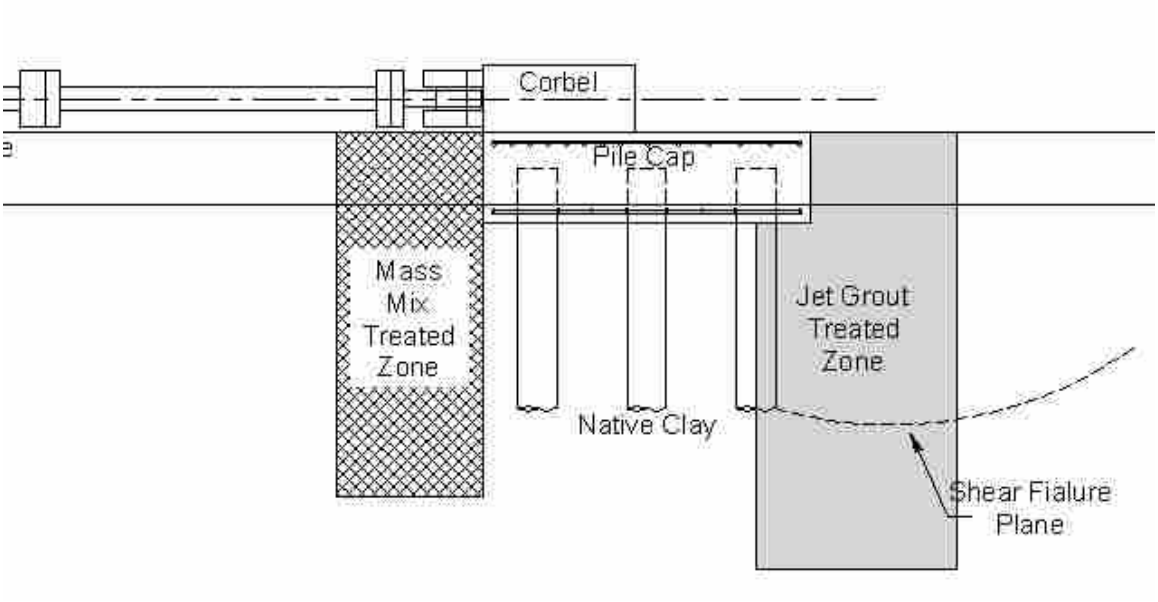

Figure 13-6 Profile view of a shear failure scenario for the soilcrete block.

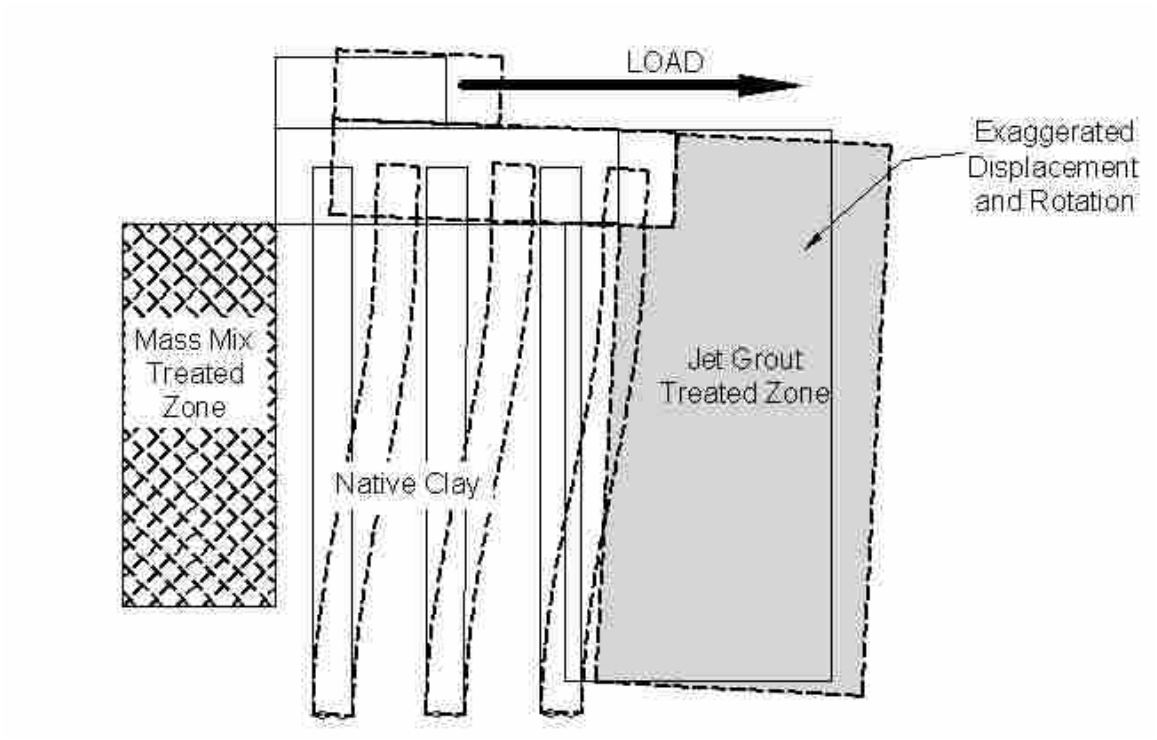

Figure 13-7 Exaggerated profile view of jet grout treated zone adjacent to pile cap 1 displacing as a rigid block.

13.2.3 Shear Failure

In evaluating the first scenario, that the soilcrete experienced a shear failure, the shear strength of the soilcrete along a potential shear plane would need to be estimated. The laboratory compressive strength of the soilcrete was determined in Figure 5-9 to be between 550-650 psi for tests 3 through 6. However, the design/in-situ compressive strength recommended for use by Hayward Baker was only between 200-250 psf. In reality, the in situ strength of the soil is probably somewhere between that achieved in the laboratory and that recommended by Hayward Baker for design. Thus, an in situ compressive strength of 450 psf was used. The shear strength, τ, of the soilcrete is one-half of the unconfined compressive strength or 225 psi, which is equal to 32,400 psf. By multiplying the shear strength of the soilcrete by the design soilcrete area of 13 feet by 6.6 feet in plan view, the shear capacity of the mass mix would be about 2780 kips. This shear capacity is considerably greater than the maximum load applied to the soilcrete of 612 kips, making it highly unlikely that a shear failure occurred. Even if the compressive strength of the in-situ soilcrete were as low as that recommended by Hayward Baker for design, the soilcrete would have more than adequate shear strength to resist failure.

13.2.4 Rigid Block Failure - Calculation of Ultimate Soil Resistance

A better understanding of the forces acting on the soilcrete block would be helpful in understanding the behavior of the zone and in analyzing potential failure mechanisms from shear and bending. This analysis would also be useful in determining if the increased lateral resistance produced by the soilcrete block can be adequately accounted for using basic geotechnical design concepts. If the soilcrete mass failed as a

rigid block, a majority of the increased strength would be caused by displacing the soilcrete block through the weak clay soil. The soil resistance acting on the soilcrete block consists of the passive soil resistance acting on the face of the soilcrete block and the skin friction or adhesive resistance acting on the bottom and the sides of the block.

The Rankine passive earth pressure theory was used to determine the ultimate passive soil resistance that would act on the face of the displacing soilcrete block. The Rankine passive earth pressure theory predicts the passive force equation

$$\frac{1}{2}(\gamma)(H^2)(B)(K_p) + 2(c_u)(H)(B)(\sqrt{K_p}) \quad \textbf{(13-1)}$$

where γ is the unit weight of soil, H is the height of the block or pile cap, B is the base width perpendicular to the plane of loading, c_u is the undrained shear strength of the soil, and K_p is the passive earth pressure coefficient. For the undrained conditions involved, the friction angle is taken as 0 and K_p is equal to 1.0. The desiccated nature of the clay caused the upper 2.5 feet of the clay to be significantly stronger than the clay below the depth of 2.5 feet. The undrained shear strength of the upper zone was estimated to be approximately 1040 psf with an average unit weight of 117.5 pcf, which is consistent with the results in. The undrained shear strength of the upper zone was back-calculated using Rankine theory based upon the results of test 2, which showed that approximately 50 kips of passive force was provided by the virgin clay acting on the 9 ft wide and 2.5 ft deep pile cap. was used to determine the potential shear strengths and average unit weights for the clay between 2.5 and 12 feet below the ground surface. It was determined that the shear strength of the clay for these depths was between 300 and 350 psf, with a mean shear strength of 325 psf. This equals an

average shear strength of between 454 psf and 494 psf for the upper 12 ft of clay. These shear strengths are consistent with the results from the analysis on the mass mix treated zone placed on the south side of pile cap 1, which determined that the average shear strength for the upper 10 feet of soil was 475 psf (Herbst, 2008). Figure 13-10 provides a comparison between the undrained shear strengths used in the analysis and those measured during the filed investigations.

The average unit weight for this depth range was estimated to be 112 pcf. The in-situ geometry of the soilcrete columns was never verified by excavating the ground in the field. Therefore, soilcrete column diameters which varied from the 4 ft design diameter were used in two additional analyses of the lateral resistance. Soilcrete column diameters of between 3 feet and 5 feet were used to define possible base widths (B) of the soilcrete mass. These columns diameters equate to a base width of between 12 and14 feet, with a mean of 13 ft for the 4-ft diameter column. The height of the soilcrete columns (H) was precisely controlled by the drill rig and was considered to be 12 feet. The relatively rapid loading of the soil necessitated an undrained analysis be performed. Thus, the soil friction angle was 0 degrees, which correlates to a passive earth pressure coefficient (K_p) of 1.0. From the above parameters, the ultimate passive soil resistance acting on the face of the pile cap was calculated to be between 229 and 281 kips, with a mean for the 4 ft column diameter of 255 kips. The passive soil resistance pressure distribution on the face of the soilcrete mass for the analyses is found in Figure 13-8.

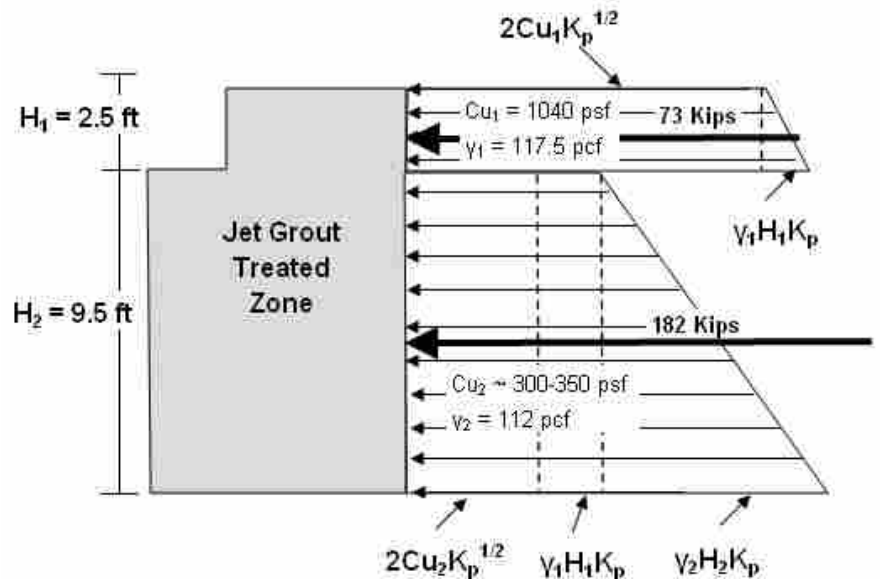

Figure 13-8 Fully developed passive pressure distribution from Rankine theory along the face of the soilcrete mass using mean analysis soilcrete block dimensions.

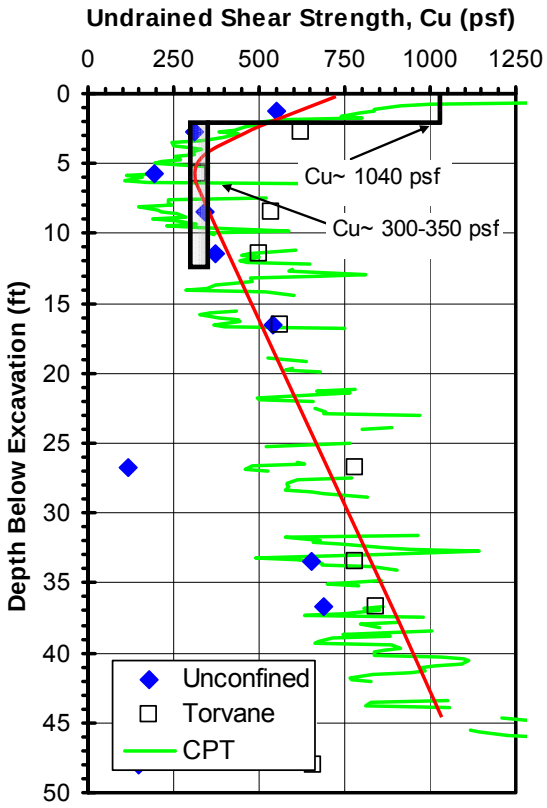

Figure 13-9 Range of undrained shear strengths used in PYCAP and adhesive strength analysis compared to measured strengths.

The adhesive force of the soft clay acting on the block was then determined. It was assumed that the adhesive force acted on the sides and the bottom of the soilcrete mass, and that the "adhesion" between the soilcrete and clay was equal to the "undrained cohesion" or undrained shear strength of the clay. length of the block in the direction of loading below the pile cap. It is assumed that the block would have extended 1.0 ft underneath the pile cap for a 3 ft diameter column, 2.0 feet under the pile cap for a 5 ft diameter column and 1.5 ft for the 4 ft diameter column.

The total side surface area contributing to the adhesive soil resistance on the soilcrete mass would have been between 139 and 182 ft^2. The area components for the top 2.5 feet and bottom 9.5 feet were multiplied by the shear strengths for those particular depths to determine the adhesive soil resistance contribution from the sides of the soilcrete mass. The calculated resistance was found to be between 60 and 84 kips, with a mean of 72 kips. The frictional or adhesive resistance along the bottom of the soilcrete mass was then determined. The bottom surface area was calculated to be between 72.0 and 112.0 ft^2. It was also determined from Figure 3-3 that shear strength at a depth of 12 ft was between 350 and 375 psf, with a mean of 365 psf. Thus, the adhesive resistance from the bottom of the mass was between 25 and 42 kips, with a mean of 33 kips. Therefore, the total adhesive resistance from the sides and bottom of the soilcrete mass ranged between 85 and 126 kips, with a mean of 105 kips. Adding the total adhesive resistance to the ultimate passive resistance yielded a total soil resistance of between 315 and 407 kips, with a mean of 360 kips. All of the calculations for the upper bound, lower bound, and mean analysis can be found in the Appendix C.

13.2.5 Rigid Block Failure – Soil Resistance vs. Displacement Relationship

The total adhesive and passive forces computed in the previous section are developed as the soilcrete block displaces through the soil. Typically, the adhesive resistance on the side of a wall or a pile have been found to fully develop with relatively small movements, while the passive force becomes fully developed after larger movements. Therefore, the soil resistance-displacement curves for each component of resistance have been developed separately and then combined to compute the total soil resistance-displacement curve for the soilcrete block.

To estimate the development of the passive resistance on the face of the soilcrete block, an analysis was done using the spreadsheet PYCAP created by R. L. Mokwa and J. M. Duncan (2001) and treating the soilcrete block as an equivalent pile cap. The spreadsheet computes the ultimate passive force and then uses a hyperbolic curve to compute the development of passive force/resistance with displacement. For the undrained loading case, with ϕ=0, PYCAP computes the ultimate passive force using the Rankine theory described above. The shear zones at the end of the wall are assumed to form parallel to the direction of loading so that 3-D effects need not be considered. PYCAP develops the hyperbolic force-displacement curve using the initial soil modulus to define the initial stiffness and the ultimate passive resistance as an asymptote as shown in Figure 13-10. Using the hyperbolic model in PYCAP, hyperbolic curves were created using a range of possible input parameters. Parameters were chosen which defined an upper and lower range, along with best estimates. Only two parameters, the soilcrete block width and the shear strength of the bottom 9.5 feet of soil, were varied to define the upper and lower range curves.

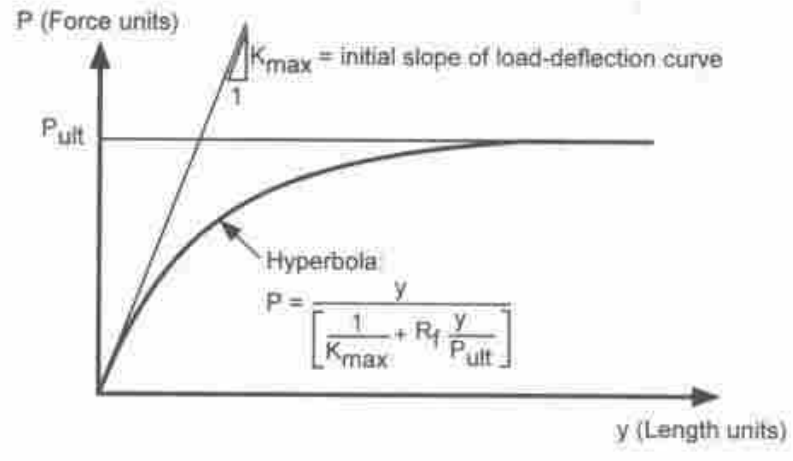

Figure 13-10 Graphic of the hyperbolic model (Duncan and Mokwa, 2001).

The variations in soilcrete block width and the shear strength for the bottom 9.5 feet were discussed in the previous section. The parameters used for each of these respective analyses are shown in

Table 13-1 through Table 13-2. The average shear strengths for the upper 12 ft zone were used in these analyses, in stead of the separate shear strengths for the upper 2.5 feet and lower 9.5 feet of the soil profiles as were discussed previously. Using the weighted shear strengths will not affect the ultimate passive force calculation in the previous section.

The soilcrete columns were installed up to the top of the pile cap. Thus, there was no embedment depth for the equivalent pile cap. The initial soil modulus was estimated using the following equation

$$E_i \approx \frac{15 \cdot C_u}{I_p(\%)} \qquad \textbf{(13-2)}$$

where E_i is the initial soil modulus, C_u is the undrained shear strength of the soil (coehsion), and I_p is the plasticity index (%), which in this case in 25. A value of 0.5 was used for the Poisson's ratio of the clay. The average soil unit weight was determined to be 113.1 pcf, by averaging the unit weights discussed in the previous section and displayed in Figure 13-8. An adhesion factor of 1.0 would appear appropriate based on research regarding unit side resistance of piles in soft clay (API 1986). columns. The percent of wall height used to mobilize full passive resistance (Δ_{max}/H) was 1.5%, which is consistent with the findings of Brandenberg et al. (2005) for cohesive soils. This equals a displacement of 2.16 inches. In the context of the hyperbolic model this corresponds to a failure ration, R_f, of 0.83. The hyperbolic passive soil resistance vs. block displacement curve for each strength case are presented in Figure 13-11 through Figure 13-13.

Table 13-1 Parameters used in PYCAP analysis for the lower range curve.

Cap width, b (ft)	**12.00**
Cap height, H (ft)	**12.00**
Embedment depth, z (ft)	**0.00**
Surcharge, qs (psf)	**0.0**
Cohesion, c (psf)	**454.2**
Soil friction angle, Φ (deg.)	**0.0**
Wall friction, δ (deg.)	**0**
Initial soil modulus, Ei (kip/ft^2)	**272.5**
Poisson's ratio, v	**0.50**
Soil unit weight, γ_m (pcf)	**113.1**
Adhesion factor, α	**1.00**
Δ_{max}/H	**0.015**

Table 13-2 Parameters used in PYCAP analysis for the mean or best estimates.

Cap width, b (ft)	**13.00**
Cap height, H (ft)	**12.00**
Embedment depth, z (ft)	**0.00**
Surcharge, qs (psf)	**0.0**
Cohesion, c (psf)	**475.0**
Soil friction angle, Φ (deg.)	**0.0**
Wall friction, δ (deg.)	**0**
Initial soil modulus, Ei (kip/ft^2)	**285**
Poisson's ratio, v	**0.50**
Soil unit weight, γ_m (pcf)	**113.1**
Adhesion factor, α	**1.00**
Δ_{max}/H	**0.015**

Table 13-3 Parameters used in PYCAP analysis for the upper range.

Cap width, b (ft)	**14.00**
Cap height, H (ft)	**12.00**
Embedment depth, z (ft)	**0.00**
Surcharge, qs (psf)	**0.0**
Cohesion, c (psf)	**493.8**
Soil friction angle, Φ (deg.)	**0.0**
Wall friction, δ (deg.)	**0**
Initial soil modulus, Ei (kip/ft^2)	**296.3**
Poisson's ratio, v	**0.50**
Soil unit weight, γ_m (pcf)	**113.1**
Adhesion factor, α	**1.00**
Δ_{max}/H	**0.015**

To compute the development of the force due to adhesive resistance on the bottom and sides of the soilcrete block, it was necessary to estimate the movement required to develop full skin friction resistance. Evaluation of current literature suggests that maximum skin resistance based on load tests for both piles and drilled shafts is on the order of 0.12 to 0.4 inches (Bowles 1996). Another source suggests that skin friction is developed at about 1/10 of the displacement required to mobilize the end bearing resistance (Budhu 2007). In the PYCAP analysis, a displacement equal to 1.5% of the mass mixed zone height was used as the displacement necessary to develop full

passive resistance. Using the method suggested by Budhu, and considering the passive resistance behind the mass mixed zone as end bearing, a displacement equal to one-tenth of 1.5% times the height of 12 feet or .216 inches would be necessary to mobilize full skin friction. This value is consistent with the range suggested by Bowles and for simplicity was rounded down to 0.2 for use in these analyses. Therefore, the development of side shear and base shear was assumed to be linear up to a displacement of 0.2 inches and then remain constant. The adhesive soil resistance vs. soilcrete block displacement curves is displayed for each of the analyses in the Figure 13-11 and Figure 13-12, along with the hyperbolic curves measured with the PYCAP spreadsheet.

The PYCAP hyperbolic curves and the adhesive soil resistance curves were superimposed to create the total soil resistance curves. The total soil resistance curves from the lower and upper range analysis are compared to the total measured increase soil resistance curve (Figure 13-4) in Figure 13-14. The maximum capacity of the actuators (~600 kips) did not allow pile cap 1 to be displaced beyond the 0.75 inch mark. Thus comparisons are not able to be made at the displacement level where ultimate soil resistance was developed (2.16 inches). The total soil resistance calculated from the lower range analysis was 263 kips at a displacement of 0.72 inches, which equals about 66% of the actual measured strength increase. The mean curve resulted in a resistance of 302 kips at 0.72 inches of displacement, which is 76% of the measured resistance. For the upper range, the total soil resistance at 0.72 inches of displacement was 342 kips, which equals about 87% of the total strength increase at that displacement.

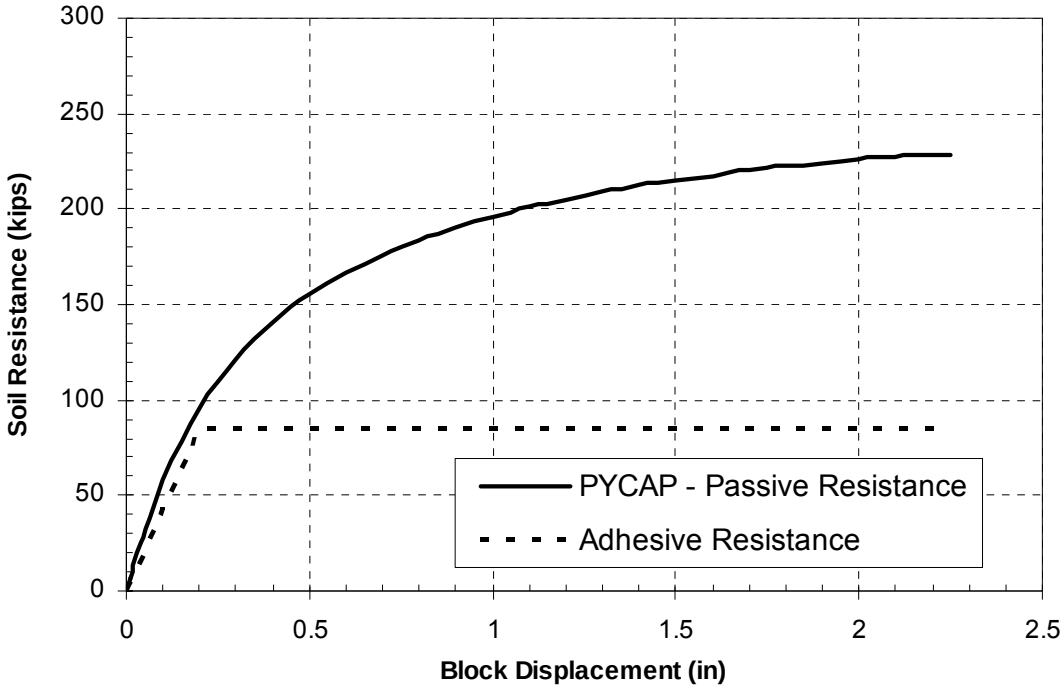

Figure 13-11 Hyperbolic passive soil resistance vs. soilcrete block displacement curve from PYCAP analysis, along with adhesive soil resistance vs. soilcrete block displacement curve for the lower bound analysis.

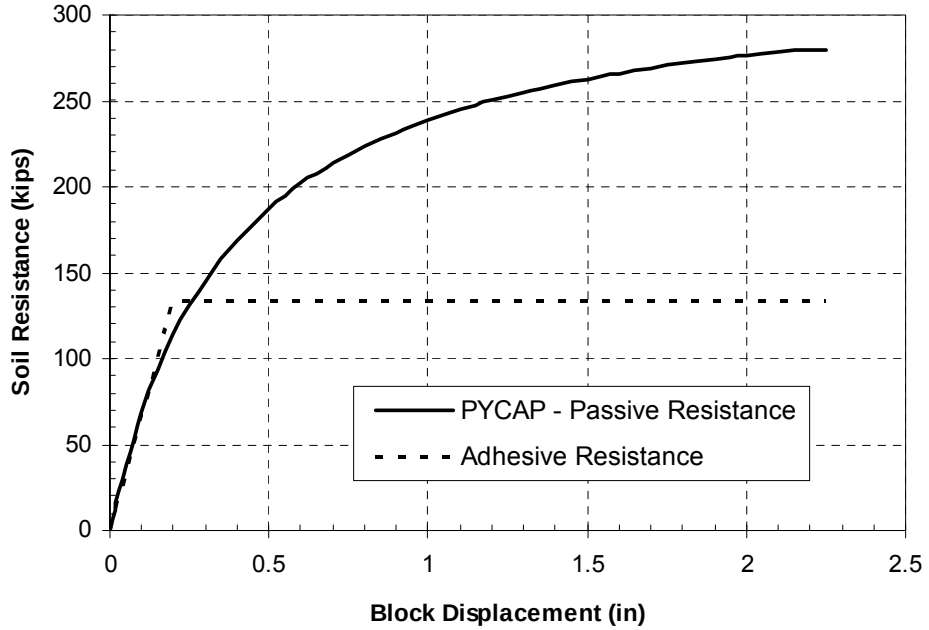

Figure 13-12 Hyperbolic passive soil resistance vs. soilcrete block displacement curve from PYCAP analysis, along with adhesive soil resistance vs. soilcrete block displacement curve for the upper bound conditions.

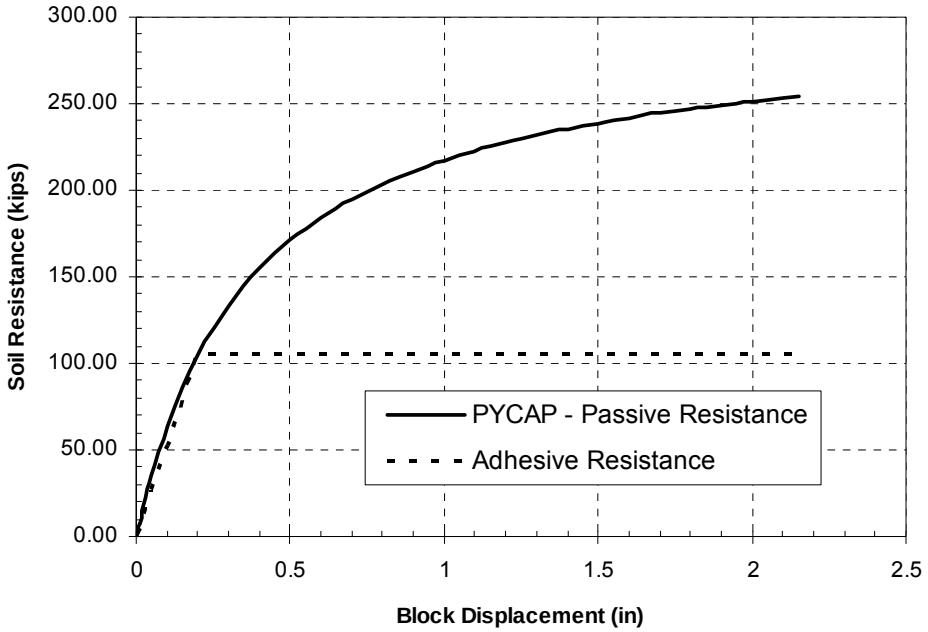

Figure 13-13 Hyperbolic passive soil resistance vs. soilcrete block displacement curve from PYCAP analysis, along with adhesive soil resistance vs. soilcrete block displacement curve for the mean conditions.

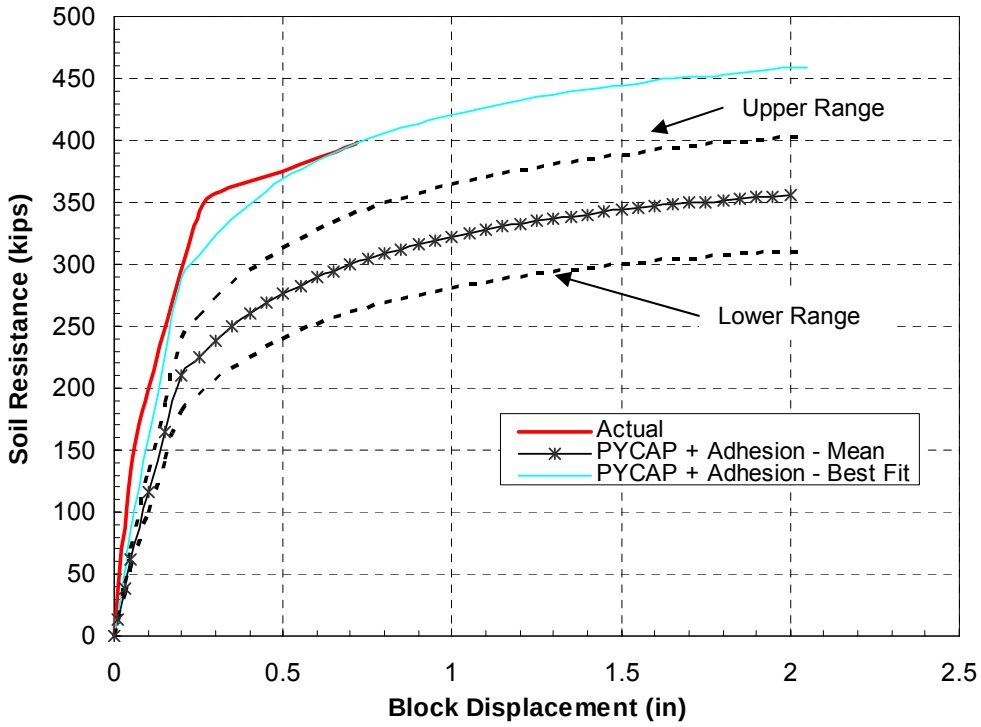

Figure 13-14 Comparison of total measured increased soil resistance with calculated increased soil resistance from PYCAP and adhesive strength analysis for pile cap 1.

A best-fit curve is also shown in Figure 13-14. This best-fit curve was back-calculated by using all of the same parameters as the mean bound curve, except that the average shear strength of the soil on the periphery and the bottom 9.5 feet of the soilcrete block was increased from the average of 325 psf until the computed curve matched best with the measured curve. The best-fit with the measured curve was obtained with a uniform undrained strength of about 650 psf, from using 1040 psf for the shear strength of the upper 2.5 feet and 550 psf for the strength of the lower 9.5 feet of the block. This strength is considerably higher than the measured values and suggests that the difference in measured resistance is likely due to some other source.

The difference in resistance between the soil resistance curves calculated with the PYCAP analysis plus the adhesive resistance and the actual measured increased resistance is likely due to the interaction between the strengthened soil and the piles. A detailed analysis of how the piles interact with the strengthened soil is beyond the scope of this thesis and will be left for the subsequent investigations. However, having such high percentages of the strength increase calculated from procedure described above, strongly suggests that the soilcrete mass did move as a rigid block. Figure 13-15 shows the portion of resistance due to displacement of the soilcrete block and soil-pile interaction for the mean analysis. For comparison with the results of pile cap 2, the best-fit curve from Figure 13-14 will be used to extrapolate the actual measured increase curve.

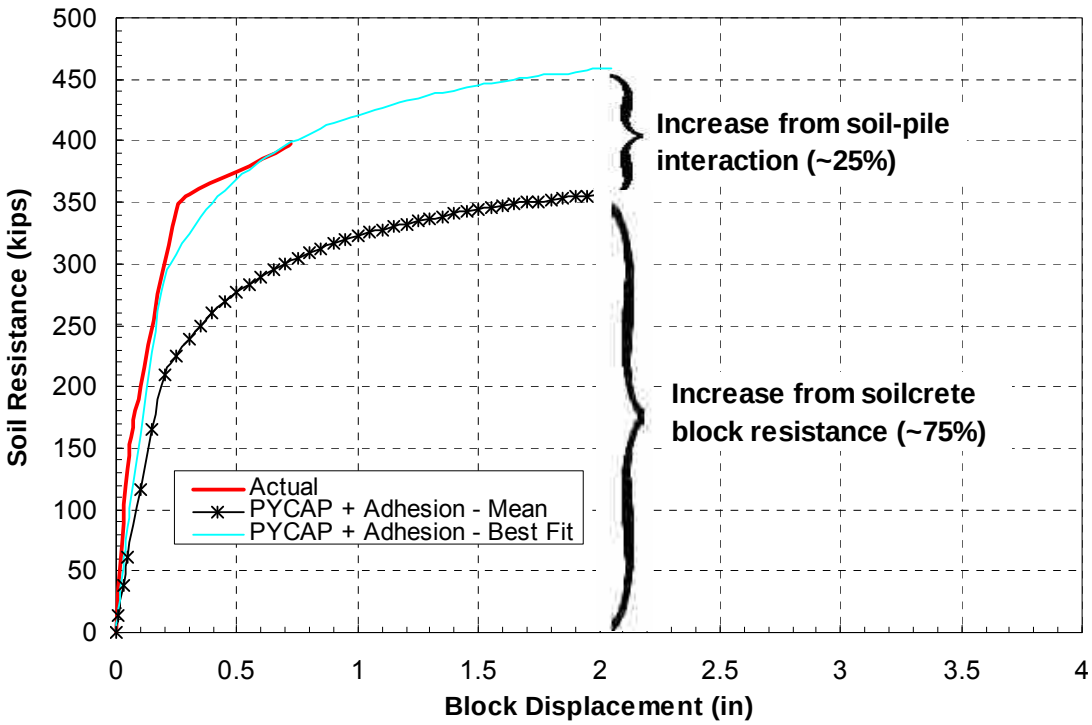

Figure 13-15 Breakdown of strength increase due to soilcrete block resistance and soil-pile interaction.

13.2.6 Rigid Block Failure – Rigid Block Bending Moment Capacity

In the previous sections, all of the potential forces acting on the soilcrete block were quantified. During testing, only a portion of the ultimate passive soil resistance calculated was developed due to the relatively small displacement values of the pile cap. However, the adhesive soil resistance acting on the soilcrete mass was fully developed. From these results, the maximum predicted bending moment occurring in the soilcrete block can be determined. Figure 13-16(a) shows the developed forces acting on the soilcrete block from the mean analysis performed previously. The total force transferred from the piles and pile cap onto the soilcrete block was determined from the mean analysis; however the actual stress distribution was not able to be determined. Since the bottom of the soilcrete was hypothesized to translate or slide through the soil, the

bending shear force and bending moment in the soilcrete block was determined to be zero at the base of the block. From this information, the stress distribution which enabled both the shear force and bending moment diagrams The distributed load acting on the left side of the block comes from the total developed force calculated for the mean analysis. Figure 13-16(b) displays the shear force diagram which would be expected in the soilcrete block calculated from beam mechanics, and assuming the bottom of the soilcrete block is fixed. In section 13.2.3 it was determined that a shear failure is highly unlikely, and the shear force diagram shows that the magnitude maximum shear force is only 22 kip-ft at a depth of 2.5 feet from the top of the pile cap, which is considerably lower than the shear capacity of the soilcrete block.

Figure 13-16(c) shows the bending moment diagram derived from the shear diagram. From the diagram, the maximum moment applied to the mass mixed zone would be about 65 kip-ft, occurring at a depth of 6.5 feet below the pile cap. Typical tensile strength for concrete occurs on the order of about 8% to 15% the unconfined compressive strength (MacGregor and Wight 2005). If it is assumed that the soilcrete would crack at about 12% of its unconfined compressive strength of 250 psi (design strength), then the theoretical bending moment to initiate cracking would be about 84.5 kip-ft. (Hand calculations for this procedure are found in Appendix D) Since the maximum moment was only 65 kip-ft, even the low design estimate for the soilcrete strength is adequate to resist cracking due to the generated bending moment. This helps to further validate that the soilcrete mass experienced rigid block failure.

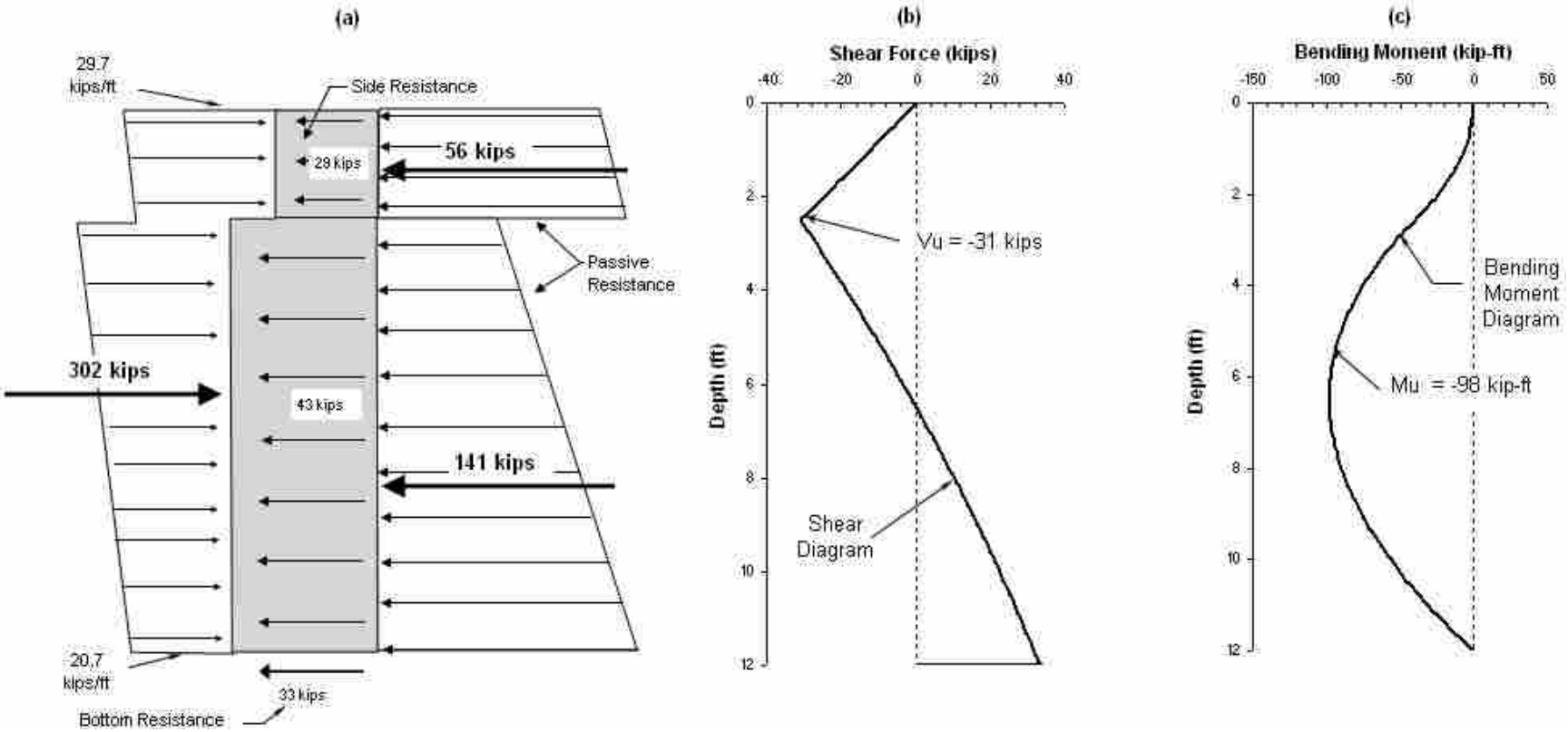

Figure 13-16 (a) The free body diagram defining the horizontal forces on the soilcrete block as passive soil resistance, adhesive soil resistance, and the load transferred from the pile cap and piles. (b) The shear diagram of the soilcrete block defining the maximum shear as -31 kips at a depth of 2.5 feet below the ground surface. (c) The bending moment diagram of the soilcrete block defining the maximum bending moment as -98 kip-ft at a depth of 6.5 feet below the ground surface.

13.3 Jet Grout Test Comparisons for Pile Cap 2

The results from pile cap 1 for both the mass mix treated zone (Herbst, 2008), and the jet grout treated zone, suggest that the soilcrete mass below pile cap 2 also displaced as a rigid block. In fact, it is high unlikely that the mass would have experienced a shear or bending moment failure, since it was "reinforced" with piles which extended through the entire thickness of the soilcrete block. Therefore, it is unnecessary to check the shear and bending moment capacity of the soilcrete block beneath pile cap 2. However, a PYCAP and adhesive resistance analysis will be performed to determine the strength increase that would be expected for the sliding soilcrete block.

13.3.1 Load vs. Displacement Comparison

Figure 13-17 displays the peak load-displacement curves for all of the tests involving pile cap 2 following jet grouting. The results from the virgin tests are also shown for comparison. In this figure it can be seen that the results from test 3 and test 4 can be combined to produce a "virgin" load displacement curve for pile cap 2 in the jet grout treated soil. The final peak point on the load-displacement curve for test 3 is neglected when producing the combined curve. Refer to section 9.1 for a detailed discussion on this issue.

The reloading of the soil at pile cap deflections less than 3 inches would have significantly decreased the soil resistance acting on the pile group. Also, the passive pressure acting on the pile group did not begin to develop until the pile cap began displacing beyond the point of initial displacement. Shifting the load-displacement

curve closer to the origin helps to compensate for this decrease in the strength from reloading and change in initial pile cap displacement. Therefore, the load deflection curve for test 5 has been shifted back to the origin in order to make valid comparisons between the tests performed before and after excavation of the soil on the face of the pile cap. Test 6 was shifted the same amount to the right. The shifted results from tests 5 and 6 can be combined in similar fashion to tests 3 and 4 to produce the load-displacement curve with no passive soil resistance behind the pile cap.

Figure 13-18 displays the combined curves after jet grouting in comparison with the virgin load-displacement curves. It can be seen that combined load-displacement curve for the pile cap before excavation can be separated into three distinct parts. The initial 0.3 inches of the curve are fairly linear. At a displacement of 0.3 inches the curve shows an abrupt change in slope. A second linear portion of the curve extends from 0.3 to about 1.6 inches of displacement. The third portion of the curve following 1.6 inches of displacement is flat with a slight drop off in strength after 2.1 inches of displacement. This shape is much different than the hyperbolic shape of the load-displacement curve for the virgin tests. The linear portions of the combined load-displacement curve following excavation are somewhat less defined due to reloading effects, but the same general trends in the shape of the load-deflection curve would be expected for this load-deflection curve if the soilcrete mass beneath pile cap 2 displaced as a rigid block.

The initial stiffness of the load-displacement curve for the “Jet Grout” curve in Figure 13-18 is considerably higher than the initial stiffness during virgin loading. The pile cap only displaced .016 inches at a load of 200 kips. The initial stiffness of the “Jet-

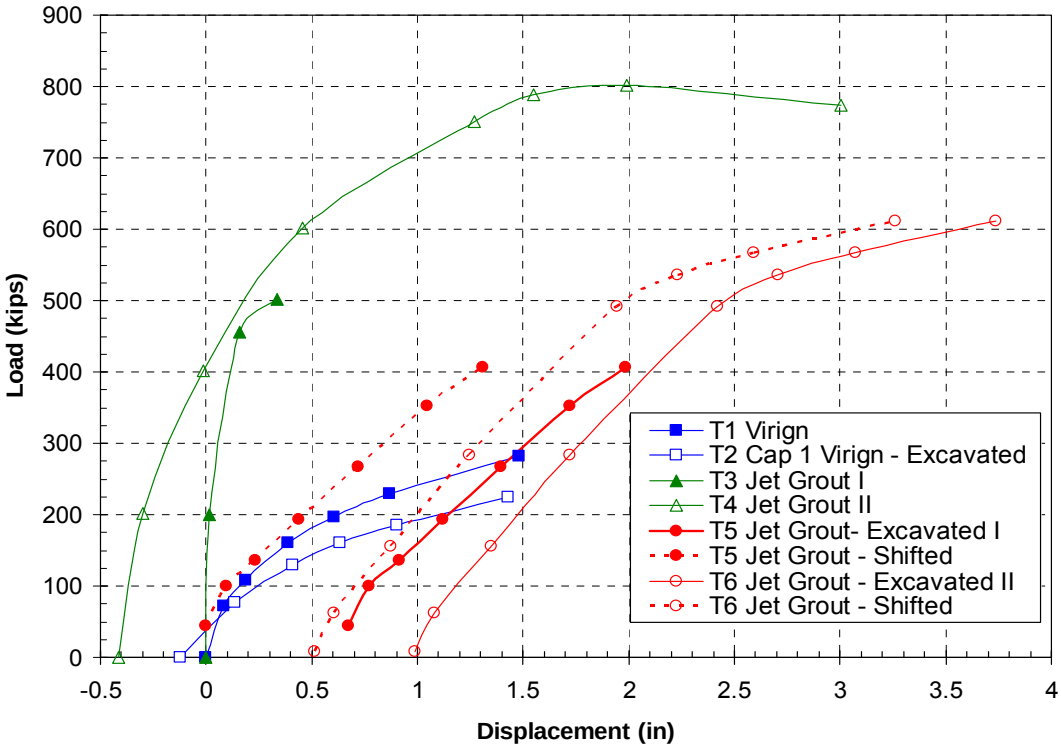

Figure 13-17 Load-displacement curves for all tests performed on pile cap 2 following jet grouting. The results from the virgin test are also shown for comparison.

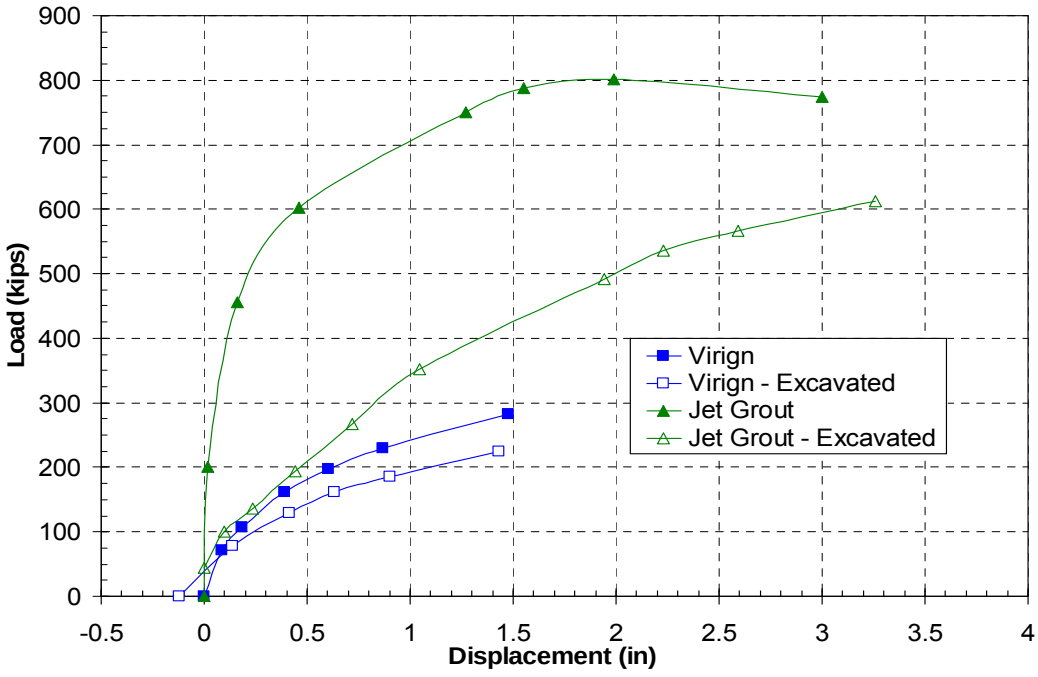

Figure 13-18 Combined load-displacement curves for tests performed on pile cap 2 following jet grouting. The results from the virgin test are also shown for comparison.

Grout – Excavation" curve is not any higher than the initial stiffness during the virgin tests, and is due to weakening of the soil through reloading.

The increase in total lateral resistance from improving the soil beneath pile cap 2 with jet grout can be found by comparing the load-displacement curve from the virgin test in native soil (test 1) with the combined load-displacement curves from test 3 and 4 after jet grout treatment. The increased lateral resistance of pile cap 2 due to jet grouting is plotted as a function of displacement in Figure 13-19. This curve was generated by taking the difference between the load for "Jet Grout" and the load for "Virgin" curves in Figure 13-18 at several displacement levels. From the curve it can be seen that the ultimate increase in soil resistance was 495 kips, and this resistance was fully developed at a deflection of 2 inches. Comparing the resistance at a displacement of 1.5 inches, jet grouting increased the lateral pile cap resistance from 282 kips to nearly 782 kips. This increase of 500 kips equates to an increase in total resistance of about 2.6 times or 160%.

13.3.2 Development of Soil Resistance vs. Block Displacement Curves

A profile schematic drawing of how the soilcrete mass would have displaced as a rigid block is shown in Figure 13-20. The block would have displaced in this manner before and after excavation of the soil at the face of the pile cap. Just as for pile cap 1, it is assumed that a majority of the increased strength was caused by displacing the soilcrete block through the weak clay soil. The soil resistance acting on the soilcrete block consisted of the passive soil resistance acting on the face of the soilcrete block and the adhesive force acting on the bottom and the sides of the block.

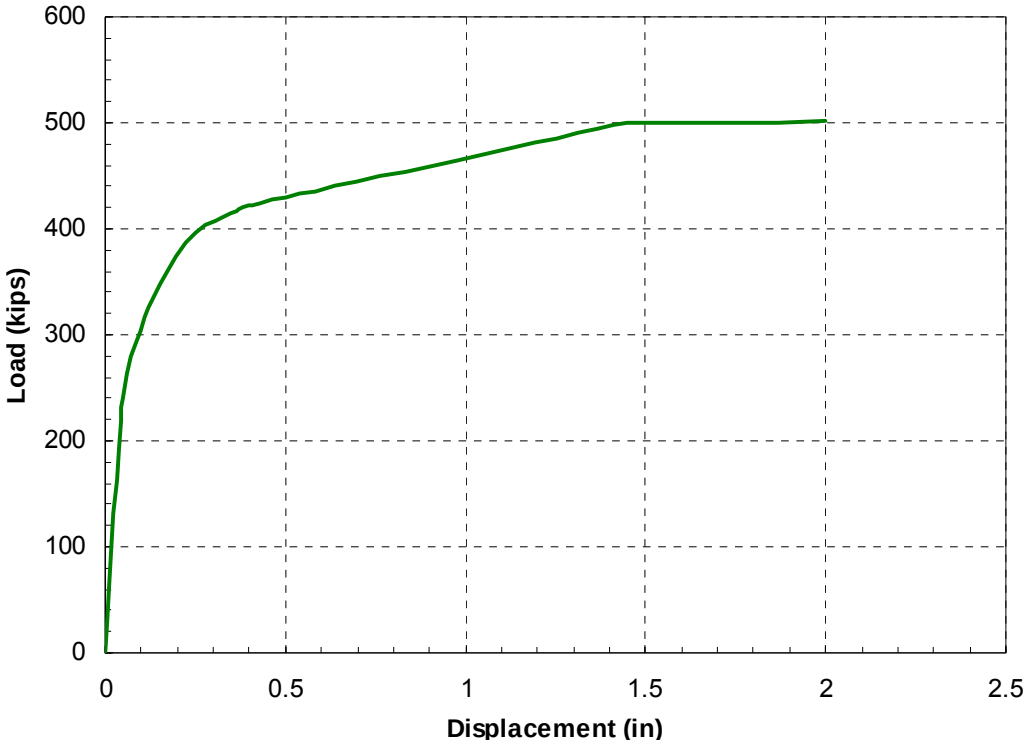

Figure 13-19 Total measured increased lateral resistance from jet grouting below pile cap 2.

The PYCAP spreadsheet tool was again used to estimate the development of the passive resistance on the face of the soilcrete block. Thus, the input parameters selected for the PYCAP analysis are generally the same as those used to compute the ultimate passive earth pressure for pile cap 1, and the following section will only outline the development of the soil-resistance vs. block displacement curve. Using the hyperbolic model in PYCAP, hyperbolic curves were created using a range of possible input parameters. The equivalent pile cap dimension and the shear strength of the soil were varied once again to define the upper range, mean, and lower range curves.

The parameters used for each of these respective analyses are shown in .

Table 13-4 through Table 13-6. The actual in-situ geometry of the soilcrete columns was never determined. Therefore, soilcrete diameters from 4-6 ft, which varied

from the 5 ft design diameter, were used in the analyses. The range of equivalent pile cap widths was from 10-12 ft, with a mean width of about 11 ft. The height of the soilcrete columns was precisely controlled by the drill rig, and was assumed to be 10 feet for each of theanalyses. The soilcrete columns were inserted just below the pile cap. Thus, the embedment depth of the equivalent pile cap was 2.5 feet or the height of the pile cap. The cohesion or shear strength of the soil was determined from the results displayed in Figure 3-3. The average shear strength of the soil for a depth range of 2.5 – 10 feet was determined to be 300 psf for the lower bound and 350 psf for the upper bound, with a mean shear strength of 325 psf. These are the same shear strengths as those used in the pile cap 1 analysis (Figure 13-9). The relatively rapid loading of the soil necessitated an undrained analysis be performed. Thus, the soil friction angle was 0 degrees, which correlates to a passive earth pressure coefficient (K_p) of 1.0. The initial soil modulus was estimated using Equation 7-1, with the plasticity index being 25. A value of 0.5 was used for the Poisson's ratio of the saturated clay.

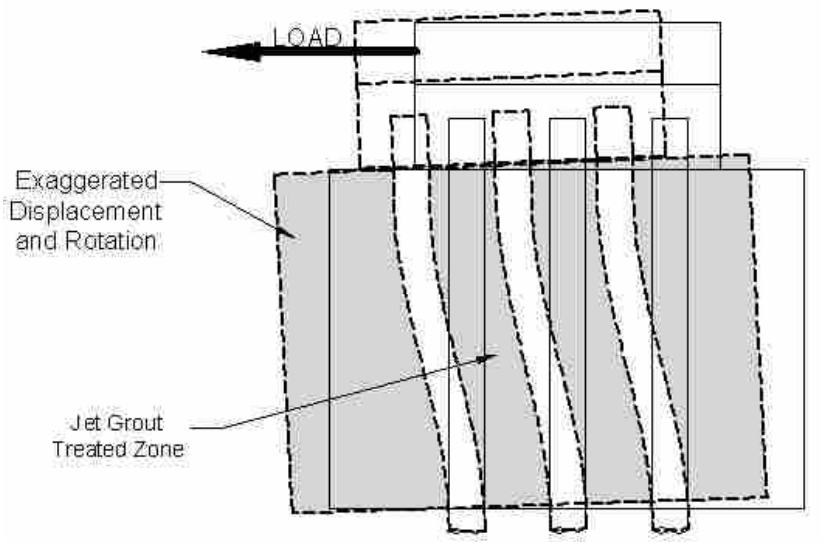

Figure 13-20 Exaggerated profile view of jet grout treated zone beneath pile cap 2 displacing as a rigid block.

Table 13-4 Parameters used in PYCAP analysis for the lower range curve.

Cap width, b (ft)	**10.00**
Cap height, H (ft)	**10.00**
Embedment depth, z (ft)	**2.50**
Surcharge, qs (psf)	**0.0**
Cohesion, c (psf)	**300.0**
Soil friction angle, Φ (deg.)	**0.0**
Wall friction, δ (deg.)	**0**
Initial soil modulus, Ei (kip/ft^2)	**180**
Poisson's ratio, v	**0.50**
Soil unit weight, γ_m (pcf)	**112.0**
Adhesion factor, α	**1.00**
Δ_{max}/H	**0.015**

Table 13-5 Parameters used in PYCAP analysis for the mean curve.

Cap width, b (ft)	**11.00**
Cap height, H (ft)	**10.00**
Embedment depth, z (ft)	**2.50**
Surcharge, qs (psf)	**0.0**
Cohesion, c (psf)	**325.0**
Soil friction angle, Φ (deg.)	**0.0**
Wall friction, δ (deg.)	**0**
Initial soil modulus, Ei (kip/ft^2)	**195**
Poisson's ratio, v	**0.50**
Soil unit weight, γ_m (pcf)	**112.0**
Adhesion factor, α	**1.00**
Δ_{max}/H	**0.015**

Table 13-6 Parameters used in PYCAP analysis for the upper range curve.

Cap width, b (ft)	**12.00**
Cap height, H (ft)	**10.00**
Embedment depth, z (ft)	**2.50**
Surcharge, qs (psf)	**0.0**
Cohesion, c (psf)	**350.0**
Soil friction angle, Φ (deg.)	**0.0**
Wall friction, δ (deg.)	**0**
Initial soil modulus, Ei (kip/ft^2)	**210**
Poisson's ratio, v	**0.50**
Soil unit weight, γ_m (pcf)	**112.0**
Adhesion factor, α	**1.00**
Δ_{max}/H	**0.015**

The average soil unit weight was determined to be 112 pcf (Table 3-1). An adhesion factor of 1.0 was used, because it was assumed that the interlock between the soft clay and the soilcrete was quite high. The percent of wall height used to mobilize full passive resistance (Δmax/H) was 1.5%, which is consistent with the findings of Brandenberg et al. (2005) for naturally occurring cohesive soils. Thus, a displacement of 1.8 inches (R_f = 0.86) would be needed to fully develop passive resistance. The passive soil resistance hyperbolic curve vs. block displacement is presented for each of the analyses in Figure 13-22 through Figure 13-24. The ultimate passive resistance was 145 kips for the low range and 186 kips for the high range, with a mean resistance of 165. The passive soil resistance pressure distribution on the face of the soilcrete mass for each of the respective analyses is also illustrated in Figure 13-21.

The adhesive resistance of the soft clay acting on the block was then determined. Because the clay is soft, an adhesion factor of 1.0 would appear appropriate based on research regarding unit side resistance of piles in clay (API, 1986). An adhesion factor of 1.0 indicates that the adhesion between the clay and soilcrete is equal to the cohesive strength of the clay. It was assumed that the adhesive force acted on the sides and the bottom of the soilcrete mass. The lengths of the sides of the soilcrete mass for the lower bound analysis were 14 feet, 15 feet for the mean, and 16 feet for the upper range analysis. For a height of 10 ft, the total side surface area contributing to the adhesive soil resistance on the soilcrete mass for the upper and lower range tests between 280-320 ft^2, with a mean of 300 ft^2. These areas were then multiplied by the cohesive strength of the clay (300-350 psf) to calculate the fully developed adhesive soil resistance contribution from the sides of the soilcrete block.

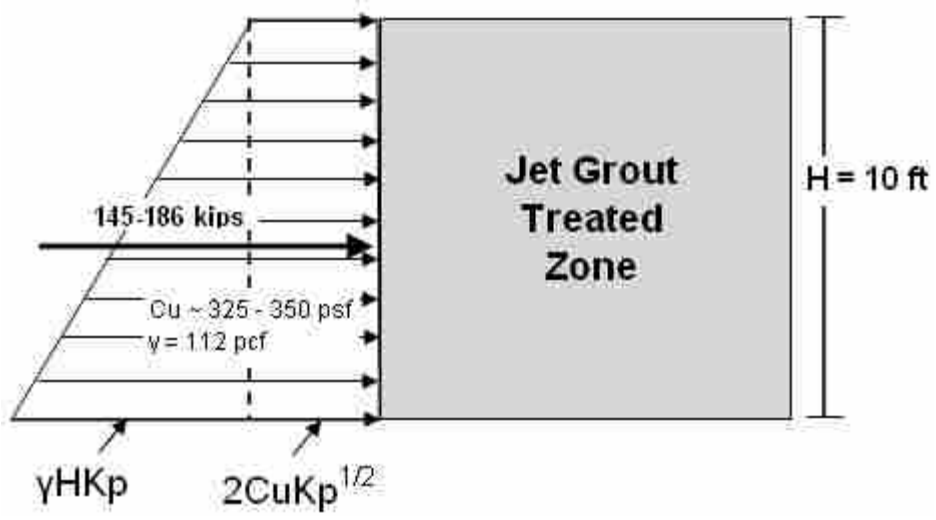

Figure 13-21 Passive soil pressure distribution on face a soilcrete mass for PYCAP analysis.

The side adhesive resistance was calculated to be between 84 and 112 kips, with a mean of 97.5 kips. The area of the bottom of the soilcrete block was between 154 ft^2 and 208 ft^2. The range of undrained shear strengths for the soil on the bottom of the block were assumed to be between 350-375 psf, with a mean strength of 365 psf. These are the same shear strengths used in the previous analysis. The adhesive soil resistance acting on the bottom of the block was calculated to be 49 kips for the low range and 72 kips for the upper range, and 60 kips for the mean. Thus, the total adhesive soil resistance acting on the sides and the bottom of the block was between 133 and 184 kips, with a mean of 158 kips. It was once again assumed that the application of the adhesive force on the sides of the block increased linearly until if was fully developed at a displacement of 0.2 inches (Budhu, 2007). The adhesive soil resistance vs. soilcrete block displacement curves are displayed for each of the analyses in the Figure 13-22 through Figure 13-23, along with the hyperbolic curves measured with the PYCAP spreadsheet.

The PYCAP hyperbolic curves and the adhesive soil resistance curves were then superimposed to create the total soil resistance curves. The total soil resistance curves from the three analyses are compared to the total measured increase soil resistance curve (Figure 13-19) in Figure 13-25. The total soil resistance calculated from the PYCAP and adhesive strength analysis for the lower range was 278 kips at a displacement of 2 inches, which equals about 56% of the total strength increase. For the upper range, the calculated soil resistance at 2 inches of displacement was 370 kips, which equals about 74% of the total strength increase. The mean analysis yielded a soil resistance of 323 kips or 65% of the measured increase. A best-fit curve is also shown in Figure 13-25. This best-fit curve was calculated by using all of the same parameters as the mean curve, but the average shear strength of the soil around the periphery and bottom of the soilcrete block was increased to 600 psf.

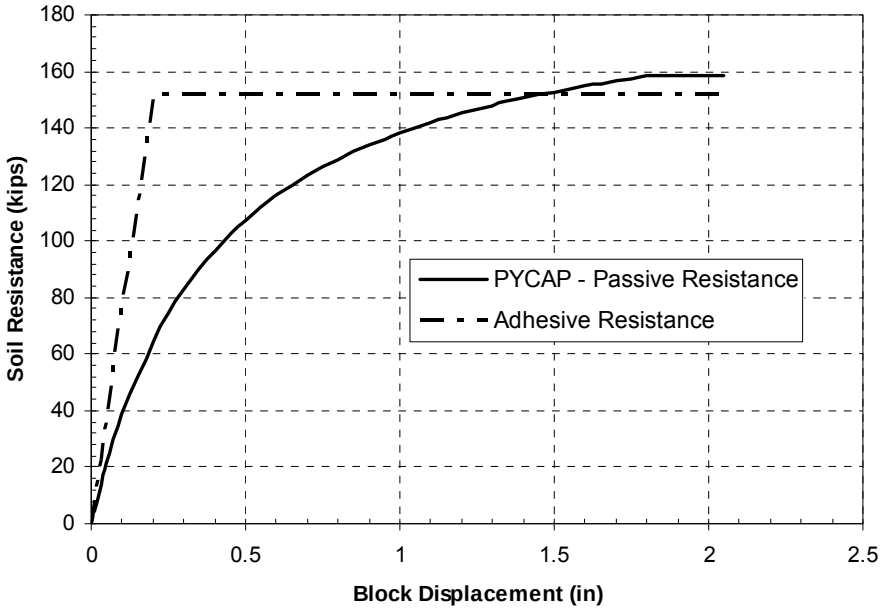

Figure 13-22 Hyperbolic passive soil resistance vs. soilcrete block displacement curve from PYCAP analysis, along with adhesive soil resistance vs. soilcrete block displacement curve for the lower bound analysis.

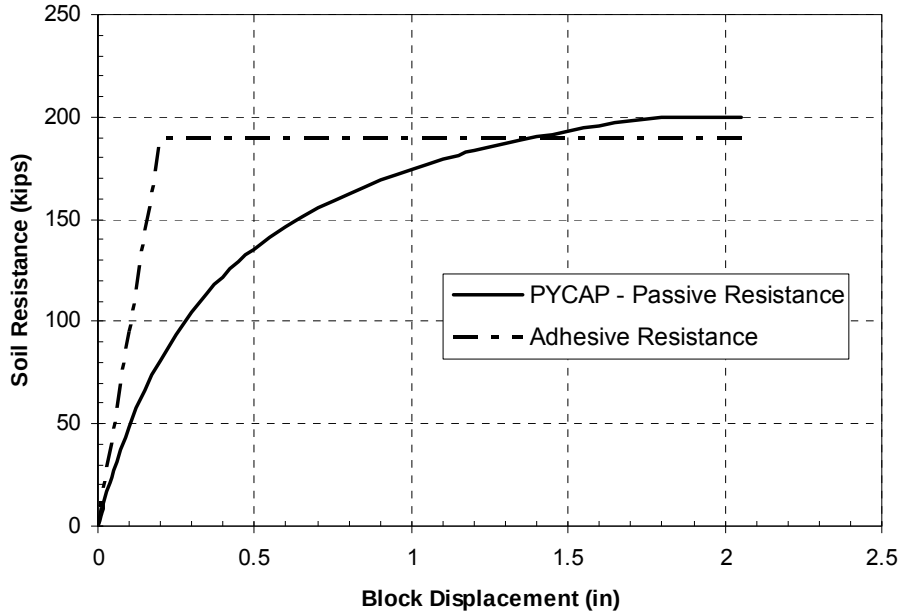

Figure 13-23 Hyperbolic passive soil resistance vs. soilcrete block displacement curve from PYCAP analysis, along with adhesive soil resistance vs. soilcrete block displacement curve for the upper bound analysis.

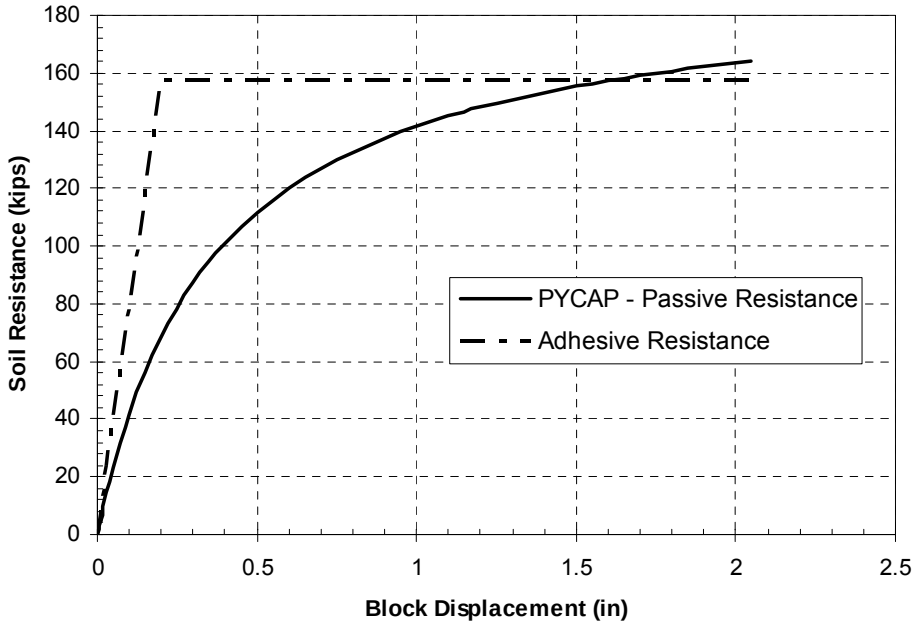

Figure 13-24 Hyperbolic passive soil resistance vs. soilcrete block displacement curve from PYCAP analysis, along with adhesive soil resistance vs. soilcrete block displacement curve for the upper bound analysis.

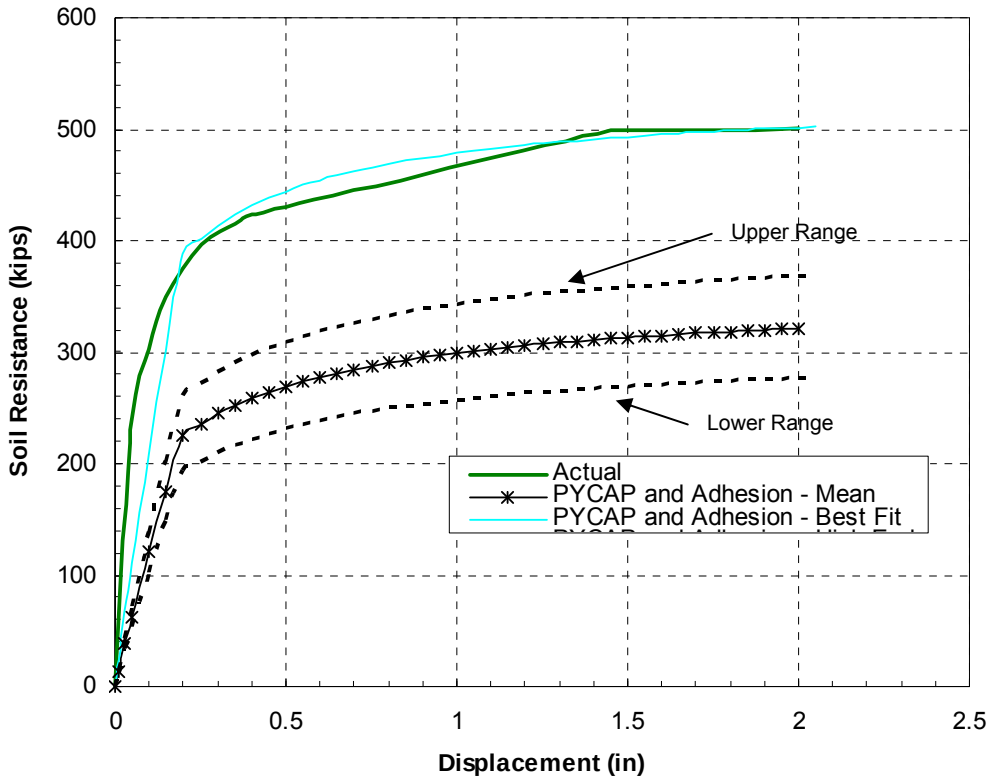

Figure 13-25 Comparison of total measured increased soil resistance with calculated increased soil resistance from PYCAP and adhesive strength analysis for pile cap 2.

Additionally, a breakdown of the portions of resistance coming from soilcrete block resistance and soil-pile interactions for the mean analysis is also displayed in Figure 13-26. These results are comparable with the results from the soilcrete block installed adjacent to pile cap 1; however, the mean analysis on pile cap 1 provided for 75% (compared to 65% for pile cap 2) of the measured increase in lateral resistance from the passive and adhesive force calculations performed for the soilcrete block. This means that a greater percentage of the increased lateral resistance is coming from soil-pile interaction for pile cap 2. This behavior is expected because the soilcrete installed beneath the pile cap interacts with all 9 piles of the pile group, where as the soilcrete installed adjacent to pile cap 1 only interacts with the lead row of piles in pile cap 1.

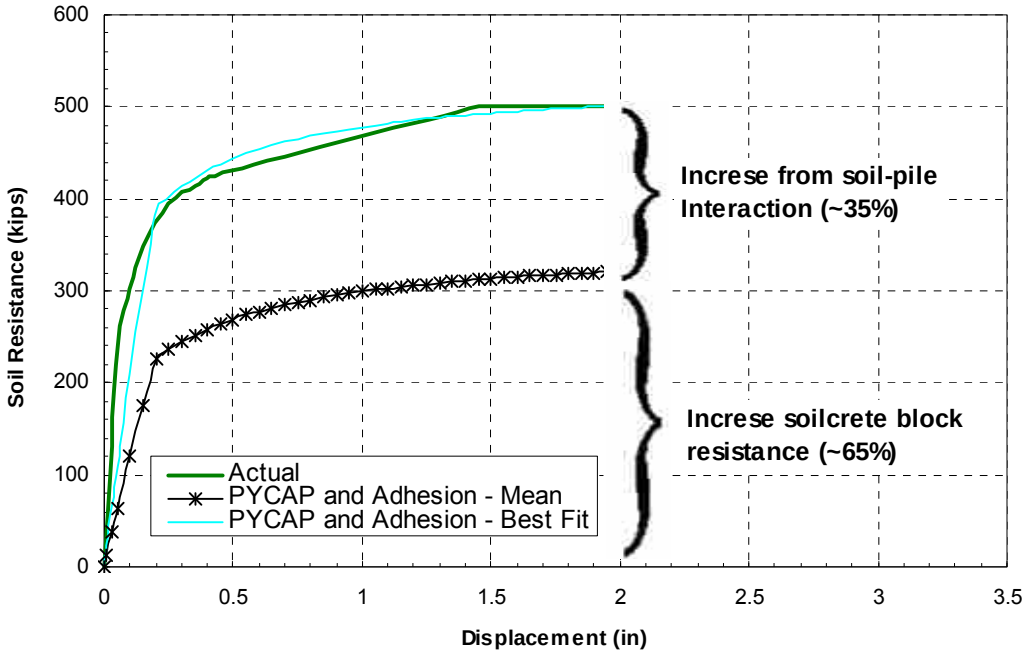

Figure 13-26 Breakdown of strength increase due to soilcrete block resistance and soil-pile interaction for pile cap 2 analysis.

The shape of each of the curves is very similar, with each curve being broken up into 2 segments. This suggests that the failure mechanism presented and analyzed is potentially correct. The first linear segment has a relatively steep slope, and extends to a displacement of about 0.2 inches. The following segment has a much flatter slope and a hyperbolic shape. This second segment extends until failure at about 1.5 inches. This suggests that the adhesive and passive soil resistance were increasing with increasing displacement during the initial 0.2 inches of displacement. The adhesive resistance became fully developed at 0.2 inches, and only the passive soil resistance increased with increasing displacement after further displacements.

An average undrained shear strength of 600 psf was needed to match the actual increased resistance curve using the PYCAP and adhesive soil resistance procedure. From Figure 13-10 above, it can be seen that an average of 600 psf for the soil profile

from 2.5 to 12.5 feet below the ground surface is greater than what was measured during field testing. Thus, the difference between the actual measured increased resistance curves and those calculated following the above procedure is probably not only due to a underestimation of undrained soil shear strength. The difference in resistance between the soil resistance curves calculated with the PYCAP analysis plus the adhesive force and the actual measured increased resistance is likely due to the interaction between the strengthened soil and the piles. A detailed analysis of how the piles interact with the strengthened soil will be left for the subsequent parametric studies and finite element analysis.

Additionally, if the jet grout mass did move as a rigid block, then it would be assumed that the difference in lateral resistance between the tests performed with and without soil directly behind the pile cap on the post jet grouted pile cap 2 would only be 50 kips; which was the passive force acting on the face of the pile cap calculated from test 2. However, the combined load-displacement curve from the tests performed after excavation of the soil from the face of pile cap 2 in Figure 13-18 shows a difference of 200 kips between the tests performed before and after excavation at a displacement of about 1.5 inches. The difference in soil resistance above 50 kips is likely due to reloading effects, which would decreased the measured soil resistance by an additional 20% or 150 kips from the previous test.

The 10% difference in resistance during reloading seen during the virgin test, was the difference is resistance at previous peak displacements. Pile cap 2 had been displaced about 4 inches during the inclinometer testing of test 4, and thus a decrease is

resistance of 10% would be expected at a pile cap displacement 4inches; however, at a displacements less than 4 inches, a decrease in resistance greater than 10% is expected.

13.4 Jet Grout - Pile Cap 1 and Pile Cap 2 Comparison

Figure 13-27 displays the combined curves from both pile caps 1 and 2 following jet grouting. The curve was pile cap 1 was extrapolated to a displacement of 2.3 inches. The extrapolated portion of the curve shows the predicted shape of the curve, had the pile cap been displaced over 2 inches. The ultimate load from extrapolated curve was predicted to be between 750 and 760 kips at a deflection of about 2.0 inches. The best-fit curve from the previous PYCAP and adhesive soil resistance analysis (Figure 13-14), which calculated a total increase in soil resistance of 458 kips at a displacement of 2.0 inches, was added to the virgin load displacement curve at displacements greater than ~0.7 inches to create the extrapolated portion of the curve. It was assumed that the soil resistance on the soilcrete block adjacent to pile cap 1 would have peaked at approximately 2 inches of displacement. It can be seen that the ultimate load to displace pile cap 1 about 2 inches is approximately 40-50 kips below the ultimate load measured for the tests on pile cap 2. Figure 13-28 compares the increased resistance from treating the soil surrounding the separate pile caps with jet grouting. It can be seen that each of the curves has a fairly similar shape. This further validates that a majority of the increased soil resistance can be attributed to displacing the soilcrete mass below or adjacent to the pile cap as rigid block through the native soil. About 50 percent more soil was treated beneath pile cap 2 compared with the soil treated adjacent to pile cap 1. However, the difference in the ultimate increase in soil

resistance of about 50 kips is relatively small compared with the additional amount of treated soil beneath pile cap 2. According to the previously performed analysis, the soil resistance on the soilcrete block came from both passive pressure on the face of the block and adhesive resistance on the sides and bottom of the block. The greater volume of the soilcrete block beneath pile cap 2 yielded a greater block surface area, and, subsequently, a greater adhesive soil force.

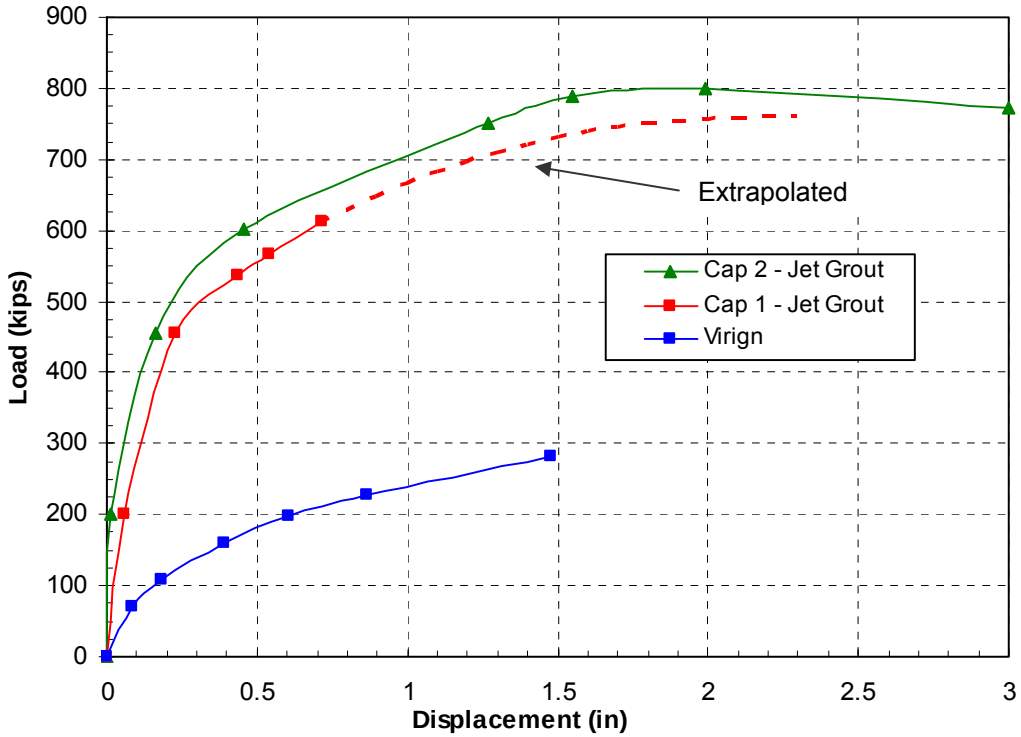

Figure 13-27 Comparison of combined load- displacement curves from the tests on pile caps 1 and 2 following jet grouting. The virgin curve is also displayed for comparison.

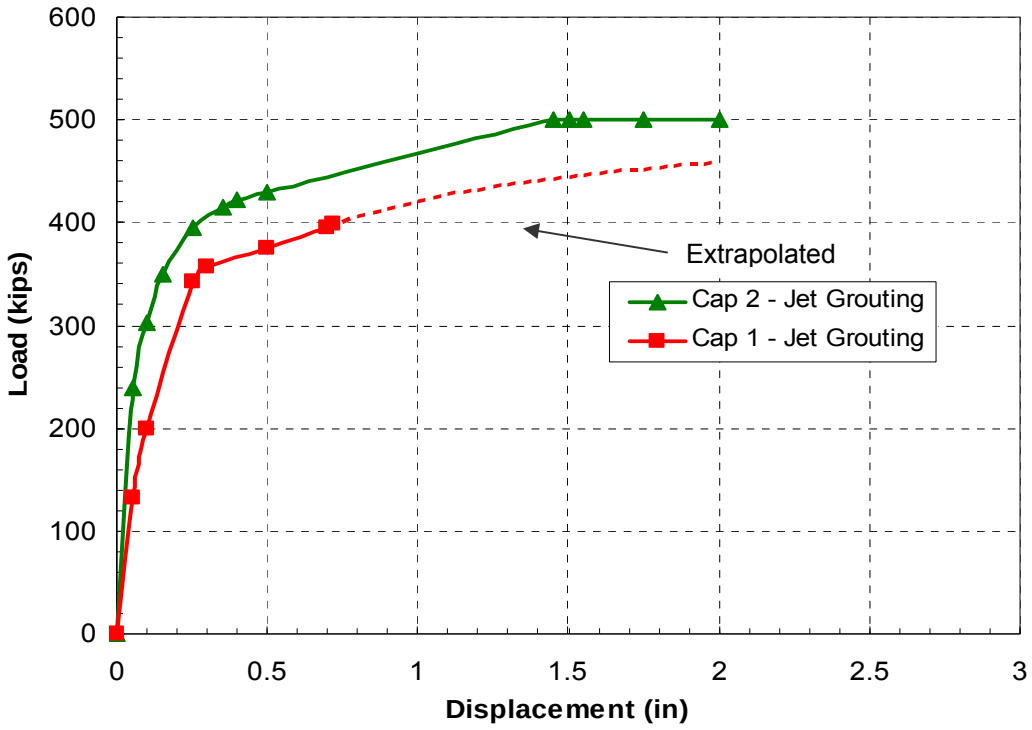

Figure 13-28 Total measured increased lateral resistance from jet grouting below pile caps 1 and 2.

However, the passive resistance acting on the block beneath pile cap 2 was less than the passive resistance acting on the face of block adjacent to pile cap 1. The reason for this difference in passive resistance is the length of the face of the soilcrete mass perpendicular to the direction of loading. This dimension is equal to the "B" parameter from the Rankine passive pressure theory displayed in Equation 13-1. The face of the block adjacent to pile cap 1 was approximately 2-3 feet wider than the face of the soilcrete block beneath pile cap 2. This increased the passive soil pressure on the face of the block, and partially counteracted the decrease in adhesive soil resistance on the block adjacent to pile cap 1. This can be confirmed by analyzing Figure 13-11 through Figure 13-14 and Figure 13-22 through Figure 13-24.

13.5 Rotation vs. Load Comparison

Although an exhaustive study of the increased lateral resistance due to the soil pile interaction will be left for the parametric studies. A simple comparison of the pile head rotation behavior before and after treatment with jet grouting can help to verify that there was increased lateral resistance which came from soil-pile interaction. Figure 13-29 below provides the pile head rotations in pile cap 1 before and after treatment with jet grouting. The rotations from test 6 in Figure 13-29, which represent the rotations of pile cap 1 following jet grouting, were taken relative to the beginning of test 6, in stead of relative to the beginning of test 3 as was presented in section 12.2. This was done to more easily determine the amount of pile head rotation as the pile cap was displaced during test 6. From the figure it can be seen that pile cap 1 experienced much less rotation for loads greater than 250 kips.

The average initial rotations measured from the shape arrays during test 6 are somewhat larger than initial pile cap 1 rotations from test 1. This is likely due to the reloading of the soil, or the gap created by having an initial pile cap displacement of "negative" 0.5 inches. The pile cap had also been previously been loaded to 500 kips and a displacement of 0.3 inches during test 3. Nevertheless, the pile head rotation after soil treatment is considerably decreased during the larger loadings, which is sufficient to prove that the lateral stiffness of the piles had been increased due the installation of soilcrete columns adjacent to pile cap 1.

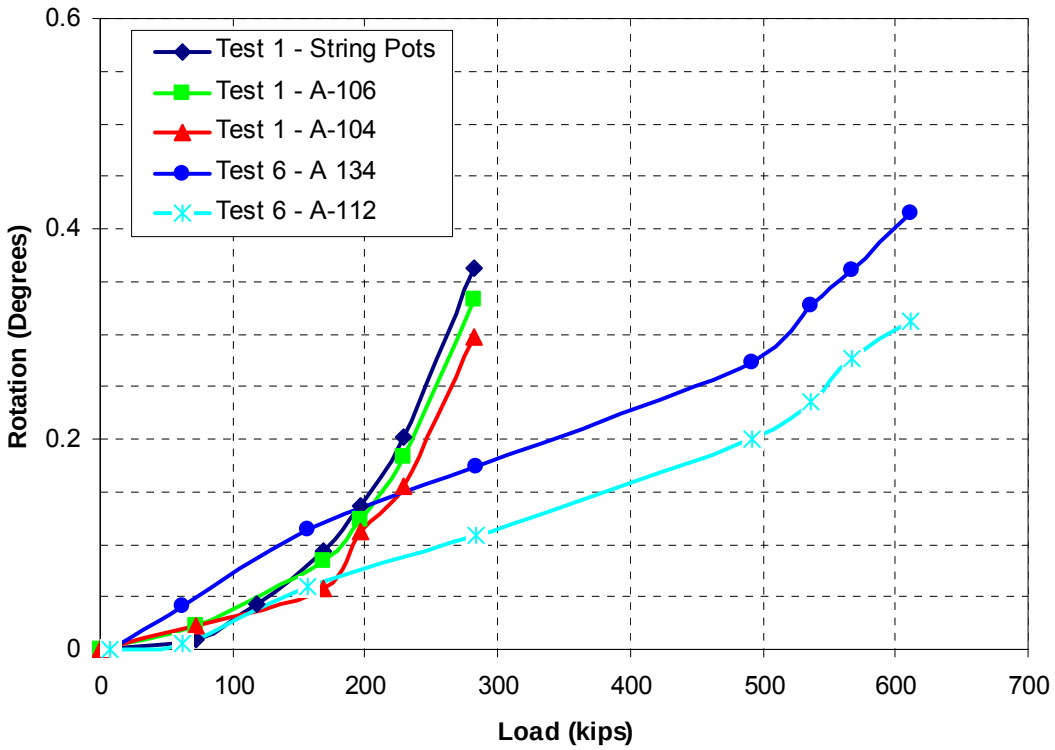

Figure 13-29 Pile head rotation comparison for pile cap 1 before and after soil treatment with jet grouting.

Figure 13-30 provides the pile head rotations taken during test 4 for pile cap 2 compared with the rotations measured during the virgin test. The rotations from test 4 are also shown relative to the beginning of test 4. In this figure it can be seen that the rotations measured during test 4 also show decreased pile head rotation, which proves that the lateral stiffness of the piles had also been increased through installing soilcrete columns beneath pile cap 2. The results from each of the pile caps suggests that the difference between the actual measured increase in lateral resistance and the increased passive and adhesive soil resistance calculated for the pile caps in Figure 13-14 and Figure 13-25 could potentially be attributed to soil-pile interaction.

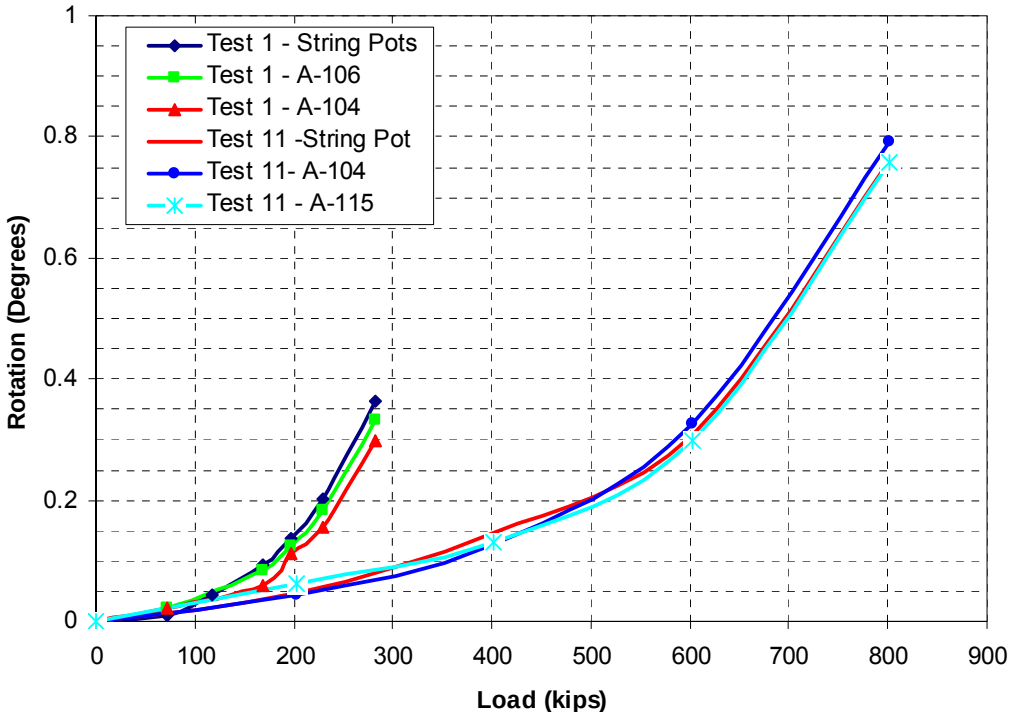

Figure 13-30 Pile head rotation comparison for pile cap 2 before and after soil treatment with jet grouting.

13.6 Bending Moment Comparison

If the soilcrete masses beneath pile cap 2 and adjacent to pile cap 1 did fail as a rigid block, it is assumed that this would decrease the deflection of the piles with depth. The bending moment calculations were based solely on the curvature or the measured deflections of the piles. Reduced bending moments are evidence that the piles experienced smaller deflections at depth. Figure 13-31 and Figure 13-32 display the maximum load vs. resulting maximum positive bending moment in the piles of pile cap 1 before and after treatment with jet grouting. In these plots it can be seen that the post jet grouting bending moments in the piles (Tests 4 and 6) of pile cap 1 experience less bending moment than the piles before jet grouting at loads greater than 250 kips.

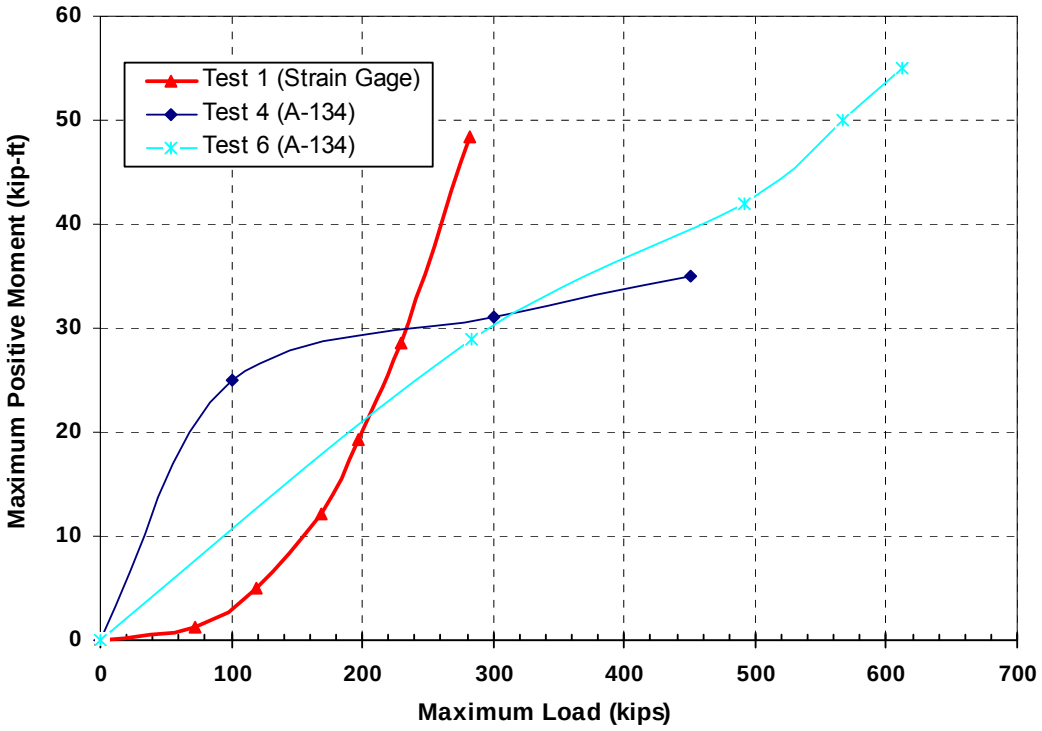

Figure 13-31 Comparison in measured bending moment in the south center pile of pile cap 1 (1-S) before and after soil treatment with jet grouting.

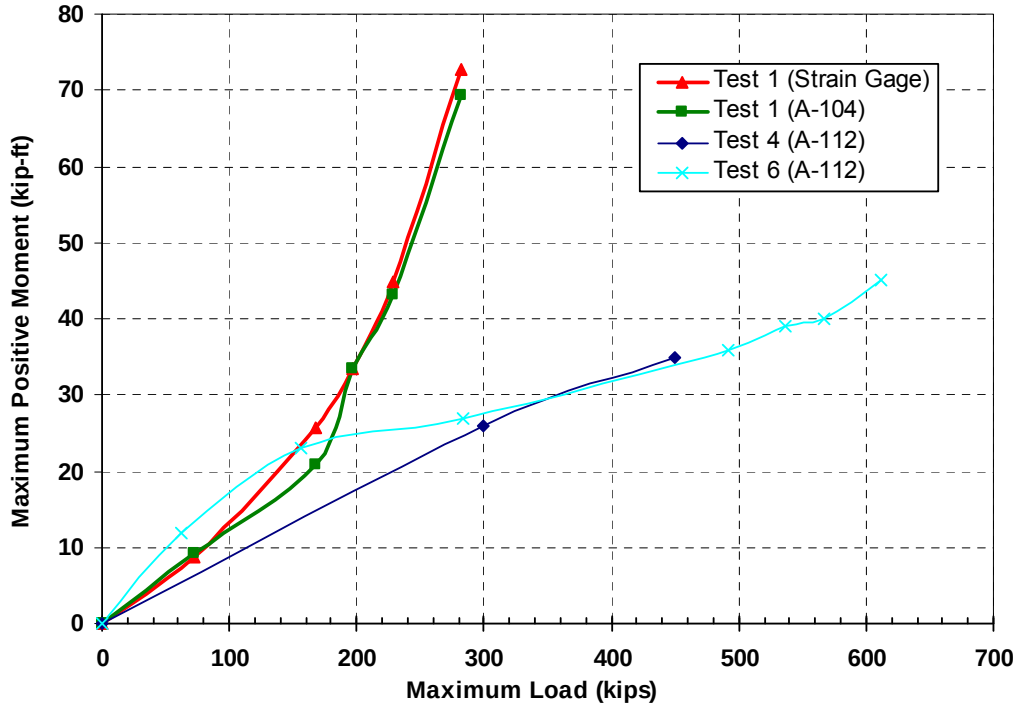

Figure 13-32 Comparison in measured bending moment in the middle center pile of pile cap 1 (1-M) before and after soil treatment with jet grouting.

At loads less than 250 kips, the piles generally experience greater bending moments. The piles and pile cap had been loaded multiple times at smaller load increments, but very few times at loads greater than 250 kips. The multiple loadings at smaller loads caused the piles to deflect more at these smaller increments during the tests performed following jet grouting. However, the general trends at the higher loadings proves that the piles are deflecting less at these loads than during virgin testing. This is evidence that the piles deflected less following soil treatment with jet grouting.

Figure 13-33 and Figure 13-34 display the maximum load vs. resulting maximum bending moment in the piles of pile cap 2 before and after treatment with jet grouting. Once again, the piles experienced greater bending moments at the smaller load increments following jet grouting; but at higher load increments the bending moments experienced in the piles were considerably lower. This is especially true for the bending moments obtained from test 4, which was the first test following jet grouting, for which the pile cap and piles experienced pile head deflections equal to those experienced during virgin testing. Once again, the results from this simple bending moment analysis proves that the piles experienced considerable less deflection at similar loads following installation of soilcrete columns. This helps to further validate that the soilcrete mass did displace as a rigid block.

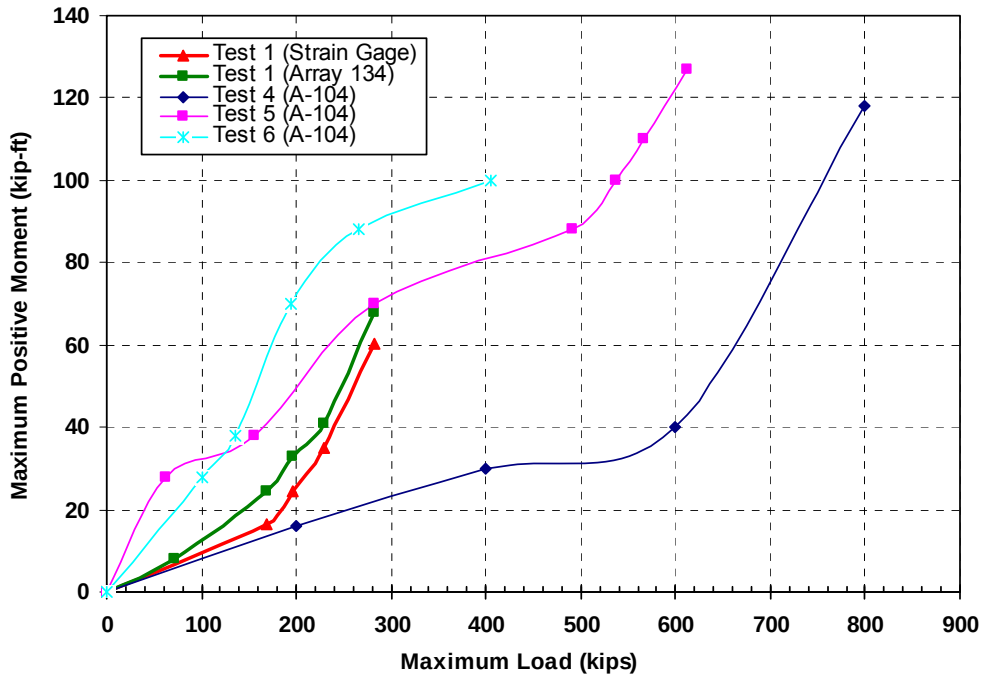

Figure 13-33 Comparison in measured bending moment in the north center pile of pile cap 2 (2-N) before and after soil treatment with jet grouting.

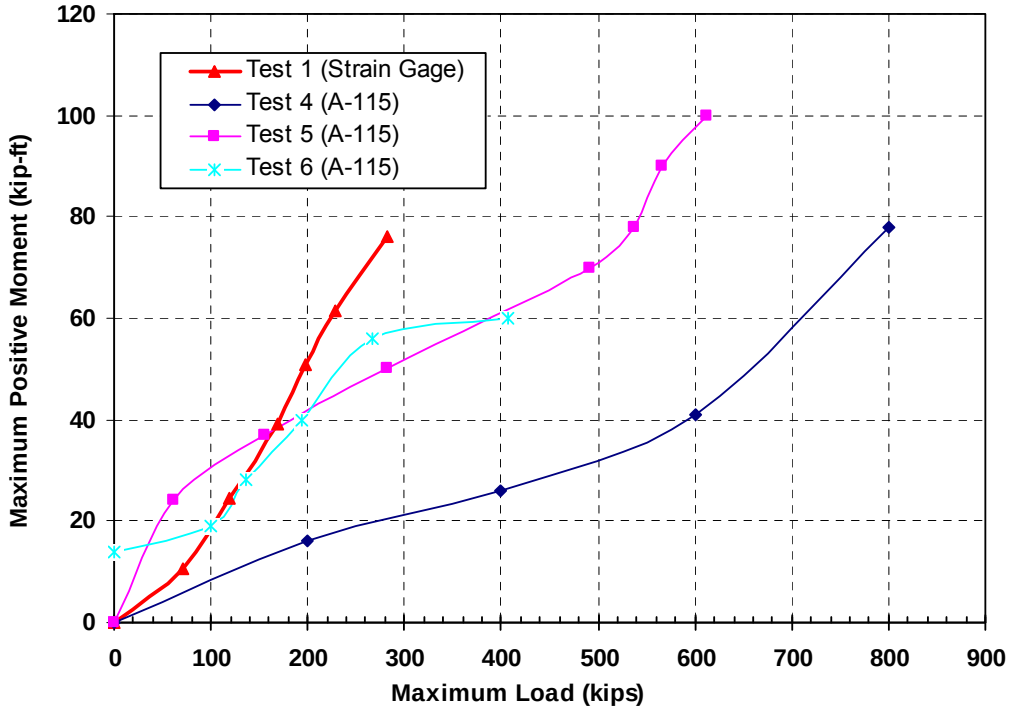

Figure 13-34 Comparison in measured bending moment in the south center pile of pile cap 2 (2-S) before and after soil treatment with jet grouting.

13.7 Basic Cost and Effectiveness Considerations

It was observed that jet grouting beneath the foundations increased the lateral resistance of the pile group by 500 kips, while jet grouting adjacent to pile cap 1 was predicted to increase the lateral resistance by about 450 kips. The cost of producing this increased lateral resistance due to soil improvement needs to be quantified to determine if it can be considered as not only a viable solution, but as a cost-effective solution as well. To do this, a rough estimate of the cost incurred to produce the jet grout treated zones will be compared to the alternative of adding more piles and expanding the pile cap.

There are two key cost elements associated with jet grouting. The first is the cost associated with mobilizing equipment and qualified operators and technicians to a particular site. These costs include: mobilization of equipment and operators to a site, equipment set-up, equipment tear-down, and demobilization of equipment. The mobilization costs are highly variable, depending upon the type of equipment needed and the location of the project. A good estimation of total mobilization costs for the Utah region is between $65,000 and $85,000. The second key cost element for jet grouting is the cost of performing the soil treatment. Local cement costs play a key role in this cost element, accounting for up to 40% of the total cost of treatment. Thus, the treatment costs of jet grouting are also highly variable. The range of possible costs can be as low as $100 per cubic yard of treated soil for large scale of economy projects with easy access, and up to $1000 per cubic yard of treated soil smaller projects with difficult access. An appropriate cost range for the Utah region is from $300 to $650 per cubic yard of treated soil (Ivanetich, 2008). Hayward Baker donated all of the labor and

equipment costs for this project. Therefore the actual costs associated with jet grouting were never determined.

Approximately 60 cubic yards of soil were treated beneath pile cap 2, with 40 cubic yards of soil being treated adjacent to pile cap 1. This correlates to a cost of between $21,000 and $36,000 to treat the soil beneath pile cap 2, and between $14,000 and $24,000 to treat the soil adjacent to pile cap 1. Thus, the total cost for treating the soil beneath pile cap 2 was between $86,000 and $121,000, and between $79,000 and $109,000 for treating the soil adjacent to pile cap 1 if mobilization costs are added separately to each foundation. Generally, however, the mobilization costs would be distributed evenly to each of the portions of the same project. A summary table of the costs associated with the jet grouting for this project are found Table 13-7. Treating the soil adjacent to pile cap 1 caused nearly the same increase in lateral resistance for the pile group and it was also the cheapest treatment method to install. Also, there are additional costs and technical issues associated with jet grouting through an existing foundation which are not shown in the cost summary. Therefore, jet grouting adjacent to an existing foundation is recommended as a more preferable option than jet grouting beneath an existing foundation.

Table 13-7 Summary of costs associated with jet grouting for this project.

Treatment Elements	Jet Grouting Beneath Pile Cap 2	Jet Grouting Adjacent to Pile Cap 1
Mobilization Cost	$65,000 - $85,000	$65,000 - $85,000
Treated Soil Volume (yd^3)	60	40
Cost per Volume of Treated Soil (yd3)	$350 - $600	$350 - $600
Total Cost to Treat Soil	$21,000 - $36,000	$14,000 - $24,000
Total Cost	$86,000 - $121,000	$79,000 - $109,000

One common alternative to jet grouting would be to simply add more piles and increase the size of the pile cap. According to the test results for cap 1 during test 2, the maximum lateral load resisted by the nine pile group was about 230 kips. If this load is distributed evenly, each pile would have carried about 26 kips. To obtain the same lateral resistance of 450-550 kips that was achieved through jet grouting beneath pile cap 2 or adjacent to pile cap 1, about 16-20 piles would have to be added. Creating an additional 4x4 or 4x5 pile configuration, which would need to be connected to the existing 3x3 pile group. Steel pipe pile costs during the project were on the order of $30/ft. Assuming typical pile lengths of 80 feet, 16-20 additional piles would cost $38,400 to $48,000. Mobilization costs to bring the steel piles and a pile driver to the site range between $15,000 and $20,000.

The driving costs are approximately for piles in the Utah area is approximately $12 per ft of driven pile. Therefore, the 16-20 additional piles would cost between $15,400 and $19,200 to drive into place. The average cost for concrete and reinforcement on the project was about $300 per cubic yard. The volume of concrete needed to fill the additional 16-20 piles would be 37.2 to 46.5 cubic yards, and would amount to an additional $11,200 to $14,000 of concrete and steel to reinforce the piles. Assuming the same pile spacing of 3 feet on center, the addition to the pile cap would have dimensions 12'x12'x2.5' for the 4x4 pile configuration, and dimensions of 12'x15'x2.5' for the 4x5 pile configuration. This equals pile cap volumes of 13.3 cubic yards and 16.67 cubic yards, respectively. That would amount to $4,000 for the cost of steel and concrete for the 4x4 configuration and $5,000 for the 5x5 pile configuration. Therefore, the total estimated cost of driving additional piles and expanding the pile cap

to obtain an increase in lateral resistance of 450-500 kips is from $84,000 to $106,000. A summary table of the costs associated with driving additional piles and expanding the pile cap is found in Table 13-8.

The cost difference between retrofitting with jet grouting or structurally retrofitting the existing foundation seems to be somewhat minimal when comparing the total costs associated with each retrofitting method. However, the mobilization costs for jet grouting are approximately 70-80% of the total cost of jet grouting; whereas the mobilization costs for structurally retrofitting the foundation are only 15-20% of the total cost. The actual treatment costs associated with jet grouting are significantly lower than those associated with driving the additional piles and constructing the pile cap addition. Thus, jet grouting would be an extremely cost effective solution for larger scale projects, where the mobilization costs could be distributed over a much larger project scope. Jet grouting could also be a cost effective solution for smaller scale projects; however, the mobilization costs and local costs of cement would need to be evaluated to determine if jet grouting would be an appropriate retrofitting method. Of course, this analysis is rough and the precise cost difference may differ from this analysis. Nevertheless, this example clearly illustrates how jet grouting can be a viable and cost-effective solution to increasing the lateral resistance of driven pile foundations.

Table 13-8 Summary of costs associated with structurally retrofitting the existing foundation for this project to achieve a comparable strength gain with jet grouting.

Cost Elements of Driving Additional Piles and Expanding the Pile Cap	4x4 Pile Configuration	4x5 Pile Configuration
Mobilization Costs	$15,000 - $20,000	$15,000 - $20,000
Steel Costs for Piles	$38,400	$48,000
Driving Cost for Piles	$15,400	$19,200
Reinforcement Cost for Piles	$11,200	$14,000
Pile Cap Expansion Cost	$4,000	$5,000
Total Cost	$84,000-$89,000	$101,000 - $106,000

14 Conclusions

In light of the findings in this thesis the following conclusions can be made in regards to using jet grouting as a soil improvement method to increase the lateral resistance of deep foundations in cohesive soils.

1. Jet grouting with a grout slurry with a 1:1 water-cement ratio by weight (S.G. = 1.52) was able to increase the average compressive strength of a soft, plastic clay from an average of 6 to 8 psi to an average above 400 psi. This result is consistent with past performance.
2. Installation of a soilcrete block (12 ft deep, 12-14 ft wide, and 6-8 ft long) adjacent to an existing nine-pile foundation with a pile cap (9 ft square and 2.5 ft deep) increased the lateral resistance of the pile group from 214 kips to 612 kips at a pile cap displacement of 0.75 inches. This increase of about 400 kips represents a 185% increase in lateral resistance. It is predicted that the fully developed lateral resistance would have been 750-760 kips at a pile cap displacement of 2.0 inches. This represents an approximate increase of 150-155% from an estimated virgin resistance of 300 kips at 2.0 inches of displacement.

3. Subsequent testing, after excavation to the base of the pile cap of a soilcrete block installed adjacent to an existing pile cap, yielded similar results for increased resistance as the soilcrete block before excavation. This suggests that the soilcrete block displaced as a rigid block during testing.
4. Analyses suggest that the soilcrete block (12 ft deep, 12-14 ft wide, and 6-8 ft long) with a design compressive strength of 250 psi installed adjacent to an existing nine-pile foundation with a 9 ft square by 2.5 ft deep pile cap was sufficient for lateral loads in excess of 610 kips. Additionally, the bending moment capacity of the soilcrete block installed adjacent to the nine-pile group was also sufficient to prevent cracking of the soilcrete block. These analyses further suggest that the soilcrete mass failed as a rigid block.
5. Installation of a soilcrete block (10 ft deep, 10-12 ft wide, and 14-16 ft long) below an existing nine pile group with a 9 ft square by 2.5 ft deep pile cap increased the lateral resistance from about 282 kips to 782 kips at a pile cap displacement of 1.5 inches. This increase of about 500 kips represents a 175-180% increase in lateral resistance.
6. The initial stiffness of the load-displacement curve following jet-grouting adjacent to and beneath the pile cap of an existing nine-pile foundation was increased substantially.
7. Analyses suggest that a 75% of the increased lateral soil resistance for the soilcrete block installed adjacent pile cap of a nine pile group can be attributed to the passive soil resistance acting on the face of the soilcrete block and adhesive soil resistance acting on the sides and bottom of the block as it is

displaced through the soil. These resistances can be calculated using basic geotechnical principles. The remaining 25% soil resistance not accounted for by the passive and adhesive soil resistance can potentially be attributed to increased soil pile interaction, which is predicted due to the decrease in pile head rotation during loading following soil treatment.

8. Analyses suggest that a 65% of the increased lateral soil resistance for the soilcrete block installed beneath the pile cap of a nine pile group can be attributed to the passive soil resistance acting on the face of the soilcrete block and adhesive soil resistance acting on the sides and bottom of the block as it is displaced through the soil. These resistances can be calculated using basic geotechnical principles. The remaining 35% soil resistance not accounted for by the passive and adhesive soil resistance can potentially be attributed to increased soil pile interaction, which is predicted due to the decrease in pile head rotation during loading following soil treatment.
9. Jet grouting adjacent to the pile cap of a nine pile group resulted in a 1% increase in lateral resistance per 7.3 ft^3 of treated soil, while jet grouting beneath the pile cap of an existing nine-pile group resulted in a 1% increase per 10.2 ft^3 of treated soil. Therefore, jet grouting adjacent to an existing pile foundation is preferred to jet grouting beneath an existing foundation.
10. When compared with retrofitting with additional piles and an expanded pile cap, retrofitting with jet grouting is economically comparable; especially when dealing with large scale projects.

15 References

American Petroleum Intstitute (API). (1986). "API Recommended Practice for Planning, Designing, and Constructing Fixed Offshore Platforms." Report RP-2A.

Bowles, J. E. (1996). Foundation Analysis and Design; McGraw Hill Incorporated, USA. pp. 1066.

Brandenberg, S. J., Boulanger, R. W., Kutter, B. L., and Chang, D. (2005). "Behavior of Pile Foundations in Laterally Spreading Ground during Centriufuge Tests". Journal of Geotechnical and Geoenvironmental Engineering, 131(11), 1389.

Budhu, M. (2007). Soil Mechanics and Foundations. John Wiley and Sons Inc. 111 River St, Hobokan, NJ 07030-5774. pp. 407.

Burke, G. (2004). "Jet Grouting Systems: Advantages and Disadvantages". ASCE Geotechnical Special Publication No. 12, pp. 875-886.

Duncan, J. M. and Mokwa, R.L. (2001). "Passive Earth Pressures: Theories and Test." Journal of Geotechnical and Geoenvironmental Engineering, 127(3), 248-257.

Hayward Baker Inc. (2007). Jet Grouting Services. Accessed February 2007, from http://www.haywardbaker.com/services/jet_grouting.htm

Herbst. M. (2008). Impact of Mass Mixing on the Lateral Resistance of Driven-pile Foundations. Brigham Young University Masters Thesis.

Ivanetich, K. (2008). Area Manager, Hayward Baker. Concord, California. Personnal communication.

Lemme, N. (In Press). Imapct of Compacted Fill and Rammed Aggreagate Piers on the Lateral Resistance of Diven-pile Foundations. Brigham Young University Masters Thesis.

MacGregor, J.G. and Wight, J.K. (2005). Reinforced Concrete Mechanics and Design. Prentice Hall, Upper Saddle River, New Jersey 07458. pp. 60.

Riaud, J. and Miran, J. (1992). The Cone Penetrometer Test. Washigton, D.C.

Appendix A. Corbel Specifications and Design

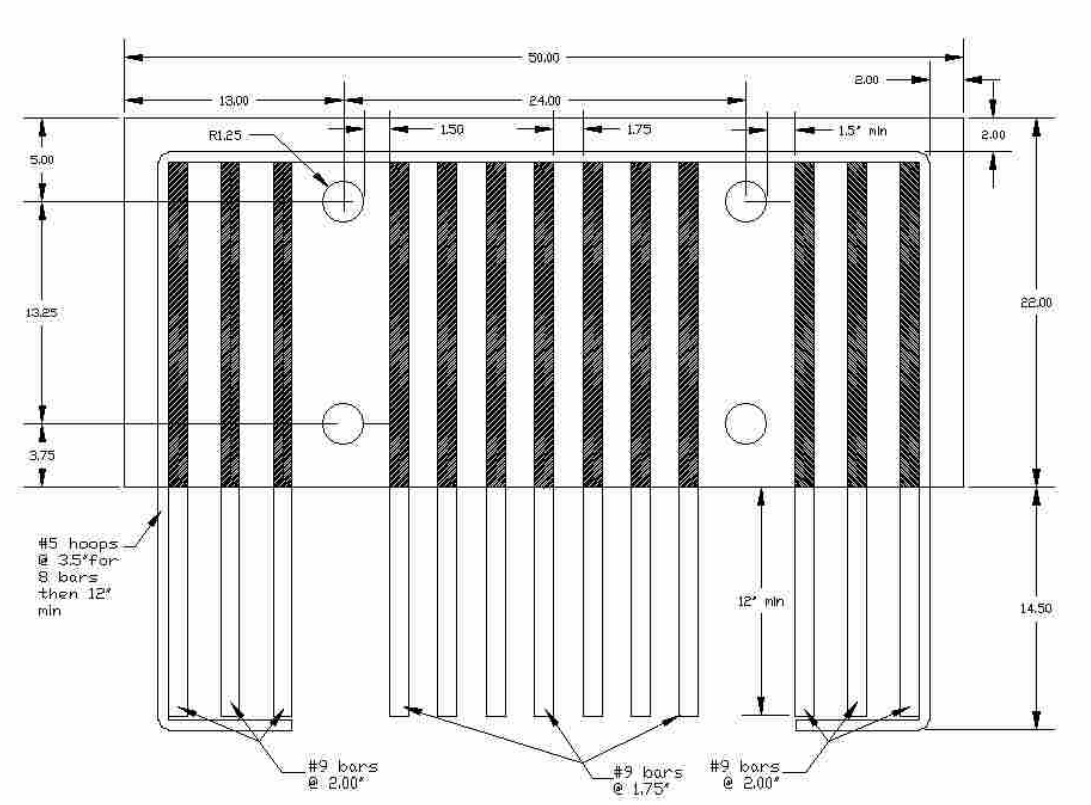

Figure 15-1– Front view of the corbel steel where the actuator would connect to the corbel.

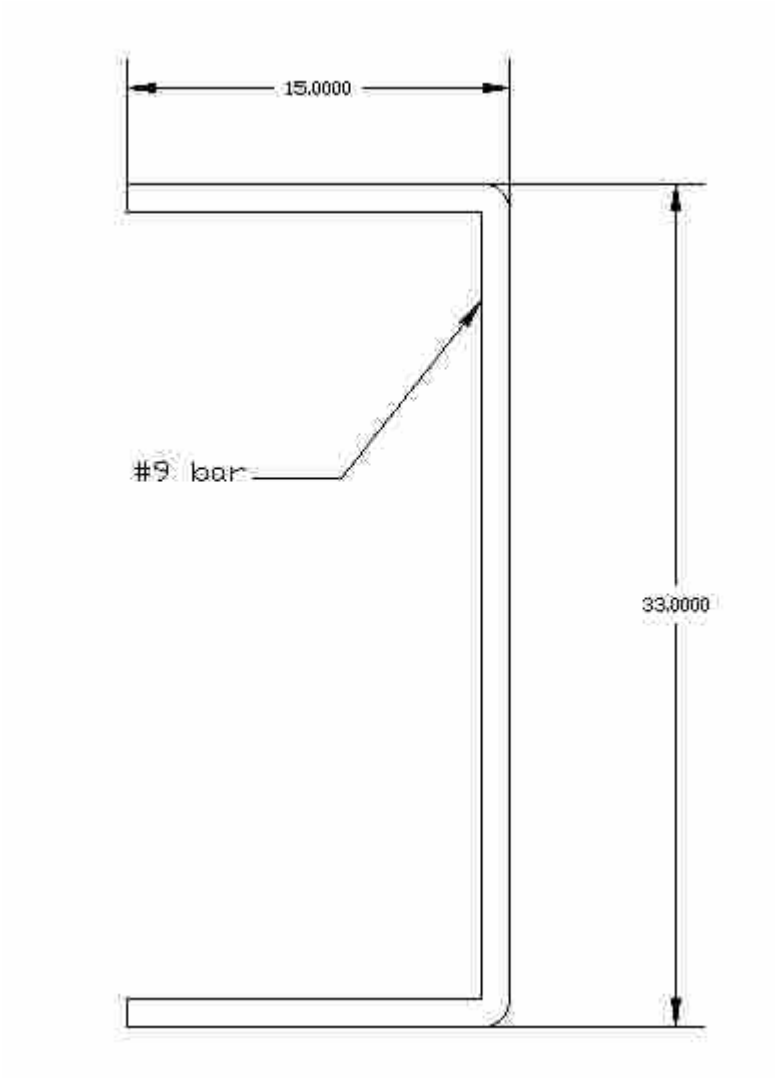

Figure 15-2 – The #9 bar main reinforcement for the corbel.

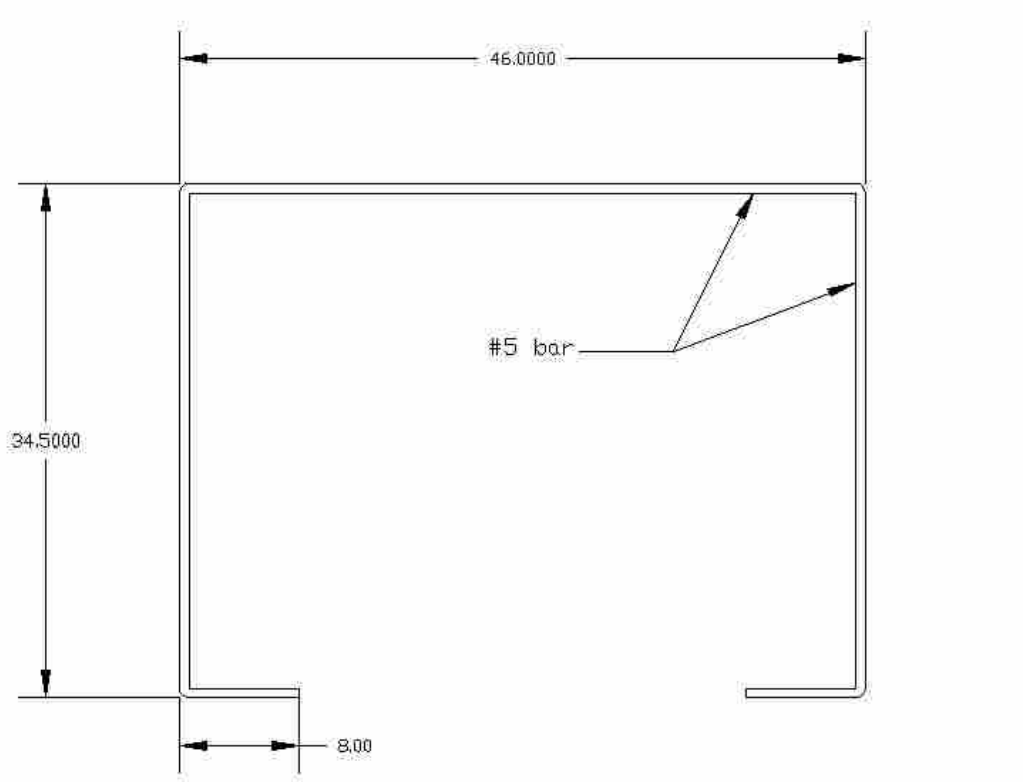

Figure 15-3 – The transverse or hoop reinforcement for the corbel.

Mark Herbst
Corbel Design

	Enter Value
	Guess or Over Ride
	Calculated Value

Parameters		
F'c	5000	psi
Vu (factored)	840	kips
Fy	60000	psi
Bw (guess)	50	inches

Bearing Plate Calcs				
b dim of plate	30			
Φ	0.65			
Bstress	2.7625	ksi		
Plate width	10.13574661	inches	try	
L dim of plate	20	in min	30 x20x1.5	OK
L	22			

Depth of Corbel				
Vn(d)	50			
Vn(d)	40			
Used Vn(d)	40		Say	
d min	28	inches	48	in
Φ	0.75			

Forces		
Nuc	168	kips
Av	10.5	in
h	50	in
d	48	
Mu	9156	kip-in
Φ	0.75	

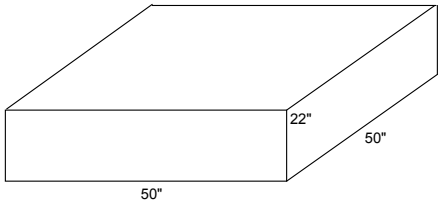

Shear Friction Steel		
λ	1	
Avf	13.33	in^2

Flexural Reinforcement		
Assume	d-a/2 = .9d	
Af	4.71	in^2
recompute a	1.33	
recompute Af	4.30	
An	3.733333333	in^2

Tension Tie Reinforcment	
Asc1	8.03
Asc2	12.62222222
Ascmin	8
	12.62

Bar Sizes	Area in^2	Diameter in	# Bars	Area	Total DofA w/#4 stirup	Spacing Cl	1 row clearance
3	0.11	0.378	115	12.6500	44.47	117	-111.47
4	0.2	0.5	64	12.8000	33	66	-49
5	0.31	0.625	41	12.7100	26.625	43	-19.625
6	0.44	0.75	29	12.7600	22.75	31	-3.75
7	0.6	0.875	22	13.2000	20.25	24	5.75
8	0.79	1	16	12.6400	17	18	15
9	1	1.128	13	13.0000	15.664	16.536	17.8
10	1.27	1.27	10	12.7000	13.7	14.43	21.87
11	1.56	1.41	9	14.0400	13.69	14.28	22.03
14	2.25	1.693	6	13.5000	11.158	11.465	27.377
18	4	2.257	4	16.0000	10.028	9.771	30.201

Size	#Bars	As	Enough Steel
9	13	13	YEP!

Area of Horizontal Stirrups		
Ah	4.44	in^2

Bar Sizes	Area in^2	Diameter in	# Bars	Area	Total DofA w/#4 stirup	Spacing Cl	1 row clearance
3	0.11	0.378	41	4.5100	16.498	43	-9.498
4	0.2	0.5	23	4.6000	12.5	25	12.5
5	0.31	0.625	15	4.6500	10.375	17	22.625

Size	#Bars	As	Enough Steel
5	8 Double leg	4.96	YEP!

Development Length				
Ldh	10.72	in	say 12	
Db	1.128	in		
Reg Ld	62.21	in	5.1845069	ft
α	1.3			
β	1			
γ	1			
λ	1			
12*d	13.536		say 14	

Figure 15-4 – Corbel design calculated values using ACI section 11.9.

Appendix B. Detailed Jet Grouting Production Logs

HAYWARD BAKER INC.

JET GROUT PRODUCTION LOG

Job # 53864 **Date: 7-25-07**

Job Name: Lateral Load Test **Job Location: Salt Lake City, Utah**

Column number	D	C	H				
Start time	10:33	11:31	12:37				
Stop time	10:58	11:54	1:02				
Construction time	25	23	25				
Start depth (feet)	16 ft	16 ft	16 ft				
Stop depth (feet)	6 ft	6 ft	6 ft				
Length treated	10 ft	10 ft	10 ft				
Start gallons	0	0	0				
Stop gallons	2208	2041	2100				
Total gallons	2208	2041	2100				
Column diameter	5 ft	5 ft	5 ft				
Grout pressure	6000 psi	6000 psi	6000 psi				
Grout flow rate	90 gpm	90 gpm	90 gpm				
Rotation speed	7 rpm	7 rpm	7 rpm				
Pull rate	20 cpm	20 cpm	20 cpm				

Total length treated today	30 FT

Figure B-1 Hayward Baker production log for jet grouting soil treatment on July 25, 2007.

HAYWARD BAKER INC.

JET GROUT PRODUCTION LOG

Job # 53864 **Date: 7/26/07**

Job Name: Lateral Load Test **Job Location: Salt Lake City, Utah**

Column number	A	B	G				
Start time	10:52	11:40	12:52				
Stop time	11:17	12:03	1:18				
Construction time	25 min	23 min	26 min				
Start depth (feet)	16 ft	16 ft	16 ft				
Stop depth (feet)	6 ft	6 ft	6 ft				
Length treated	10 ft	10 ft	10 ft				
Start gallons	0	0	0				
Stop gallons	2177	2021	2209				
Total gallons	2177	2021	2209				
Column diameter	5 ft	5 ft	5 ft				
Grout pressure	6000 psi	6000 psi	6000 psi				
Grout flow rate	90 gpm	90 gpm	90 gpm				
Rotation speed	7 rpm	7 rpm	7 rpm				
Pull rate	20 cpm	20 cpm	20 cpm				

Total length treated today	30 ft

Figure B-2 Hayward Baker production log for jet grouting soil treatment on July 26, 2007.

HAYWARD BAKER INC.

JET GROUT PRODUCTION LOG

Job # 53864 **Date: 7/27/07**

Job Name: Lateral Load Test **Job Location: Salt Lake City, Utah**

Column number	E	F	1	2	3	4	
Start time	7:23	8:02	11:58	12:30	1:12	1:57	
Stop time	7:45	8:53	12:18	12:54	1:35	2:17	
Construction time	22 min	51 min	20 min	24 min	23 min	20 min	
Start depth (feet)	16 ft	16 ft	16 ft	16 ft	16 ft	16 ft	
Stop depth (feet)	6 ft	6 ft	4 ft	4 ft	4 ft	4 ft	
Length treated	10 ft	10 ft	12 ft	12 ft	12 ft	12 ft	
Start gallons	0	0	0	0	0	0	
Stop gallons	2013	2226	1514	1837	1773	1520	
Total gallons	2013	2226	1514	1837	1773	1520	
Column diameter	5 ft	5 ft	4 ft	4 ft	4 ft	4 ft	
Grout pressure	6000 psi	6000 psi	6000 psi	6000 psi	6000 psi	6000 psi	
Grout flow rate	90 gpm	90 gpm	90 gpm	90 gpm	90 gpm	90 gpm	
Rotation speed	7 rpm	7 rpm	8 rpm	8 rpm	8 rpm	8 rpm	
Pull rate	20 cpm	20 cpm	25 cpm	25 cpm	25 cpm	25 cpm	

Total length treated today	68 lf

Figure B-3 Hayward Baker production log for jet grouting soil treatment on July 27, 2007.

HAYWARD BAKER INC.

JET GROUT PRODUCTION LOG

Job # 53864 **Date: 7/30/07**

Job Name: Lateral Load Test **Job Location: Salt Lake City, Utah**

Column number	5	6	7				
Start time	9:43	10:20	10:55				
Stop time	10:10	10:40	11:19				
Construction time	26 min	20 min	23 min				
Start depth (feet)	16 ft	16 ft	16 ft				
Stop depth (feet)	4 ft	4 ft	4 ft				
Length treated	12 ft	12 ft	12 ft				
Start gallons	0	0	0				
Stop gallons	1904	1836	2100				
Total gallons	1904	1836	2100				
Column diameter	4 ft	4 ft	4 ft				
Grout pressure	6000 psi	6000 psi	6000 psi				
Grout flow rate	90 gpm	90 gpm	90 gpm				
Rotation speed	8 rpm	8 rpm	8 rpm				
Pull rate	25 cpm	25 cpm	25 cpm				

Total length treated today	36 lf

Figure B-4 Hayward Baker production log for jet grouting soil treatment on July 30, 2007.

Appendix C. Passive and Adhesive Resistance

Due to the difficulty of transferring text from MATHCAD software to Wordpreocessing software, the following figures are screen captured from MATHCAD version 14.

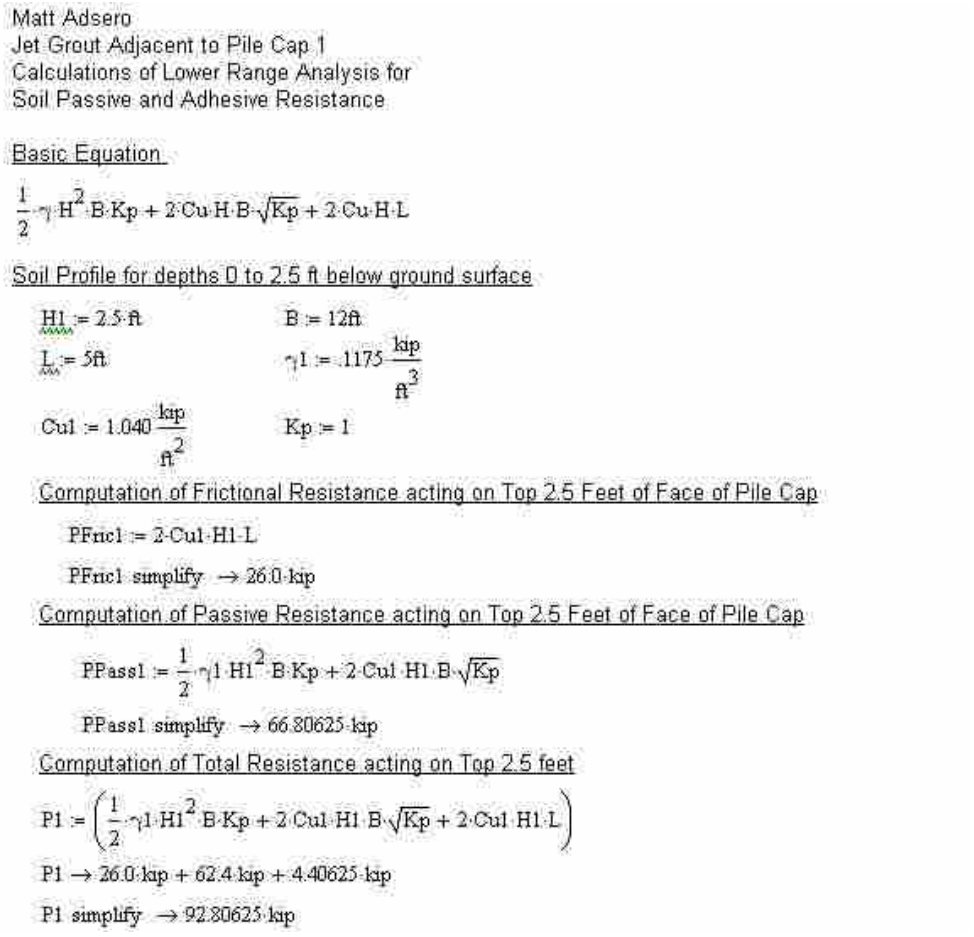

Figure C-1 Calculations performed in MATHCAD computational software for the top 2.5 feet of soilcrete block adjacent to pile cap 1 for the lower bound adhesive and passive soil resistance analysis.

Soil Profile for depths 2.5 to 10 ft below ground surface

$H2 := 9.5\,ft$ $\quad B := 12ft$

$L := 6ft$ $\quad \gamma 2 := .112\,\frac{kip}{ft^3}$

$Cu2 := .30\,\frac{kip}{ft^2}$ $\quad Kp := 1$

Computation of Frictional Resistance acting on Top 2.5 Feet of Face of Pile Cap

$PFric2 := (2 \cdot Cu2 \cdot H2 \cdot L)$

PFric2 simplify $\rightarrow 34.2\,kip$

Computation of Passive Resistance acting on Bottom 9.5 Feet of Face of Pile Cap

$$PPass2 := \frac{1}{2} \cdot \gamma 2 \cdot H2^2 \cdot B \cdot Kp + (2 \cdot Cu2 \cdot B \cdot \sqrt{Kp} + \gamma 1 \cdot H1 \cdot B \cdot Kp) \cdot H2$$

PPass2 simplify $\rightarrow 162.5355\,kip$

Computation of Total Resistance acting on Bottom 9.5 feet

$$P2 := \frac{1}{2} \cdot \gamma 2 \cdot H2^2 \cdot B \cdot Kp + (2 \cdot Cu2 \cdot B \cdot \sqrt{Kp} + \gamma 1 \cdot H1 \cdot B \cdot Kp) \cdot H2 + 2 \cdot Cu2 \cdot H2 \cdot L$$

$P2 = 196.736\,kip$

Bottom Friction

$Cu3 := .35\,\frac{kip}{ft^2}$

$PFric3 := L \cdot B \cdot Cu3$

$PFric3 = 25.2\,kip$

Total Frictional Resistance

$PFric\_Tot := PFric1 + PFric2 + PFric3$

PFric_Tot simplify $\rightarrow 85.4\,kip$

Total Passive Resistance

$PPass\_Tot := PPass1 + PPass2$

PPass_Tot simplify $\rightarrow 229.34175\,kip$

Total Resistance Passive + Friction

$Ptotal := P1 + P2 + PFric3$

$Ptotal = 314.742\,kip$

Figure C-2 Calculations performed in MATHCAD computational software for bottom 9.5 feet of soilcrete block adjacent to pile cap 1 for the lower bound adhesive and passive soil resistance analysis. The total resistance from 0 to 12 feet is also shown.

Matt Adsero
Jet Grout Beneath Pile Cap 2
Calculations of Mean Analysis for
Soil Passive and Adhesive Resistance

Basic Equation

$$\frac{1}{2}\cdot\gamma\cdot H2^2\cdot B\cdot Kp + 2\cdot Cu\cdot H2\cdot B\sqrt{Kp} + 2\cdot Cu\cdot H2\cdot L$$

Soil Profile for depths 2.5 to 12.5 ft below ground surface

$B := 10ft$ $\quad \gamma 1 := .1175\cdot\frac{kip}{ft^3}$ $\quad H1 := 2.5ft$

$L := 14ft$ $\quad H2 := 10ft$

$Cu2 := .300\frac{kip}{ft^2}$ $\quad \gamma 2 := .112\cdot\frac{kip}{ft^3}$ $\quad Kp := 1$

Computation of Adhesive Resistance acting on Sides of Soilcrete Mass

$PFric1 := (2\cdot Cu2\cdot H2\cdot L)$

$PFric1\ simplify \rightarrow 84.0\cdot kip$

Computation of Passive Resistance acting on Face of Soilcrete Mass

$$PPass2 := \frac{1}{2}\cdot\gamma 2\cdot H2^2\cdot B\cdot Kp + \left(2\cdot Cu2\cdot B\sqrt{Kp} + \gamma 1\cdot H1\cdot B\cdot Kp\right)\cdot H2$$

$PPass2\ simplify \rightarrow 145.375\cdot kip$

Bottom Adhesive Resistance

$$Cu3 := .350\cdot\frac{kip}{ft^2}$$

$PFric2 := L\cdot B\cdot Cu3$

$PFric2 = 49\cdot kip$

Total Adhesive Resistance

$PFric\_Tot := PFric1 + PFric2$

$PFric\_Tot\ simplify \rightarrow 133.0\cdot kip$

Total Passive Resistance

$PPass\_Tot := PPass2$

$PPass\_Tot\ simplify \rightarrow 145.375\cdot kip$

Figure C-3 Calculations performed in MATHCAD computational software the soilcrete block beneath pile cap 2 for the lower bound adhesive and passive soil resistance analysis.

Appendix D. Soilcrete Bending Moment Capacity

Matt Adsero
Soilcrete Bending Capacity
Calculations
Mcr Analysis

Solving for Mcr

$$\sigma := \frac{M \cdot Y}{I} \rightarrow M := \frac{\sigma \cdot I}{Y} \rightarrow Mcr := \frac{Fr \cdot I}{Y}$$

As a rough estimate we will assume Fr equals 12% of unconfined compression strength.

$Fr := 0.12 \cdot 250psi$ $Fr = 30\ psi$

Sloving for I

$b := 11ft$ $h := 4ft$

$$I := \frac{b \cdot h^3}{12} \quad I = 1.217 \times 10^6\ in^4$$

$Y := 24in$

$$Mcr := \frac{Fr \cdot I}{Y} \quad Mcr = 126.72\ kip \cdot ft$$

Figure D-1 Calculations performed in MATHCAD to determine the bending moment capacity of the hardened soilcrete.